Académie universitaire Wallonie-Europe
University of Liège, Belgium

Faculty of Applied Sciences
GIGA-In Silico Medicine
Thermodynamics of Irreversible Processes

Model-Based Prediction of the Response to Vascular Filling Therapy

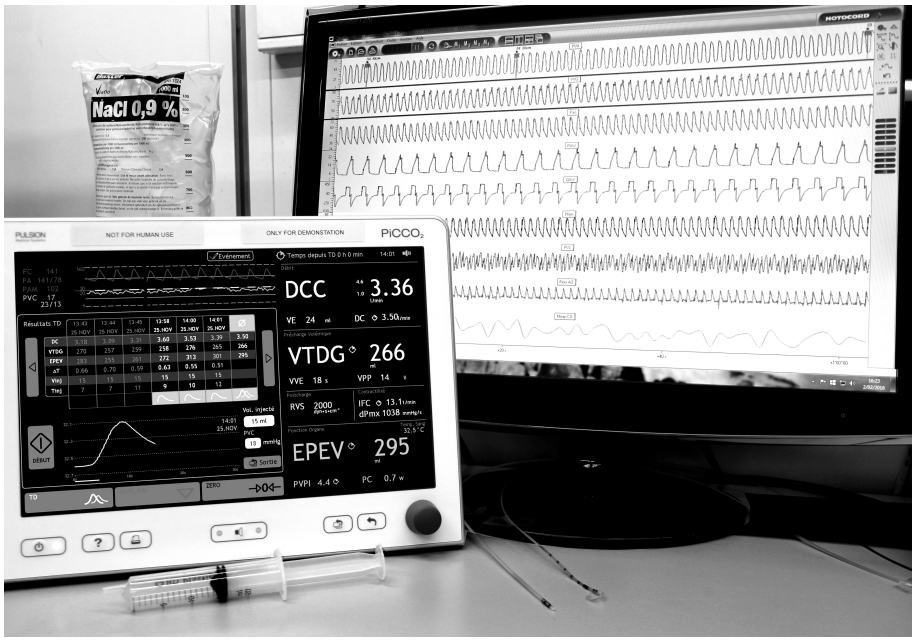

By **Antoine Pironet**, Master in Biomedical Engineering

Supervised by Thomas Desaive, Ph.D.

A thesis submitted in partial fulfilment of the requirements for the degree of Doctor of Philosophy in Engineering Sciences

February 2016

"Prediction is very difficult, especially about the future."

Niels Bohr

The present dissertation has been evaluated by the jury members:

Dr T. Desaive (supervisor)
University of Liège, Liège, Belgium

Dist. Prof. J. G. Chase,
University of Canterbury, Christchurch, New Zealand

Prof. P. C. Dauby,
University of Liège, Liège, Belgium

Prof. L. Geris,
University of Liège, Liège, Belgium

Prof. P. Kolh,
University of Liège and CHU de Liège, Liège, Belgium

Dr P. Morimont,
CHU de Liège, Liège, Belgium

Dr C. Phillips,
University of Liège, Liège, Belgium

Prof. J.-P. Ponthot,
University of Liège, Liège, Belgium

The research described in the present dissertation was financially supported by the Belgian National Funds for Scientific Research, F.R.S.-FNRS, and the French Community of Belgium (Actions de Recherches Concertées, Académie Wallonie-Europe).

Résumé

Le remplissage vasculaire est l'une des interventions les plus fréquentes dans les unités de soins intensifs, l'effet attendu étant une augmentation du débit cardiaque. Cependant, cette réponse est observée dans seulement environ 50 % des cas. De plus, un remplissage vasculaire trop important peut mener à des effets délétères, comme l'œdème pulmonaire, qui augmentent la durée de la respiration mécanique, de l'hospitalisation, la mortalité et les coûts. Les médecins sont donc à la recherche d'indices fournissant *a priori* une information sur les effets du remplissage vasculaire. Cette thèse présente une méthode de prédiction de la réponse au remplissage vasculaire basée sur un modèle mathématique. Un modèle mathématique est un ensemble d'équations représentant le comportement d'un système donné, par exemple le système cardio-vasculaire.

Des éléments de base d'anatomie et de physiologie cardio-vasculaire sont présentés dans la première partie de cette thèse, car ils sont nécessaires à la compréhension des principes du remplissage vasculaire. Ensuite, des détails supplémentaires sont fournis sur la thérapie de remplissage vasculaire, ainsi que sur les indices actuellement utilisés par les médecins pour en prédire les effets. Les indices dits statiques sont faciles à obtenir, mais peu efficaces. Les indices dits dynamiques, basés sur les interactions cardio-pulmonaires, sont plus performants, mais sont invasifs et difficiles à implémenter en clinique. Un nouvel indice, le volume total de sang sous pression, pourrait s'avérer utile, mais est également difficile à obtenir en clinique. Ce travail développe et utilise des modèles du système cardio-vasculaire pour rendre ce paramètre disponible aux médecins.

Sur base des éléments de physiologie développés dans la première partie, la seconde partie de cette thèse décrit comment modéliser les composants actifs et passifs du système cardio-vasculaire sous forme d'éléments agrégés, comme des compartiments, des valves et des résistances. Deux modèles du système cardio-vasculaire, comptant respectivement trois et six compartiments, sont ensuite construits à partir de tels éléments. Ces deux modèles impliquent un petit nombre de paramètres, représentant notamment le volume total sous pression dans le modèle.

La troisième partie de cette thèse explique comment identifier les paramètres des deux modèles du système cardio-vasculaire. L'identification des paramètres a pour but de trouver les valeurs des paramètres qui rendent les simulations du modèle aussi proches que possible des données mesurées. Les données disponibles sont donc décrites en premier lieu, en fonction de l'endroit où elles sont mesurées : dans un laboratoire expérimental ou une unité de soins intensifs. Ensuite, il est mathématiquement démontré que tous les paramètres du modèle peuvent théoriquement être identifiés à partir de données disponibles dans une unité de soins intensifs. Cependant, d'un point de vue pratique, certains paramètres ne peuvent être identifiés, car ils ont peu d'influence sur les simulations, ou ont le même effet que d'autres paramètres. En dernier lieu, des méthodes numériques pour identifier les paramètres à partir d'un ensemble de données cliniques sont présentées et comparées.

La dernière partie de cette thèse présente deux applications des modèles du système cardio-vasculaire à des données expérimentales. Premièrement, tous les paramètres du modèle du système cardio-vasculaire à six compartiments sont identifiés à partir de données provenant d'une expérience de réduction de précharge. Ce résultat constitue la première validation quantitative du modèle à six compartiments en situation transitoire. Deuxièmement, tous les paramètres du modèle à trois compartiments, y compris le volume total sous pression, sont identifiés à partir de données provenant d'expériences de remplissage vasculaire. Les résultats montrent que le volume total sous pression est systématiquement lié au changement de débit cardiaque après remplissage. Ce dernier indice fournit donc, pour la première fois, une méthode basée sur un modèle pour prédire la réponse au remplissage vasculaire.

Abstract

Vascular filling is one of the most frequent interventions in intensive care units. Its expected effect is to increase cardiac output. However, this increase is only observed in approximately 50 % of cases. In addition, excessive vascular filling can lead to deleterious effects, such as pulmonary oedema, which increase length of ventilation, stay, mortality and cost. Clinicians are thus looking for indices to provide *a priori* knowledge of the effect of vascular filling. This thesis focuses on a mathematical model-based approach to predict the response to vascular filling. Mathematical models are sets of equations representing the behaviour of a given system as, for instance, the cardiovascular system.

To understand the concept of vascular filling, basic elements of cardio-vascular anatomy and physiology are presented in the first part of this thesis. Then, further details about vascular filling therapy are given, as well as the current indices used by clinicians to predict its effects. The static indices are easy to obtain, but do not perform well. The dynamic indices, based on cardio-pulmonary interactions, perform better, but are difficult and highly invasive to implement clinically. A new index, total stressed blood volume, also seems to perform well, but is not easy to obtain clinically. This work develops and then uses models of the cardio-vascular system to make this parameter available to clinicians.

Building on the elements of physiology provided in the first part, the second part of this thesis describes ways to model the components of the cardio-vascular system as lumped elements, such as chambers, valves and resistances. Two models of the cardio-vascular system, comprising respectively three and six chambers, are built from such elements. These two models involve a small number of parameters, including the total stressed volume in the model.

The third part of this thesis describes the potential and methods to identify the parameters of the two cardio-vascular system models. Parameter identification aims at finding the parameter values that make model simulations as close as possible to measured data. The available data is thus first described, according to whether it is collected in an experimental laboratory or an intensive care unit. Then, it is mathematically demonstrated that all model parameters can theoretically be identified from data available in an intensive care unit. However,

practically speaking, some parameters are difficult to identify, because they have little influence on the simulations, or have the same effect as other parameters. Finally, computational methods to perform parameter identification are presented and compared.

The last part of this thesis presents two applications of the cardio-vascular system models to experimental data. First, all parameters of the six-chamber cardio-vascular system model are identified from data recorded during a preload reduction experiment. This result provides the first quantitative validation of the six-chamber model in transient conditions. Second, all parameters of the three-chamber cardio-vascular system model, including total stressed volume, are identified from data recorded during vascular filling experiments. The total stressed volume parameter is shown to be systematically related to the change in cardiac output after vascular filling. This last index thus provides, for the first time, a model-based means of predicting the response to vascular filling.

Contents

List of Figures

List of Tables

List of Acronyms

Chapter 1

Introduction

1.1 Vascular Filling

Vascular filling is one of the most frequent interventions in intensive care units (ICUs) and represents "*the cornerstone of haemodynamic management in ICUs*" [1–3]. This therapy consists in intravenous administration of a given quantity of fluid to a patient. The type of fluid, the quantity and the duration of the infusion vary widely across ICUs. The goal of vascular filling is to increase the amount of fluid in the blood circulation and, subsequently, to increase the pumping ability of the heart. This therapy is the key element in case of shock, a condition that concerns up to one third of ICU patients [4].

However, most studies performed in ICUs agree on the fact that vascular filling is effective in only approximately 50 % of cases [3]. This observation is linked to the fact that ICU patients present very different cardio-vascular problems, and patient state is rapidly changing. In addition, an excess of intra-vascular fluid can lead to severe complications, such as pulmonary oedema, right ventricular dysfunction or haemodilution [5, 6], which increase length of ventilation, length of stay, mortality and cost. Clinicians are thus in need of robust, readily available indices to predict the effect of vascular filling.

Prediction of the patient response to vascular filling is difficult, because the clinical data available in an ICU is mostly coming from the periphery of the cardio-vascular system (CVS). The decision to perform vascular filling thus largely depends on the experience of the medical staff.

To make a decision about vascular filling, ICU clinicians typically rely on one of the available physiological measurements, which include:

- Pressure in the central veins,
- Pressure in the peripheral arteries,
- Cardiac output.

The *static* values of these measurements, that is, their mean values, have repeatedly been shown to be poor predictors over the last decade [5,7,8]. However, they are still the current practice in 36 % of ICUs [1]. More recently, changes in measurements caused by external influences, or *dynamic* values, have been suggested as predictors. Several studies have demonstrated the better predictive ability of dynamic indices [5,7]. However, others have emphasised the difficulty of practically using them [9].

1.2 Approach

This work aims to contribute to the reliable prediction of the response to vascular filling, in a way that complies with the recently published European guideline stating that "*fluid resuscitation should be guided by more than one single hemodynamic variable*" [4]. To do so, this thesis relies on an original approach, one that processes several ICU available measurements to create a reliable predictor. The processing is performed using two tools: a mathematical model and a parameter identification procedure to turn clinical data into a patient-specific, model-based metric of patient state.

1.2.1 Mathematical Model

A mathematical model is a set of equations representing the behaviour of a given system. In general, the goal of a modelling process is one of the following: description, interpretation, prediction or explanation of the modelled phenomenon [10]. In the present case, a mathematical model of the CVS could be used to help interpret the clinical data [11] and predicting fluid responsiveness.

A model of the CVS intended for prediction of fluid responsiveness must be applicable in the ICU without requiring additional measurements. The model would also have to be robust to make correct predictions for different patients and conditions, and fast enough to predict significant changes in real time. Finally, it needs to provide a reasonably correct picture of the intrinsic haemodynamics, which are not available from the ICU data alone.

As for all systems, there exists an infinite number of ways to model the CVS. The more detailed the model, the more realistic the description it provides. For instance, the most detailed models of the CVS thoroughly study the dynamics of blood and muscle fibres [12]. However, more detailed models contain more equations, which are also more complex, and thus, more computational time is required to obtain a solution. The design of a model thus depends on the desired

goal. Following the model's intended use, the model designer chooses to neglect some phenomena.

Since real-time prediction is crucial in the ICU, the models used in this work will be simpler ones. These models are called *lumped* models, because they aggregate several parts of the CVS. Lumped models, even if simple, still need to take into account complex effects, such as cardiac contraction and valve dynamics. Such lumped models are bold approximations of the reality, but can reproduce well the macro-physiologic trends. Thanks to their simplicity, their equations can be solved in a few seconds on a standard computer.

Every model contains several *a priori* unknown quantities, called *parameters* and linking the variables involved in the model. Values have to be assigned to these parameters for the model equations to be solved. In addition, reasonable values have to be chosen so that the model simulations correctly represent the reality of the modelled system.

In lumped CVS models, the number of parameters is limited. These parameters usually represent the resistance to flow of small vessels and valves, and the elastance, or stiffness, of large vessels and cardiac chambers. Another very important parameter of mathematical models of the CVS is the total stressed blood volume contained by the system, capturing the ability of the heart and vessels to generate pressure.

1.2.2 Parameter Identification

Parameter identification is sometimes called the *inverse problem*. It aims at finding the parameter values that make model simulations as close as possible to a set of experimental measurements. In the ICU case, example of available measurements have been given in Section 1.1, and their limited number thus governs the model complexity for patient-specific applications.

Identifying the parameters of a CVS model using the measurements available in an ICU provides parameter values that concentrate all the available information. The term *patient-specific* is used to emphasise that, thanks to the parameter identification process perfomed on patient data, the model can be adapted to each patient at a given point in time. The resulting parameter values can then be used for cardio-vascular monitoring over time, potentially including prediction of the response to vascular filling.

Parameter identification is not a simple task. For instance, several parameter sets could lead to the same model outputs. In this case, the two parameter sets cannot be distinguished and the model is said to be structurally non-identifiable. The models developed in this work will thus be demonstrated to be structurally

identifiable. In other words, it should be possible to uniquely retrieve their parameters values from the available data.

Even for a structurally identifiable model, parameter identification can go wrong because of the data quality. All data are indeed limited and imperfect, which can cause a structural identifiable model to be practically non-identifiable. Using the models and the available data, the practical identifiability should also be investigated. This analysis is usually done by observing the individual effects of parameters on the simulations, through a *sensitivity analysis*, and the joint effects of parameters, through a *correlation analysis*.

For non-linear models, which are necessary to represent cardio-vascular and physiological reality with sufficient accuracy, parameter identification is not an immediate process. Instead, several model simulations have to be performed with different parameter sets, to find which one is the best. Several methods exist to do so. A method that will allow fast and reliable estimation of CVS model parameters thus needs to be selected, derived or adapted.

1.3 Goals

The goals of this work are:

- To develop simple models of the CVS usable in the ICU,
- To demonstrate that the parameters of these models can be identified from readily available ICU data, proving structural and practical identifiability,
- To verify the models using clinical data, to predict the response to vascular filling.

This thesis is organised in four parts: one introductory part and three main parts, each corresponding to these three goals.

1.4 Overview

The first part of this thesis provides the physiological and medical background on which the next three parts will be built. Chapter 2 of this work describes the elements of anatomy and physiology of the CVS that are useful to understand the effects of vascular filling and the development of CVS models. Chapter 3 describes vascular filling in further details and presents the commonly used indices of fluid responsiveness.

The second part of this thesis deals with the development of simple models of the CVS. Chapters 4 and 5 describe the building blocks of such models. Passive elements, such as resistances, valves and chambers are detailed in Chapter 4 and

active elements, such as ventricles and atria, are modelled in Chapter 5. Finally, in Chapter 6, two models are built from the previously introduced elements.

The third part of this thesis studies parameter identification of the two models from ICU data. First, Chapter 7 describes the type of data that can be obtained in an ICU, and the sensors that need to be used. Chapter 8 then mathematically demonstrates that all model parameters can theoretically be obtained from such data. In practice, however, the beat-to-beat nature of the data can prevent correct parameter identification. Chapter 9 thus provides tests to ensure that parameters can be practically identified. Finally, Chapter 10 presents a comparison of the different methods that can be used to obtain the parameter values.

The last part of this thesis uses the models and identification methods to predict the response to vascular filling therapy. The first developed CVS model is quantitatively validated in Chapter 11. Then, Chapter 12 shows that one parameter of the second CVS model, representing total stressed blood volume, is an index of fluid responsiveness. Finally, Chapter 13 presents conclusions and ideas for future improvements.

1.5 Summary

This introductory chapter detailed the elements mentioned in the title of this thesis, vascular filling and mathematical models. Vascular filling is a very frequent therapy in the ICU, but its positive effect on the circulation is not granted and difficult to predict. To solve this problem, this work proposes to use a mathematical model-based approach. Mathematical models are useful tools for prediction, but a preliminary requirement is that their parameters have to be identified from available data.

The three goals of this work were stated: development of CVS models, identification of CVS model parameters, and prediction of fluid responsiveness using the models. The organisation of the thesis in three main parts according to these three goals was detailed. An additional part, which directly comes after this paragraph, describes the medical background necessary for understanding this thesis.

Part I

Medical Background

Introduction

Part I contains two chapters, which aim at explaining the medical concepts on which the rest of this work is based. Chapter 2 presents an anatomical and physiological summary of the CVS. Using the terminology introduced in Chapter 2, Chapter 3 presents vascular filling therapy in more detail, along with its predictors and outcomes.

Chapter 2

The Cardio-Vascular System

2.1 Introduction

This chapter introduces the basic elements of CVS anatomy and physiology necessary for this work. A general overview of the CVS is provided first, with a short description of the heart and vessels. In the second part of this chapter, the functioning of the CVS is described and indices used by clinicians to assess its state are presented.

2.2 Overview of the Cardio-Vascular System

Blood supplies all cells of the organism with the nutrients and oxygen necessary for proper functioning, and collects the waste and carbon dioxide created. The role of the CVS is to maintain enough blood flow through the body, to provide a permanent flow of nutrients, ensure perfusion of the organs, and permanently removing waste. To perform this function, the CVS consists of a pump, the heart, and a closed network of blood vessels.

The CVS is closely associated with the respiratory system, which is responsible for the removal of carbon dioxide and the supply of oxygen, from and to the blood. The first part of the vascular system connects the heart to the lungs and back to the heart, and is called the *pulmonary circulation*. The second part, which connects the heart to every cell of the body and its return to the heart, is called the *systemic circulation*.

The pulmonary and systemic circulations both involve the same three types of blood vessels: arteries, capillaries and veins. When the heart contracts, it propels blood into the *arteries*, which are large and deformable blood vessels. Downstream of the heart, arteries branch out into increasingly smaller vessels. The smallest of these vessels are called the *capillaries*. The wall of the capillaries is

porous, allowing the exchange of chemical species between blood and other body cells in the systemic circulation, or between blood and the air in the lungs in the pulmonary circulation. Further away, capillaries branch together and form increasingly larger vessels, the *veins*. The veins are the vessels through which blood returns to the heart. The situation is illustrated in Figure 2.1.

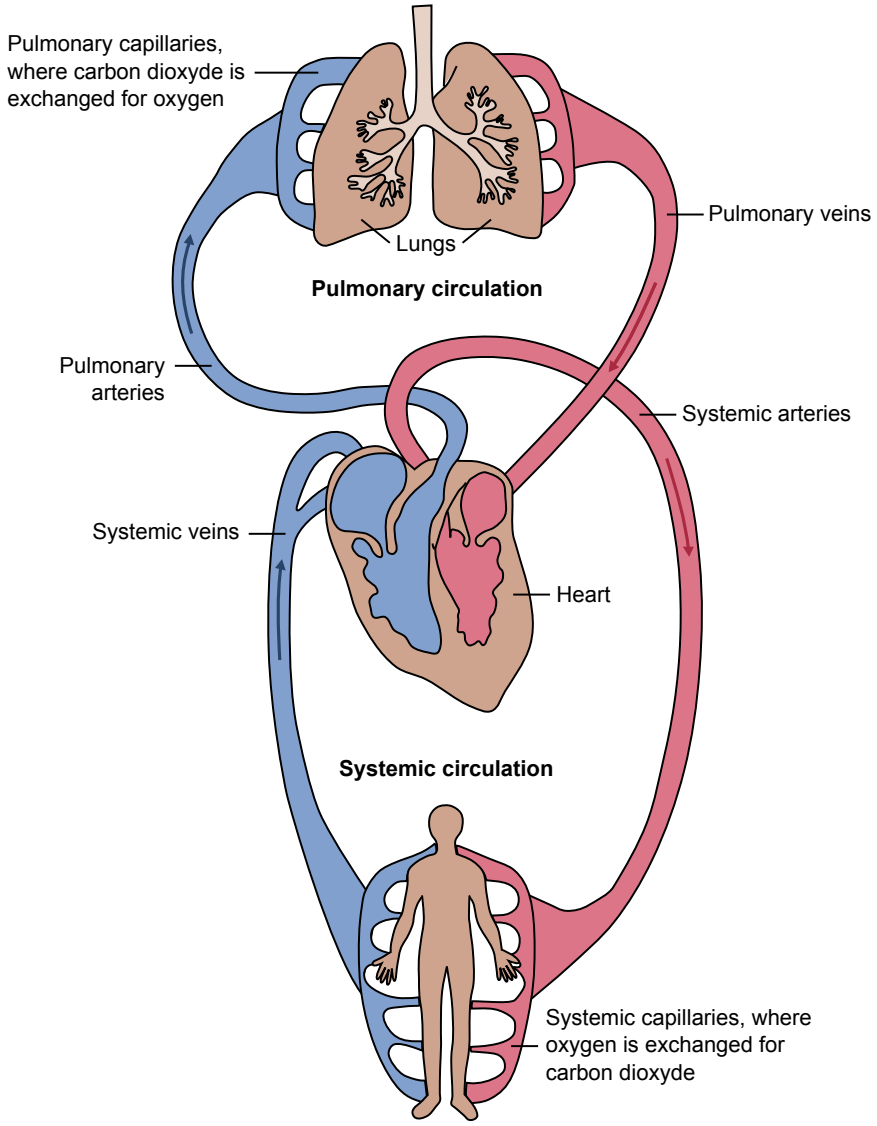

Figure 2.1: Simplified illustration of the cardio-vascular system (adapted from [13], with permission). Red is used to depict oxygenated blood and blue represents de-oxygenated blood.

2.2.1 The Heart

The heart is a muscular pump that connects the systemic and pulmonary circulations. It consists of two parts, left and right, separated by a central wall called the *septum*. The right part of the heart collects de-oxygenated blood coming from the

systemic circulation and drives it to the pulmonary circulation, while the left part collects oxygenated blood coming from the pulmonary circulation and drives it to the systemic circulation.

The left and right parts of the heart are both composed of two contractile chambers: an *atrium* and a *ventricle*. Two valves are located up and downstream of each ventricle and prevent blood from flowing back. The valve located between the left atrium and the left ventricle is called the *mitral valve*, the one located between the right atrium and ventricle is called the *tricuspid valve*. These two valves are referred to as the *atrio-ventricular valves*. Finally, the valve located between the left ventricle and the aorta, the major systemic artery, is the *aortic valve* and the valve located between the right ventricle and the pulmonary artery is the *pulmonary valve*. These last two valves are called the *ventriculo-arterial valves*. Figure 2.2 presents an illustration of the heart and its valves.

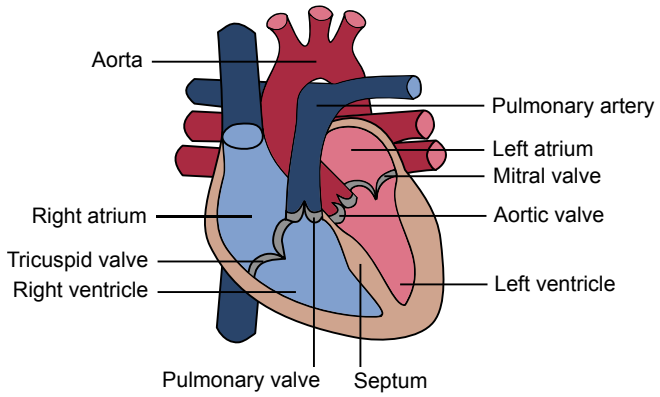

Figure 2.2: Section of the heart showing the four chambers and the four valves (adapted from [13], with permission).

The heart is enclosed in a serous and fibrous envelope, the *pericardium* [14]. Because of its rigidity, the pericardium prevents an excessive distension of cardiac chambers. Consequently, if one of the ventricles is distended, the other will be compressed through the motion of the septum. This interaction is called the *direct interaction of the ventricles*.

2.2.2 The Vessels

The *aorta* is the vessel located downstream of the left ventricle and the aortic valve. It is the main systemic artery and forms the beginning of the systemic circulation, and it thus contains oxygenated blood. The *pulmonary artery* is the vessel located downstream of the right ventricle and the pulmonary valve. It forms the beginning of the pulmonary circulation and contains de-oxygenated blood on the way to the lungs.

The *superior* and *inferior venae cavae* are the two veins that bring de-oxygenated blood back from the upper and lower parts of the body to the right atrium. The four *pulmonary veins* are the vessels that bring oxygenated blood back from the lungs to the left atrium. The arteries and the veins are the largest blood vessels. They are also relatively elastic. In particular, veins can serve as reservoirs to store blood and re-equilibrate pressures in the system, if necessary [15]. In these large vessels, blood flows easily.

2.3 Physiology of the Cardio-Vascular System

2.3.1 The Cardiac Cycle

During a cardiac cycle, the heart muscle successively contracts to eject blood and then relaxes to allow filling. Since this behaviour repeats in time, one must choose a starting point to describe the cardiac cycle. In this section, the chosen starting point is the end of ejection, marked by the closing of the aortic and pulmonary valves.

Isovolumic Relaxation

At the closing of the aortic and pulmonary valves, the heart is still contracted. It then starts to relax by keeping a constant volume, because all the valves are closed, as the mitral and tricuspid valves closed at a prior time of the cardiac cycle. This relaxation at a constant volume causes a pressure decrease. This action is the *isovolumic relaxation* phase. It is represented in Figure 2.3.

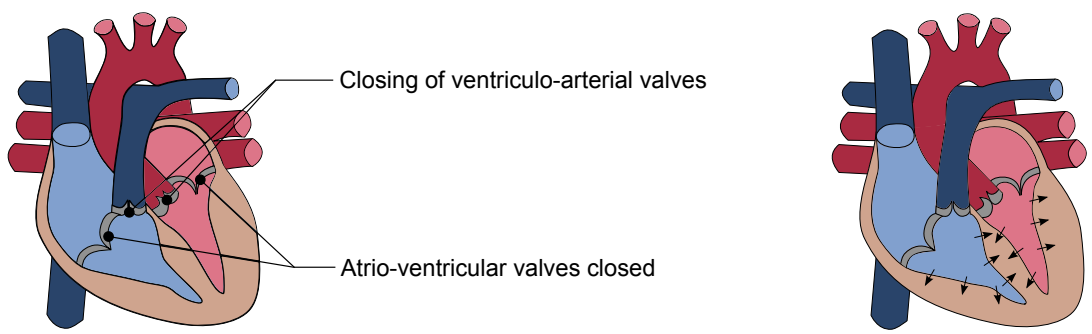

Figure 2.3: Situation of the heart during the isovolumic relaxation phase (adapted from [13], with permission).

Filling

The atrio-ventricular valves eventually open because of the ventricular pressure drop, which causes the blood to spontaneously flow from the atria to the ventricles. This change marks the beginning of the *early filling* phase, marked by a rapid blood flow. It is represented in Figure 2.4.

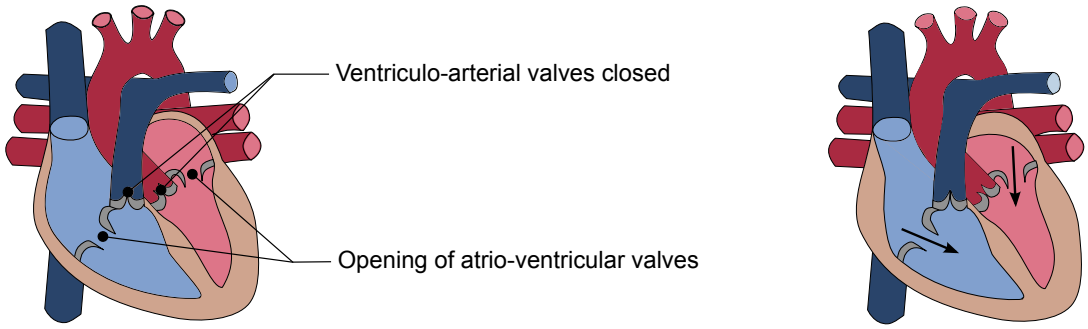

Figure 2.4: Situation of the heart during the early filling phase (adapted from [13], with permission).

The accumulation of blood in the ventricles causes an increase in pressure. Therefore, the pressure difference between the atria and the ventricles is gradually compensated and blood flow from the atria to the ventricles rapidly slows down. At some point, the flow becomes nearly zero, marking the phase of *diastasis*, as depicted in Figure 2.5.

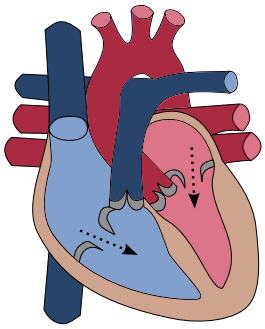

Figure 2.5: Situation of the heart during the diastasis phase (adapted from [13], with permission).

The last part of the ventricular filling is the *atrial contraction*. During this phase, the atria contract and *kick* a supplementary amount of blood into the ventricles, as illustrated in Figure 2.6.

During the whole filling phase, the aortic and pulmonary valves remain closed, preventing the backflow of the blood ejected during the previous contraction.

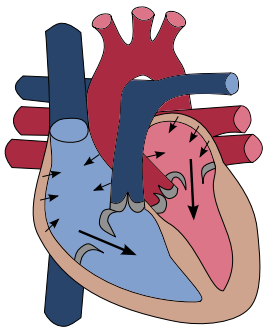

Figure 2.6: Situation of the heart during the atrial contraction phase (adapted from [13], with permission).

Shortly after atrial contraction, ventricular contraction initiates, causing the atrio-ventricular valves to close and marking the end of the *filling* phase.

Isovolumic Contraction

Ventricular contraction continues with all four valves closed, meaning that the ventricular volume remains constant. This phase is thus termed the *isovolumic contraction*. It is depicted in Figure 2.7.

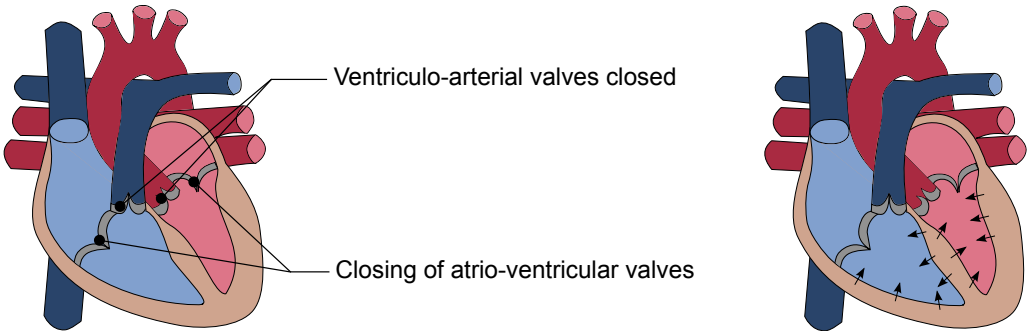

Figure 2.7: Situation of the heart during the isovolumic contraction phase (adapted from [13], with permission).

Ejection

Finally, the further increasing ventricular pressure causes the aortic and pulmonary valves to open, which allows the ejection of blood into the main arteries, the aorta and pulmonary arteries. This phase is called *ejection* and is represented in Figure 2.8. Blood flows into the arteries until the pressures in the arteries become larger than the pressures in the ventricles. At this moment, the aortic and pulmonary valves close, marking the end of the ejection phase. The cardiac cycle then continues with the next phase, isovolumic relaxation.

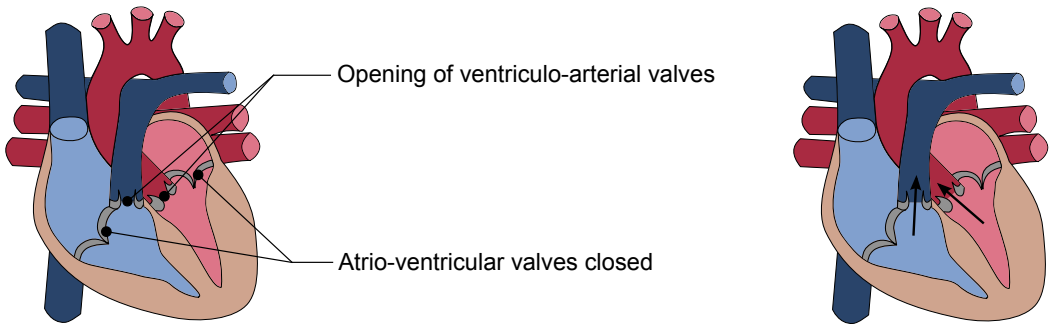

Figure 2.8: Situation of the heart during the ejection phase (adapted from [13], with permission).

2.3.2 Evolution of Pressures and Volumes

As implied in the previous section, the succession of events during a cardiac cycle is closely related to the concept of pressure. Consequently, it is usual to represent the evolution of pressures during a cardiac cycle on a diagram, such as the one of Figure 2.9. In more detail, Figure 2.9 represents pressures in the left part of the circulation, left atrium, left ventricle and aorta, and volume in the left ventricle. Throughout this work, pressures will be expressed in millimetres of mercury (mmHg; 1 mmHg = 1/760 atm $\approx$ 133.3 Pa).

All curves presented in Figure 2.9 are periodic, with a period equal to the cardiac period. Aortic pressure increases during cardiac ejection, since the aorta fills with blood. At the end of ejection, marked by the closing of the aortic valve, the aortic pressure presents a small dip, called the *dicrotic notch* or *incisura* [15]. Once the aortic valve is closed, aortic pressure slowly decays because the stored blood volume is flowing to the systemic circulation.

Left ventricular pressure usually ranges between approximately 0 mmHg and a value higher than the maximum aortic pressure. During the isovolumic phases, contraction and relaxation, ventricular pressure rises and falls very rapidly. The effect of atrial contraction can sometimes be seen through an increase in ventricular pressure at the same moment, as in Figure 2.9.

Left atrial pressure varies to a much lesser extent than left ventricular and aortic pressures. Therefore, it is very often assumed to be constant in the first approximation. In reality, the left atrial pressure curve is rather complex and consists of several crests and troughs. After the opening of the mitral valve, left atrial pressure decreases because blood is passively flowing into the left ventricle. At the end of ventricular filling, the left atrium contracts, causing an increase in pressure called the *a-wave* [15]. After atrial contraction, the mitral valve closes and atrial pressure presents a second crest, called the *c-wave*. The c-wave is not

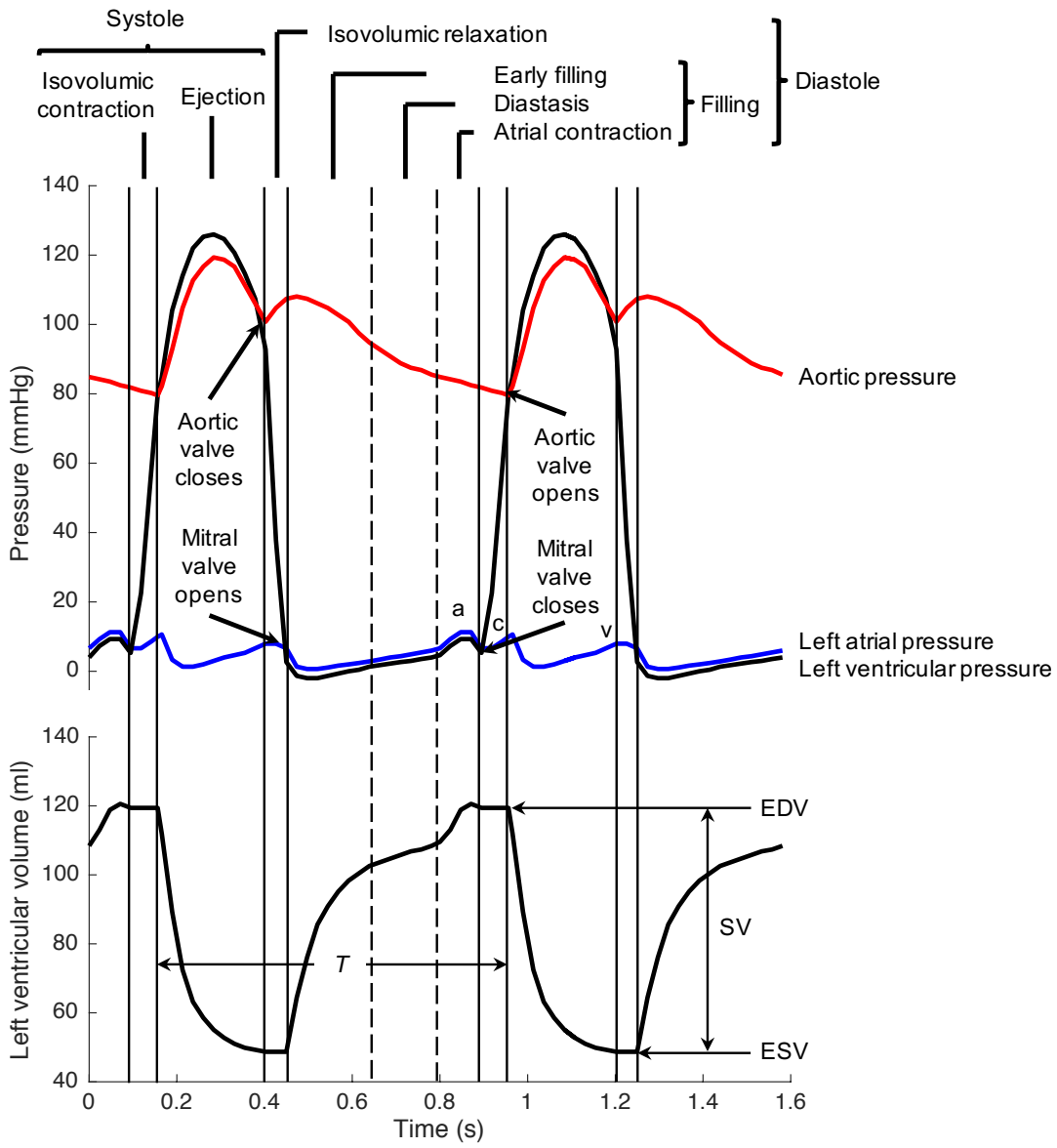

Figure 2.9: Evolution of left atrial, left ventricular and aortic variables during two cardiac cycles. *Top:* left ventricular pressure (*black*), aortic pressure (*red*) and left atrial pressure (*blue*) with specific waves (a, c and v waves) indicated. *Bottom:* left ventricular volume. Data points were extracted from [15].

always present and its physiological origins are uncertain [15]. Once the mitral valve is closed, left atrial pressure increases owing to the blood inflow from the veins. When the mitral valve reopens, left atrial pressure starts decreasing again. On the pressure tracing, this rising and falling translates by a crest called the *v-wave*.

Finally, left ventricular volume decreases during ejection and remains constant during isovolumic phases, relaxation and contraction. As explained in the previous section, the increase of left ventricular volume during filling happens in two phases: the first increase is due to passive blood flow from the left atrium to

the left ventricle, which eventually slows down, while the second increase is due to left atrial contraction. The contribution of left atrial contraction to left ventricular filling volume can be seen in Figure 2.9.

Figure 2.9 also introduces the definition of the two important sub-periods of the cardiac cycle. Specifically, systole and diastole. As evidenced in the figure, *systole* encompasses ventricular contraction and ejection, while *diastole* refers to ventricular relaxation and filling [15].

2.3.3 Conventional Indices of the Cardiac Function

As explained in the previous section, haemodynamic signals have complex shapes, including several local maxima and minima during one cardiac period. In addition, these signals can strongly vary from patient to patient, especially in pathological situations. Consequently, clinicians usually focus on beat-to-beat indices derived from the pressure or volume curves, rather than on the whole curves.

Another explanation for relying on beat-to-beat indices is that the entirety of the curves is not always clinically available. Several important indices of the cardiac function are presented in the following sections, and indices of the vascular state are presented in Section 2.3.4.

Cardiac Period and Heart Rate

The *cardiac period*, T, is the time interval separating two heart beats. For instance, in Figure 2.9, T is approximately equal to 0.8 s. The *heart rate (HR)*, also called *cardiac frequency*, is the inverse of the cardiac period:

$$\mathrm{HR} = \frac{1}{T}. \tag{2.1}$$

If period is expressed in seconds, then HR is expressed in hertz (Hz; 1 Hz $=$ 1 s^{-1}). If period is expressed in minutes, HR is expressed in beats per minute, which is the most frequently encountered unit.

In Figure 2.9, the HR is approximately equal to $1/0.8 = 1.25$ Hz, or $1.25 \times 60 =$ 75 beats per minute. For humans, the HR and T can vary to large extents, so that the CVS can quickly adapt to various situations, for instance if a person is exercising or changes its posture [15].

End-Diastolic Volume

End-diastolic volume (EDV) is the volume of a ventricle at the end of diastole, that is, the maximum ventricular volume during a cardiac cycle. In Figure 2.9, the left ventricular end-diastolic volume (LVEDV) is approximately equal to 120 ml.

End-Systolic Volume

End-systolic volume (ESV) is the volume of a ventricle at the end of systole, that is, the minimum ventricular volume during a cardiac cycle. In Figure 2.9, the left ventricular ESV is approximately equal to 50 ml.

Stroke Volume, Stroke Volume Index, Cardiac Output and Cardiac Index

Stroke volume (SV) is defined as the volume of blood ejected by a ventricle at each cardiac cycle. It is computed:

$$\mathrm{SV} = \mathrm{EDV} - \mathrm{ESV} \tag{2.2}$$

and is usually expressed in millilitres. For humans, the SV is usually around 70 ml [15]. In Figure 2.9, left ventricular SV is approximately equal to $120 - 50 = 70$ ml. Since the left and right ventricle are connected in series, left and right ventricular SVs are equal in average. Otherwise, blood would build up in either the systemic or the pulmonary circulation. The *stroke volume index (SVI)* is equal to the ratio of SV to body surface area [16]. It is therefore expressed in $\mathrm{ml/m^2}$.

Cardiac output (CO) is the average blood flow exiting the heart. It is computed:

$$\mathrm{CO} = \frac{\mathrm{SV}}{T}. \tag{2.3}$$

CO is consequently expressed in ml/s or litres per minute. CO usually ranges between 5 and 6 litres per minute [15]. Using the data of Figure 2.9, CO equals $70/0.8 \approx 88$ ml/s, or $88 \times 0.06 = 5.25$ litres per minute. Finally, *cardiac index (CI)* is defined as the "*ratio of CO to body surface area*" [17]. It is consequently expressed in $\mathrm{ml/(s\ m^2)}$.

2.3.4 Conventional Indices of the Vascular State

Indices Derived from the Arterial Pressure Curve

As shown in Figure 2.9, aortic pressure changes in a large extent during a cardiac cycle. Its maximum value occurs during systole and is therefore called *systolic arterial pressure (SAP)* [15]. In Figure 2.9, SAP is approximately equal to 120 mmHg.

Arterial pressure reaches its minimum during diastole; this minimum value is called *diastolic arterial pressure (DAP)* [15]. In Figure 2.9, DAP is approximately equal to 80 mmHg.

Arterial pulse pressure (PP) is defined as the difference between the maximum (SAP) and minimum (DAP) values of arterial pressure [15]:

$$\text{Arterial PP} = \text{SAP} - \text{DAP}. \tag{2.4}$$

In Figure 2.9, arterial PP approximately equals $120 - 80 = 40$ mmHg. In this work, the definition of PP will be applied to any measured pressure signal (central venous, pulmonary arterial, *etc.*). PP thus represents the difference between the maximum and minimum values of a measured pressure signal.

Mean arterial pressure (MAP) represents the mean value of arterial pressure during one cardiac cycle. In Figure 2.9, MAP is equal to 97 mmHg. The exact computation of MAP requires a continuous arterial pressure measurement, which is not always available [18]. The following formula has thus been developed to approximate MAP when only SAP and DAP are available:

$$\text{MAP} \approx \frac{1}{3}\text{SAP} + \frac{2}{3}\text{DAP}. \tag{2.5}$$

Using this approximate formula, MAP in Figure 2.9 is equal to $120/3 + 2 \times 80/3 \approx 93$ mmHg.

The definitions presented in this section can be transposed to the pulmonary artery, hence leading to the introduction of *systolic* and *diastolic pulmonary arterial pressures*, *mean pulmonary arterial pressure (MPAP)* and *pulmonary arterial PP*.

Systemic Vascular Resistance

Systemic vascular resistance (SVR) represents the resistance to blood flow exerted by the systemic circulation. It is computed [15]:

$$\text{SVR} = \frac{\text{MAP} - \text{CVP}}{\text{CO}}, \tag{2.6}$$

where *central venous pressure (CVP)* represents the pressure in the systemic venous circulation, assumed to be constant. The equation for SVR represents the ratio of the driving force for blood flow, defined as the pressure difference between the beginning and end of the systemic circulation, to the resulting flow. Consequently, the lower the SVR, the more easily the blood flows through the systemic vasculature. SVR is expressed in mmHg s/ml.

Pulmonary Vascular Resistance

Pulmonary vascular resistance (PVR) represents the pulmonary counterpart of SVR and is thus computed as [19,20]

$$\mathrm{PVR} = \frac{\mathrm{MPAP} - \mathrm{PVP}}{\mathrm{CO}} \tag{2.7}$$

where pulmonary venous pressure (PVP) is also assumed constant. PVR is also expressed in mmHg s/ml.

2.3.5 Determinants of Cardiac Output

CO is generally considered to be determined by four factors: preload, contractility, afterload and HR. Each of these factors describes the heart's ability as a pump or the forces around the heart. They are described below.

Preload

Preload represents the stretching of the heart muscle fibres before contraction begins [5,15]. More generally, preload describes the ability of the heart to fill. The *Frank-Starling mechanism* states that the larger the preload, the larger the contraction force generated, and thus, the larger the SV [15]. The effect of preload on SV is thus often represented using the Frank-Starling curve, shown in Figure 2.10. The important feature to observe on the Frank-Starling curve is that, at some point, increasing preload will not lead to an increase in SV. Some authors also believe that, if preload increases beyond that limit point, SV will eventually decrease [21].

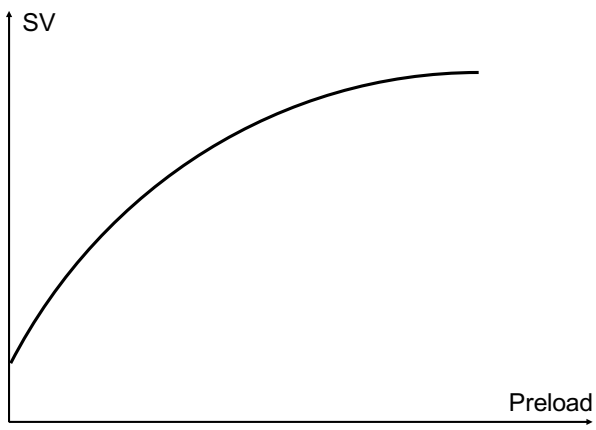

Figure 2.10: Frank-Starling curve representing the effect of preload on SV.

The EDV is widely used as an index of preload. Indeed, it represents the ventricular volume just before contraction. Therefore, it can be associated with the stretching of the muscle fibres at that moment [5, 15].

Contractility

Contractility is the ability of the heart muscle to generate force. At a given preload, the larger the contractility, the larger the contraction force generated, and thus, the larger the SV. Consequently, increasing contractility moves the Frank-Starling curve to the upper-left part of the plane, as shown in Figure 2.11.

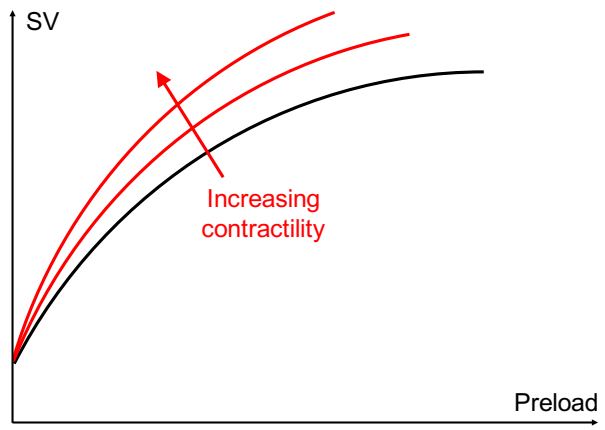

Figure 2.11: Effect of increasing contractility on the Frank-Starling curve.

An important index of contractility is the concept of *end-systolic elastance* [22]. It will be described in detail in Section 5.2.1, but captures this strength capacity of the heart for a given volume. Other indices of contractility include the maximum value of the time derivative of the left ventricular or arterial pressure signals, respectively termed the *left ventricular* and *arterial* $\mathrm{d}P/\mathrm{d}t_{\mathrm{max}}$ [22].

Afterload

Afterload is the resistance the ventricle has to overcome to eject blood [15]. This resistance is caused by everything located downstream of the ventricle, for instance, the ventriculo-arterial valve and the pressure of the blood in the arteries. At a given preload and contractility, the larger the afterload, the lower the SV. As a consequence, increasing afterload moves the Frank-Starling curve to the lower-right part of the plane, as shown in Figure 2.12.

SVR is usually used as an index of left ventricular afterload, as it represents the resistance of the total systemic vasculature. Other indices of afterload exist, but are less commonly used and thus will not be described here. Overall, a low afterload implies less work required to achieve a given blood flow and perfusion.

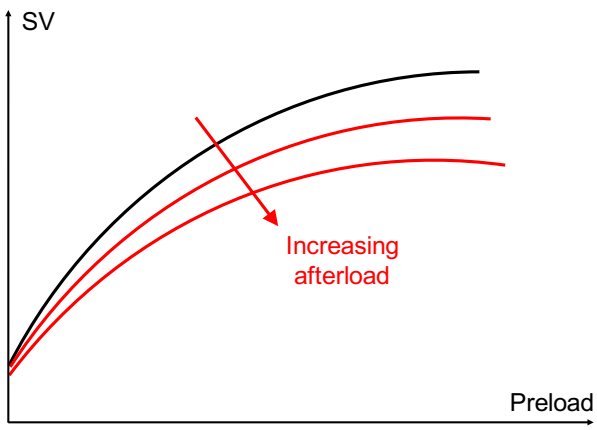

Figure 2.12: Effect of increasing afterload on the Frank-Starling curve.

Heart Rate

The previous three elements, preload, contractility and afterload, determine the SV, which is the volume of blood ejected at each heartbeat. A fourth element enters into play when considering the CO. Specifically, the HR, which, with these factors, determines the total volume pumped per minute based on the number of times the heart beats every minute.

2.4 Summary

In this chapter, the heart and the blood vessels were both described in several ways. First, their particular anatomy was briefly described. Second, their functioning was explained, with a particular emphasis on the complex way pressures and volumes vary in the different structures of the CVS. Third, the essential features of the pressure and volume curves in the heart and the vessels were summarised in important indices. Finally, the four determinants of CO (preload, contractility, afterload and HR) were detailed.

Chapter 3

Fluid Responsiveness

3.1 Introduction

3.1.1 Vascular Filling

Vascular filling, the intravenous administration of fluid to a patient, is a circulatory management therapy. It takes several other different names in the literature:

- Fluid therapy,
- Volume expansion [5, 23],
- Fluid resuscitation [5, 24, 25].

Vascular filling aims to increase circulating volume, and subsequently CO. The overall goal is to improve tissue perfusion[1] as a result [1, 27]. Vascular filling is frequently used to treat acute circulatory shock [6]. This therapy is one of the most frequent interventions in the ICU [1–3].

The type and volume of fluid used for vascular filling vary, along with the duration of the infusion. The fluids typically used are either crystalloids or colloids. Crystalloids are aqueous fluids that only contain small chemical elements. Examples of widely used crystalloids include normal saline, Ringer's lactate and Hartmann's solution [24]. Colloids contain both small and macromolecular chemical components. Examples of colloids include albumin, hydroxyethyl starch, dextran and gelatin [24].

For adults, the volume of fluid infused ranges from 100 ml [7] to 750 ml [5]. In the majority of cases, the volume is 500 ml. Other authors use a volume proportional to the patient's actual or ideal weight, varying between 7 and 20 ml/kg [25]. The duration of the fluid infusion usually ranges from 1 to 45 minutes [25]. Taking the volume infused and the duration of the infusion into account, the rate at

[1] The red blood cell concentration, and thus, haemoglobin concentration are decreased by vascular filling. However, a low haemoglobin concentration seems to be well tolerated thanks to various regulatory mechanisms [26].

which the volume is infused varies between 500 ml/h [5] and 6000 ml/h [28] or, when the volume depends on the patient's weight, from 16 ml/(kg h) [29] to 60 ml/(kg h) [30].

3.1.2 Fluid Responsiveness

The problem with vascular filling is that it is only effective in approximately 50 % of the cases it is used [3, 6, 31], which leads to a distinction between situations of *fluid responsiveness* and *non-responsiveness*. Furthermore, even if vascular filling improves the haemodynamic state of certain patients, excessive fluid administration can lead to deleterious effects, such as pulmonary oedema, right ventricular dysfunction or haemodilution [5, 6]. Clinicians are thus looking for reliable predictors of fluid responsiveness [5].

At this stage, it is important to emphasise that the success of a fluid infusion depends on several factors:

- The volume of fluid used for the infusion,
- The patient's state before the infusion,
- The type of fluid infused and
- The duration of the infusion.

These highly variable factors underline the complexity of predicting fluid responsiveness in a general population or for any specific patient. Especially, if only simple haemodynamic metrics are used or available. Many indices of fluid responsiveness exist, but, for the previously mentioned reasons, none of them is perfect. Consequently, European guidelines do not recommend the use of a particular index [4].

Several indices of fluid responsiveness are presented and reviewed in this chapter. Before describing such indices, the following section first presents the statistical tools needed to assess the performance of a given index.

3.2 Assessment of Index Performance

In most cases, fluid responsiveness is measured by the effect of a fluid infusion on CO, SV or their indexed values, SVI and CI. However, since changes in CO, SV, CI or SVI *relative to the situation before filling* are used in the vast majority of studies, the effect of body surface area cancels out. Consequently, relative changes in CO are strictly equivalent to relative changes in CI, and relative changes in SV are strictly equivalent to relative changes in SVI. An index of fluid responsiveness will thus be considered as performing if it is able to predict the change in CO

or SV caused by vascular filling. Three statistical tools have been used in the literature to assess the performance of indices.

3.2.1 Quantitative Prediction: Linear Regression

The simplest way to assess the performance of an index of fluid responsiveness is to perform a linear regression between this index and the relative change in CO or SV after vascular filling. The quality of the index is then assessed using the r or r^2 value of the linear regression. The closer r^2 is to one, the greater the index captures the observed variability and thus the better the index. An example is given in Figure 3.1 using an index called *total stressed blood volume* that will be described in Section 3.5. The data in this figure is far from a perfect line, causing the low value of $r^2 = 0.13$, indicating only 13 % of observed variability is explained by the regression line.

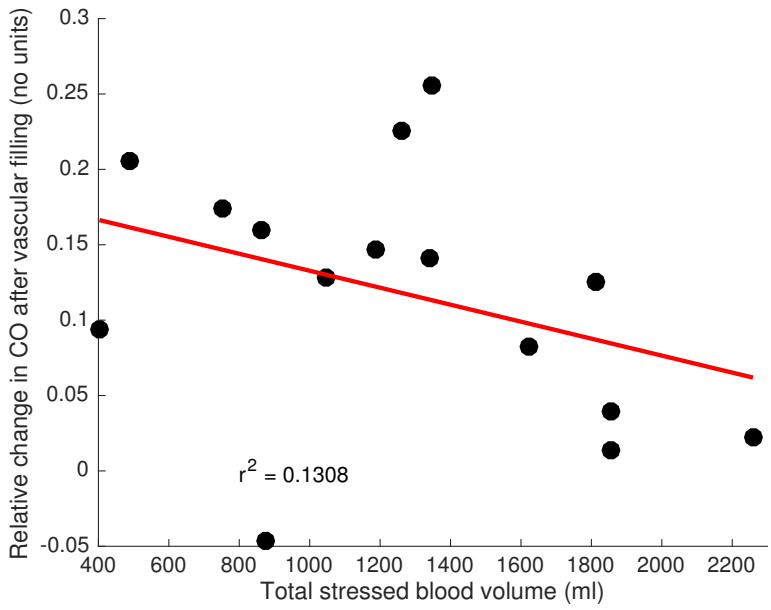

Figure 3.1: Linear regression between change in CO and total stressed blood volume. The data points were obtained from [32].

3.2.2 Binary Prediction

The remaining two methods require defining an arbitrary threshold for fluid responsiveness. This threshold usually lies between 5 and 15 % relative change in CO, SV, CI or SVI after vascular filling [5, 25, 33]. Using this criterion, each filling step can be qualified as successful or unsuccessful, without concern for the quantitative value of the change in CO or SV.

t-Test

To perform such a test, the values of the index must first be separated according to the associated positive or negative response to vascular filling. Two mean values of the index are computed for all positive and negative responses. Performing a t-test allows investigating whether these two mean values are statistically different. The t-test provides a p-value, which is equal to the probability of the observed difference between the mean indices happening by chance [34]. The lower the p-value, the better the predictive power of the index. A p-value lower than 0.05 is usually considered as statistically significant.

As an example, using the data of Figure 3.1 and defining a threshold for fluid responsiveness as a change in CO $> 12\%$, there are 9 positive responses to filling and 6 negative ones. The index is equal to 1122 ± 390 ml (mean $\pm$ standard deviation) for positive responses, and to 1478 ± 698 ml for negative ones. The associated p-value equals 0.22, and the means are thus not significantly different.

Receiver-Operator Characteristic Curve

This analysis requires defining a test based on the index value. A positive result to the test should be associated with fluid responsiveness. For instance, Figure 3.2 represents the situation when the test for fluid responsiveness is that total stressed blood volume is lower than 1000 ml and fluid responsiveness is defined as a relative change in CO larger than 12 %.

The second step consists in counting the data points falling into each category of the contingency table presented in Table 3.1 [34]. The columns indicate whether the test is successful or not, and the rows indicate whether there was a positive or a negative response to filling. For an index that is not perfect, there will be cases for which the test was successful, but the patient did not respond to filling. These cases are *false positives*: the test was positive, but the outcome was not. Conversely, there will be cases for which the test was unsuccessful, but the patient still responded to filling. These cases are *false negatives*.

Table 3.1: Contingency table.

	Test successful	Test unsuccessful
Positive response	True positive (TP)	False negative (FN)
Negative response	False positive (FP)	True negative (TN)

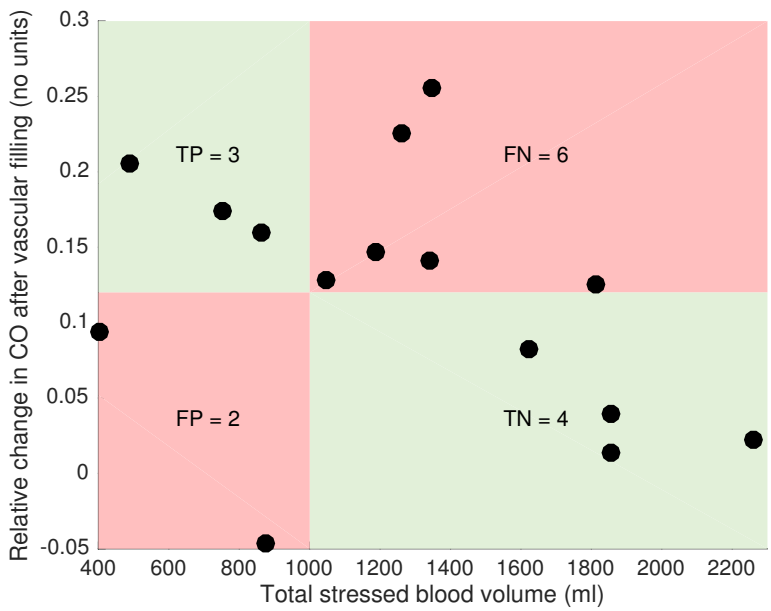

Figure 3.2: Separation of the data points from [32] according to the positive response to vascular filling (change in CO > 12 %) and the value of total stressed blood volume (greater or less than 1000 ml).

The precision of this test can be assessed by the following two quantities [34]:

$$\text{Sensitivity} = \frac{\text{TP}}{\text{TP} + \text{FN}} \tag{3.1}$$

$$\text{Specificity} = \frac{\text{TN}}{\text{TN} + \text{FP}}. \tag{3.2}$$

The closer the sensitivity is to 1, the better the test identifies positive responses to filling. The closer the specificity is to 1, the better the test identifies negative responses to filling.

According to the data presented in Figure 3.2,

$$\text{Sensitivity} = \frac{\text{TP}}{\text{TP} + \text{FN}} = \frac{3}{3+6} \approx 0.33 \tag{3.3}$$

$$\text{Specificity} = \frac{\text{TN}}{\text{TN} + \text{FP}} = \frac{4}{4+2} \approx 0.67. \tag{3.4}$$

The sensitivity and specificity both depend on the value chosen for the index threshold. In Figure 3.2, the threshold was set at 1000 ml.

To choose the best threshold, it is useful to investigate how the sensitivity and the specificity vary when the threshold is changed. Such an investigation results in two curves, sensitivity as a function of the threshold, and specificity as a function of the threshold. An example is given in Figure 3.3.

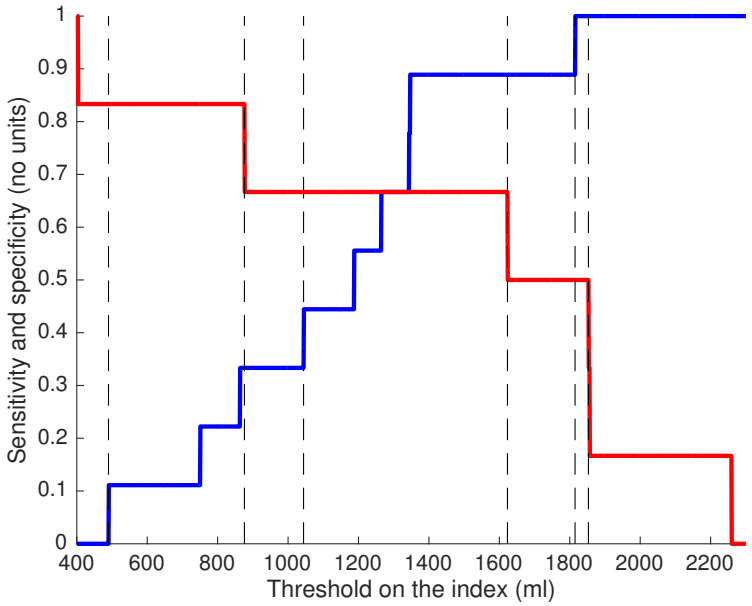

Figure 3.3: Sensitivity (*blue*) and specificity (*red*) of the test for fluid responsiveness based on total stressed blood volume being lower than a given threshold.

The receiver operating characteristic (ROC) curve combines the previous two functions in one. It represents the points with coordinates (1 − Specificity, Sensitivity) for all possible threshold values. Figure 3.4 presents the ROC curve corresponding to the curves of Figure 3.3. The best threshold is often chosen as the one that maximises the sensitivity and the specificity, that is, the one that corresponds to the upper-left corner of the ROC curve. In Figure 3.4, the best threshold is thus 1623 ml.

An ideal predictor gives no FP or FN. Its sensitivity and specificity are thus both equal to 1. The corresponding ROC curve is shown in green in Figure 3.4. A random predictor gives as much TPs as FPs, and as much TNs as FNs. The sum of its sensitivity and specificity thus always equals 1. A corresponding ROC curve is shown in red in Figure 3.4. If the ROC curve of an index is under the ROC curve of a random predictor, then the index is less efficient than flipping a coin to make a decision about vascular filling.

Finally, the measure of the quality of an index for prediction of fluid responsiveness is the area under the ROC curve. The area under the ROC curve of an ideal predictor is equal to 1 and the area under the ROC curve of a random predictor is equal to 0.5. The closer the area under the ROC curve of an index is to 1, the better the index.

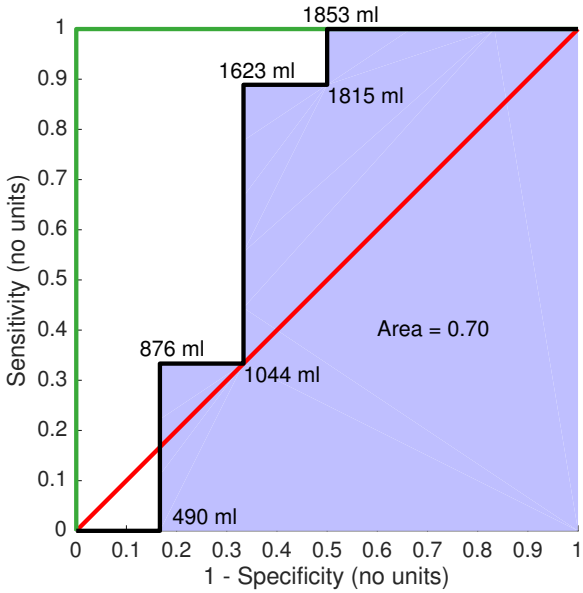

Figure 3.4: ROC curve for the example test of fluid responsiveness using the data of Figure 3.1. The numbers indicate the corresponding values of the threshold. The green line represents the ROC curve of a perfect predictor, the red line represents the ROC curve of a random predictor.

3.3 Static Indices of Fluid Responsiveness

The original reasoning behind vascular filling was based on the Frank-Starling curve presented in Figure 2.10. According to this curve, if CO is insufficient, a larger CO can be obtained by increasing preload, which will increase SV, and thus CO. Consequently, vascular filling can be performed based on low indices of preload, such as LVEDV or right ventricular end-diastolic volume (RVEDV) [5, 35]. However, since EDV is not easily measured, more readily measurable surrogates are often used instead, such as:

- CVP [16, 21, 31, 33, 36–50],
- Pulmonary artery occlusion pressure (PAOP), defined in Section 7.3.3 [5, 8, 30, 33, 35, 36, 40, 44, 51–55],
- Right atrial pressure (RAP) [5, 30, 51–53],
- Global end-diastolic volume (GEDV), defined in Section 7.3.5 [25, 46, 56].

Table 3.2 provides the values of the three performance measures introduced in Section 3.2 as reported for each static index in the literature. Because of their weak performance, static indices of fluid responsiveness are currently considered to be inefficient [5, 7–9]. One explanation for this ineffectiveness is that, as explained in Section 2.3.5, the effect of preload on SV also depends on contractility and afterload [6], creating a multifunctional problem not easily captured. Despite its

low performance, CVP was found to be the most frequently used index of fluid responsiveness in a recent study conducted in 46 countries [1], likely due to its frequent measurement in ICU care.

Table 3.2: Performance measures of the static indices of fluid responsiveness.

	r^2	p-value	Area ROC	References
LVEDV		0.005 to > 0.05		[5]
RVEDV		< 0.001 to < 0.002		[5, 35]
CVP	0.003 to 0.31	< 0.001 to 0.4	0.43 to 0.71	[16, 21, 31, 33, 36–50]
PAOP	0.001 to 0.46	0.001 to 0.3	0.40 to 0.77	[5, 30, 33, 35, 36]
				[40, 44, 51–55]
RAP	0.029 to 0.25	0.04 to > 0.05	0.51	[5, 30, 51–53]
GEDV		> 0.05	0.52 to 0.69	[25, 46, 56]

3.4 Dynamic Indices of Fluid Responsiveness

3.4.1 Cardio-Pulmonary Interactions

So-called *dynamic* indices of fluid responsiveness have been defined based on cardio-pulmonary interactions during mechanical ventilation. Mechanical ventilation, *i.e.* the use of a respirator to ventilate sedated patients in ICUs, causes transient changes in lung pressures. Since the heart and the lungs are enclosed in a rigid cavity, the thorax, a larger lung pressure increases the pressure acting on the outside of the heart and large vessels. Therefore, mechanical ventilation alters left and right ventricular preload and afterload [5], and thus, the overall functioning of the heart.

More specifically, during forced inspiration, lung pressure increases and, as a consequence, the pressure acting on the heart and pulmonary circulation also increases[2]. Because they are under pressure, the right atrium and ventricle fill with more difficulty, and right ventricular preload decreases [5,8,57]. According to the Frank-Starling mechanism, right ventricular SV is then also decreased. Within a few heartbeats, flow entering the left ventricle is also decreased and, in turn, left ventricular SV is eventually diminished [5,7,8,57].

During expiration, the opposite phenomena occur: lung pressure decreases, which makes right ventricular filling easier. Right ventricular SV increases, and, a few heartbeats later, left ventricular SV also increases. Other, more complex,

[2]Normal inspiration is caused by different physiological mechanisms [26].

haemodynamic effects occur during mechanical ventilation [7], but do not alter the main conclusion that mechanical ventilation affects both left and right ventricular SV.

The systemic arteries are located directly downstream of the left ventricle and carry the ejected blood. As a consequence of the respiratory influence on left ventricular SV, the systemic arteries carry different quantities of blood during the different phases of the respiratory cycle. This influence is observed by transient increases and decreases in arterial pressure during a breath. The ventilation-induced changes in left ventricular SV and systemic arterial pressure are illustrated in Figure 3.5.

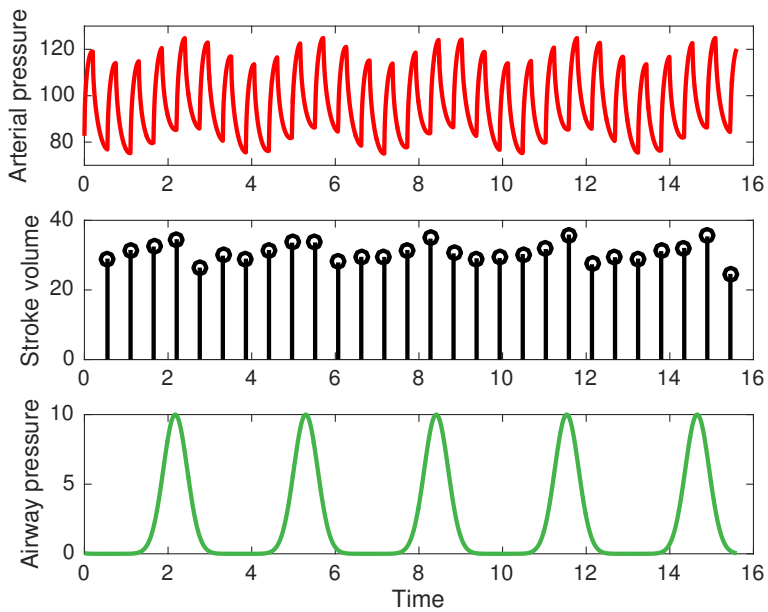

Figure 3.5: Ventilation-induced changes in systemic arterial pressure (*red*) and left ventricular stroke volume (*black*). The figure was built using data from [58].

3.4.2 Definition of the Dynamic Indices

According to Figure 3.6, a given transient change in preload due to the effects of mechanical ventilation, causes larger changes in SV for patients being on the increasing part of the Frank-Starling curve [7]. This statement, along with other observations, explains how hypovolemic conditions could be detected by high variations in SV during mechanical ventilation [7].

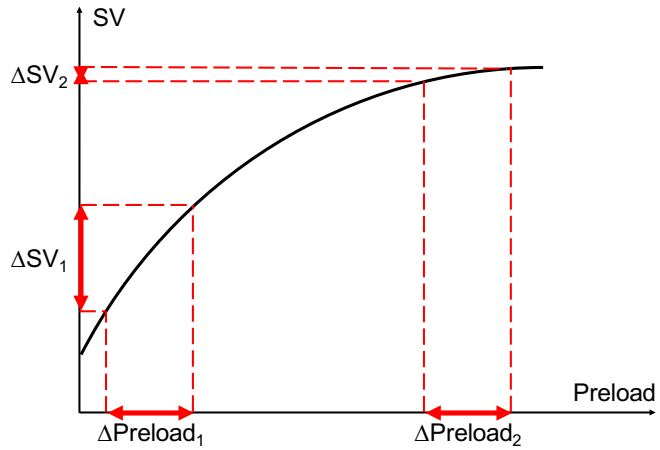

Figure 3.6: Frank-Starling curve, where the nonlinear, saturable stroke volume as a function of preload illustrates how a given change in preload can yield different changes in stroke volume, depending on the initial level of preload.

Stroke Volume Variation

Based on the idea introduced above, the *stroke volume variation (SVV)* index is defined [5]:

$$\mathrm{SVV} = 2\frac{\mathrm{SV}_{\mathrm{max}} - \mathrm{SV}_{\mathrm{min}}}{\mathrm{SV}_{\mathrm{max}} + \mathrm{SV}_{\mathrm{min}}} \tag{3.5}$$

where $\mathrm{SV}_{\mathrm{max}}$ and $\mathrm{SV}_{\mathrm{min}}$ are the maximum and minimum values of SV observed during a respiratory cycle. SVV quantifies the magnitude of the transient changes in SV caused by mechanical ventilation.

Figure 3.7 displays arterial pressure, arterial PP and SV for the first respiratory cycle of Figure 3.5. For the respiratory cycle displayed in Figure 3.7:

$$\mathrm{SVV} = 2\frac{35 - 26}{35 + 26} \approx 30\ \%. \tag{3.6}$$

Pulse Pressure Variation

Since SV is not easy to assess beat-by-beat in the ICU, other dynamic indices have been introduced, based on blood pressure measurements, which are more readily available. For instance, systemic arterial PP represents the arterial reflection of SV, and may thus be a useful surrogate. The *pulse pressure variation (PPV)* is defined [6]:

$$\mathrm{PPV} = 2\frac{\mathrm{PP}_{\mathrm{max}} - \mathrm{PP}_{\mathrm{min}}}{\mathrm{PP}_{\mathrm{max}} + \mathrm{PP}_{\mathrm{min}}} \tag{3.7}$$

where $\mathrm{PP}_{\mathrm{max}}$ and $\mathrm{PP}_{\mathrm{min}}$ are the maximum and minimum values of arterial PP observed during a respiratory cycle. Since pressures are often measured in real-

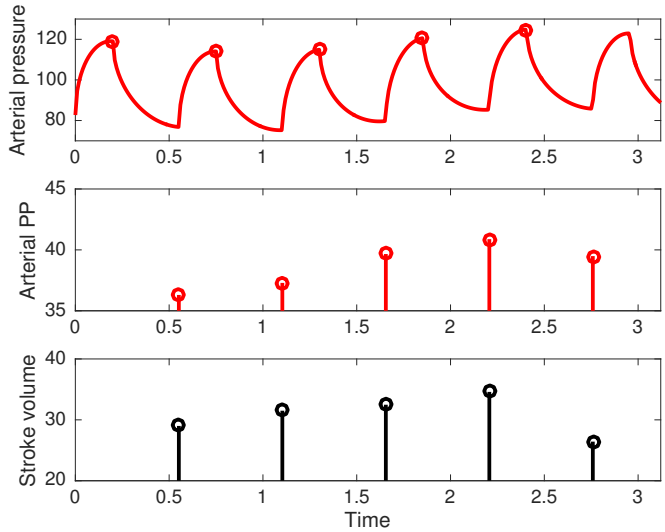

Figure 3.7: Arterial pressure (*top*), arterial pulse pressure (*centre*) and stroke volume (bottom) during the first respiratory cycle of Figure 3.5.

time in the ICU, PPV is far more readily available than SV. Using the example of Figure 3.7:

$$\mathrm{PPV} = 2\frac{41-36}{41+36} \approx 13\ \%. \tag{3.8}$$

Systolic Pressure Variation

A third important dynamic index of fluid responsiveness is the *systolic pressure variation (SPV)*, which characterises the changes of SAP with mechanical ventilation [53]:

$$\mathrm{SPV} = 2\frac{\mathrm{SAP}_{\mathrm{max}} - \mathrm{SAP}_{\mathrm{min}}}{\mathrm{SAP}_{\mathrm{max}} + \mathrm{SAP}_{\mathrm{min}}} \tag{3.9}$$

where $\mathrm{SAP}_{\mathrm{max}}$ and $\mathrm{SAP}_{\mathrm{min}}$ are the maximum and minimum values of SAP observed during a respiratory cycle. The computation of SPV using the data of Figure 3.7 yields:

$$\mathrm{SPV} = 2\frac{125-114}{125+114} \approx 9\ \%. \tag{3.10}$$

3.4.3 Performance

Table 3.3 summarises the performance measures of the SVV, PPV and SPV indices, as reported in the literature. Overall, the dynamic indices are better predictors of fluid responsiveness than the static indices introduced in Section 3.3. However the reported performance measures are very different between studies.

Table 3.3: Performance measures of the dynamic indices of fluid responsiveness.

	r^2	p-value	Area ROC	References
SVV	0.12 to 0.55	< 0.0001 to 0.232	0.50 to 0.92	[16, 33, 37, 39, 41, 59]
				[25, 43, 45, 47, 48, 60–62]
SPV	0.52 to 0.69	0.0001 to 0.017	0.63 to 0.94	[16, 36, 43, 48, 53–55, 63]
PPV	0.054 to 0.94	< 0.0001 to 0.107	0.51 to 0.99	[21, 25, 28–31, 36, 39–48]
				[53, 56, 60, 62–66]

3.4.4 Limitations

Because of their numerous underlying hypotheses, dynamic indices of fluid responsiveness suffer many limitations. Some of these limitations are described in the present section.

First, because of the underlying mechanisms, the dynamic indices cannot be applied to all ICU patients. Patients presenting the following physiological limitations are excluded:

- Spontaneous breathing [9, 48, 67, 68],
- Open thorax [69],
- Arrhythmias [3, 9, 48, 67, 68].

The first limitation is important, as the current trend in ICUs is to let patients breathe spontaneously as early as possible.

Second, the dynamic indices are based on a cascade of cardio-pulmonary interactions, which can be affected by many physiological variables, including:

- Tidal (inspired) volume [8, 48, 57, 67–70],
- Lung compliance [8, 67, 71],
- Chest wall compliance [57, 67],
- Abdominal pressure [69],
- Left and right cardiac contractility [57, 67, 71] and compliance [8],
- Systemic and pulmonary arterial compliance [8, 67, 71],
- SVR and PVR [3, 8, 71],

All these variables exert an influence on the dynamic indices that is not related to the patient's volume status. These influences make it very difficult to compare values of the dynamic indices across patients and for a given patient when any of these variables is changed. Hence, Table 3.3 has often poor values of r^2, p and area under the ROC curve, as this variability is not explained or captured by the metric.

Two recent studies indicate that these influencing variables and patient requirements mean dynamic indices can only be applied to a fraction of ICU pa-

tients, ranging from 2 % [9] to 42 % [68]. In a recent study, Cecconi *et al.* recorded the actual use of dynamic indices in only 22 % of patients [1].

Third, technical issues have also been reported to influence the computed value of the dynamic indices. For instance:

- The number of respiratory cycles on which SVV, PPV and SPV are computed [48],
- The number of cardiac cycles per respiratory cycle [69],
- The site of pressure measurement [67],
- The lack of reliability and reproducibility of PPV measurements provided by cardio-vascular monitoring devices [3].

All these issues can significantly alter the metric value and may thus explain some of the performance variability in Table 3.3.

3.4.5 Other Dynamic Indices

Several other dynamic indices have been proposed in the literature, but are less documented. Some of these indices are:

- Respiratory variation in superior vena cava diameter [38],
- Respiratory variation in inferior vena cava diameter [50, 72],
- Dynamic arterial elastance, defined as the ratio of PPV to SVV [57, 73].

Other authors also developed specific tests to cause transient increases in preload, replacing the cyclic influence of mechanical ventilation. For instance, the passive leg raising manoeuvre [23, 48, 56, 66, 74, 75] and the end-expiratory occlusion test [48, 56]. A sufficient increase in CO during the test is considered as predictive of fluid responsiveness.

3.5 Total Stressed Blood Volume

The *total stressed blood volume (SBV)* is defined as the total *pressure-generating* blood volume in the circulation [32]. This concept is thus particularly interesting in the context of vascular filling therapy.

Indeed, in 15 ICU patients, Maas *et al.* computed SBV and recorded the change in CO following a 500 ml fluid infusion. The results of their study were presented in Figures 3.1 to 3.4 and were used as the example of Section 3.2. The performance metrics of this index are thus $r^2 = 0.13$, $p = 0.22$ and area under the ROC curve of 0.70. Even if these performance metrics are far from optimal, they are similar to those of the clinically used indices, displayed in Tables 3.2 and 3.3. SBV thus has the potential to be used as an index of fluid responsiveness.

However, SBV cannot currently be used to guide vascular filling therapy, because its experimental determination is cumbersome and highly invasive. First, the heart has to be stopped to let the CVS reach its equilibrium pressure, called the *mean circulatory filling pressure (MCFP)* [76]. Then, a given fluid volume is infused in the CVS and the heart is stopped again. The MCFP is now higher than before fluid infusion. These steps of fluid infusion and cardiac arrest can be repeated. Finally, a linear regression of the infused volume-MCFP points allows estimation of SBV as the volume that should be *withdrawn* for MCFP to be zero. The method and concept are illustrated in Figure 3.8.

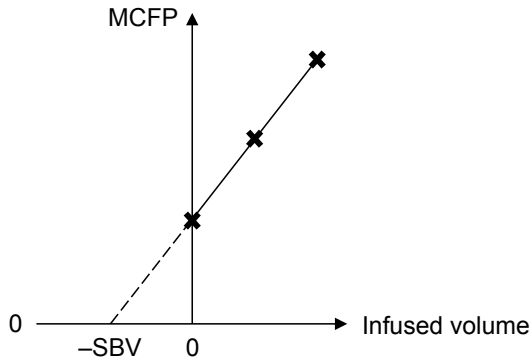

Figure 3.8: Illustration of the experimental method to determine SBV.

Such experiments have been performed in pigs [77] and dogs [78–83], but are inconceivable and unethical in humans. For humans, Maas *et al.* [32] determined SBV by stopping blood flow and measuring MCFP in the arm instead of the whole body. However, even that approach is invasive and, equally impossible to validate.

The current method to compute SBV has many drawbacks. First, it involves repeated circulatory arrests, either global or regional. Second, fluid has to be infused, which can be useless if there is no positive response, or even harmful. Particularly, if the goal is to determine fluid responsiveness in the first case. Third, it is time-consuming, requiring more than 20 minutes [32]. Finally, it relies on the concept of MCFP, which is not a pressure encountered in normal situations.

However, a model-based method using measurements typically available in an ICU could obviate all of these concerns. The goal of this work is thus to develop a mathematical model of the CVS, which will provide access to a model-based surrogate of SBV.

3.6 Summary

This chapter introduced the concepts of vascular filling and fluid responsiveness, which represent the core of this work. As implied in this chapter, there are various ways to assess fluid responsiveness, static indices, dynamic indices or SBV, with no clear consensus.

The present work aims to develop a new method to estimate a surrogate of SBV without requiring circulatory arrests or fluid administration. This method is based on the use of mathematical models of the CVS, of which the SBV surrogate is a parameter. The following part will therefore focus on how to translate the functioning of the CVS, described in Chapter 2, into mathematical terms.

Part II

Modelling of the Cardio-Vascular System

Introduction

To assist physicians, engineers have developed a wide range of mathematical models, in particular of the CVS. There exists a large number of ways to mathematically represent the behaviour of the CVS, with various complexities and objectives. The main goals range from clinical input to deeper physiological understanding.

At one extreme of the spectrum lie *distributed* models of the CVS, which are complex, three-dimensional finite elements models, involving millions of degrees of freedom [12, 84]. These models can be used to gain precise understanding on local parts of the CVS. However, because of the time required to perform a single simulation of a finite-element CVS model, such models cannot currently be used to perform cardiac and circulatory monitoring. Furthermore, building such models requires large amounts of medical data, coming from three-dimensional scans of the anatomy, such as from magnetic resonance imaging [85] or computed tomography.

At the other end of the spectrum lie *lumped* models of the CVS [86–102]. Lumped models present a discrete representation of the CVS, where the variables of interest are considered only at specific points called *nodes*. Between the nodes, whole sections of the CVS are represented as single elements, cardiac chambers or vascular resistances, for instance.

A consequence is that these models cannot be used to gain detailed local understanding of the CVS. They do not perfectly reproduce the reality, but focus more on the macro-physiological trends. However, thanks to their simplicity, the involved equations can be solved in a few seconds on a standard computer. Furthermore, lumped CVS models involve a low number of unknown parameters. Consequently, these parameters can be more readily identified from clinical data, and in real time [103].

The intermediate class of models comprises *pulse-wave propagation* models of the CVS [104]. These models are based on an approach similar to the *lumped* models of the CVS. The difference is that more nodes are used, leading to more precise representations of some anatomical structures, typically the arterial tree

[104–106]. As a consequence, the number of unknown parameters increases, and identifiability and bedside use decrease.

Patients in the ICU are difficult to treat, which is in part due to the fact that a diagnosis is hard to establish in circulatory or CVS dysfunction. The two main reasons are that the patient state is highly variable [11] and the amount of measurements available is limited. In addition, these measurements are mainly peripheral, such as CVP, arterial pressure and electrocardiograms, and thus do not provide accurate information on the central functioning of the CVS. Yet, this kind of information is of extreme interest in the study of many diseases.

A mathematical model of the CVS can be used to provide a picture of the central haemodynamics from such limited and peripheral data. Such a model should be usable at bedside and, consequently, should only require commonly available measurements. Second, the model has to be computationally fast, to predict changes in real time. Since these real-time and few data aspects are the most important for an application in the ICU, the models used in this work belong to the lumped family.

Before presenting complete lumped CVS models in Chapter 6, the following chapters first present the building blocks of such models. Chapter 4 describes *passive* elements, namely vessels and chambers and Chapter 5 describes *active* chamber elements.

Chapter 4

Passive Elements: Resistances, Valves and Chambers

4.1 Introduction

Lumped CVS models represent the circulatory system as a more or less complex interconnection of elastic *chambers* and non-deformable vessels, called *resistances*. Another very important feature of the CVS is the presence of *valves*, which also have to be taken into account in any realistic model of the CVS and its regulated flow. Resistances, valves and chambers are termed passive elements because they do not generate pressure, unlike the heart. Mathematical models for these passive elements are described in the present chapter.

4.2 Omh's Law - Resistances

A vessel is represented in Figure 4.1. As evidenced in the figure, one side of the vessel is submitted to a pressure $P_{\text{up}}(t)$, while the other side is submitted to $P_{\text{down}}(t)$. The flow $Q(t)$ in the vessel is usually described:

$$Q(t) = \frac{P_{\text{up}}(t) - P_{\text{down}}(t)}{R}, \tag{4.1}$$

where R is a proportionality constant, called the *resistance* of the vessel [90, 107, 108]. This equation is identical to Ohm's law in electricity, which states that electrical current, the flow of electrons, is equal to the ratio of the voltage difference, the driving force, to the resistance of the wire. By extension, Equation 4.1 is also referred to as Ohm's law.

Equation 4.1 is also very similar to Poiseuille's equation, which describes the steady flow of an incompressible fluid through a rigid tube. Poiseuille's equation

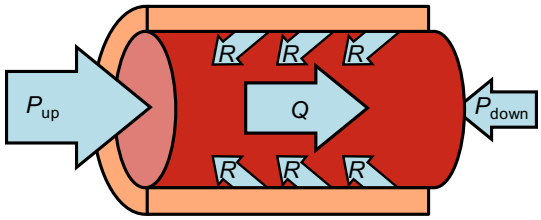

Figure 4.1: Illustration of Ohm's law.

reads [109]:

$$Q = \frac{(P_{\text{up}} - P_{\text{down}})\pi r^4}{8\eta l}, \tag{4.2}$$

where η is the viscosity of blood, l is the length of the vessel and r, its radius. It is thus often stated that $R = 8\eta l/\pi r^4$. However, the hypotheses formulated to derive Poiseuille's equation, steady and laminar flow, rigid and perfectly cylindrical vessel, are not valid in the CVS, meaning that R cannot be computed using Equation 4.2.

The plot on the left of Figure 4.2 shows the linear relation assumed in Equation 4.1. The right panel of Figure 4.2 displays the diagram and notation that will be used later to represent resistance elements.

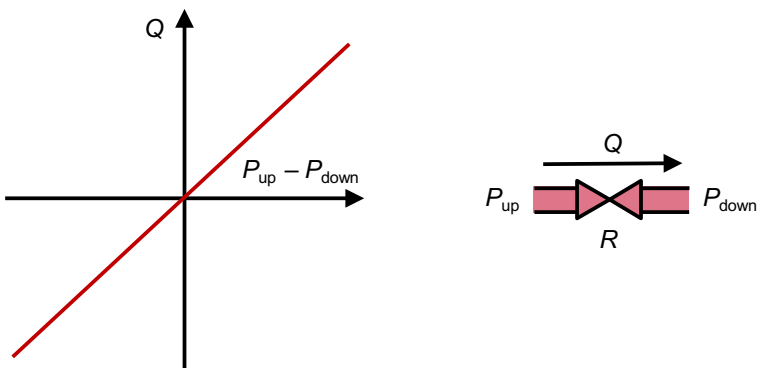

Figure 4.2: Relationship between flow and pressure difference (*left*), and symbol (*right*) of a resistance element.

4.2.1 Inertances

Equation 4.1 assumes that blood flow stops as soon as the pressure gradient reaches zero. This simplification neglects the blood's inertia. Some models [90,98, 107,108,110–112] involve elements called *inertances* to represent this phenomenon.

In such cases, Equation 4.1 is modified to read:

$$Q = \frac{P_{\text{up}}(t) - P_{\text{down}}(t)}{R} - \frac{L}{R}\frac{\mathrm{d}Q}{\mathrm{d}t}(t), \tag{4.3}$$

where L denotes the value of the inertance.

The term $-(L/R)\mathrm{d}Q(t)/\mathrm{d}t$ implies that blood will keep on flowing for some time, even if the pressure gradient reaches zero. The notation L used for inertance also results from an electrical analogy between inertances and inductors. In an electrical circuit, inductors also oppose changes of current, the flow of electrons, in a similar way.

4.3 Valve law

The simplest model of a heart valve assumes that:

1. there is flow through the valve only when the pressure upstream of the valve is higher than the pressure downstream, and
2. the flow through an open valve can also be described by Ohm's law.

Hence, one can define [107, 108]:

$$Q(t) = \begin{cases} \dfrac{P_{\text{up}}(t) - P_{\text{down}}(t)}{R} & \text{if } P_{\text{up}}(t) > P_{\text{down}}(t) \\ 0 & \text{otherwise.} \end{cases} \tag{4.4}$$

Figure 4.3 displays the diagram and notation for a valve element, and also illustrates Equation 4.4. The plot of Figure 4.3 shows linearity, but only when $P_{\text{up}} > P_{\text{down}}$. There is a close similarity between the valve element presented in this section and the behaviour of an ideal electric diode.

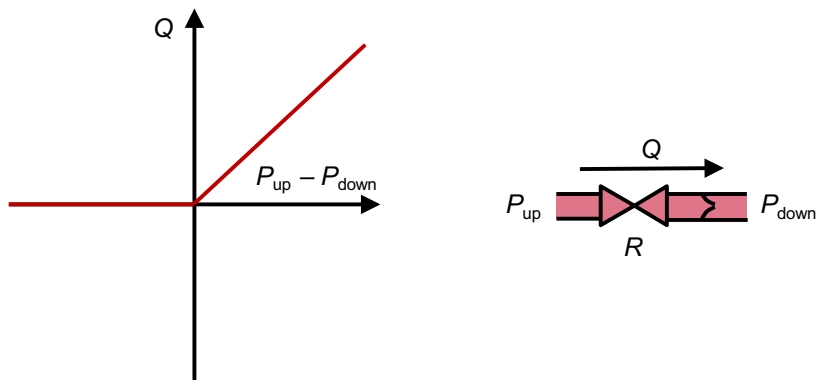

Figure 4.3: Relationship between flow and pressure difference (*left*), and symbol (*right*) of a valve element.

Equation 4.4 can also be adapted to take the blood's inertia into account. Such a valve model allows to reproduce the fact that the valves "*open on pressure and close on flow*" [89,113]. However, adapting Equation 4.4 to include inertances is not an easy task because the differential Equation 4.3 has to be solved *a priori* to know when Q becomes negative, making simulation more computationally intensive.

4.4 Pressure-Volume Relationships of the Chambers

In lumped models of the CVS, passive elastic chamber elements are used to account for the deformable properties of the large vessels, namely the arteries and veins. As its name indicates, the pressure-volume relationship of a chamber describes the relationship between the blood volume inside the chamber and the pressure exerted by the chamber. The pressure-volume relationship is often described using a convex function $P(V)$ [109,114], an example of which is displayed in Figure 4.4.

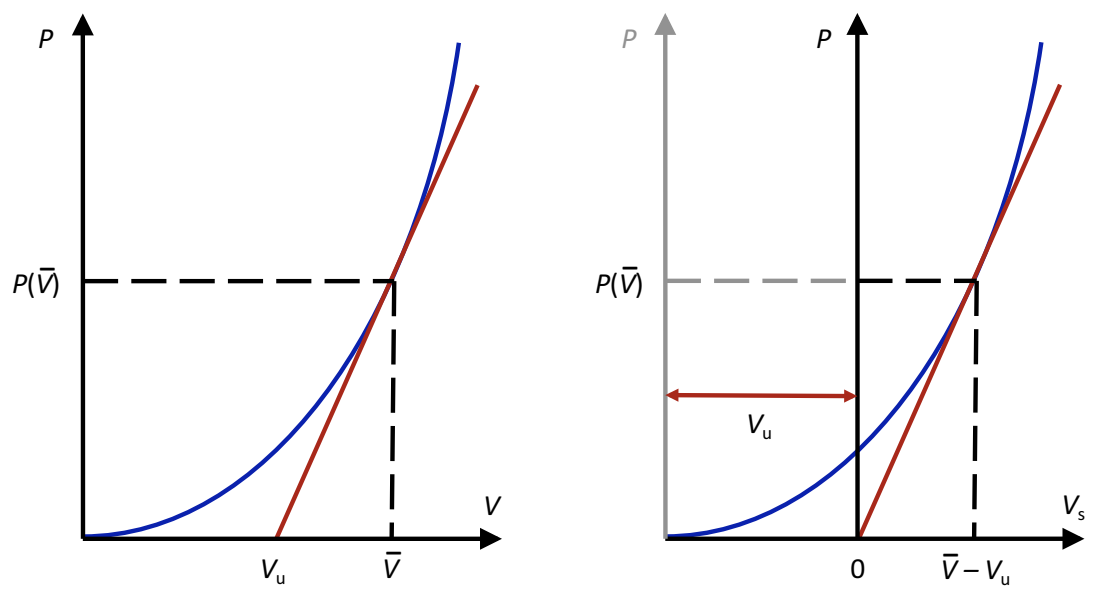

Figure 4.4: *Left:* illustration of $P(V)$ and its first-order Taylor approximation. *Right:* illustration of the change of variables in Equation 4.11.

A first-order Taylor approximation of this function around a chosen *working point* [109] $V = \bar{V}$, yields

$$P(V) \approx P(\bar{V}) + \left.\frac{\mathrm{d}P}{\mathrm{d}V}\right|_{V=\bar{V}} (V - \bar{V}). \tag{4.5}$$

The *elastance* E of the chamber is defined as the slope of its pressure-volume relationship at $V = \bar{V}$:

$$E = \left.\frac{\mathrm{d}P}{\mathrm{d}V}\right|_{V=\bar{V}}. \tag{4.6}$$

More specifically, the elastance is the increase in pressure caused by a unit change in volume. The linear approximation implies that E is assumed to be constant. Equation 4.5 thus becomes:

$$P(V) \approx P(\bar{V}) + E(V - \bar{V}). \tag{4.7}$$

As defined, Equation 4.7 is difficult to use, as it requires the knowledge of $P(\bar{V})$, E and $\bar{V}$ to compute P from V. It will thus be further manipulated to substitute two of the three unknown quantities.

First, let V_u, for *unstressed* volume, be the volume at which pressure is equal to zero, according to the first-order approximation. Inserting this quantity in Equation 4.7 gives:

$$0 \approx P(\bar{V}) + E(V_\mathrm{u} - \bar{V}). \tag{4.8}$$

$$\Leftrightarrow P(\bar{V}) \approx E(\bar{V} - V_\mathrm{u}). \tag{4.9}$$

Substituting $P(\bar{V})$ into Equation 4.7 finally gives:

$$P(V) \approx E(V - V_\mathrm{u}). \tag{4.10}$$

Equation 4.10 now only requires two parameters to compute pressure from volume. However, the quantity V_u is very difficult to estimate. Indeed, it represents the volume at which pressure is zero, assuming that the linear model is valid. However, in reality, pressure is zero at a volume that is usually very different from V_u, as seen in Figure 4.4.

A further simplification consists in performing the following change of variable:

$$V_\mathrm{s} = V - V_\mathrm{u} \Leftrightarrow V = V_\mathrm{s} + V_\mathrm{u}. \tag{4.11}$$

This change leads the model to work only with the *stressed* volume ,V_s, rather than the total volume. The vessel volume V is thus virtually divided in two components: the unstressed volume V_u, that does not contribute to pressure generation, and the stressed volume V_s, that solely contributes to pressure.

Equation 4.10 then becomes:

$$P(V_\mathrm{s}) \approx EV_\mathrm{s}. \tag{4.12}$$

Equation 4.12 now only requires the knowledge of E for computation of pressure from stressed volume. Passive vessels, such as arteries and veins, will be described using Equation 4.12. Figure 4.5 displays the symbol that will be used to represent a chamber element. Finally, when using Equation 4.12, it is extremely important to remember that stressed volume does not correspond to a physical volume.

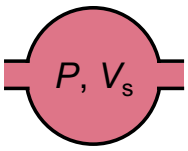

Figure 4.5: Symbol of a chamber element.

It is worth mentioning that pressure-volume relationships of arteries and veins are affected by several factors. These factors include: reflex constrictions, passive recoil, viscoelastic properties and myogenic activation of the smooth muscle around the vessels [78, 115]. This observation implies that parameters E and V_u are not constant with time and can be affected by all the aforementioned factors.

Here also, an electrical analogy can be made, as the behaviour of a chamber element is similar to that of a capacitor in electricity. A capacitor accumulates electrons, which proportionally increases the voltage difference between its two plates. Equivalently, the chamber accumulates blood, which increases the pressure inside the chamber.

4.5 The Continuity Equation - Closing the Loop

The continuity equation states that there can be no loss of matter. In lumped CVS models, it implies no loss of volume or blood. It can be written:

$$\frac{\mathrm{d}V(t)}{\mathrm{d}t} = Q_{\mathrm{in}}(t) - Q_{\mathrm{out}}(t). \tag{4.13}$$

This equation states that the volume change of a chamber $\mathrm{d}V/\mathrm{d}t$ is equal to the difference between flows coming in, Q_{in}, and going out, Q_{out}, of the chamber. In other words, flow coming into a chamber either contributes to a volume increase of the chamber or goes out of the chamber and total volume is conserved. The continuity equation is illustrated in Figure 4.6.

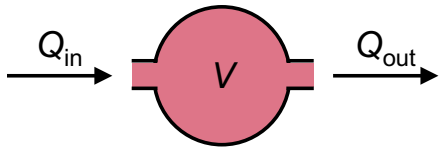

Figure 4.6: Illustration of the continuity equation.

Using the change of variables introduced in Equation 4.11, Equation 4.13 can equivalently be written in terms of stressed volume:

$$\frac{\mathrm{d}V_{\mathrm{s}}(t)}{\mathrm{d}t} = Q_{\mathrm{in}}(t) - Q_{\mathrm{out}}(t). \tag{4.14}$$

The continuity equation is also valid for active chambers, which will be presented in the next chapter. Summing Equation 4.14 for all model chambers, active and passive, gives

$$\sum_i \frac{\mathrm{d}V_{\mathrm{s},i}(t)}{\mathrm{d}t} = \sum_i Q_{\mathrm{in},i}(t) - \sum_i Q_{\mathrm{out},i}(t). \tag{4.15}$$

Since the CVS is a closed loop, the flow coming out of a chamber is the flow going into the next one, and the right-hand side of the previous equation cancels out, leaving:

$$\sum_i \frac{\mathrm{d}V_{\mathrm{s},i}(t)}{\mathrm{d}t} = 0. \tag{4.16}$$

Consequently, the total stressed volume contained in the system is constant, and thus defined:

$$\sum_i V_{\mathrm{s},i}(t). \tag{4.17}$$

This quantity represents a model-based equivalent of SBV. The goal of this work is to estimate this parameter and test it as an index of fluid responsiveness.

For large time scales, the total stressed volume is not necessarily constant. Indeed, total stressed volume can be modified by sympathetic nervous actions, time-dependent vascular properties, fluid exchange through the capillaries, haemorrhage and others [78,108]. Equally, as described in Chapter 3, clinical treatment can add fluid. The total stressed volume is thus constant over shorts and intermediate periods where changes are known and accounted for.

4.6 Summary

This chapter presented the passive elements used in most lumped CVS models: resistances, valves, inertances and chambers. To model the CVS, a description of its central element, the heart, is still needed. The following chapter presents different models for the active elements of the CVS: the ventricles and the atria.

Chapter 5

Active Elements: Ventricles and Atria

5.1 Introduction

Lumped CVS models represent the ventricles and atria as chambers as they have pressure and volume. However, according to physiology, these chambers are active, meaning that they are able to generate a pressure increase through contraction. Consequently, the pressure generated by the chamber does not solely depend on the volume inside of the chamber, but also depends on time, namely the phase of the cardiac cycle currently happening.

This chapter first presents two ways of describing the active ventricular behaviour. The first model described is the time-varying elastance theory, the most simple and commonly applied model of active ventricular behaviour. The second section deals with models built to account for the drawbacks of time-varying elastance theory. The last part of this chapter deals with the application of these two ventricular models to the smaller, but also active, atria.

5.2 The Ventricles

5.2.1 Time-Varying Elastance Theory

When ventricular pressure and volume are plotted against one another, the result is a pressure-volume loop, as shown in Figure 5.1. On this loop, the four main phases of the cardiac cycle can be distinguished:

- Filling (pressure is more or less constant at a small value, volume increases),
- Isovolumic contraction (pressure increases, volume is constant),
- Ejection (pressure is more or less constant at a high value, volume decreases),

- Isovolumic relaxation (pressure decreases, volume is constant).

The width of the pressure-volume loop is equal to the SV.

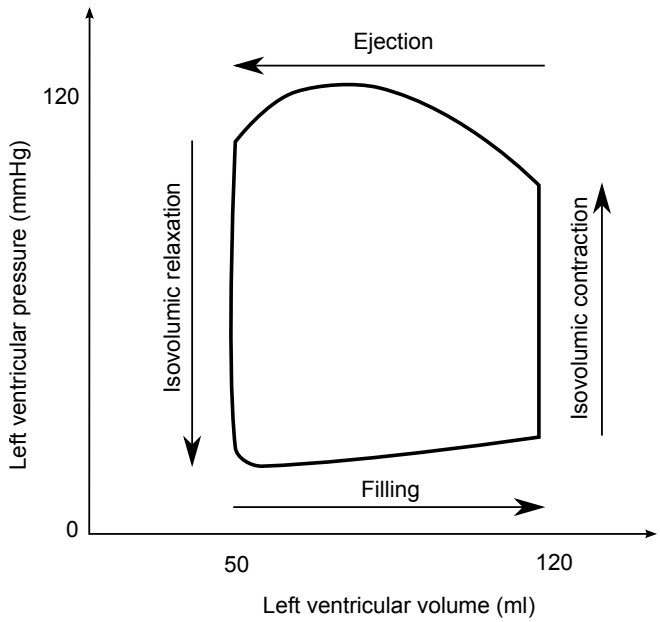

Figure 5.1: Left ventricular pressure-volume loop (adapted from [13], with permission).

The time-varying elastance, also termed *time-varying pressure-volume ratio*, has been introduced by Suga *et al.* [116]. These authors observed various pressure-volume loops corresponding to different levels of afterload. They identified the top-left point of each of these loops, and observed that these points lay approximately on a straight line, as shown in Figure 5.2. The equation of the straight line can be stated as:

$$P = E_{\mathrm{ES}}(V - V_{\mathrm{u}}) \tag{5.1}$$

where E_{ES} is the slope of the line and V_{u} is its intercept with the volume axis. The V_{u} value is referred to as the *left ventricular unstressed volume*. It is the extrapolated volume at which left ventricular pressure would be zero.

When the experiment was repeated after epinephrine infusion, Suga *et al.* observed an increase of E_{ES}, but virtually no change in V_{u}. This major result indicates that E_{ES} is an index of ventricular contractility. Figure 5.2 presents an illustration of the experiment. This experiment also indicates that E_{ES} is independent of afterload, since all points obtained at different afterload levels lie on the same straight line.

Suga *et al.* performed a second experiment with varying preload levels, and found that the top-left pressure-volume points also lay on the same curve. Consequently, E_{ES} represents a preload and afterload independent index of ventricular

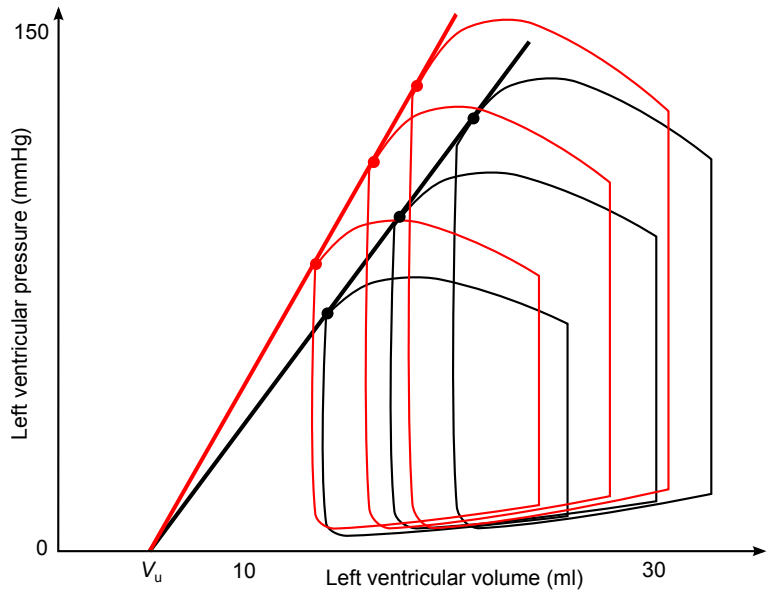

Figure 5.2: Illustration of the experiment of Suga *et al.* [116]. *Black:* baseline pressure-volume loops; *red:* pressure-volume loops obtained after epinephrine infusion.

contractility. The E_{ES} value is called the *end-systolic elastance*, because the top-left point of a pressure-volume loop approximately corresponds to the end of systole. Similarly, the line given by Equation 5.1, is called the *end-systolic pressure-volume relationship (ESPVR)*.

Suga *et al.* also defined the following pressure-volume ratio:

$$E(t) = \frac{P(t)}{V(t) - V_u} \tag{5.2}$$

and computed it over an entire cardiac cycle. The resulting $E(t)$ is shown in Figure 5.3. The maximum value of $E(t)$ is E_{ES}, since E_{ES} was computed using the top-left points of the loops, approximately at maximum pressure and minimum volume.

Finally, Suga *et al.* normalised $E(t)$ with respect to amplitude:

$$e(t) = \frac{E(t)}{E_{ES}} = \frac{P(t)}{E_{ES}(V(t) - V_u)}. \tag{5.3}$$

The function $e(t)$ thus has a maximum value of 1. It is plotted in Figure 5.3 (centre). The function $e(t)$ was also normalised with respect to time:

$$e_N(t/t_{ES}) = e(t), \tag{5.4}$$

where t_{ES} is the time at which $E(t) = E_{ES}$.

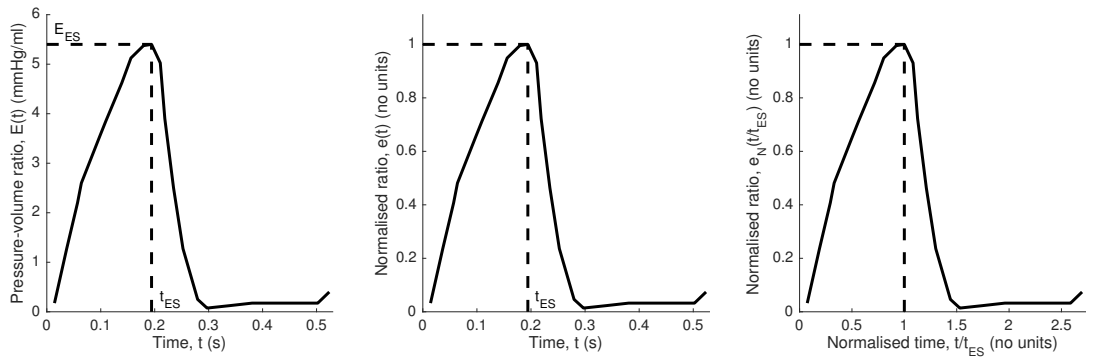

Figure 5.3: Example of $E(t)$, $e(t)$ and $e_{\mathrm{N}}(t/t_{\mathrm{ES}})$. Data points were extracted from [116].

Suga *et al.* showed that $e_{\mathrm{N}}(t/t_{\mathrm{ES}})$ was independent on contractility, preload, afterload and cardiac period, meaning that it can be used to describe the heart in any loading condition. This finding has been confirmed for humans by Senzaki *et al.* [117]. As a result, $e(t)$ can be obtained through a contraction or an expansion of the generic $e_{\mathrm{N}}(t/t_{\mathrm{ES}})$ to account for different cardiac periods.

Consequently, ventricular pressure $P(t)$ can be computed at any time of the cardiac cycle from the sole knowledge of $e(t)$, $V(t)$, E_{ES} and V_{u} using Equation 5.3, yielding:

$$P(t) = e(t)E_{\mathrm{ES}}(V(t) - V_{\mathrm{u}}) \tag{5.5}$$

at any time of the cardiac cycle. The link between pressure and volume thus only depends on two parameters and one function The function $e(t)$ is often called the *activation* or *driver function*.

There is an interesting similarity between Equations 5.5 and 4.10. The only difference between these two equations is that the elastance of the heart is equal to $e(t)E_{\mathrm{ES}}$ and is thus not constant. Hence, its name *time-varying elastance*. Performing the change of variables in Equation 4.11, Equation 5.5 becomes:

$$P(t) = e(t)E_{\mathrm{ES}}V_{\mathrm{s}}(t). \tag{5.6}$$

This time-varying ventricular model will be represented by the symbol displayed in Figure 5.4.

Extension

During filling, ventricular pressure is close to zero, and so is $e(t)$, as shown in Figures 5.1 to 5.3. Precise description of the ventricular behaviour during filling using the time-varying elastance theory thus requires an accurate knowledge of

Figure 5.4: Symbol of a time-varying ventricle element.

the small value of $e(t)$. Because it is practically complex, some authors have assumed $e(t)$ to be zero during filling. Doing so, they could adapt the time-varying elastance theory to include a more precise description of the diastolic behaviour.

In such cases, Equation 5.5 is modified to become:

$$P(t) = e(t)E_{\mathrm{ES}}(V(t) - V_{\mathrm{u}}) + (1 - e(t))P_{\mathrm{ED}}\big(V(t)\big) \tag{5.7}$$

where $P_{\mathrm{ED}}\big(V(t)\big)$ is a pressure-volume curve describing the behaviour of the ventricle during diastole, when $e(t) = 0$. The curve $P_{\mathrm{ED}}(V)$ is called the *end-diastolic pressure-volume relationship* [15]. Several equations have been proposed for the end-diastolic pressure-volume relationship, most of them curvilinear [96, 98, 118–120].

Limitations

Despite its many advantages described in the previous section, many criticisms have been raised against the time-varying elastance concept. First, its biggest advantage, namely that it allows a simple relationship between ventricular pressure and volume, is also its biggest drawback. Indeed, this *ad hoc* approach does not consider the fact that cardiac muscle contraction begins at a microscopic scale.

Second, more recent experiments have shown the ESPVR to be more parabolic than linear in shape [109, 118, 121, 122]. As a consequence, some researchers have observed negative values of V_{u} [109, 122, 123]. A negative value of V_{u} is not seen as physiologically impossible. Indeed, V_{u} is nothing, but the result of a linear regression on a series of pressure-volume points. If ventricular volume was actually decreased until ventricular pressure reached zero, the resulting volume would indeed be positive. This inconsistency is due to the parabolic shape of the ESPVR. Some researchers subsequently modified the time-varying elastance theory to include various nonlinear pressure-volume relationships [124–126].

Third, instantaneous ventricular pressure has also been shown to be negatively dependent on instantaneous flow out of the ventricle, an effect that has been termed the *internal resistance* of the ventricle [127–129]. The authors that made these observations added their *ad hoc* modifications to the time-varying

elastance theory to account for this resistive effect by including a flow term in Equation 5.2, yielding:

$$E(t) = \frac{P(t)}{V(t) - V_{\mathrm{u}}} - RQ(t) \tag{5.8}$$

where R is a resistance and $Q(t)$ is the flow out of the ventricle.

Finally, the relationship between ventricular pressure and volume has been demonstrated to depend on the mechanical load exerted on the ventricle [130]. This result implies the load dependence of the ESPVR, in turn indicating that the ESPVR is not unique. This effect cannot be accounted for by any generic modification of the time-varying elastance theory. A similar observation has been made for the right ventricle [131]. In addition, for the right ventricle, it was found that V_{u} was not constant during a cardiac cycle and also changed with epinephrine administration.

5.2.2 Multi-Scale Models

The objections presented in the previous section have led many authors to gain deeper knowledge of the fundamental mechanisms underlying cardiac contraction. From this knowledge, they built multi-scale ventricular models whose contraction is described at the level of a cardiac muscle unit, a *sarcomere* [91,118,132–135]. The previously cited multi-scale ventricular models are built on the same two elements: a sarcomere model describing force generation at the muscle unit level, and a ventricle model converting sarcomere force into ventricular pressure and sarcomere length into ventricular volume. The situation is depicted in Figure 5.5

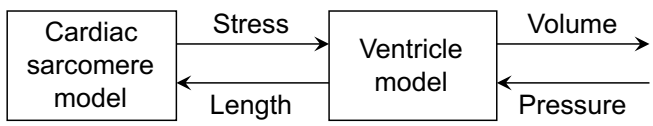

Figure 5.5: Multi-scale model of a ventricle, built as the interconnection of two models.

Sarcomere Models

Sarcomere models describe active stress, σ_{a}, generated by a single sarcomere as the product of two quantities, the deformation, ε, of the sarcomere, and its con-

tractile state, C:

$$\sigma_a = \varepsilon(L)C(L, ...), \tag{5.9}$$

where L is the length of the sarcomere and is computed from the ventricular volume as described in the following section.

The models available in the literature vary widely in the level of detail used to describe the sarcomere's contractile state, C. The simplest model [132] describes C as the solution to an empirical differential equation. The others describe the chemical pathways of calcium in the sarcomere using a four-state model [91, 118, 133–135]. Contractility is then defined as the concentration of the protein troponin attached to another protein, thus generating contraction.

Total stress, σ, generated by the sarcomere is given by the sum of the active stress, σ_a, and a passive component, σ_p, generated by a nonlinear spring, yielding:

$$\sigma = \sigma_\mathrm{a} + \sigma_\mathrm{p}, \tag{5.10}$$

where σ_p only depends on L.

Ventricle Models

Ventricle models available in the literature assume the ventricle to be a tube [132], a sphere [91, 118, 133] or a hemisphere [134, 135]. These geometrical assumptions allow the derivation of a relationship between sarcomere length and ventricular volume:

$$L = L(V). \tag{5.11}$$

The geometrical assumptions performed to build the ventricle model also allow the linking of sarcomere stress, σ, to ventricular pressure. As a general rule, pressure is directly related to sarcomere stress, σ, and nonlinearly related to ventricular volume V:

$$P = \sigma f(V) \tag{5.12}$$

where f is a shape function depending on the assumed ventricular geometry. The simplest version of Equation 5.12 reads:

$$P = \frac{2h\sigma}{r} \tag{5.13}$$

where h is the constant wall thickness and r is the radius of the sphere (or the hemisphere). In haemodynamics, Equation 5.13 is called the *law of Laplace* [109, 134, 135].

5.3 The Atria

The previous sections presented two ways of modelling the ventricular behaviour, the time-varying elastance theory and multi-scale models. The following section discusses the application of these two types of models to the two other active cardiac chambers. Specifically, the atria, located just before the ventricles.

5.3.1 Time-Varying Elastance Theory

The typical evolution of left atrial and left ventricular pressures and left atrial volume is shown in Figure 5.6. When left atrial pressure and volume are plotted against one another, the result is a closed curve in the pressure-volume plane, called the left atrial pressure-volume loop. An example of such a loop is given in Figure 5.7 . This loop is composed of two lobes, giving it a particular figure-eight shape. The right lobe, at higher volumes, is the *v loop*, and represents the passive properties of the atrium. The left lobe, at lower volumes, is the *a loop*, which is caused by active contraction of the atrium.

Only two groups have experimentally computed a time-varying elastance curve for the left atrium [136, 137]. Both found the $E(t)$ curve for an ejecting atrium has two local maxima. In addition, only the group of Alexander *et al.* [136] tested the load independence of the atrial $E(t)$ and came up with a negative conclusion. Specifically, that the atrial $E(t)$ is different for ejecting and non-ejecting beats. More recently, other groups [138–140] also plotted pressure-volume loops for differently loaded left atrial beats, but did not explicitly compute an atrial elastance curve. Thus, the application of the time-varying elastance concept to the atria remains very uncertain.

Despite all these theoretical issues regarding the use of an atrial time-varying elastance, many models available in the literature rely on this concept [90, 102, 141–146]. In addition, these models only use atrial elastance curves similar to the ventricular one. More specifically, one with only one maximum per cardiac cycle. This approach holds largely due to the simplicity of the time varying elastance theory, even though experiments have proven these curves were different.

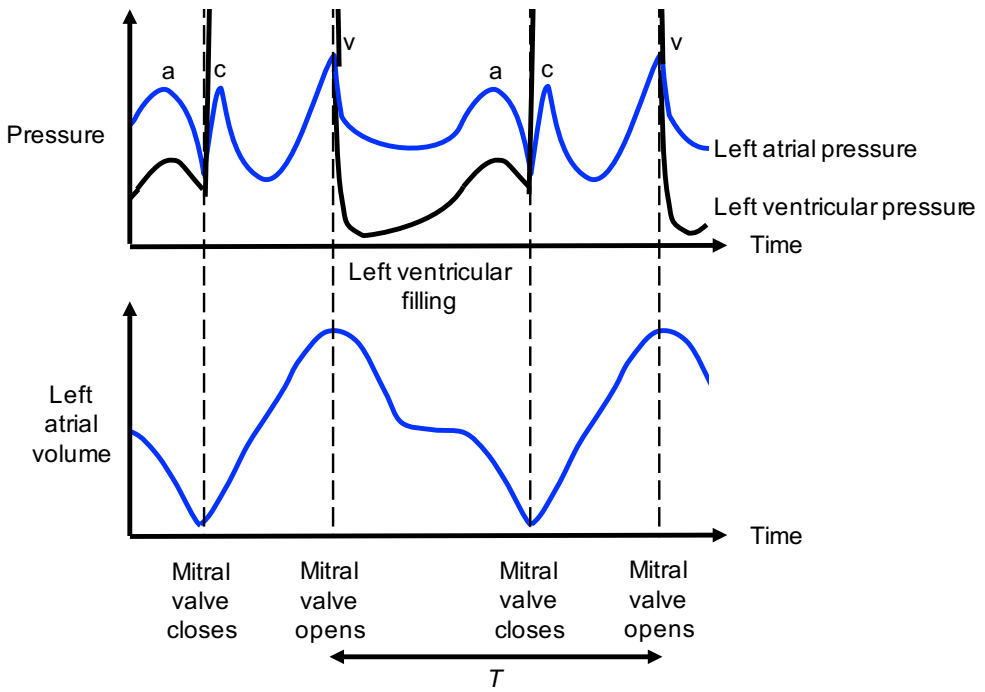

Figure 5.6: Evolution of left atrial and left ventricular variables during two cardiac cycles [134]. *Top:* left ventricular pressure (*black*) and left atrial pressure (*blue*) with specific waves (a, c and v waves) indicated. *Bottom:* left atrial volume.

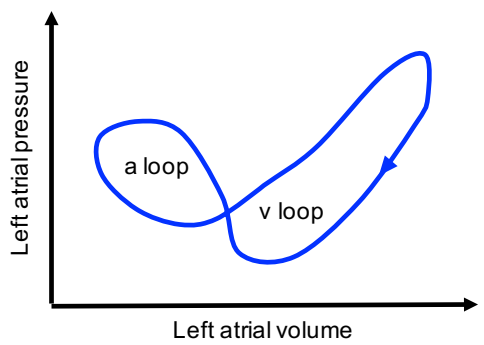

Figure 5.7: Sketch of a typical left atrial pressure-volume loop [134].

5.3.2 Multi-Scale Models

As with the ventricles, some multi-scale models of the atrial behaviour have been developed in the literature [132, 134]. Since multi-scale models are based on a microscopic-scale description of contraction, they can easily be transposed from the ventricles to the atria, whose contraction happens on the same physiological basis. The atrial equations are thus similar to Equations 5.9 to 5.12, but some parameter values are different to account for the differences between the atria and the ventricles, including, for instance, the geometry and timing of the contraction.

5.4 Summary

This chapter first presented the most commonly used model to describe ventricular contraction in lumped CVS models, namely the time-varying elastance theory. The simplicity of this theory makes it a very convenient tool, but this simplicity comes with neglecting many complex phenomena happening during ventricular contraction. Multi-scale ventricular models were developed to overcome the lack of physiological grounds of the time-varying elastance theory. Such models are particularly interesting in the case of the atria since there exists no accurate time-varying elastance model applicable to these chambers.

Chapter 6

Models of the Cardio-Vascular System

6.1 Introduction

This chapter presents two CVS models involving the passive and active elements described in Chapters 4 and 5. The first model is a very simple three-chamber model, describing the heart using the time-varying elastance theory. The second is a more complete model, involving six chambers and taking into account both the systemic and the pulmonary circulation.

6.2 Three-Chamber Model

The three-chamber CVS model is presented in Fig. 6.1. It consists of three elastic chambers representing the heart (h), the arteries (a) and the veins (v). The three model chambers are linked by vessel resistances representing an input (R_{i}) and output (R_{o}) heart valve, and the circulation (R_{c}). This model can be linked to the work of Danielsen and Ottesen [87], in which the venous chamber is replaced by a constant pressure generator. The three-chamber model is also somewhat similar to the one introduced by Parlikar and Verghese [147], the main difference lying in the way the valves are modelled. More recently, Rüschen *et al*. have used a nearly identical model to estimate CO in animals equipped with a left ventricular assist device [148]. In their model, the input valve was not included, and the heart was bypassed by the left ventricular assist device.

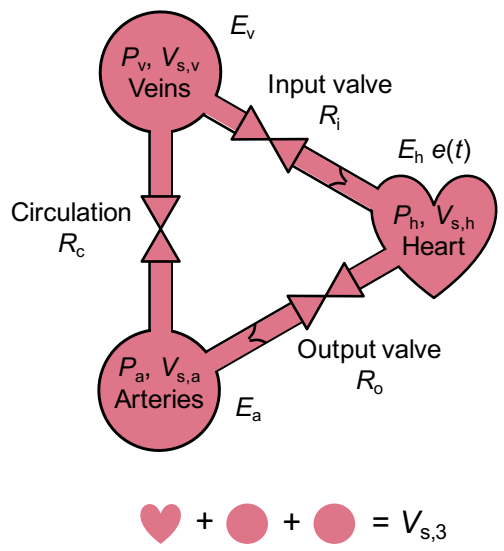

Figure 6.1: Schematic representation of the three-chamber CVS model.

6.2.1 Equations

The arteries and veins in this model are described:

$$P_a(t) = E_a V_{s,a}(t) \tag{6.1}$$

$$P_v(t) = E_v V_{s,v}(t) \tag{6.2}$$

where P_a, E_a and $V_{s,a}$ respectively denote arterial pressure, elastance and stressed volume. The equivalent venous quantities are denoted using the subscript v.

The cardiac chamber is modelled using the time-varying elastance theory from Equation 5.6:

$$P_h(t) = e(t) E_h V_{s,h}(t) \tag{6.3}$$

where P_h, E_h and $V_{s,h}$ respectively denote cardiac pressure, elastance and stressed volume.

Flow Q_c through the circulation is described by Ohm's law from Equation 4.1:

$$Q_c(t) = \frac{P_a(t) - P_v(t)}{R_c} \tag{6.4}$$

where R_c denotes the resistance of the circulation. Flows Q_i and Q_o, through the input and output valves, are described using the simple valve model of Equa-

tion 4.4:

$$Q_{\mathrm{i}}(t) = \begin{cases} \dfrac{P_{\mathrm{v}}(t) - P_{\mathrm{h}}(t)}{R_{\mathrm{i}}} & \text{if } P_{\mathrm{v}}(t) > P_{\mathrm{h}}(t) \\ 0 & \text{otherwise} \end{cases} \tag{6.5}$$

$$Q_{\mathrm{o}}(t) = \begin{cases} \dfrac{P_{\mathrm{h}}(t) - P_{\mathrm{a}}(t)}{R_{\mathrm{o}}} & \text{if } P_{\mathrm{h}}(t) > P_{\mathrm{a}}(t) \\ 0 & \text{otherwise.} \end{cases} \tag{6.6}$$

where R_{i} and R_{o} denote the resistances of the input and output valves.

Finally, the continuity equation seen in Equation 4.14 gives the rate at which the stressed volumes of the chambers change and results in:

$$\frac{\mathrm{d}V_{\mathrm{s,h}}(t)}{\mathrm{d}t} = Q_{\mathrm{i}}(t) - Q_{\mathrm{o}}(t), \tag{6.7}$$

$$\frac{\mathrm{d}V_{\mathrm{s,a}}(t)}{\mathrm{d}t} = Q_{\mathrm{o}}(t) - Q_{\mathrm{c}}(t), \tag{6.8}$$

$$\frac{\mathrm{d}V_{\mathrm{s,v}}(t)}{\mathrm{d}t} = Q_{\mathrm{c}}(t) - Q_{\mathrm{i}}(t). \tag{6.9}$$

Summing Equations 6.7 to 6.9 gives:

$$\frac{\mathrm{d}V_{\mathrm{s,h}}(t)}{\mathrm{d}t} + \frac{\mathrm{d}V_{\mathrm{s,a}}(t)}{\mathrm{d}t} + \frac{\mathrm{d}V_{\mathrm{s,v}}(t)}{\mathrm{d}t} = 0. \tag{6.10}$$

Consequently, the total stressed volume contained in the CVS model is a constant parameter that can be expressed:

$$V_{\mathrm{s,h}}(t) + V_{\mathrm{s,a}}(t) + V_{\mathrm{s,v}}(t) = V_{\mathrm{s,3}}. \tag{6.11}$$

6.2.2 Parameters

The three-chamber CVS model has eight parameters:

- T, cardiac period,
- E_{h}, cardiac end-systolic elastance,
- E_{a}, arterial elastance,
- E_{v}, venous elastance,
- R_{i}, input valve resistance,
- R_{o}, output valve resistance,
- R_{c}, resistance of the circulation and
- $V_{\mathrm{s,3}}$, total stressed volume.

The model is set going using a driver function $e(t)$ and initial conditions for $V_{\mathrm{s,h}}$, $V_{\mathrm{s,a}}$ and $V_{\mathrm{s,v}}(t)$ respecting Equation 6.11.

6.2.3 Simulation

Figure 6.2 displays the result of a simulation of the three-chamber CVS model using the parameter values given in Table 6.1. These values were chosen to produce physiological pressure and volume curves. The simulation displayed in Figure 6.2 begins during diastole, so the input valve of the heart is open, while the output valve is closed. Accordingly, flow through the input valve, Q_i, is positive and proportional to the pressure difference between the veins and the heart, $P_\mathrm{v} - P_\mathrm{h}$. In contrast, flow through the output valve, Q_o, is zero because the pressure in the arteries, P_a is higher than that of the heart, P_h. Consequently, venous stressed volume, $V_\mathrm{s,v}$, is decreasing, while cardiac stressed volume, $V_\mathrm{s,h}$, is increasing. Since the heart is filling, cardiac pressure, P_h gradually increases. On the pressure-volume loop, filling is seen in the low pressure area.

Table 6.1: Parameter values for the simulation of the three-chamber CVS model presented in Figure 6.2.

Parameter	Units	Value
T	s	1.1
E_h	mmHg/ml	1.4
E_a	mmHg/ml	1.2
E_v	mmHg/ml	0.2
R_i	mmHg s/ml	0.05
R_o	mmHg s/ml	0.04
R_c	mmHg s/ml	2
$V_\mathrm{s,3}$	ml	250
$e(t)$	-	$\exp\left[-20\left((t \bmod T) - \frac{T}{2}\right)^2\right]$

At a moment dictated by the driver function, cardiac contraction initiates, causing a rapid rise in cardiac pressure, which then becomes larger than the upstream venous pressure. The input valve subsequently closes, marking the end of diastole. This closure allows the veins to fill, which is translated by a small increase in pressure. Since the output valve is still closed, the cardiac volume remains constant at its end-diastolic value. On the pressure-volume loop, this period is illustrated by the vertical line at high volume.

Cardiac contraction is still going on, meaning that cardiac pressure keeps increasing, until it becomes larger than arterial pressure. At this moment, the output valve opens, marking the beginning of systole. Blood flows to the arteries, consequently filling the arteries and emptying the heart. Arterial pressure sub-

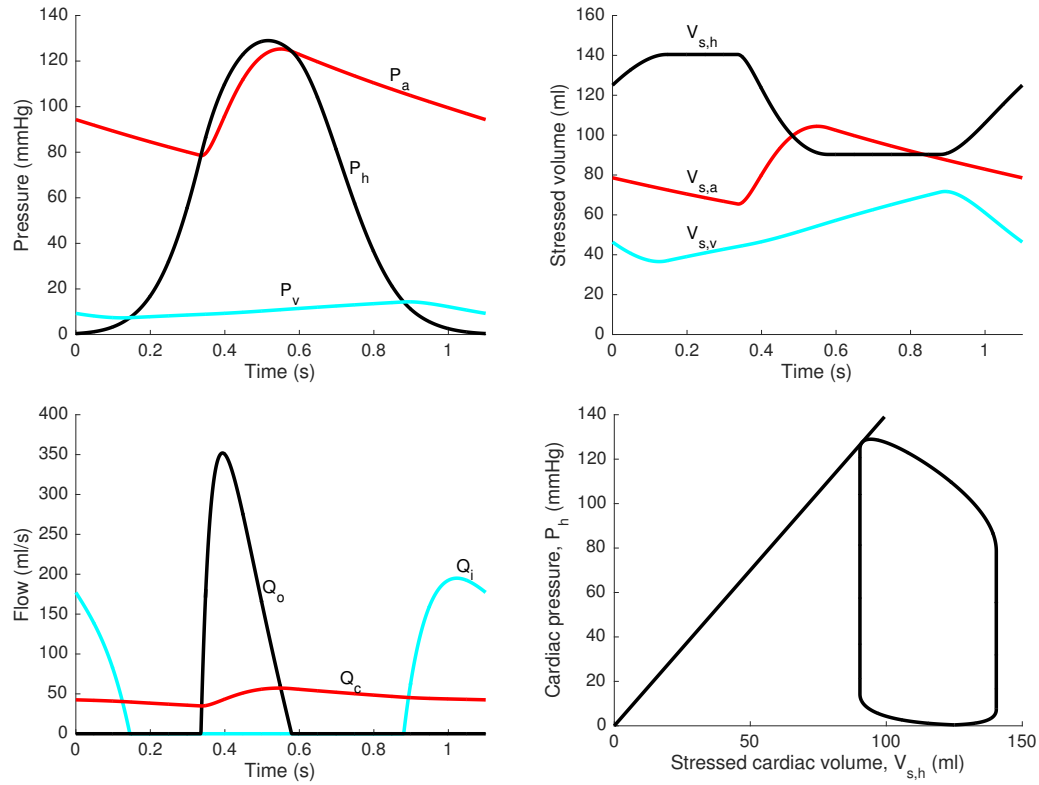

Figure 6.2: Simulation of the three-chamber CVS model using the parameters of Table 6.1. *Top-left:* cardiac (P_{h}, *black*), arterial (P_{a}, *red*) and venous (P_{v}, *cyan*) pressures. *Top-right:* cardiac ($V_{\mathrm{s,h}}$, *black*), arterial ($V_{\mathrm{s,a}}$, *red*) and venous ($V_{\mathrm{s,v}}$, *cyan*) stressed volumes. *Bottom-left:* input (Q_{i}, *cyan*), output (Q_{o}, *black*) and circulatory (Q_{c}, *red*) flows. *Bottom-right:* cardiac pressure-volume loop and the corresponding ESPVR.

sequently increases proportionally to the increase in arterial volume. This part of the cardiac cycle corresponds to the top of the pressure-volume loop, where pressures are large and volume is decreasing.

Arterial pressure, increasing because of filling, soon passes over ventricular pressure, which is decreasing because of the drop in ventricular volume and because the heart starts to relax. At this moment, the output valve closes, marking the end of systole. The output flow goes back to zero. Since the input valve is still closed, the cardiac volume remains constant at its end-systolic value. On the pressure-volume loop, this behaviour is seen in a vertical line at low volume.

Finally, cardiac pressure keeps decreasing, until it becomes lower than the upstream venous pressure. At this moment, the input valve opens, and the cardiac cycle resumes. Thus, several cardiac cycles may be simulated if desired, thanks to the modulo operator inserted in the driver function.

6.2.4 Discussion

The pressures depicted in Figure 6.2 reproduce quite well the physiological ones presented in Section 2.3.2. Simulated arterial pressure ranges between approximately 80 and 120 mmHg, which is its expected physiological range. As can be seen from the arterial pressure waveform, the three-chamber CVS model does not reproduce the dicrotic notch, defined in Section 2.3.2. This problem can be solved using inertance elements, described in Section 4.2.1, and using two chambers to describe the arteries [149]. Venous pressure is approximately constant, as physiologically observed. Please note that simulated cardiac pressure is approximately symmetrical only because the chosen driver function is symmetrical. This formulation of the driver function was chosen because it is the simplest possible, involving only two parameters. The use of a more complex driver function, closer to the experimental one depicted in Figure 5.3, yields a more realistic cardiac pressure curve [86–88, 92, 141, 150].

As a reminder, the outputs of the simulation are *stressed* volumes, which means that they cannot be compared to actual volumes without knowing the value of the corresponding *unstressed* volume, as defined in Equation 4.11. However, a difference of stressed volumes can be compared to a difference of actual volumes, since unstressed volume is subtracted from itself during the computation. For instance, in Figure 6.2, the range of the cardiac stressed volume curve equals:

$$\Delta V_{\mathrm{s,h}} = V_{\mathrm{s,h}}(t_{\mathrm{EF}}) - V_{\mathrm{s,h}}(t_{\mathrm{EE}}) \approx 140 - 90 = 50 \text{ ml}, \tag{6.12}$$

where t_{EF} and t_{EE} denote the end of filling and the end of ejection. The range of actual cardiac volume is identical to the previous quantity, since:

$$\Delta V_{\mathrm{h}} = V_{\mathrm{h}}(t_{EF}) - V_{\mathrm{h}}(t_{EE}) = V_{\mathrm{s,h}}(t_{EF}) + V_{\mathrm{u,h}} - V_{\mathrm{s,h}}(t_{EE}) - V_{\mathrm{u,h}} = \Delta V_{\mathrm{s,h}}. \tag{6.13}$$

The previous quantity is the model-based equivalent of SV. As for SV, it is also equal to the width of the pressure-volume loop. The model-based equivalent of CO can be obtained as:

$$\frac{\Delta V_{\mathrm{s,h}}}{T} \approx \frac{50}{1.1} \approx 45 \text{ ml/s}. \tag{6.14}$$

Equations 6.7, 6.8 and 6.9 dictate that the changes in chamber (stressed) volumes are equal to the difference between flows coming in and going out of the chambers. This statement can be checked from the plots of Figure 6.2. Please note that during cardiac ejection, cardiac volume decreases and arterial volume increases, but not by the same amount. Indeed, part of the volume ejected by the heart flows directly into the vein, as will be discussed later. In a more general fashion, the sum of all stressed volumes is constant at all times and equal to $V_{\mathrm{s},3}$.

As expected from model Equations 6.1 and 6.2, the ratio of arterial (or venous) pressures and volumes in Figure 6.2 is equal to E_a (or E_v).

One can also observe on the bottom-left panel of Figure 6.2 that the flow curves have the shape of the differences between up and downstream pressures, as dictated by Equations 6.4, 6.5 and 6.6. The integral of all three flows over one heartbeat, the areas under the flow curves, is equal to $\Delta V_{s,h}$. In particular, at each cardiac cycle, this volume leaves the heart, goes through the circulation, and comes back into the heart, to be ejected at the next heartbeat.

The bottom-right panel of Figure 6.2 displays the pressure-volume loop simulated by the three-chamber model and the corresponding ESPVR, whose equation is $P = E_h V_{s,h}$. The ESPVR crosses the origin because the graph represents stressed volume. When absolute volume is represented, the equation of the ESPVR is $P = E_h(V - V_{u,h})$, repeating Equation 5.1, and the ESPVR does not cross the origin, unless $V_{u,h} = 0$. As dictated by Equation 6.3, the pressure-volume loop meets the ESPVR near end-systole or, more precisely, when $e(t)$ is equal to one.

6.2.5 Limitations

Besides the hypotheses formulated to establish the equations of the lumped elements presented in Chapters 4 and 5, the building of the three-chamber CVS model itself also relies on a series of assumptions. These assumptions are discussed in the following sections.

Only One Circulation

The biggest limitation of the three-chamber CVS model presented is the difficulty to interpret it in terms of cardio-vascular physiology. Indeed, as explained in Chapter 2, the CVS consists of two parallel circuits, the systemic and pulmonary circulations, which are not represented in the model. The assumption underlying the building of the three-chamber CVS model is that the systemic and pulmonary circulations can be merged or considered separately. Other authors [147,148,151] have previously proposed models representing only one circulation.

No Thoracic Pressure

As mentioned in Section 3, the heart and sections of the largest blood vessels are enclosed in the thorax, resulting in part of the lung pressure being transmitted to these structures. Taking thoracic pressure into account in the three-chamber model is difficult because of the absence of two distinct circulations. Indeed, the

effects of respiration on the left ventricle are different than on the right [14, 152]. This aspect cannot be correctly reproduced using the three-chamber CVS model, since it includes only one cardiac chamber. Furthermore, the modelled passive chambers, the arteries and the veins, are physiologically both partially located in the thorax. Therefore, it is difficult to apply thoracic pressure in an anatomical fashion in the model [153].

No Ventricular Interaction

As mentioned in Section 2.2.1, the heart is enclosed in a rather rigid structure, called the pericardium. Consequently, an increase in left ventricular volume compresses the right ventricle and reciprocally. Since there is only one cardiac chamber in the three-chamber CVS model, inserting the direct interaction of the ventricles in this model is not relevant.

No Atria

As explained in Section 5.3, the time-varying elastance theory has not yet been demonstrated to be applicable to the atria. Consequently, the only way to represent the atria is to use a multi-scale model. However, multi-scale models involve a large number of unknown parameters that cannot be identified from the limited amount of clinical data available. For instance, the model developed by Pironet *et al.* involves 21 parameters, only to represent the left atrial behaviour [134]. Since the goal of the present work is an application in the ICU, the atria have been neglected in establishing the three-chamber CVS model.

It is estimated that left atrial contraction can account for 15 to 30 % of left ventricular filling [154–156]. However, the absence of atrial contraction in the model will not lead to an underestimation of ventricular filling. Indeed, the model parameters can be adjusted so that model simulations match experimental data, as explained in Part III of this work. Since all ventricular filling in the model is caused by passive blood flow to the ventricles, the identified inflow resistance parameter, R_i will thus likely be lower than in reality, to allow for equivalent filling that is totally passive.

No Inertances

The inertance elements introduced in Section 4.2.1 were not included in the three-chamber CVS model, for several reasons. First, they have been shown to have small values and to weakly affect model dynamics [149, 157]. Second, neglecting these inertial parameters reduces uncertainty in the parameter estimation pro-

cess. Finally, these parameters are difficult to measure and not well defined, and thus difficult to validate even if used.

6.3 Six-Chamber Model

The six-chamber CVS model captures both circuits. It represents the left (LV) and right (RV) ventricles, the systemic (SA) and pulmonary arteries (PA), and the systemic (SV) and pulmonary veins (PV). The six chambers are linked by resistive vessels, representing the four heart valves (mitral: MV, aortic: AV, tricuspid: TV and pulmonary: PV) and the systemic and pulmonary circulations (sys and pul). The model is presented in Figure 6.3.

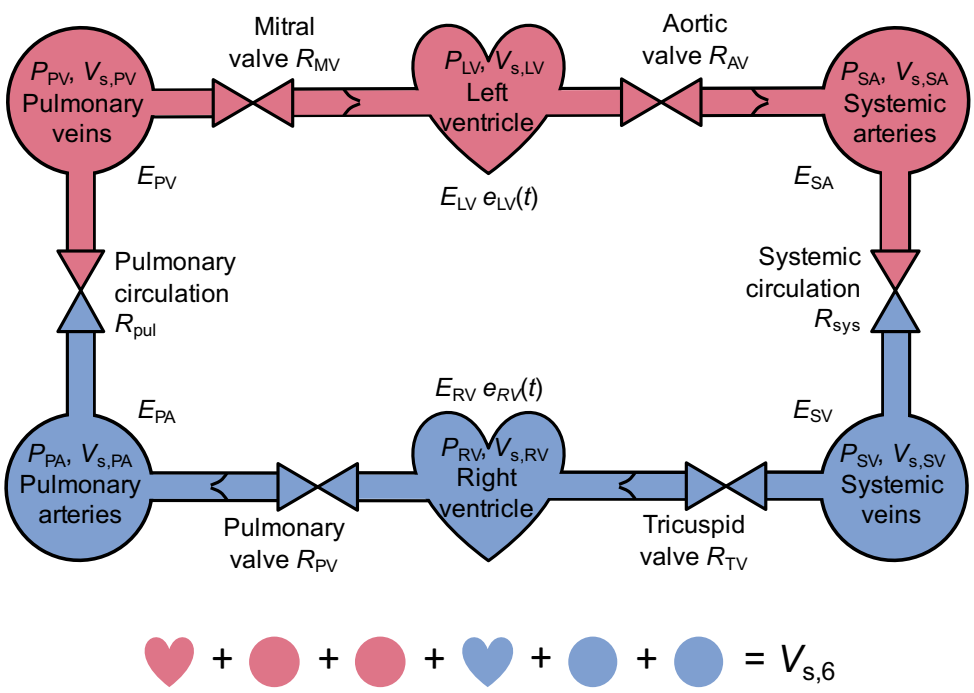

Figure 6.3: Schematic representation of the six-chamber CVS model.

The six-chamber CVS model used in this work has previously been presented by Burkhoff and Tyberg [86]. This model is the simplest model to consider both the systemic and pulmonary circulations. It has allowed theoretical studies assessing the consequences of left ventricular dysfunction [86] and ventricular interaction [96, 112]. From an experimental point of view, a similar model has been used for haemodynamic monitoring during septic shock [95] and pulmonary embolism [94, 101].

6.3.1 Equations

The systemic and pulmonary arteries and veins are modelled as passive chambers using Equation 4.12:

$$P_{\mathrm{SA}}(t) = E_{\mathrm{SA}} V_{\mathrm{s,SA}}(t) \tag{6.15}$$

$$P_{\mathrm{SV}}(t) = E_{\mathrm{SV}} V_{\mathrm{s,SV}}(t) \tag{6.16}$$

$$P_{\mathrm{PA}}(t) = E_{\mathrm{PA}} V_{\mathrm{s,PA}}(t) \tag{6.17}$$

$$P_{\mathrm{PV}}(t) = E_{\mathrm{PV}} V_{\mathrm{s,PV}}(t), \tag{6.18}$$

where P_{SA}, E_{SA} and $V_{\mathrm{s,SA}}$ respectively denote systemic arterial pressure, elastance and stressed volume. The equivalent sytemic venous, pulmonary arterial and pulmonary venous quantities are denoted using the subscripts SV, PA and PV, respectively.

The left and right ventricles are active chambers. Thus, the relationship between pressure and volume is time-varying per Equation 5.6:

$$P_{\mathrm{LV}}(t) = e_{\mathrm{LV}}(t) E_{\mathrm{LV}} V_{\mathrm{s,LV}}(t) \tag{6.19}$$

$$P_{\mathrm{RV}}(t) = e_{\mathrm{RV}}(t) E_{\mathrm{RV}} V_{\mathrm{s,RV}}(t), \tag{6.20}$$

where P_{LV}, $e_{\mathrm{LV}}(t)$, E_{LV} and $V_{\mathrm{s,LV}}(t)$ respectively denote left ventricular pressure, elastance, driver function and stressed volume. The equivalent right ventricular quantities are denoted using the subscript RV.

In the systemic and pulmonary circulations, flows Q_{sys} and Q_{pul} are given by Ohm's law in Equation 4.1:

$$Q_{\mathrm{sys}}(t) = \frac{P_{\mathrm{SA}}(t) - P_{\mathrm{SV}}(t)}{R_{\mathrm{sys}}} \tag{6.21}$$

$$Q_{\mathrm{pul}}(t) = \frac{P_{\mathrm{PA}}(t) - P_{\mathrm{PV}}(t)}{R_{\mathrm{pul}}}. \tag{6.22}$$

where R_{sys} and R_{pul} denote the resistance of the systemic and pulmonary circulations. In the case of the valves, the model assumes that there is only flow when

the pressure difference across the valve is positive, using Equation 4.4:

$$Q_{\mathrm{MV}}(t) = \begin{cases} \dfrac{P_{\mathrm{PV}}(t) - P_{\mathrm{LV}}(t)}{R_{\mathrm{MV}}} & \text{if } P_{\mathrm{PV}}(t) > P_{\mathrm{LV}}(t) \\ 0 & \text{otherwise} \end{cases} \tag{6.23}$$

$$Q_{\mathrm{AV}}(t) = \begin{cases} \dfrac{P_{\mathrm{LV}}(t) - P_{\mathrm{SA}}(t)}{R_{\mathrm{AV}}} & \text{if } P_{\mathrm{LV}}(t) > P_{\mathrm{SA}}(t) \\ 0 & \text{otherwise} \end{cases} \tag{6.24}$$

$$Q_{\mathrm{TV}}(t) = \begin{cases} \dfrac{P_{\mathrm{SV}}(t) - P_{\mathrm{RV}}(t)}{R_{\mathrm{TV}}} & \text{if } P_{\mathrm{SV}}(t) > P_{\mathrm{RV}}(t) \\ 0 & \text{otherwise} \end{cases} \tag{6.25}$$

$$Q_{\mathrm{PV}}(t) = \begin{cases} \dfrac{P_{\mathrm{RV}}(t) - P_{\mathrm{PA}}(t)}{R_{\mathrm{PV}}} & \text{if } P_{\mathrm{RV}}(t) > P_{\mathrm{PA}}(t) \\ 0 & \text{otherwise,} \end{cases} \tag{6.26}$$

where, Q_{MV} and R_{MV} denote the flow through and the resistance of the mitral valve. The equivalent quantities, linked to the aortic, tricuspid and pulmonary valves, are denoted using the subscripts AV, TV and PV, respectively.

Finally, volume change in any of the six chambers is given by the difference between flows in and out of the chamber using Equation 4.14:

$$\frac{\mathrm{d}V_{\mathrm{s,LV}}(t)}{\mathrm{d}t} = Q_{\mathrm{MV}} - Q_{\mathrm{AV}} \tag{6.27}$$

$$\frac{\mathrm{d}V_{\mathrm{s,SA}}(t)}{\mathrm{d}t} = Q_{\mathrm{AV}} - Q_{\mathrm{sys}} \tag{6.28}$$

$$\frac{\mathrm{d}V_{\mathrm{s,SV}}(t)}{\mathrm{d}t} = Q_{\mathrm{sys}} - Q_{\mathrm{TV}} \tag{6.29}$$

$$\frac{\mathrm{d}V_{\mathrm{s,RV}}(t)}{\mathrm{d}t} = Q_{\mathrm{TV}} - Q_{\mathrm{PV}} \tag{6.30}$$

$$\frac{\mathrm{d}V_{\mathrm{s,PA}}(t)}{\mathrm{d}t} = Q_{\mathrm{PV}} - Q_{\mathrm{pul}} \tag{6.31}$$

$$\frac{\mathrm{d}V_{\mathrm{s,PV}}(t)}{\mathrm{d}t} = Q_{\mathrm{pul}} - Q_{\mathrm{MV}}. \tag{6.32}$$

Summing Equations 6.27 to 6.32 gives:

$$\frac{\mathrm{d}V_{\mathrm{s,LV}}(t)}{\mathrm{d}t} + \frac{\mathrm{d}V_{\mathrm{s,SA}}(t)}{\mathrm{d}t} + \frac{\mathrm{d}V_{\mathrm{s,SV}}(t)}{\mathrm{d}t} + \frac{\mathrm{d}V_{\mathrm{s,RV}}(t)}{\mathrm{d}t} + \frac{\mathrm{d}V_{\mathrm{s,PA}}(t)}{\mathrm{d}t} + \frac{\mathrm{d}V_{\mathrm{s,PV}}(t)}{\mathrm{d}t} = 0. \tag{6.33}$$

and integrating Equation 6.33 yields:

$$V_{\mathrm{s,LV}}(t) + V_{\mathrm{s,SA}}(t) + V_{\mathrm{s,SV}}(t) + V_{\mathrm{s,RV}}(t) + V_{\mathrm{s,PA}}(t) + V_{\mathrm{s,PV}}(t) = V_{\mathrm{s},6}. \tag{6.34}$$

Equation 6.33 expresses that, since the model is a closed-loop, there is no net flow going in or out of the whole CVS. Equation 6.34 expresses that, as a consequence, total stressed volume in the model is conserved and set as a constant, denoted $V_{s,6}$.

6.3.2 Parameters

The six-chamber model counts fourteen parameters:

- T, cardiac period ,
- E_{LV}, left ventricular end-systolic elastance,
- E_{RV}, right ventricular end-systolic elastance,
- E_{SA}, systemic arterial elastance,
- E_{PA}, pulmonary arterial elastance,
- E_{SV}, systemic venous elastance,
- E_{PV}, pulmonary venous elastance,
- R_{MV}, mitral valve resistance,
- R_{AV}, aortic valve resistance,
- R_{TV}, tricuspid valve resistance,
- R_{PV}, pulmonary valve resistance,
- R_{sys}, resistance of the systemic circulation,
- R_{pul} resistance of the pulmonary circulation, and
- $V_{s,6}$ total stressed volume.

This model requires two driver functions $e_{LV}(t)$ and $e_{RV}(t)$, for the left and right ventricles, respectively.

6.3.3 Simulation

Figure 6.4 shows the result of the simulation of the six-chamber CVS model using the parameter values in Table 6.2. The timing of the cardiac cycle is physiologically correct, as shown in Figure 6.4. The first phase represented in Figure 6.4 is filling of the left and right ventricles. Mitral and tricuspid valves closure occurs when ventricular pressures rise at the initiation of a new contraction. Isovolumic contraction then begins. During this phase, ventricular pressures increase until the aortic and pulmonary valves open due to crossover of ventricular and downstream arterial pressures.

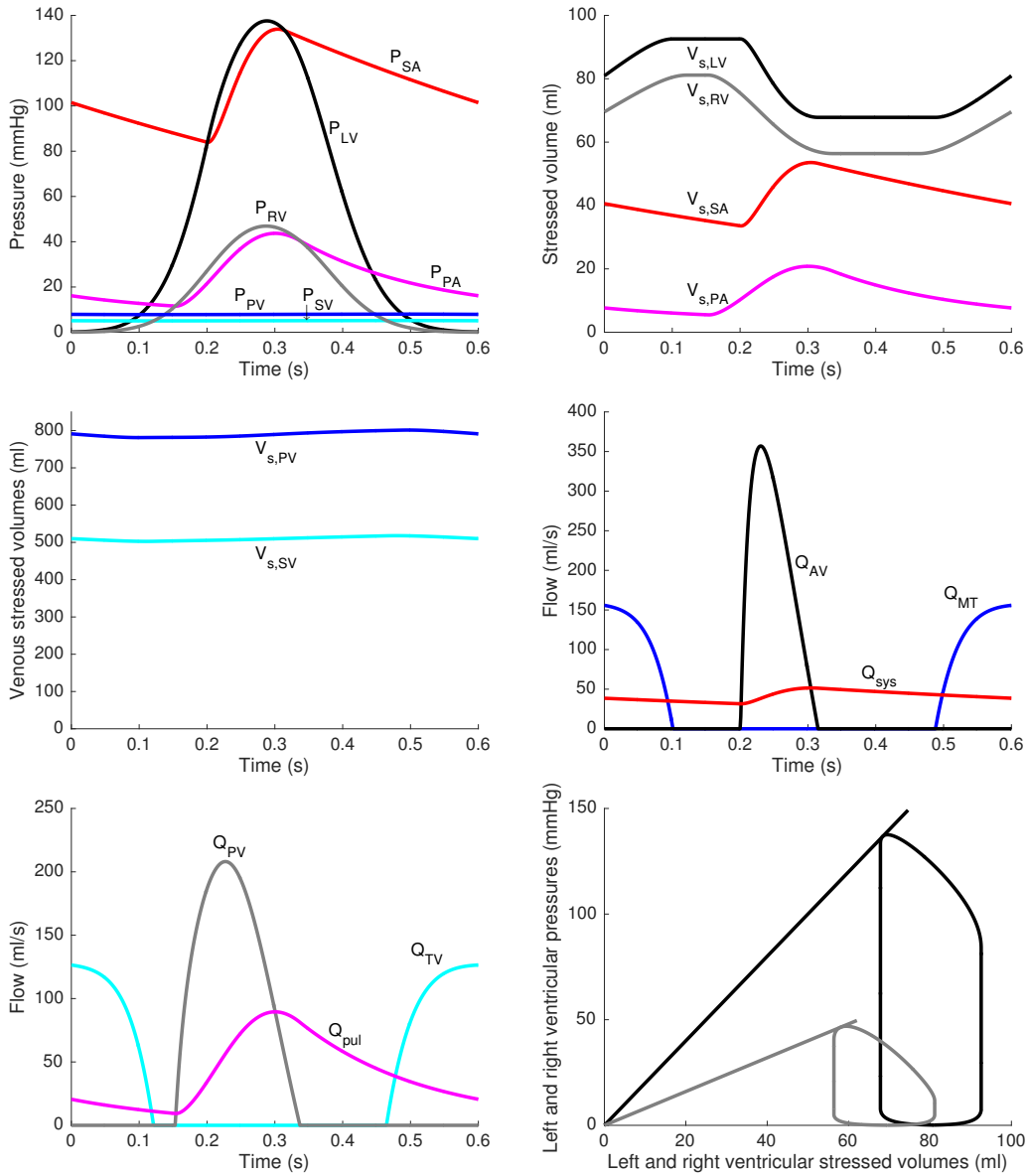

Figure 6.4: Simulation of the six-chamber CVS model using the parameters of Table 6.2. *Top-left:* left (P_{LV}, *black*) and right (P_{RV}, *grey*) ventricular, systemic (P_{SA}, *red*) and pulmonary arterial (P_{PA}, *magenta*), systemic (P_{SV}, *light blue*) and pulmonary venous (P_{PV}, *blue*) pressures. *Top-right:* left ($V_{\mathrm{s,LV}}$, *black*) and right ($V_{\mathrm{s,RV}}$, grey) ventricular, systemic ($V_{\mathrm{s,SA}}$, *red*) and pulmonary arterial ($V_{\mathrm{s,PA}}$, *magenta*) stressed volumes. *Centre-left:* systemic ($V_{\mathrm{s,SV}}$, *light blue*) and pulmonary venous ($V_{\mathrm{s,PV}}$, *blue*) stressed volumes. *Centre-right:* mitral (Q_{MV}, *blue*), aortic valvular (Q_{AV}, *black*) and systemic (Q_{sys}, *red*) flows. *Bottom-left:* tricuspid (Q_{TV}, *light blue*), pulmonary valvular (Q_{PV}, *grey*) and pulmonary (Q_{pul}, *magenta*) flows. *Bottom-right:* left (*black*) and right (*grey*) ventricular pressure-volume loops and the corresponding ESPVRs.

Table 6.2: Parameter values for the simulation of the six-chamber CVS model presented in Figure 6.4.

Parameter	Units	Value
T	s	0.6
E_{LV}	mmHg/ml	2
E_{RV}	mmHg/ml	0.8
E_{SA}	mmHg/ml	2.5
E_{PA}	mmHg/ml	2.1
E_{SV}	mmHg/ml	0.01
E_{PV}	mmHg/ml	0.01
R_{MV}	mmHg s/ml	0.05
R_{AV}	mmHg s/ml	0.04
R_{TV}	mmHg s/ml	0.04
R_{PV}	mmHg s/ml	0.03
R_{sys}	mmHg s/ml	2.5
R_{pul}	mmHg s/ml	0.4
$V_{\mathrm{s},6}$	ml	1500
$e_{\mathrm{LV}}(t)$	-	$\exp\left[-80\left((t \bmod T) - \frac{T}{2}\right)^2\right]$
$e_{\mathrm{RV}}(t)$	-	$\exp\left[-80\left((t \bmod T) - \frac{T}{2}\right)^2\right]$

During ejection, the aorta and pulmonary artery fill up with blood, increasing their pressures until they exceed the ventricular pressures. At this moment, the aortic and pulmonary valve closes, denoting the beginning of isovolumic relaxation. When ventricular pressures drop below upstream venous pressures, the mitral and tricuspid valves open, allowing filling of the ventricles, and the cycle resumes.

The four phases of cardiac contraction, namely filling, isovolumic contraction, ejection and isovolumic relaxation can clearly be distinguished on the two pressure-volume loops of Figure 6.4 (bottom-right).

The model thus captures the fundamental dynamics of the CVS. The choice of a simple driver function as that of Table 6.2 only affects the overall shape of the pressure and volume curves.

6.3.4 Discussion

All comments that were made in Section 6.2.4 regarding the three-chamber model can be reproduced here for the six-chamber model. Here also, the model-based equivalent of SV can be computed as the height of the ventricular stressed volume curves or the width of the pressure-volume loops. The computations yield

$$\Delta V_{\mathrm{s,LV}} = \Delta V_{\mathrm{s,RV}} \approx 25 \text{ ml}. \tag{6.35}$$

The model-based equivalent of CO is equal to:

$$\frac{\Delta V_{\mathrm{s,LV}}}{T} = \frac{\Delta V_{\mathrm{s,RV}}}{T} \approx \frac{25}{0.6} \approx 42 \text{ ml/s}. \tag{6.36}$$

Left and right ventricular model-based SVs and COs are equal, which is to be expected[1] when the CVS model is simulated with constant determinants of CO (contractility, preload, afterload and HR, as explained in Section 2.3.5).

As physiologically expected, pressures in the pulmonary circuit are lower than in the systemic circuit [15]. Left and right ventricular contractions occur at approximately the same time, which is due to the fact that left and right driver functions used in this simulation are identical. However, this behaviour could be made more realistic with small, physiological changes to the driver functions used.

6.3.5 Limitations

The hypotheses underlying the formulation of the six-chamber CVS model are detailed in this section.

No Thoracic Pressure

A more elaborated version of the six-chamber model takes thoracic pressure into account [112]. However, in this work, simulations of the six-chamber model will be compared to measurements obtained during open-chest and open-pericardium experiments, meaning that the effects of thoracic pressure are cancelled. Consequently, for a consistent comparison, these effects were not introduced in the six-chamber model in this study, but can be readily added.

[1] The contrary would imply a constant accumulation of volume in some area of the CVS model.

No Ventricular Interaction

As previously mentioned, ventricular interaction occurs through two structures: the septum, which separates both ventricles, and the pericardium, which encloses the whole heart. Smith *et al.*'s version of the six-chamber model also takes these two structures into account [112]. Santamore and Burkhoff developed another version of the six-chamber model, in wich ventricular interaction can be turned on or off [96].

As explained in the previous section, the measurements to which simulations will be compared are taken during open-chest and open-pericardium experiments. As a consequence, the effects of pericardial pressures are cancelled and ventricular interaction only occurs through the septum. For a consistent comparison with these experimental data, the pericardium was not introduced in the six-chamber model. The effect of the septum, on the other hand, will be merged in the identified values of the parameters E_{LV} and E_{RV}.

No Atria

A version of the six-chamber model in which the left atrium is taken into account using a multi-scale model has been developed by Pironet *et al.* [134]. However, as already mentioned in Section 6.2.5, this multi-scale model involves many parameters, that cannot be identified from data available in an ICU. Hence, it is not used in this study of overall haemodynamics.

No Inertances

Some versions of the six-chamber model also include inertances [98]. For the reasons listed in Section 6.2.5, these elements were not taken into account in the version of the six-chamber model used in this work.

6.4 Summary

This chapter presented two very simple lumped models of the CVS. The models presented were voluntarily kept as simple as possible, so that the number of parameters involved, as listed in Sections 6.2.2 and 6.3.2, was as low as possible. As a result, identification of the model parameters can be performed using smaller amounts of data, typically available in an ICU. Now that the CVS models have been presented, the next part of this work describes how the parameter identification of these models is performed.

Part III

Identification of Cardio-Vascular System Models

Introduction

The goal of parameter identification is to find the model parameter values that make simulations as close as possible to the data. Having discussed the models in Part II, Part III first describes what kind of data is available for parameter identification. Chapter 8 investigates what data is absolutely necessary to perform parameter identification. Chapter 9 discusses the concept of how to practically find the *best* parameter values. Finally, Chapter 10 compares different methods to perform parameter identification.

Chapter 7

Available Data

7.1 Introduction

Parameter identification requires data, and model parameter values are then adjusted so the simulation results are as close as possible to the data. As a consequence, the data of interest must correspond to variables of the previous chapter: pressures, volumes and flows.

In this work, experimental animal data from a haemodynamics laboratory will be used. Since the methodology is aimed to be implemented in the ICU, the data available in an ICU must also be considered. While the type of data recorded remains the same in the laboratory and in the ICU, the available quantity of data and the way to record them are very different. These two settings will therefore be described in two separate sections of the present chapter. Finally, please note that this chapter only presents the sensors needed for the comprehension of the following chapters and thus does not provide an extensive review of all available cardio-vascular monitoring devices.

7.2 Experimental Data

The experimental data used in this work comes from three different sets of experiments performed on pigs. These experiments were performed in the Haemodynamics Laboratory of the GIGA-Cardiovascular Siences (University of Liège), with the approval of the Ethics Commission for the Use of Animals at the University of Liège. The experimental procedures are detailed in Chapters 11 and 12, while the sensors used during these experiments are described in the present section.

7.2.1 Pressure Catheters

In a haemodynamics laboratory, pressure catheters are the most commonly used data acquisition devices. Such catheters are tipped with a piezoelectric pressure sensor [114], which is able, after a calibration step, to measure pressure changes with respect to atmospheric pressure. Such sensors can then be positioned in a wide range of anatomical locations, such as the aorta, vena cava, left atrium, pulmonary artery, and others. They can then provide the continuous evolution of pressures in these areas.

7.2.2 Pressure-Volume Catheters

As their name indicates, pressure-volume catheters are able to simultaneously measure pressure and the volume of blood surrounding them. This dual measurement is particularly useful to plot ventricular pressure-volume loops, such as the one presented in Figure 5.1. They thus measure the fundamental CVS curve directly at its location.

The principle of pressure measurement is similar to the one presented in the previous section. To measure blood volume, the pressure-volume catheter actually measures the electric conductance, the inverse of resistance, of the surrounding blood. In more detail, the catheter consists of several electrode pairs [158,159]. A small alternating current is applied between the two extreme electrodes and the voltage is measured between a pair of inner electrodes, as illustrated in use in Figure 7.1. From the knowledge of current and voltage, the conductance can be derived. The total conductance is, in turn, proportional to the blood volume around the catheter [158, 159].

The main disadvantage of the conductance method is that the measured conductance also takes into account the conductance of the tissues surrounding the blood [158, 159]. Various methods have been designed to estimate the conductance of the tissues. These methods include the injection of saline solution, which changes the conductance of the blood, but not that of the tissues.

Another way of estimating the conductance of tissues makes use of the alternating nature of voltages and currents [159,160]. In that case, the resulting signal is called *admittance*. Because blood and tissue have different frequency responses, their contributions to the total admittance can be separated.

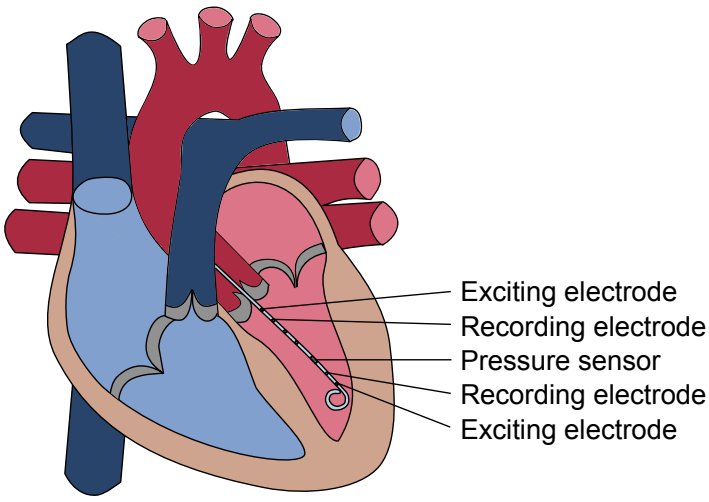

Figure 7.1: Illustration of a pressure-volume catheter (adapted from [13], with permission).

7.3 Clinical Data

7.3.1 Pressure-Volume Catheters

The use of pressure-volume catheters is very rare in the ICU. Indeed, such catheters are meant to be placed into the ventricles, which is a highly invasive procedure. Hence, they are not usually used clinically on humans.

7.3.2 Pressure Catheters

Pressure sensors used in the ICU rely on a different principle from those used in the laboratory. They consist of a needle introduced in the vessel of interest, which is often a peripheral vessel, such as the inferior vena cava or the femoral, radial, brachial or axillary arteries [18]. Behind the needle is a plastic catheter filled with saline fluid. Hence, the name *fluid-filled* catheter. Pressure is transmitted by the two fluids, blood and saline, through the catheter to a pressure transducer located at the end of the catheter [114].

7.3.3 The Pulmonary Artery Catheter

The pulmonary artery catheter is often referred to using the name of its designers, Swan and Ganz. As its name indicates, the first purpose of this catheter is measurement of pulmonary arterial pressure. What differentiates it from other pressure catheters is the presence of a balloon at its tip, which helps correctly position the catheter in the pulmonary artery.

The placing of a pulmonary artery catheter is illustrated in Figure 7.2. The pulmonary artery catheter is first inserted through the subclavian or jugular vein [18]. It is then advanced in the superior vena cava, where the balloon is inflated to help the catheter follow the blood flow. Thanks to the balloon, the catheter can be advanced into the right atrium, then into the right ventricle. The pressure curves provided by the catheter help in knowing its current position [18]. The catheter is then pushed through the pulmonary valve into the pulmonary artery.

The catheter is again pushed further, until it gets wedged in a pulmonary artery. Because the catheter is wedged, it prevents blood from flowing in the vessel. Consequently, the pressure measured at the tip of the balloon, called the *pulmonary artery occlusion pressure (PAOP)* or the the *wedge pressure* [161], is a reflection of the downstream pressures, namely pulmonary venous pressure and left atrial pressure.

Finally, the balloon is deflated while the catheter is left at its current position, thereby allowing blood to flow in the pulmonary artery. The catheter now provides a measurement of pulmonary arterial pressure.

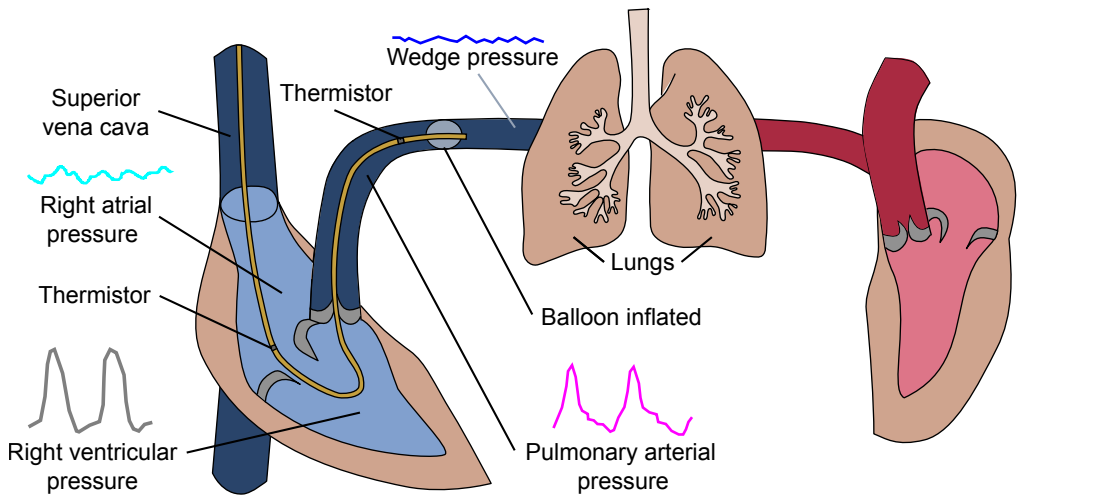

Figure 7.2: Illustration of the placement of a pulmonary artery catheter.

Pulmonary artery catheters also contain two thermistors, which are temperature sensors. The first is located close to the tip of the catheter and the second one, further from the balloon. When the catheter is correctly positioned, the first thermistor should be located in the pulmonary artery and the second one, in the right atrium [18]. These sensors can be used for measurement of CO by thermodilution, as explained in the next section.

7.3.4 Thermodilution

The thermodilution technique allows determination of CO [18]. It requires two thermistors, usually located upstream and downstream of the heart [161]. Before the thermodilution, the blood temperature upstream and downstream of the heart is equal to T_b. To estimate CO, a given volume, V_i, of cold fluid (at temperature T_i) is quickly injected at the upstream site. The cold fluid subsequently enters the heart, before being ejected. When the cold fluid progressively reaches the downstream thermistor, a drop in the downstream temperature, $T_d(t)$, is detected. The downstream temperature goes back to normal at a rate that is directly proportional to the blood flow, in other words, to the CO.

Mathematically speaking, the relation reads:

$$\mathrm{CO} = \frac{(T_b - T_i)V_i K}{\int_0^{+\infty} (T_b - T_d(t))\,\mathrm{d}t} \tag{7.1}$$

where K is a correction constant [161]. The previous equation is often called the *Stewart-Hamilton equation*. A *thermodilution curve* refers to a plot of $T_b - T_d(t)$. Such a curve is depicted in Figure 7.3.

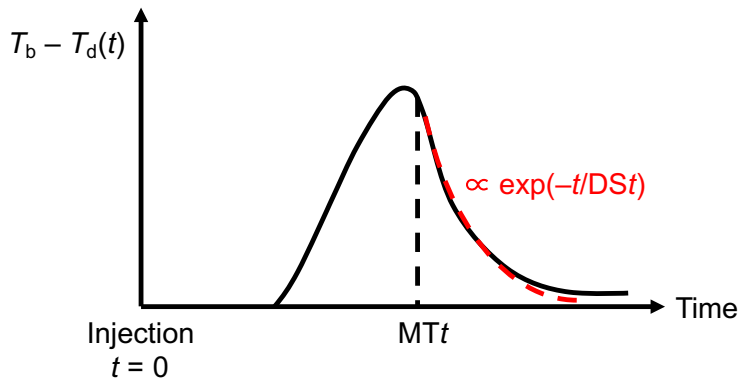

Figure 7.3: Example of a thermodilution curve.

7.3.5 The PiCCO

The PiCCO is a hemodynamic monitoring device manufactured by Pulsion AG (Germany). Its placement is depicted in Figure 7.4. The PiCCO requires the use of arterial and venous catheters, located in the femoral artery and superior vena cava in Figure 7.4. These two catheters are fluid-filled pressure catheters. The arterial catheter can also measure temperature through a thermistor [162, 163].

The purpose of the thermistor is to provide an estimate of CO using thermodilution. With the PiCCO, as for the pulmonary artery catheter, the cold fluid

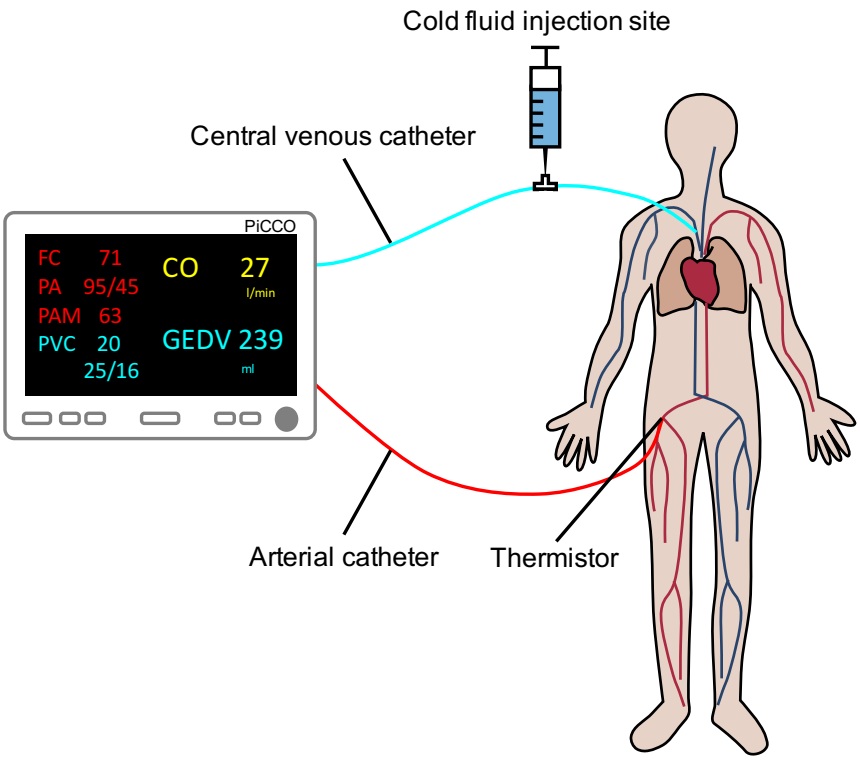

Figure 7.4: Illustration of the PiCCO monitoring device.

is injected in the superior vena cava [163]. However, with the PiCCO, the cold fluid goes through both the right and left sides of the heart, as illustrated in Figure 7.5, before being detected by the thermistor located in the femoral artery. The cold fluid thus goes through the whole pulmonary circulation before being detected. Therefore, this version of the thermodilution method is called *transpulmonary thermodilution* [162, 163].

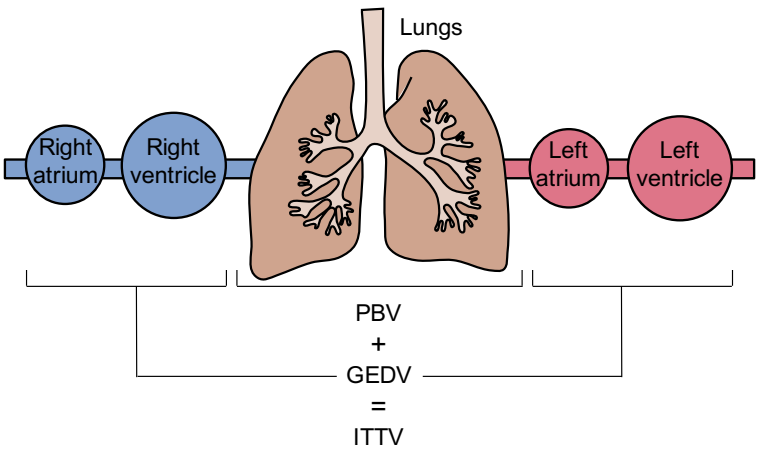

Figure 7.5: Overview of the structures through which the cold fluid goes during a transpulmonary thermodilution.

During the transpulmonary thermodilution, the cold fluid is successively pumped in the right atrium, right ventricle, lungs, left atrium, left ventricle and in the arteries, as shown in Figure 7.5. Thanks to the thermodilution curve, the PiCCO is also able to provide estimates of several pulmonary and cardiac volumes [162]. Among these volumes, the first one is the intrathoracic thermal volume (ITTV). It is the volume through which a temperature drop is felt during the transpulmonary thermodilution process. It consists of blood in the heart, lung water, and a fraction of the heart and vessel walls. It is computed:

$$\mathrm{ITTV} = \mathrm{CO}\,\mathrm{MT}t \tag{7.2}$$

where MTt is the mean transit time of the cold fluid [161], as depicted in Figure 7.3. The second volume of interest is the pulmonary blood volume (PBV). It can be determined by knowing that the transpulmonary thermodilution curve decays in an exponential fashion, as exemplified in Figure 7.3. The time constant of the exponential decay is called the *downslope time* (DSt). It is determined by the volume of the largest compartment through which the fluid circulates, the lungs [161]. Consequently, the PBV can be determined from the DSt:

$$\mathrm{PBV} = \mathrm{CO}\,\mathrm{DS}t. \tag{7.3}$$

Finally, the volume of the combined four heart chambers, called the *global end-diastolic volume (GEDV)*, can be estimated by subtracting PBV from ITTV:

$$\mathrm{GEDV} = \mathrm{ITTV} - \mathrm{PBV}. \tag{7.4}$$

In addition, the PiCCO uses the thermodilution-derived CO to compute the parameters of its own mathematical model for CO. This approach allows beat-to-beat estimation of CO, while the thermodilution only provides intermittent values of CO. This continuous estimation of CO is reliable as long as arterial properties do not change [164]. Otherwise, the system must be recalibrated using a new thermodilution.

Finally, thanks to the catheter placed in the femoral artery, the PiCCO is able to continuously compute the PPV index of fluid responsiveness [21]. In addition, the continuous estimation of CO allows the PiCCO to continuously display the SVV index of fluid responsiveness [162]. Note that the PPV and SVV indices were introduced in Section 3.4.

7.4 Summary

This chapter presented the data available in the two settings investigated in this work: the animal laboratory and the ICU. In the animal laboratory, pressures can be measured in nearly any location of the CVS using dedicated catheters. Furthermore, ventricular volumes are also accessible, using ventricular pressure-volume catheters.

However, in the ICU, ventricular volumes are typically not accessible and measured pressures are usually peripheral ones. Consequently, to obtain cardiac information such as CO, the thermodilution technique is often used. Two devices were presented with which this technique can be performed: the pulmonary artery catheter and the PiCCO. Both of these devices are able to measure a wide range of other useful parameters, which will be of interest in the rest of this work.

Chapter 8

Structural identifiability

8.1 Introduction

Chapter 6 presented two different mathematical models of the CVS. For these models to be clinically relevant, they should be able to reproduce any given patient's condition. To do so, the model parameters, presented in Tables 6.2.2 and 6.3.2, have to be identified from measured data so that simulations of the models match the clinical data. This task is not obvious due to the indirect nature of the typically available clinical data, as explained in Chapter 7.

Importantly, as will be shown in this chapter, there are several measurement sets from which the parameters of these models cannot be uniquely computed. The key question is thus: *can we find a measurement set that allows unique identification of all model parameters?* In more theoretical terms, this question can be stated as: *what is the set of model outputs one has to include in the model definition for the model to be structurally globally identifiable?*

8.1.1 Structural Identifiability

Structural identifiability analysis of a model determines whether all model parameters can be uniquely retrieved under perfect conditions of noise-free and continuous measurements of the model outputs. If the answer is yes, then the model is said to be *structurally globally identifiable* [165, 166]. Otherwise, if there exists multiple parameter values for the given model outputs, the model is *structurally locally identifiable* to a set of limited possible values. Finally, if there is an infinite number of possible parameter values, the model is termed *structurally non-identifiable* and no unique values can be retrieved.

Structural identifiability is called structural because it only depends on the model structure, that is, its equations. Therefore, it depends on the roles of the parameters and the nature and number of the available model outputs. For in-

stance, if the number of model outputs is too low with respect to to the number of parameters to identify, the model is likely to be non-identifiable, and there will not be enough unique measurements to separate parameter values.

Taking the measurement noise and the practically finite number of data points into account and investigating if the model parameters can still be uniquely determined relates to a different topic, called practical identifiability [167], and discussed in Chapter 9. Structural identifiability is a necessary condition for practical identifiability. It is therefore risky to perform a parameter identification procedure on a model that has not been shown to be structurally identifiable.

8.1.2 Goal

This chapter aims to prove the structural identifiability of the three-chamber model described in Section 6.2 from a typical clinically available output set. As said above, this structural identifiability analysis is a necessary step to ensure that results obtained when identifying the model parameters from limited clinical data are unique, and thus, relevant.

8.2 Methods

8.2.1 Parameter Set

The model is defined in Equations 6.1 to 6.11 and the parameter set to identify, $\mathbf{p}$, consists of seven elements:

$$\mathbf{p} = (E_\mathrm{a}\ E_\mathrm{v}\ E_\mathrm{h}\ R_\mathrm{i}\ R_\mathrm{o}\ R_\mathrm{c}\ V_{\mathrm{s},3}). \tag{8.1}$$

This parameter set is different from the list in Section 6.2.2 because the cardiac period, T, and the driver function, $e(t)$ are missing. The cardiac period is indeed trivial to obtain from any haemodynamic signal, and the form of the driver function does not matter in the following specific analysis, as long as it is T-periodic and ranges from 0 (diastole) to 1 (end-systole).

8.2.2 Output Sets

In this section, three different model output sets, $\mathbf{y}^k$ ($k = 1$, 2 or 3), are proposed for the three-chamber model. Structural identifiability of the model is then assessed for each of these output sets.

Output Set $\mathbf{y}^1$ Containing Only Volumes

To show a first example of structural non-identifiability, it is assumed that all chamber stressed volumes are model outputs. Consequently, the outputs of the three-chamber model are:

- Stressed volume in the arteries, $V_{\mathrm{s,a}}(t)$,
- Stressed volume in the veins, $V_{\mathrm{s,v}}(t)$,
- Stressed volume in the heart, $V_{\mathrm{s,h}}(t)$,

and the output set is:

$$\mathbf{y}^1 = (V_{\mathrm{s,a}}(t)\ V_{\mathrm{s,v}}(t)\ V_{\mathrm{s,h}}(t)). \tag{8.2}$$

Output Set $\mathbf{y}^2$ Containing Only Pressures

For the second example of structural non-identifiability, it is assumed that all chamber pressures are model outputs. Consequently, the outputs of the three-chamber model are:

- Pressure in the arteries, $P_{\mathrm{a}}(t)$,
- Pressure in the veins, $P_{\mathrm{v}}(t)$,
- Pressure in the heart, $P_{\mathrm{h}}(t)$,

and the output set is:

$$\mathbf{y}^2 = (P_{\mathrm{a}}(t)\ P_{\mathrm{v}}(t)\ P_{\mathrm{h}}(t)). \tag{8.3}$$

Clinically Available Output Set $\mathbf{y}^3$

Finally, to show structural identifiability, the outputs of the three-chamber model are chosen to be the following clinically available measurements:

- Pressure in the arteries, $P_{\mathrm{a}}(t)$,
- Pressure in the veins, $P_{\mathrm{v}}(t)$,
- Integral of the ejected flow during one cardiac period, $\int_0^T Q_{\mathrm{o}}(t)\ \mathrm{d}t$.

The availability of these measurements in a clinical setting is explained in Section 8.4. The output set is thus defined:

$$\mathbf{y}^3 = \left(P_{\mathrm{a}}(t)\ P_{\mathrm{v}}(t)\ \int_0^T Q_{\mathrm{o}}(t)\ \mathrm{d}t\right). \tag{8.4}$$

8.3 Results

As previously mentioned, there are certain measurement sets from which the model parameters cannot be uniquely determined. In these cases, the model is structurally non-identifiable. Two such cases are first described in this section.

8.3.1 Output Set $\mathbf{y}^1$ Containing Only Volumes

From the model equations, it can be seen that all simulated volumes will be exactly the same if all elastances, E_a, E_v and E_h, and resistances, R_i, R_o and R_c, are multiplied by the same factor. Indeed, expressing Equations 6.7, 6.8 and 6.9 solely in terms of volumes by substituting pressures and flows using Equations 6.1 to 6.6 results in:

$$\frac{\mathrm{d}V_{\mathrm{s,h}}(t)}{\mathrm{d}t} = \mathrm{r}\left[\frac{E_\mathrm{v}V_{\mathrm{s,v}}(t) - E_\mathrm{h}e(t)V_{\mathrm{s,h}}(t)}{R_\mathrm{i}}\right] - \mathrm{r}\left[\frac{E_\mathrm{h}e(t)V_{\mathrm{s,h}}(t) - E_\mathrm{a}V_{\mathrm{s,a}}(t)}{R_\mathrm{o}}\right] \tag{8.5}$$

$$\frac{\mathrm{d}V_{\mathrm{s,a}}(t)}{\mathrm{d}t} = \mathrm{r}\left[\frac{E_\mathrm{h}e(t)V_{\mathrm{s,h}}(t) - E_\mathrm{a}V_{\mathrm{s,a}}(t)}{R_\mathrm{o}}\right] - \frac{E_\mathrm{a}V_{\mathrm{s,a}}(t) - E_\mathrm{v}V_{\mathrm{s,v}}(t)}{R_\mathrm{c}} \tag{8.6}$$

$$\frac{\mathrm{d}V_{\mathrm{s,v}}(t)}{\mathrm{d}t} = \frac{E_\mathrm{a}V_{\mathrm{s,a}}(t) - E_\mathrm{v}V_{\mathrm{s,v}}(t)}{R_\mathrm{c}} - \mathrm{r}\left[\frac{E_\mathrm{v}V_{\mathrm{s,v}}(t) - E_\mathrm{h}e(t)V_{\mathrm{s,h}}(t)}{R_\mathrm{i}}\right], \tag{8.7}$$

where $\mathrm{r}(x)$ is the ramp function, defined:

$$\mathrm{r}(x) = \begin{cases} x & \text{if } x > 0 \\ 0 & \text{otherwise.} \end{cases} \tag{8.8}$$

Equations 8.5 to 8.7 only involve the following ratios of elastances to resistances:

$$\frac{E_\mathrm{v}}{R_\mathrm{i}}, \frac{E_\mathrm{h}}{R_\mathrm{i}}, \frac{E_\mathrm{h}}{R_\mathrm{o}}, \frac{E_\mathrm{a}}{R_\mathrm{o}}, \frac{E_\mathrm{a}}{R_\mathrm{c}}, \frac{E_\mathrm{v}}{R_\mathrm{c}}. \tag{8.9}$$

Therefore, including only stressed volumes in the output vector results in a case of structural non-identifiability.

8.3.2 Output Set $\mathbf{y}^2$ Containing Only Pressures

Once again, from the model equations, it can be seen that all simulated pressures will be exactly the same if all elastances , E_a, E_v and E_h, and resistances, R_i, R_o and R_c, are multiplied by the same factor, while $V_{\mathrm{s},3}$ is divided by this factor. Hence, like the first case, it is not structurally identifiable as there is an infinite number of such multipliers.

8.3.3 Clinically Available Output Set $\mathbf{y}^3$

It can be shown that all seven parameters of the three-chamber model can be uniquely retrieved from the output set $\mathbf{y}^3$. The corresponding demonstration is quite technical and is provided in the following section. This outcome, in turn, proves that the three-chamber CVS model is structurally globally identifiable from these specific output signals. Consequently, given all required mea-

surements of the outputs, there exists one and only one possible parameter set corresponding to these measurements, a unique solution.

8.3.4 Demonstration of Structural Identifiability from the Third Output Set, $\mathbf{y}^3$

To perform the structural identifiability of a model, it is assumed that the outputs can be perfectly and continuously measured [168]. Consequently, they can be differentiated as much as necessary. As a reminder, the outputs of the three-chamber model were chosen to be:

- Pressure in the arteries, $P_\mathrm{a}(t)$,
- Pressure in the veins, $P_\mathrm{v}(t)$,
- Integral of the ejected flow during one cardiac period, $\int_0^T Q_\mathrm{o}(t)\,\mathrm{d}t$.

Furthermore, it will also be assumed that the driver function, $e(t)$, is known.

In the following sections, it is shown that unique relationships can be established between the seven model parameters in $\mathbf{p}$ and the three model outputs in $\mathbf{y}^3$ in Equation 8.4. This outcome implies that the three-chamber model is identifiable from this output set.

During the Whole Cardiac Cycle

Integrating Equation 6.4 over a whole heartbeat, from $= 0$ to $t = T$, yields:

$$\int_0^T Q_\mathrm{c}(t)\,\mathrm{d}t = \frac{\int_0^T [P_\mathrm{a}(t) - P_\mathrm{v}(t)]\,\mathrm{d}t}{R_\mathrm{c}}. \tag{8.10}$$

Rearranging this equation gives:

$$R_\mathrm{c} = \frac{\int_0^T [P_\mathrm{a}(t) - P_\mathrm{v}(t)]\,\mathrm{d}t}{\int_0^T Q_\mathrm{c}(t)\,\mathrm{d}t}. \tag{8.11}$$

This result shows that the parameter R_c is the model-based equivalent of the SVR, introduced in Section 2.3.4.

Integrating Equation 6.8 during one cardiac cycle gives:

$$\int_0^T \frac{\mathrm{d}V_\mathrm{s,a}(t)}{\mathrm{d}t}\,\mathrm{d}t = \int_0^T Q_\mathrm{o}(t)\,\mathrm{d}t - \int_0^T Q_\mathrm{c}(t)\,\mathrm{d}t \tag{8.12}$$

$$\Leftrightarrow V_\mathrm{s,a}(T) - V_\mathrm{s,a}(0) = \int_0^T Q_\mathrm{o}(t)\,\mathrm{d}t - \int_0^T Q_\mathrm{c}(t)\,\mathrm{d}t. \tag{8.13}$$

Since the simulated signals are all T-periodic, the left-hand side is equal to zero, leading directly to:

$$\int_0^T Q_\mathrm{o}(t)\,\mathrm{d}t = \int_0^T Q_\mathrm{c}(t)\,\mathrm{d}t. \tag{8.14}$$

Combining Equations 8.11 and 8.14 gives:

$$R_\mathrm{c} = \frac{\int_0^T [P_\mathrm{a}(t) - P_\mathrm{v}(t)]\,\mathrm{d}t}{\int_0^T Q_\mathrm{o}(t)\,\mathrm{d}t}, \tag{8.15}$$

Equation 8.15 makes it possible to compute R_c, since all elements of the right-hand side are known.

During Ejection

At the beginning of ejection, $t = t_\mathrm{BE}$, cardiac pressure equals arterial pressure:

$$P_\mathrm{a}(t_\mathrm{BE}) = P_\mathrm{h}(t_\mathrm{BE}). \tag{8.16}$$

Using Equation 6.3 gives:

$$P_\mathrm{a}(t_\mathrm{BE}) = E_\mathrm{h} e(t_\mathrm{BE}) V_\mathrm{s,h}(t_\mathrm{BE}) \tag{8.17}$$

$$\Leftrightarrow V_\mathrm{s,h}(t_\mathrm{BE}) = \frac{P_\mathrm{a}(t_\mathrm{BE})}{E_\mathrm{h} e(t_\mathrm{BE})} \tag{8.18}$$

Similarly, at the end of ejection, $t = t_\mathrm{EE}$, cardiac pressure once again equals arterial pressure:

$$P_\mathrm{a}(t_\mathrm{EE}) = P_\mathrm{h}(t_\mathrm{EE}) \tag{8.19}$$

$$= E_\mathrm{h} e(t_\mathrm{EE}) V_\mathrm{s,h}(t_\mathrm{EE}) \tag{8.20}$$

$$\Leftrightarrow V_\mathrm{s,h}(t_\mathrm{EE}) = \frac{P_\mathrm{a}(t_\mathrm{EE})}{E_\mathrm{h} e(t_\mathrm{EE})} \tag{8.21}$$

Integrating Equation 6.7 during ejection results in:

$$\int_{t_\mathrm{BE}}^{t_\mathrm{EE}} \frac{\mathrm{d}V_\mathrm{s,h}(t)}{\mathrm{d}t}\,\mathrm{d}t = \int_{t_\mathrm{BE}}^{t_\mathrm{EE}} Q_\mathrm{i}\,\mathrm{d}t - \int_{t_\mathrm{BE}}^{t_\mathrm{EE}} Q_\mathrm{o}\,\mathrm{d}t \tag{8.22}$$

$$\Leftrightarrow V_\mathrm{s,h}(t_\mathrm{EE}) - V_\mathrm{s,h}(t_\mathrm{BE}) = \int_{t_\mathrm{BE}}^{t_\mathrm{EE}} Q_\mathrm{i}\,\mathrm{d}t - \int_{t_\mathrm{BE}}^{t_\mathrm{EE}} Q_\mathrm{o}\,\mathrm{d}t. \tag{8.23}$$

During ejection, flow going into the heart, Q_i, is equal to zero. In addition, flow going out of the heart, Q_o, is different from zero only during ejection. Conse-

quently, Equation 8.23 can also be written:

$$V_{\mathrm{s,h}}(t_{\mathrm{EE}}) - V_{\mathrm{s,h}}(t_{\mathrm{BE}}) = -\int_0^T Q_{\mathrm{o}}\,\mathrm{d}t. \tag{8.24}$$

Combining Equations 8.18, 8.21 and 8.24 gives:

$$\frac{P_{\mathrm{a}}(t_{\mathrm{EE}})}{E_{\mathrm{h}}e(t_{\mathrm{EE}})} - \frac{P_{\mathrm{a}}(t_{\mathrm{BE}})}{E_{\mathrm{h}}e(t_{\mathrm{BE}})} = -\int_0^T Q_{\mathrm{o}}\,\mathrm{d}t. \tag{8.25}$$

$$\Leftrightarrow E_{\mathrm{h}} = \frac{1}{\int_0^T Q_{\mathrm{o}}\,\mathrm{d}t}\left(\frac{P_{\mathrm{a}}(t_{\mathrm{BE}})}{e(t_{\mathrm{BE}})} - \frac{P_{\mathrm{a}}(t_{\mathrm{EE}})}{e(t_{\mathrm{EE}})}\right). \tag{8.26}$$

Since the right side of Equation 8.26 is known, it provides the second identifiable parameter E_{h}.

During cardiac ejection, the input valve is closed because cardiac pressure is higher than venous pressure, $P_{\mathrm{h}}(t) > P_{\mathrm{v}}(t)$. Consequently, the combination of Equations 6.4, 6.5 and 6.9 can be written:

$$\frac{\mathrm{d}V_{\mathrm{s,v}}(t)}{\mathrm{d}t} = Q_{\mathrm{c}} = \frac{P_{\mathrm{a}}(t) - P_{\mathrm{v}}(t)}{R_{\mathrm{c}}} \tag{8.27}$$

Combining this equation with Equation 6.2 gives:

$$\frac{\mathrm{d}P_{\mathrm{v}}(t)}{\mathrm{d}t} = E_{\mathrm{v}}\frac{P_{\mathrm{a}}(t) - P_{\mathrm{v}}(t)}{R_{\mathrm{c}}}. \tag{8.28}$$

Equation 8.28 thus shows that E_{v} is identifiable, since R_{c} is already known:

$$E_{\mathrm{v}} = \frac{\mathrm{d}P_{\mathrm{v}}(t)}{\mathrm{d}t}\frac{R_{\mathrm{c}}}{P_{\mathrm{a}}(t) - P_{\mathrm{v}}(t)}. \tag{8.29}$$

Since the data is assumed to be perfect, the right-hand side of Equation 8.29 is exactly equal to E_{v} at any time during cardiac ejection.

During Filling

During cardiac filling, $P_{\mathrm{a}}(t) > P_{\mathrm{h}}(t)$, and the combination of Equations 6.4, 6.6 and 6.8 gives:

$$\frac{\mathrm{d}V_{\mathrm{s,a}}(t)}{\mathrm{d}t} = -Q_{\mathrm{c}} = -\frac{P_{\mathrm{a}}(t) - P_{\mathrm{v}}(t)}{R_{\mathrm{c}}}. \tag{8.30}$$

Using Equation 6.1, Equation 8.30 becomes:

$$\frac{\mathrm{d}P_{\mathrm{a}}(t)}{\mathrm{d}t} = -E_{\mathrm{a}}\frac{P_{\mathrm{a}}(t) - P_{\mathrm{v}}(t)}{R_{\mathrm{c}}}. \tag{8.31}$$

This equation can be solved for E_a, proving that this parameter is identifiable:

$$E_a = -\frac{dP_a(t)}{dt}\frac{R_c}{P_a(t) - P_v(t)}. \tag{8.32}$$

Since the data is assumed to be perfect, the right-hand side of Equation 8.32 is entirely known and exactly equal to E_a at any time during cardiac filling.

During cardiac filling, $P_v(t) > P_h(t)$, thus flow through the input valve is positive. The combination of Equations 6.2, 6.4, 6.5 and 6.9 yields:

$$\frac{dP_v(t)}{dt} = E_v\left(\frac{P_a(t) - P_v(t)}{R_c} - \frac{P_v(t) - P_h(t)}{R_i}\right). \tag{8.33}$$

If Equation 8.33 is differentiated once more, the result is:

$$\frac{d^2P_v(t)}{dt^2} = E_v\left[\frac{1}{R_c}\left(\frac{dP_a(t)}{dt} - \frac{dP_v(t)}{dt}\right) - \frac{1}{R_i}\left(\frac{dP_v(t)}{dt} - \frac{dP_h(t)}{dt}\right)\right]. \tag{8.34}$$

To eliminate $dP_h(t)/dt$, the derivative of Equation 6.3 can be used:

$$\frac{dP_h(t)}{dt} = E_h\frac{de(t)}{dt}V_{s,h}(t) + E_h e(t)\frac{dV_{s,h}(t)}{dt}. \tag{8.35}$$

To eliminate the unknown $dV_{s,h}(t)/dt$ from Equation 8.35, the combination of Equations 6.5, 6.6 and 6.7 during filling yields:

$$\frac{dV_{s,h}(t)}{dt} = \frac{P_v(t) - P_h(t)}{R_i}. \tag{8.36}$$

The algebraic system formed by Equations 6.3, 8.33, 8.34, 8.35 and 8.36 has five equations and five unknowns, R_i, P_h, V_h, $dP_h(t)/dt$ and $dV_{s,h}(t)/dt$. Solving this system with a symbolic computation software (Mathematica Version 8.0, Wolfram Research Inc., Champaign, IL) shows that it has a unique solution for all t. The uniqueness of the solution, in turn, guarantees the identifiability of the parameter R_i. It also provides the curve of $V_{s,h}(t)$ during filling, which will be useful further in this demonstration.

Since arterial and venous pressures are known, as well as the elastances of the two corresponding chambers, E_a and E_v, stressed volume in these chambers can be obtained from Equations 6.1 and 6.2. And, since cardiac volume $V_{s,h}(t)$ is now also known, $V_{s,3}$ can be computed from its definition, Equation 6.11:

$$V_{s,3} = V_{s,h}(t) + V_{s,a}(t) + V_{s,v}(t) = V_{s,h}(t) + \frac{P_a(t)}{E_a} + \frac{P_v(t)}{E_v}. \tag{8.37}$$

During Ejection (Continued)

The knowledge of arterial elastance E_a from the previous section now makes it possible to obtain the value of the output valve resistance, R_o. To do so, it is necessary to return to the ejection phase and to apply a reasoning similar to the one used to compute the input valve resistance, R_i. During cardiac ejection, $P_h(t) > P_a(t)$, flow through the output valve is positive. The combination of Equations 6.1, 6.4, 6.6 and 6.8 now yields:

$$\frac{dP_a(t)}{dt} = E_a \left(\frac{P_h(t) - P_a(t)}{R_o} - \frac{P_a(t) - P_v(t)}{R_c} \right). \tag{8.38}$$

If Equation 8.38 is differentiated once more, the result is:

$$\frac{d^2P_a(t)}{dt^2} = E_a \left[\frac{1}{R_o} \left(\frac{dP_h(t)}{dt} - \frac{dP_a(t)}{dt} \right) - \frac{1}{R_c} \left(\frac{dP_a(t)}{dt} - \frac{dP_v(t)}{dt} \right) \right]. \tag{8.39}$$

The combination of Equations 6.5, 6.6 and 6.7 during ejection yields:

$$\frac{dV_{s,h}(t)}{dt} = -\frac{P_h(t) - P_a(t)}{R_o}. \tag{8.40}$$

The algebraic system formed by Equations 6.3, 8.35, 8.38, 8.39 and 8.40 has five equations and five unknowns, R_o, P_h, V_h, $dP_h(t)/dt$ and $dV_{s,h}(t)/dt$. Solving this system shows that it has a unique solution for all t. This outcome, in turn, guarantees the identifiability of the parameter R_o.

All seven model parameters have thus been shown to be computable from the selected set of model outputs, which implies that the three-chamber model is structurally globally identifiable from this set of model outputs. For a better understanding, the demonstration exposed above is summarised in Table 8.1. Each model parameter involved is linked with the equation(s) used to compute it from the output set $\mathbf{y}^3$.

8.4 Discussion

The aim of this chapter was to investigate the structural identifiability of the three-chamber CVS model, from three different output sets. The property of being structurally identifiable guarantees that all model parameters can be uniquely retrieved under the assumption of perfect measurement of the outputs. If a model cannot be shown to be structurally identifiable, performing parameter identification using real data is risky, because there is no guarantee that the resulting parameter values are unique.

Table 8.1: Summary of the demonstration of structural identifiability of the three-chamber CVS model.

Parameter	Corresponding equation(s)
R_c	8.15
E_h	8.26
E_v	8.29
E_a	8.32
R_i	6.3, 8.33, 8.34, 8.35 and 8.36
$V_{s,3}$	8.37
R_o	6.3, 8.35, 8.38, 8.39 and 8.40

The first output set, $\mathbf{y}^1$, contained stressed volumes in all three model chambers and using it resulted in a case of structural non-identifiability. Two conclusions can be derived from this result. First, the model will also be structurally non-identifiable from any output set that is a subset of $\mathbf{y}^1$, in other words, that contains only stressed volumes in part of the model chambers. Second, it can be stated that an adequate output set for this CVS model has to contain more information than only stressed volumes. For example, uniquely identifying an elastance parameter requires both volume and pressure.

Similarly, the second output set, $\mathbf{y}^2$, contained pressures in all three model chambers and also resulted in a case of structural non-identifiability. This second result implies that the model will also be non-identifiable from an output set containing only pressures in part of the model chambers. Thus, similarly, an adequate output set for the three-chamber CVS model must include more information than only pressures.

Taking these two observations together results in the conclusion that an adequate output set for the three-chamber model must combine information on both pressures and stressed volumes for the model to potentially be structurally identifiable. However, due to the lumped nature of the model and technical limitations, chamber stressed volumes are actually very difficult to measure. Hence, only one unavoidable volume measurement, the integral of the ejected flow during one cardiac period, $\int_0^T Q_o(t)\,\mathrm{d}t$, was included in the third output set, $\mathbf{y}^3$. The rest of this set consisted of arterial and venous pressures. The model was then shown to be structurally identifiable from this output set.

The measurements contained in $\mathbf{y}^3$ can readily be obtained in an ICU setting. First, the integral of the ejected flow during one cardiac period, $\int_0^T Q_o(t)\,\mathrm{d}t$, is a model-based equivalent of SV and can thus be determined using thermodilution, as explained in Section 7.3.4. In addition, model-based methods for real-time

measurement of SV are emerging [169]. Second, systemic arterial pressure and vena cava pressure can be obtained using arterial and central venous lines.

The three-chamber CVS model was thus shown to be structurally globally identifiable from a limited output set containing arterial and venous pressures and SV. However, this limited measurements set might still be reduced. It would thus be useful to investigate the structural identifiability of all model parameters from other output sets, either smaller or containing different outputs.

To reduce the number of model outputs, additional assumptions may be suitable. For instance, these assumptions can take the form of a definition of a relation between parameters. Another way to reduce the size of the output set is to fix some model parameters. For instance, a second demonstration, performed in Appendix A, shows that, if valve resistances are not identified, the remaining parameters can be identified using an output set $\mathbf{y}^4$ containing only arterial pressure, $P_{\mathrm{a}}(t)$, and $\int_0^T Q_{\mathrm{o}}(t)\ \mathrm{d}t$. In this case, venous pressure, $P_{\mathrm{v}}(t)$, does not have to be included in the outputs, which is a significant improvement, mathematically and clinically. The reason for not identifying valve resistances is that these parameters are practically difficult to identify, as will be shown in Chapter 12. Chapter 9, in turn, will provide simple formulae to obtain approximate values for these parameters.

It is also important to mention that, even if the present analysis was focused on the three-chamber CVS model, the two non-identifiability cases mentioned in Section 8.3 are not exclusive to the three-chamber CVS model. Many other CVS models, including the six-chamber model [170], suffer the same non-identifiability cases, since they involve very similar equations. For instance, Abdulla *et al.* investigated the structural identifiability of cardio-vascular feedback models [171]. Two of the four models investigated were not identifiable using only HR and MAP as outputs. For these models, including SV or CO in the outputs made the models identifiable.

The demonstration presented in Section 8.3.4 is based on the equations of the three-chamber model, and thus, cannot be applied as such to other CVS models. However, most lumped CVS models are built from elements very similar to those involved in this three-chamber model, for instance time-varying elastances of Equation 5.5 and vascular resistances of Equation 4.1. Consequently, Equations 8.15 and 8.26, that were developed to show the identifiability of these parameters, can be used with other models. In particular, a demonstration equivalent to the one presented in this chapter has been applied to prove structural identifiability of the six-chamber CVS model from SV, arterial pressure, pulmonary artery pressure, vena cava pressure and pulmonary venous pressure [170]. The

additional data, pulmonary artery and venous pressures, can be provided by a pulmonary artery catheter, as described in Section 7.3.3.

8.5 Summary

The three-chamber CVS model and others are not identifiable from a general model output set. In this chapter, two such cases of structural non-identifiability were first presented. These cases occur when the model output set only contains a single type of information, such as solely pressures or volumes.

Thus, a specific output set was chosen, mixing pressure and volume information, and containing only a limited number of clinically available measurements. Then, by manipulating the model equations involving these outputs, it was demonstrated that the three-chamber CVS model is structurally globally identifiable. The model parameters are thus unique and can theoretically be identified from the specified limited output set.

A further simplification was made, assuming known cardiac valve resistances. Under this hypothesis, the three-chamber model is structurally identifiable from an even smaller dataset involving only arterial pressure and SV.

The results of this chapter imply that parameter values computed from limited but well-chosen datasets are theoretically unique. As a consequence, the parameter identification procedure can theoretically be performed on the model from such a well-chosen dataset. The next chapter deals with the practical aspects of parameter identification.

Chapter 9

Practical Identifiability

9.1 Introduction

In the previous chapter and in Appendix A, formulae were developed involving time derivatives of physiological measurements up to the fourth order. Such formulae are impossible to use in practice because the measurement noise would be amplified by each differentiation step. Thus, the assumption of perfect and noise-free data does not hold in practice and the equations developed in Chapter 8 cannot be used to practically compute the model parameters, although they do prove the structural identifiability. The next step is to investigate how to practically identify the model parameters in the presence of actual, noisy and discrete data, thus investigating the practical identifiability of the model [167].

First, a criterion needs to be defined that will be used to decide which parameter set is the best one (Section 9.2). Section 9.3 then investigates the effect of each parameter on this criterion, while Section 9.4 investigates whether two parameters have the same effect. A parameter that does not influence the error criterion much or that has the same effect as another one is not likely to be practically identifiable. Section 9.5 shows how to decide which parameters not to identify. Finally, Section 9.6 shows how to find good initial parameter values to start the identification process.

9.2 Minimisation Criterion

The aim of the parameter identification process is to find the parameter values that make the simulations as close as possible to the data. The results thus depend on what error value is defined as close. A measure of distance is first introduced, and the goal is to minimise this value.

The output vector $\mathbf{y}$ that will be used for the rest of this work does not depend on time. The reason for this choice is twofold. First, the temporal evolution of all signals is not always available clinically, such as for ventricular volumes. Furthermore, even if haemodynamic monitors, such as the PiCCO, display the pressure curves, these data cannot always be exported. Consequently, only beat-to-beat data, such as MAP, SAP, DAP, CVP or CO are usually available when using such monitors.

Second, as explained in Sections 2.3.3 and 2.3.4, the cardiac and vascular state is not usually assessed using continuous curves. Instead beat-to-beat parameters, which are ranges and means of these curves are typically reported. Therefore, only errors on ranges and means of signals are taken into account in this chapter.

The range of a simulated pressure or volume signal $S(t)$ over one cardiac period is defined:

$$\Delta S = \max_T S(t) - \min_T S(t). \tag{9.1}$$

It is the difference between the maximum and the minimum of this signal over one cardiac period, T, which is thus twice its amplitude. The mean of a signal $S(t)$ over one cardiac period is defined using the common definition:

$$\bar{S} = \frac{1}{T} \int_T S(t) \, \mathrm{d}t. \tag{9.2}$$

Let $\mathbf{y}^{\mathrm{ref}}$ be a vector containing the N_y reference measurements and $\mathbf{y}(\mathbf{p})$, a vector containing the N_y corresponding simulated values using the parameter vector $\mathbf{p}$. The relative error vector $\mathbf{e}$ between simulated and reference values is defined:

$$e_i(\mathbf{p}) = \frac{y_i^{\mathrm{ref}} - y_i(\mathbf{p})}{y_i^{\mathrm{ref}}}, \text{ for } i = 1 \text{ to } N_y. \tag{9.3}$$

A scalar error function ψ_2 is defined as the sum of the squared components of $\mathbf{e}$:

$$\psi_2(\mathbf{p}) = \sum_{i=1}^{N_y} e_i(\mathbf{p})^2. \tag{9.4}$$

Alternatively, the error function is sometimes defined as the sum of the absolute values of the components of $\mathbf{e}$:

$$\psi_1(\mathbf{p}) = \sum_{i=1}^{N_y} |e_i(\mathbf{p})|. \tag{9.5}$$

The goal of the parameter identification process is thus to find the parameter vector $\mathbf{p}^*$ that makes ψ_2 (or ψ_1) the smallest. In mathematical terms, it can be

written:

$$\mathbf{p}^* = \arg\min_{\mathbf{p}} \psi_2(\mathbf{p}). \tag{9.6}$$

Using ψ_2, $\mathbf{p}^*$ is the best or optimal parameter vector in the *least-squares* sense [165]. If ψ_1 is used, $\mathbf{p}^*$ is the best parameter vector in the *least-modulus* sense [165].

9.3 Sensitivity Analysis

The aim of a sensitivity analysis is to know which parameters have the largest influence on the error vector. This question can be answered using the Jacobian matrix. The non-dimensionalized $N_p \times N_y$ Jacobian matrix, $\mathbf{J}$, contains the derivatives of the error vector, $\mathbf{e}$, with respect to the vector of model parameters $\mathbf{p}$ [172]:

$$\mathbf{J} = \begin{pmatrix} \frac{\partial e_1}{\partial p_1} p_1 & \frac{\partial e_2}{\partial p_1} p_1 & \cdots & \frac{\partial e_{N_y}}{\partial p_1} p_1 \\ \frac{\partial e_1}{\partial p_2} p_2 & \frac{\partial e_2}{\partial p_2} p_2 & \cdots & \frac{\partial e_{N_y}}{\partial p_2} p_2 \\ \vdots & \vdots & \ddots & \vdots \\ \frac{\partial e_1}{\partial p_{N_p}} p_{N_p} & \frac{\partial e_2}{\partial p_{N_p}} p_{N_p} & \cdots & \frac{\partial e_{N_y}}{\partial p_{N_p}} p_{N_p} \end{pmatrix}. \tag{9.7}$$

In this work, the derivatives in the Jacobian matrix are computed by central difference approximation:

$$\frac{\partial e_l}{\partial p_k} \approx \frac{e_l(\mathbf{p} + h\mathbf{l}_k) - e_l(\mathbf{p} - h\mathbf{l}_k)}{2h} \tag{9.8}$$

where h is a small step (typically 1 % of p_k) and $\mathbf{l}_k$ is a vector whose N_p entries are all zeros, except the kth one, which is equal to 1.

This method requires solving the model equations twice per parameter, yielding $2N_p$ simulations required. A more precise method exists to compute the Jacobian [173], but it implies solving $3N_p$ or $6N_p$ additional equations, depending on whether the three or six-chamber model is used. These additional equations are called the *sensitivity equations* [88].

To evaluate the sensitivity $\bar{J}_k$ of the error vector $\mathbf{e}$ to the kth parameter p_k, the Euclidean norm of the kth row of the Jacobian matrix can be computed

$$\bar{J}_k = \sqrt{\sum_{l=1}^{N_y} [\mathbf{J}]_{kl}^2}. \tag{9.9}$$

The previous number should be normalised by N_y if different Jacobian matrices need to be compared. In this work, only rows of the same Jacobian matrices are compared, so the normalisation is not needed.

9.4 Correlation Analysis

Performing a correlation analysis allows testing if any pair of parameters p_m and p_n exerts the same influence on $\mathbf{e}$. The motivation to perform such an analysis is that, if two parameters have very similar effects on the error vector, they will not be easily identifiable together. Hence, they may not be practically identifiable [167].

The probabilistic concepts introduced in this section are used when the uncertainty on the measurements is taken into account in the parameter identification process. This uncertainty is often summarised in the the variance of the error, which needs to be known. However, in the particular case of the correlation analysis, assuming the variance of the error to be a constant, denoted $\sigma_{\mathbf{e}}^2$, is sufficient.

Let $\mathbf{\Sigma}$ be the $N_p \times N_p$ *covariance matrix* of the parameter vector, $\mathbf{p}$. This matrix describes how estimates of the parameters are spread around their optimal value, $\mathbf{p}^*$, because of the uncertainty on the measurements [165]. Ideally, the components of $\mathbf{\Sigma}$ should be as small as possible, indicating a low uncertainty on the optimal parameter values.

A minimum bound on the covariance between parameters is provided by the *Cramér-Rao inequality* [165]:

$$\mathbf{\Sigma} \succeq \mathbf{F}^{-1}. \tag{9.10}$$

The previous equation actually states that $\mathbf{\Sigma} - \mathbf{F}^{-1}$ is a positive semidefinite matrix. The $N_p \times N_p$ matrix $\mathbf{F}$ is called the *Fisher information matrix* [165]. In the simplest cases, it can be computed by [174]:

$$\mathbf{F} = \sigma_{\mathbf{e}}^{-2} \mathbf{J}\mathbf{J}^{\mathrm{T}}, \tag{9.11}$$

where ^{T} denotes the transpose matrix.

Then, the $N_p \times N_p$ correlation matrix $\mathbf{C}$ can be obtained from $\mathbf{F}$ as [165, 174]

$$[\mathbf{C}]_{mn} = \frac{[\mathbf{F}^{-1}]_{mn}}{\sqrt{[\mathbf{F}^{-1}]_{mm}[\mathbf{F}^{-1}]_{nn}}} = \frac{[(\mathbf{J}\mathbf{J}^{\mathrm{T}})^{-1}]_{mn}}{\sqrt{[(\mathbf{J}\mathbf{J}^{\mathrm{T}})^{-1}]_{mm}[(\mathbf{J}\mathbf{J}^{\mathrm{T}})^{-1}]_{nn}}}. \tag{9.12}$$

The closer the element $[\mathbf{C}]_{mn}$ is to 1 (or -1), the more the parameters p_m and p_n are directly (or inversely) correlated.

9.4.1 Example on the Three-Chamber Model

The correlation analysis has been applied to the three-chamber CVS model. The reference values for the model outputs, which are the components of $\mathbf{y}^{\mathrm{ref}}$, were extracted from Figure 2.9 and are summarized in Table 9.1. Since no venous pressure curve is displayed in Figure 2.9, left atrial pressure was used instead. The parameter vector includes:

$$\mathbf{p} = (E_{\mathrm{h}}\ E_{\mathrm{a}}\ E_{\mathrm{v}}\ R_{\mathrm{i}}\ R_{\mathrm{o}}\ R_{\mathrm{c}}\ V_{\mathrm{s},3}), \tag{9.13}$$

and the parameter values at which the Jacobian matrix was computed were taken from Table 6.1.

Table 9.1: Reference output values for the parameter correlation analysis performed on the three-chamber CVS model.

Measurement	Value	Units	Reference output
Left ventricular SV	80	ml	$\Delta V_{\mathrm{s,h}}^{\mathrm{ref}}$
Aortic PP	40	mmHg	$\Delta P_{\mathrm{a}}^{\mathrm{ref}}$
Left ventricular PP	130	mmHg	$\Delta P_{\mathrm{h}}^{\mathrm{ref}}$
Mean left ventricular pressure	65	mmHg	$\bar{P}_{\mathrm{h}}^{\mathrm{ref}}$
MAP	93	mmHg	$\bar{P}_{\mathrm{a}}^{\mathrm{ref}}$
Mean left atrial pressure	10	mmHg	$\bar{P}_{\mathrm{v}}^{\mathrm{ref}}$
Mean left ventricular volume	90	ml	$\bar{V}_{\mathrm{h}}^{\mathrm{ref}}$

The computed correlation matrix $\mathbf{C}$ is displayed in Figure 9.1. As can be observed, each parameter is perfectly correlated with itself ($[\mathbf{C}]_{ii} = 1$ for $i = 1$ to 7), as should be expected. Other strong correlations, defined as $|[\mathbf{C}]_{ij}| > 0.85$, according to Olufsen and Ottesen [174], are present in the matrix. Thus, not all parameters of the model will be practically identifiable from the set of outputs in Table 9.1.

In particular, $[\mathbf{C}]_{3,7} = [\mathbf{C}]_{7,3} = -1.00$, so that there is a nearly perfect inverse correlation between venous elastance, E_{v} and total stressed volume, $V_{\mathrm{s},3}$. Indeed,

	E_h	E_a	E_v	R_i	R_o	R_c	$V_{s,3}$
E_h	1.00						
E_a	0.65	1.00					
E_v	1.00	0.67	1.00				
R_i	-1.00	-0.65	-1.00	1.00			
R_o	0.76	0.63	0.75	-0.75	1.00		
R_c	0.01	0.45	0.02	0.00	-0.18	1.00	
$V_{s,3}$	-1.00	-0.67	-1.00	1.00	-0.76	-0.02	1.00

Figure 9.1: Correlation matrix **C** for the parameters of the three-chamber CVS model and the outputs of Table 9.1.

$V_{s,3}$ can be increased arbitrarily if the venous elastance is decreased accordingly so that the venous chamber stores enough blood. This case results in the same mean venous pressure for appropriate pair of values, and thus indicates they are not both practically identifiable.

For example, Figure 9.2 shows a simulation of the three-chamber CVS model using the parameters given in Table 9.2. The $V_{s,3}$ value in Table 9.2 is twice that of Table 6.1 . The venous elastance of Table 9.2 has been decreased to compensate for this larger $V_{s,3}$, thus resulting in the same mean venous pressure $\bar{P}_V$. The two simulations of Figures 6.2 and 9.2 are thus extremely similar, the only visible differences being the venous volume curve and the amplitude of the venous pressure curve.

Since this information has not been included in the output set of Table 9.1, there is no way to distinguish between the two simulations using this output set. Consequently, venous elastance and total stressed volume cannot simultaneously be determined from the selected output set. Using such data, the model is practically non-identifiable [175].

The same kind of problem arises with the six-chamber model for an output vector that contains the elements of Table 9.1 and their counterparts for the right side of the CVS. There is a practical inability to uniquely identify the two venous elastances of this model, E_{SV} and E_{PV}, and $V_{s,6}$. However, it is more difficult

Table 9.2: Parameter values for the simulation of the three-chamber CVS model presented in Figure 9.2.

Parameter	Units	Value
T	s	1.1
E_{h}	mmHg/ml	1.4
E_{a}	mmHg/ml	1.2
E_{v}	mmHg/ml	0.034
R_{i}	mmHg s/ml	0.05
R_{o}	mmHg s/ml	0.04
R_{c}	mmHg s/ml	2
$V_{\mathrm{s},3}$	ml	500
$e(t)$	-	$\exp\left[-20\left((t \bmod T) - \frac{T}{2}\right)^2\right]$

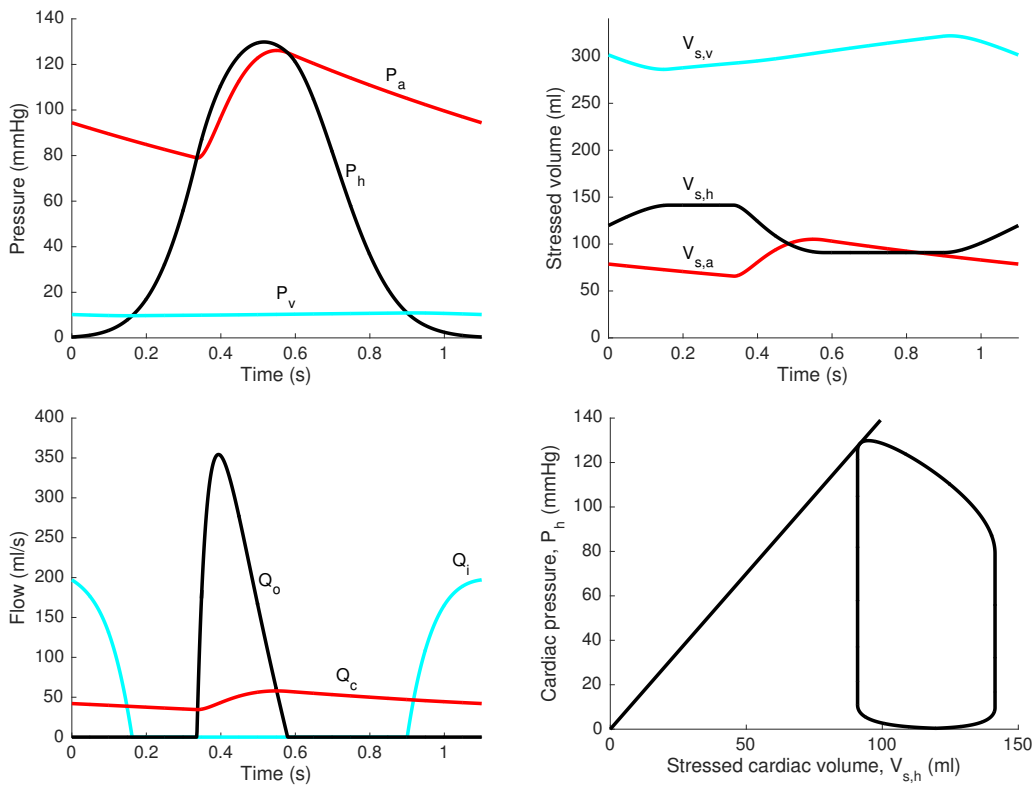

Figure 9.2: Simulation of the three-chamber CVS model using the parameters of Table 9.2. *Top-left:* cardiac (P_{h}, *black*), arterial (P_{a}, *red*) and venous (P_{v}, *light blue*) pressures. *Top-right:* cardiac ($V_{\mathrm{s,h}}$, *black*), arterial ($V_{\mathrm{s,a}}$, *red*) and venous ($V_{\mathrm{s,v}}$, *light blue*) stressed volumes. *Bottom-left:* input (Q_{i}, *light blue*), output (Q_{o}, *black*) and circulatory (Q_{c}, *red*) flows. *Bottom-right:* cardiac pressure-volume loop and the corresponding ESPVR.

to show this relationship as it involves the interplay between three parameters, rather than two.

As previously mentioned, the existence (or not) of correlations depends on the choice of model outputs used. For instance, if one output, namely venous PP, with reference value of 10 mmHg is added to the list of Table 9.1 as a reference for ΔP_{v}, parameter correlations are much less strong, as the correlation matrix of Figure 9.3 shows for this case. There remains only one strong correlation, between $V_{\mathrm{s,3}}$ and E_{a}, according to the criterion of Olufsen and Ottesen [174].

	E_h	E_a	E_v	R_i	R_o	R_c	$V_{s,3}$
E_h	1.00						
E_a	-0.14	1.00					
E_v	-0.20	0.62	1.00				
R_i	-0.28	0.63	0.56	1.00			
R_o	0.18	0.27	0.09	0.06	1.00		
R_c	-0.11	0.59	0.61	0.55	-0.29	1.00	
$V_{s,3}$	-0.05	-0.86	-0.74	-0.47	-0.35	-0.43	1.00

Figure 9.3: Correlation matrix **C** for the parameters of the three-chamber CVS model and the outputs of Table 9.1, plus venous pulse pressure, ΔP_{v}.

Consequently, when parameter correlations are present, using more data sources can solve the issue. However, this option is not always feasible. When more data are not available, some parameters have to be left out of the parameter identification procedure, because they cannot be practically identified. The next section presents an algorithm designed to select which parameters to identify, to maximise identifiability and clinical utility.

9.5 Subset Selection Algorithm

Since some parameters are not sensitive enough to be identified using the available data and some others are correlated, it is very difficult to identify them all. This issue is frequent in all classes of parameter identification problems. Conse-

quently, some authors have developed techniques to select a subset of parameters that can reliably be identified [172, 176–178].

The subset selection algorithm used in this work was introduced by Burth *et al.* [172] and was used in cardio-vascular modelling by Pope *et al.* [92]. The algorithm will be briefly described here. Further detail can be found in [92, 172].

For this method, the $N_p \times N_p$ non-dimensonalized Hessian matrix, $\mathbf{H}$, is [172]:

$$[\mathbf{H}]_{ij} = \frac{\partial^2 \psi_2}{\partial p_i \partial p_j} p_i p_j \tag{9.14}$$

$$= \frac{\partial^2}{\partial p_i \partial p_j} \left(\sum_{k=1}^{N_y} e_k^2 \right) p_i p_j \tag{9.15}$$

$$= 2 \frac{\partial}{\partial p_i} \left(\sum_{k=1}^{N_y} \frac{\partial e_k}{\partial p_j} e_k \right) p_i p_j \tag{9.16}$$

$$= 2 \left(\sum_{k=1}^{N_y} \frac{\partial^2 e_k}{\partial p_i \partial p_j} e_k + \sum_{k=1}^{N_y} \frac{\partial e_k}{\partial p_j} \frac{\partial e_k}{\partial p_i} \right) p_i p_j. \tag{9.17}$$

If the components, e_k, of the error vector are assumed to be small [172], indicating a solution near the optimum, the first term is close to zero and the previous equation can be approximated:

$$[\mathbf{H}]_{ij} \approx 2 \sum_{k=1}^{N_y} \frac{\partial e_k}{\partial p_j} \frac{\partial e_k}{\partial p_i} p_i p_j \tag{9.18}$$

$$= 2 \sum_{k=1}^{N_y} [\mathbf{J}]_{jk} [\mathbf{J}]_{ik}. \tag{9.19}$$

In matrix notation, the previous equation is written:

$$\mathbf{H} \approx 2 \mathbf{J} \mathbf{J}^{\mathrm{T}}. \tag{9.20}$$

The principle of the subset selection algorithm is to compute the N_p eigenvalues of $\mathbf{H}$ and to separate them in two subsets containing ρ and $N_p - \rho$ eigenvalues. The first subset contains the ρ largest eigenvalues and this ρ value dictates the number of parameters that can be iteratively optimised. In this work, the value of ρ is defined:

$$\rho = \arg\max_i \left(\frac{\lambda_i}{\lambda_{i+1}} \right) \text{ with } \lambda_i \geq \lambda_{i+1}. \tag{9.21}$$

That is, ρ is chosen so that the ratio between two consecutive eigenvalues (λ_i and λ_{i+1}) is the highest. In case $\rho = 1$, the second highest ratio was selected.

Let $\mathbf{V}_\rho$ be the $N_p \times \rho$ matrix containing the ρ eigenvectors of $\mathbf{H}$ associated with the ρ largest eigenvalues. To find the ρ parameters corresponding to the ρ largest eigenvalues, an $N_p \times N_p$ permutation matrix $\mathbf{P}$ is found through a QR decomposition of $\mathbf{V}_\rho^{\mathrm{T}}$:

$$\mathbf{V}_\rho^{\mathrm{T}}\mathbf{P} = \mathbf{QR}. \tag{9.22}$$

Finally, the parameter vector $\mathbf{p}$ is rearranged using $\mathbf{P}$, which gives the ρ parameters that can be used for optimization. Full details are in [172].

9.6 Initial Parameter Values

The sensitivity and correlation analyses of Sections 9.3 and 9.4 and the subset selection algorithm of Section 9.5 are local procedures, because they depend on the parameter values used to compute the Jacobian matrix. In addition, the precision of the subset selection algorithm also depends on the validity of the hypothesis $e_k \approx 0$ used to obtain Equation 9.18. Consequently, for the procedures presented in the previous sections to be relevant, it is important to choose initial parameter values that are as close as possible to the optimal ones.

This section describes how to obtain these initial values for the model parameters using simplifications of the three-chamber CVS model equations. The three-chamber model is used for simplicity. However, the formulae developed in the present section can be applied to the six-chamber model with the appropriate changes in notations, and the approach is thus general.

9.6.1 Input Valve Resistance, R_{i}

From Continuous Data

The combination of Equations 6.5 and 6.7 during filling ($Q_{\mathrm{o}} = 0$) gives:

$$\frac{\mathrm{d}V_{\mathrm{s,h}}(t)}{\mathrm{d}t} = \frac{P_{\mathrm{v}}(t) - P_{\mathrm{h}}(t)}{R_{\mathrm{i}}}. \tag{9.23}$$

Integrating this equation from beginning (t_{BF}) to end (t_{EF}) of filling gives:

$$V_{\mathrm{s,h}}(t_{\mathrm{EF}}) - V_{\mathrm{s,h}}(t_{\mathrm{BF}}) = \frac{\int_{t_{\mathrm{BF}}}^{t_{\mathrm{EF}}} (P_{\mathrm{v}}(t) - P_{\mathrm{h}}(t))\,\mathrm{d}t}{R_{\mathrm{i}}}. \tag{9.24}$$

Since $V_{\mathrm{s,h}}(t_{\mathrm{EF}})$ is the maximum of $V_{\mathrm{s,h}}$ during a cardiac cycle, and $V_{\mathrm{s,h}}(t_{\mathrm{BF}})$, its minimum, the left-hand side of the previous equation equals $\Delta V_{\mathrm{s,h}}$. Therefore,

one obtains:

$$R_{\mathrm{i}} = \frac{\int_{t_{\mathrm{BF}}}^{t_{\mathrm{EF}}} (P_{\mathrm{v}}(t) - P_{\mathrm{h}}(t))\, \mathrm{d}t}{\Delta V_{\mathrm{s,h}}}. \tag{9.25}$$

This equation can be graphically interpreted by stating that the area between venous and cardiac pressures during filling is equal to the product of $\Delta V_{\mathrm{s,h}}$ and R_{i}, as illustrated in Figure 9.4.

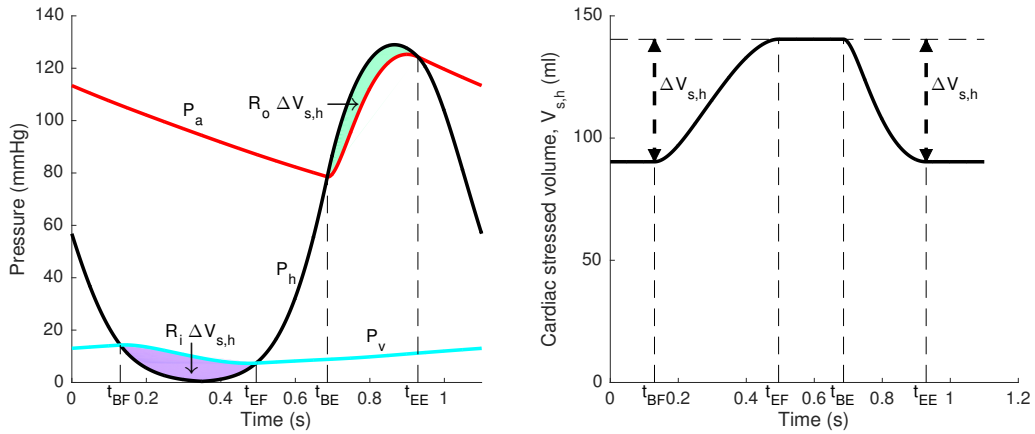

Figure 9.4: Graphical illustration of Equations 9.25 and 9.31. *Left:* venous (*light blue*), cardiac (*black*) and arterial (*red*) pressures. *Right:* cardiac stressed volume.

From Discrete Data

Assuming $P_{\mathrm{v}}(t)$ to be constant and equal to its mean value $\bar{P}_{\mathrm{v}}$, Equation 9.25 becomes:

$$R_{\mathrm{i}} \approx \frac{\int_{t_{\mathrm{BF}}}^{t_{\mathrm{EF}}} (\bar{P}_{\mathrm{v}} - P_{\mathrm{h}}(t))\, \mathrm{d}t}{\Delta V_{\mathrm{s,h}}}. \tag{9.26}$$

Neglecting cardiac pressure during filling, so that $P_{\mathrm{h}}(t) \approx 0$, gives:

$$R_{\mathrm{i}} \approx \frac{\int_{t_{\mathrm{BF}}}^{t_{\mathrm{EF}}} \bar{P}_{\mathrm{v}}\, \mathrm{d}t}{\Delta V_{\mathrm{s,h}}} \approx \frac{\bar{P}_{\mathrm{v}}}{\Delta V_{\mathrm{s,h}}} (t_{\mathrm{EF}} - t_{\mathrm{BF}}). \tag{9.27}$$

Finally, assuming $t_{\mathrm{EF}} - t_{\mathrm{BF}} = T/2$, one obtains:

$$R_{\mathrm{i}} \approx \frac{\bar{P}_{\mathrm{v}}\, T}{2\, \Delta V_{\mathrm{s,h}}}. \tag{9.28}$$

9.6.2 Output Valve Resistance, R_o

From Continuous Data

The combination of Equations 6.6 and 6.7 during ejection, when $Q_i = 0$, reads:

$$\frac{dV_{s,h}(t)}{dt} = -\frac{P_h(t) - P_a(t)}{R_o}. \tag{9.29}$$

Integrating this equation during ejection, from t_{BE} to t_{EE}, gives:

$$V_{s,h}(t_{EE}) - V_{s,h}(t_{BE}) = -\frac{\int_{t_{BE}}^{t_{EE}} (P_h(t) - P_a(t))\, dt}{R_o}. \tag{9.30}$$

Because $V_{s,h}(t_{BE})$ is the maximum value of $V_{s,h}$ and $V_{s,h}(t_{EE})$, its minimum, the left-hand side is equal to $-\Delta V_{s,h}$. Rearranging terms yields:

$$R_o = \frac{\int_{t_{BE}}^{t_{EE}} (P_h(t) - P_a(t))\, dt}{\Delta V_{s,h}}. \tag{9.31}$$

The graphical interpretation of Equation 9.31 implies that the area between cardiac and arterial pressures during ejection is equal to $\Delta V_{s,h}$ times R_o, as also shown in Figure 9.4. Using Equation 9.31 requires knowledge of cardiac pressure, which is not usually measured. Consequently, an approximation of $P_h(t)$ must be used, as described in the next section.

From Discrete Data

Assuming that cardiac stressed volume $V_{s,h}(t)$ decreases from $\bar{V}_{s,h} + 0.5\Delta V_{s,h}$ to $\bar{V}_{s,h} - 0.5\Delta V_{s,h}$ during ejection, from t_{BE} to t_{EE}, allows construction of a linear approximation of $V_{s,h}(t)$ defined:

$$\tilde{V}_{s,h}(t) = \bar{V}_{s,h} + \frac{\Delta V_{s,h}}{t_{EE} - t_{BE}} \left(\frac{t_{EE} + t_{BE}}{2} - t \right). \tag{9.32}$$

Using this approximation and Equation 6.3 yields:

$$P_h(t) \approx E_h e(t) \tilde{V}_{s,h}(t). \tag{9.33}$$

Using Equations 9.31 and 9.33, and assuming that $P_a(t) \approx \bar{P}_a$, one gets:

$$R_o \approx \frac{\int_{t_{BE}}^{t_{EE}} (E_h e(t) \tilde{V}_{s,h}(t) - \bar{P}_a)\, dt}{\Delta V_{s,h}}. \tag{9.34}$$

9.6.3 Resistance of the Circulation, R_c

The resistance of the circulation can be exactly obtained using Equation 8.15:

$$R_c = \frac{\int_0^T [P_a(t) - P_v(t)]\,dt}{\int_0^T Q_o(t)\,dt} = \frac{\bar{P}_a - \bar{P}_v}{\int_0^T Q_o(t)\,dt} T \tag{9.35}$$

where $\bar{P}_a$ and $\bar{P}_v$ are, respectively, mean arterial and venous pressures. The integral of the flow through the output valve, Q_o is equal to the volume going through the output valve during systole. In turn, this volume is exactly equal to the change of cardiac volume during systole, $\Delta V_{s,h}$. Therefore:

$$R_c = \frac{\bar{P}_a - \bar{P}_v}{\Delta V_{s,h}} T \tag{9.36}$$

For simplicity, $\bar{P}_v$ is often neglected with respect to $\bar{P}_a$, because it is much smaller [15]. Hence, Equation 9.36 simplifies to:

$$R_c \approx \frac{\bar{P}_a\, T}{\Delta V_{s,h}}. \tag{9.37}$$

9.6.4 Cardiac End-Systolic Elastance, E_h

From a Preload Reduction Manoeuvre

As explained in Section 5.2.1, the end-systolic elastance, and unstressed volume as a byproduct, must be determined using a linear regression of the end-systolic pressure-volume points during a preload reduction experiment. A dedicated method has been developed by Kass *et al.* [179]. This methods begins by finding the points with the maximum pressure-volume ratio and fitting them with a straight line. This straight line yields first estimates of E_h and $V_{u,h}$. Next, new points of end-systole are defined as those having the maximum $P_h/(V_h - V_{u,h})$ ratio. A new line is fitted to these points, and the process is repeated until convergence of E_h and $V_{u,h}$.

From a Single Beat

For simplicity reasons, many researchers have tried to determine the end-systolic elastance using a single heartbeat, rather than a preload reduction experiment (*e.g.* [117,180,181]). Since a single heartbeat only provides one end-systolic point, a further simplifying hypothesis is always necessary [182]. The simplest hypothesis consists of stating that the ventricular unstressed volume is equal to zero [93].

Under this hypothesis, Equation 5.1 for the ESPVR becomes:

$$P_{\mathrm{h}}(t_{\mathrm{ES}}) \approx E_{\mathrm{h}} V_{\mathrm{h}}(t_{\mathrm{ES}}) \tag{9.38}$$

where V_{h} is the true volume and not the stressed volume. This ESPVR line thus passes through the origin of the pressure-volume plane.

Equation 9.38 can be rearranged to yield:

$$E_{\mathrm{h}} \approx \frac{P_{\mathrm{h}}(t_{\mathrm{ES}})}{V_{\mathrm{h}}(t_{\mathrm{ES}})}. \tag{9.39}$$

In turn, assuming end-systolic cardiac pressure to be equal to maximum arterial pressure gives:

$$E_{\mathrm{h}} \approx \frac{\max_T P_{\mathrm{a}}(t)}{V_{\mathrm{h}}(t_{\mathrm{ES}})}. \tag{9.40}$$

9.6.5 Arterial Elastance, E_{a}

From Continuous Data

During diastole, volume change in the artery is described by the combination of Equations 6.4 and 6.8:

$$\frac{\mathrm{d}V_{\mathrm{s,a}}(t)}{\mathrm{d}t} = -\frac{P_{\mathrm{a}}(t) - P_{\mathrm{v}}(t)}{R_{\mathrm{c}}}. \tag{9.41}$$

If, once again, P_{v} is neglected with respect to P_{a} and Equation 6.1, is used, one gets:

$$\frac{\mathrm{d}V_{\mathrm{s,a}}(t)}{\mathrm{d}t} \approx -\frac{E_{\mathrm{a}}\, V_{\mathrm{s,a}}(t)}{R_{\mathrm{c}}}. \tag{9.42}$$

Solving this equation for $V_{\mathrm{s,a}}(t)$ yields:

$$V_{\mathrm{s,a}}(t) \approx \exp\left(-\frac{E_{\mathrm{a}}(t - t_{\mathrm{BD}})}{R_{\mathrm{c}}}\right) V_{\mathrm{s,a}}(t_{\mathrm{BD}}). \tag{9.43}$$

where t_{BD} denotes the beginning of diastole. Multiplying both sides of (9.43) by E_{a} yields:

$$P_{\mathrm{a}}(t) \approx \exp\left(-\frac{E_{\mathrm{a}}(t - t_{\mathrm{BD}})}{R_{\mathrm{c}}}\right) P_{\mathrm{a}}(t_{\mathrm{BD}}). \tag{9.44}$$

Since R_{c} can be computed from Equation 9.36 or 9.37, E_{a} can be determined by fitting the reference $P_{\mathrm{a}}(t)$ curve during diastole to Equation 9.44. An example is displayed in Figure 9.5. Estimating arterial elastance, or its inverse, called *arterial*

compliance, by fitting an exponential function to the diastolic portion of the arterial pressure curve is a well-known method [109, 183–186].

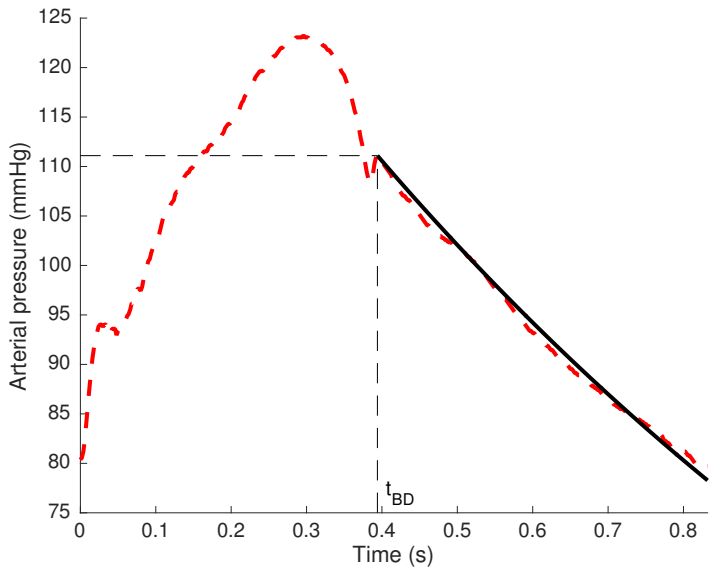

Figure 9.5: Fitting of Equation 9.44 (*black*) to arterial pressure during diastole (*red*).

From Discrete Data

If the complete curve of $P_a(t)$ is not available, and only its range ΔP_a is given, a simpler expression is required to obtain an initial value of E_a. Integrating Equation 6.8 during ejection, from t_{BE} to t_{EE}, yields:

$$V_{s,a}(t_{EE}) - V_{s,a}(t_{BE}) = \int_{t_{BE}}^{t_{EE}} Q_o(t)\,dt - \int_{t_{BE}}^{t_{EE}} Q_c(t)\,dt. \tag{9.45}$$

Multiplying both sides by E_a and using Equation 6.1 gives:

$$P_a(t_{EE}) - P_a(t_{BE}) = E_a \int_{t_{BE}}^{t_{EE}} Q_o(t)\,dt - E_a \int_{t_{BE}}^{t_{EE}} Q_c(t)\,dt. \tag{9.46}$$

As can be observed in Figure 9.4, the left-hand side is nearly equal to the range of arterial pressure, ΔP_a:

$$\Delta P_a \approx E_a \int_{t_{BE}}^{t_{EE}} Q_o(t)\,dt - E_a \int_{t_{BE}}^{t_{EE}} Q_c(t)\,dt. \tag{9.47}$$

All ejected blood goes through the output valve during systole. Consequently, the integral of Q_o is equal to $\Delta V_{s,h}$, where this substitution gives:

$$\Delta P_a = E_a \, \Delta V_{s,h} - E_a \int_{t_{BS}}^{t_{ES}} Q_c(t) \, dt. \tag{9.48}$$

Neglecting the integral of Q_c yields the following approximation for E_a:

$$E_a \approx \frac{\Delta P_a}{\Delta V_{s,h}}. \tag{9.49}$$

This assumption underestimates E_a because it assumes that the increase in arterial pressure during systole is caused entirely by $\Delta V_{s,h}$. In fact, some fraction of $\Delta V_{s,h}$, the integral of Q_c, flows through the arteries to the veins without causing an increase in arterial pressure. A more detailed discussion of the validity of this approximation can be found in [187].

9.6.6 Venous Elastance, E_v

Equation 6.9 during systole, when $Q_i = 0$, reads:

$$\dot{V}_{s,v}(t) = Q_c(t). \tag{9.50}$$

Flow through the capillaries is assumed to be constant and equal to its mean value, and thus:

$$\dot{V}_{s,v}(t) \approx \frac{\Delta V_{s,h}}{T}. \tag{9.51}$$

Integrating this equation from beginning, t_{BS}, to end, t_{ES}, of systole gives:

$$V_{s,v}(t_{ES}) - V_{s,v}(t_{BS}) \approx \frac{\Delta V_{s,h}}{T} \, (t_{ES} - t_{BS}). \tag{9.52}$$

Multiplying both sides by E_v and using Equation 6.2 gives:

$$P_v(t_{ES}) - P_v(t_{BS}) \approx E_v \, \frac{\Delta V_{s,h}}{T} \, (t_{ES} - t_{BS}). \tag{9.53}$$

Finally, assuming $P_v(t_{ES}) - P_v(t_{BS}) \approx \Delta P_v$ and $t_{ES} - t_{BS} \approx T/2$, and rearranging terms, one obtains:

$$E_v \approx \frac{2 \, \Delta P_v}{\Delta V_{s,h}}. \tag{9.54}$$

9.6.7 Total Stressed Volume, $V_{s,3}$

Equation 6.11 is averaged on one cardiac cycle, giving:

$$\bar{V}_{s,h} + \bar{V}_{s,a} + \bar{V}_{s,v} = V_{s,3}. \tag{9.55}$$

Then, Equations 6.1 and 6.2 can also be averaged, yielding:

$$\bar{V}_{s,h} + \frac{\bar{P}_a}{E_a} + \frac{\bar{P}_v}{E_v} = V_{s,3}. \tag{9.56}$$

The previous equation enables the estimation of $V_{s,3}$ if the quantities in the left-hand side are available. Therefore, the measurements needed to approximate E_a and E_v are also needed.

9.7 Summary

Throughout this chapter, the parameter identification problem was formulated. First, the objective function was introduced as the criterion defining the closeness between simulations and the measurements, that has to be made as small as possible. Because of the model structure and the limited available data, some parameters have little effect on the objective function, while others have similar effects, preventing their unique identification. Therefore, the subset selection algorithm was introduced to leave such parameters out of the identification process. Finally, formulae were designed to obtain the initial values of the parameters.

Starting from these initial values, the next step is to find a minimum of the objective function. A specific optimization method is necessary to identify the remaining model parameters. The next chapter describes and compares several such methods.

Chapter 10

Parameter Identification Methods

10.1 Introduction

To be clinically relevant, mathematical models have to be made patient-specific, which means that their parameters have to be identified so that simulations represent a patient's individual state. The parameter identification problem has been stated in the previous chapter. It aims at finding the parameters that minimise the objective function ψ_i assessing the error between simulation and clinical data. There exist several methods to find such a minimum [188–190].

To achieve real time monitoring using lumped CVS models, it is important to select the best parameter identification method, in terms of speed, efficiency and reliability. This chapter focuses on the three-chamber CVS model and investigates seven typical parameter identification methods. These methods are first described, and then, compared using *in silico* and experimental reference data [103], where *in silico* data allows the truth underlying simulations to be known.

10.2 The Methods

10.2.1 The Proportional Method

The proportional method was developed by Hann *et al.* [113, 191] specifically for parameter identification of the six-chamber CVS model. It is based on a series of *a priori* proportionality relations between parameters and outputs of the six-chamber model. More accurately, the model they used is a version of the six-chamber model where venous pressures are kept constant. For instance, the authors observed that the simulated range of systemic arterial pressure ΔP_{SA} is proportional to systemic arterial elastance E_{SA}. Consequently, during the parameter identification process, E_{SA} is successively updated using a proportional feedback

rule defined:

$$E_{\mathrm{SA}}[n+1] = E_{\mathrm{SA}}[n]\frac{\Delta P_{\mathrm{SA}}^{\mathrm{ref}}}{\Delta P_{\mathrm{SA}}(\mathbf{p}[n])}. \tag{10.1}$$

where $E_{\mathrm{SA}}[n]$ is the current value of E_{SA} and $E_{\mathrm{SA}}[n+1]$, the next one, $\Delta P_{\mathrm{SA}}^{\mathrm{ref}}$ is the target value of the range of systemic arterial pressure and $\Delta P_{\mathrm{SA}}(\mathbf{p}[n])$, its simulated value using the current parameter vector $\mathbf{p}[n]$.

The proportionality relations hypothesized in the original article [113] were:

- R_{AV} is inversely proportional to the difference between systemic arterial pressure at its inflection point and at its minimum:

$$P_{\mathrm{SA}}(t_{\mathrm{inflect}}) - \min_T P_{\mathrm{SA}}(t), \tag{10.2}$$

- E_{LV} is inversely proportional to mean left ventricular volume $\bar{V}_{\mathrm{LV}}$,
- R_{MV} is inversely proportional to the range of left ventricular volume ΔV_{LV},
- E_{SA} is directly proportional to the range of systemic arterial pressure ΔP_{SA},
- R_{sys} is directly proportional to mean systemic arterial pressure $\bar{P}_{\mathrm{SA}}$.

In subsequent versions of the method, some of these hypotheses have been altered and others have been added to identify more parameters [93, 191–193].

The biggest advantage of this method is that this *a priori* knowledge allows the parameter identification method to know in which direction to move in the parameter space without having to compute any gradients, saving significant computational effort. Its biggest drawback is that the proportionality hypotheses are approximations, and thus, are not always valid. For instance, through computation of the value of the derivative $\partial\Delta V_{\mathrm{LV}}/\partial R_{\mathrm{MV}}$, it can be shown that the second proportionality relation above can be wrong for sufficiently large values of E_{LV}. This reasoning is detailed in Appendix B. In general, if the parameter identification method gets out of the validity domain of the hypotheses, it will fail.

The proportionality relations can be summarised in a $N_p \times N_y$ matrix, defined, for the original version of the method:

$$\begin{array}{c} \\ R_{\mathrm{AV}} \\ E_{\mathrm{LV}} \\ R_{\mathrm{MV}} \\ E_{\mathrm{SA}} \\ R_{\mathrm{sys}} \end{array} \begin{array}{c} \begin{array}{ccccc} P_{\mathrm{SA}}(t_{\mathrm{inflect}}) - \min_T P_{\mathrm{SA}}(t) & \bar{V}_{\mathrm{LV}} & \Delta V_{\mathrm{LV}} & \Delta P_{\mathrm{SA}} & \bar{P}_{\mathrm{SA}} \end{array} \\ \begin{pmatrix} -1 & 0 & 0 & 0 & 0 \\ 0 & -1 & 0 & 0 & 0 \\ 0 & 0 & -1 & 0 & 0 \\ 0 & 0 & 0 & 1 & 0 \\ 0 & 0 & 0 & 0 & 1 \end{pmatrix} \end{array} = \mathbf{M}. \tag{10.3}$$

This matrix can be seen as an oversimplified version of the Jacobian matrix, where each line only has one non-zero element. Conversely to the Jacobian matrix, the non-zero elements do not quantitatively represent the derivatives of the error

vector with respect to the vector of model parameters, but rather represent them qualitatively through a plus or a minus sign.

In this work, the proportional method was implemented as follows:

1. For each parameter p_i, find the related measurement in the proportionality matrix, *i.e.* find j such that $[\mathbf{M}]_{ij} = 1$ or -1.
2. Update the parameter p_i using

$$p_i[n+1] = p_i[n] \left(\frac{y_j^{\text{ref}}}{y_j(\mathbf{p}[n])} \right)^{[\mathbf{M}]_{ij}} . \tag{10.4}$$

3. Compute the error vector with the new parameter vector and check if the jth component has decreased as expected, *i.e.* if $e_j(\mathbf{p}[n+1]) < e_j(\mathbf{p}[n])$.
4. If it is the case, update the parameter p_i four more times maximum or until the error e_j on the related measurement is lower than a fixed threshold. If not, go to step 5.
5. Go to the next parameter, *i.e.* increase i.

This procedure is repeated while the components of the error vector that are related to a parameter are higher than a given threshold.

10.2.2 The Simplex Method

The simplex method was developed by Nelder and Mead [190] for minimisation of an N_p-dimensional scalar function, ψ_i in the present case. This method works with a *simplex*, namely a surface bounded by $N_p + 1$ points in the N_p-dimensional parameter space. Thus, the simplex is a triangle if two parameters are to be optimised. At each iteration of the method, the simplex is modified according to one of the following operations [188]:

- Reflection: the point associated with the highest ψ_i value is reflected through the face of the simplex formed by all other points,
- Expansion: the simplex is stretched in the direction of the point associated with the lowest ψ_i value,
- Contraction: the simplex is contracted away from the point associated with the highest ψ_i value.

Therefore, the simplex moves on the error surface towards the lowest ψ_i regions.

10.2.3 The Direct Search Method

The direct search method has also been conceived for minimisation of an N_p-dimensional scalar function. The principle of the method is to search for a better point, with a lower ψ_i value, by taking a step from a starting point in all

the $2N_p$ possible directions. For example, steps that move up, down, left and right if two parameters are to be optimised. If a better point is found, then the search is restarted from this point. If no better point is found, then the size of the search step is reduced and the search is resumed from the current best point. The version of the direct search method that is used in this work uses random-generated search directions and investigates these directions in a random order for increased speed [193].

10.2.4 Gradient-Based Methods

The principle of gradient-based methods is to use the information contained in the gradient of the objective function, ψ_i, to find a direction in the parameter space in which ψ_i is decreasing [188]. There exists a large number of methods, each primarily differing by the size of the step they take in the direction of the gradient. In this work, the following gradient-based methods were used:

- Active set method,
- Sequential quadratic programming (SQP) method,
- Interior point method,
- Trust-region reflective (TRR) method.

The first three methods are implemented in the *fmincon* function of Matlab and the last one, in the *lsqnonlin* function. The *fmincon* function takes ψ_2 as its argument, while *lsqnonlin* takes the error vector $\mathbf{e}$ as its argument and internally computes ψ_2 from it, using Equation 9.4.

10.3 Comparison of the Methods

The seven parameter identification methods introduced in Sections 10.2.1 to 10.2.4 (proportional, simplex, direct search, active set, SQP, interior point and TRR) were tested on the three-chamber CVS model. They were tested on both simulated (*in silico*) and experimental reference data. *In silico* data allows a noise-free evaluation where the ground truth parameter values are known, to assess method accuracy.

10.3.1 Parameter Identification Process

Output Vector

The following model outputs were considered to be available:

- Range of arterial pressure, ΔP_{a},
- Range of venous pressure, ΔP_{v},

- Range of cardiac stressed volume, $\Delta V_{\mathrm{s,h}}$,
- Mean arterial pressure, $\bar{P}_{\mathrm{a}}$,
- Mean venous pressure, $\bar{P}_{\mathrm{v}}$,
- Mean cardiac stressed volume, $\bar{V}_{\mathrm{s,h}}$,
- Maximum derivative of arterial pressure, ($\max_T \mathrm{d}P_{\mathrm{a}}(t)/\mathrm{d}t$).

Accordingly, the output vector was defined:

$$\mathbf{y} = \left(\Delta P_{\mathrm{a}}\ \Delta P_{\mathrm{v}}\ \Delta V_{\mathrm{s,h}}\ \bar{P}_{\mathrm{a}}\ \bar{P}_{\mathrm{v}}\ \bar{V}_{\mathrm{s,h}}\ \max_T \frac{\mathrm{d}P_{\mathrm{a}}(t)}{\mathrm{d}t} \right). \tag{10.5}$$

Some comments have to be made regarding the composition of the output vector. First, $\Delta V_{\mathrm{s,h}}$, the model-based equivalent of SV is a necessary output for parameter identification of lumped CVS models. It thus had to be included in the available data. In addition, mean cardiac volume $\bar{V}_{\mathrm{s,h}}$ is intuitively needed for practical identification of the cardiac elastance, E_{h}, or there is no way of knowing the location of the pressure-volume loop on the volume axis, thus making E_{h} undetermined. Third, in Chapter 8, the knowledge of arterial and venous pressures was shown to be necessary for identifiability. The means and ranges of these curves, which represent their essential features, were thus included in $\mathbf{y}$. Finally, $\max_T \mathrm{d}P_{\mathrm{a}}(t)/\mathrm{d}t$ was included because it is an index of contractility [22], has been linked to identifiability of the output valve resistance [191], and was found to decrease correlations between parameters, which should improve practical identifiability. The clinical relevance of the choice of model outputs is discussed in Section 10.3.4.

Error Vector

Let $\mathbf{y}^{\mathrm{ref}}$ be a vector containing the reference values and $\mathbf{y}(\mathbf{p})$, a vector containing the corresponding simulated values. The relative error vector $\mathbf{e}$ between simulated and reference values is defined:

$$e_i = \frac{y_i^{\mathrm{ref}} - y_i(\mathbf{p})}{y_i^{\mathrm{ref}}}, \text{ for } i = 1 \text{ to } 7. \tag{10.6}$$

The goal of the parameter identification process was to minimise the sum of squared components of this vector

$$\psi_2 = e_1^2 + e_2^2 + e_3^2 + e_4^2 + e_5^2 + e_6^2 + e_7^2 \tag{10.7}$$

by varying $\mathbf{p}$, to find an optimal parameter vector $\mathbf{p}^*$.

Initial Parameter Values

The following information was assumed to be available:

- Cardiac period, T,
- Driver function, $e(t)$,
- Onset, t_{BE}, and end, t_{EE}, times of cardiac ejection.

Using this information and the data contained in the output vector $\mathbf{y}$, initial parameter values were obtained for each dataset using Equations 9.28, 9.34, 9.36, 9.49, 9.54 and 9.56 derived in Section 9.6. For estimation of initial cardiac elastance, E_{h}, Equation 9.40 was used, assuming an estimate of maximum arterial pressure that was equal to mean arterial pressure plus half the range of arterial pressure:

$$\max_{T} P_{\mathrm{a}}(t) \approx \bar{P}_{\mathrm{a}} + 0.5\,\Delta P_{\mathrm{a}}. \tag{10.8}$$

A similar hypothesis was formulated for minimum (end-systolic) cardiac volume:

$$V_{\mathrm{h}}(t_{\mathrm{ES}}) \approx \bar{V}_{\mathrm{h}} - 0.5\,\Delta V_{\mathrm{h}}. \tag{10.9}$$

Parameter Vector

As can be seen from the equality sign in Equation 9.36, no approximation has been used to obtain the value of R_{c}, which means the value of this parameter can be exactly retrieved from the selected set of model outputs. This parameter was thus not included in the parameter identification procedure. The remaining parameter vector is defined:

$$\mathbf{p} = (E_{\mathrm{h}}\ E_{\mathrm{a}}\ E_{\mathrm{v}}\ R_{\mathrm{i}}\ R_{\mathrm{o}}\ V_{\mathrm{s,3}}). \tag{10.10}$$

Adaptation of the Proportional Method

The proportional method was adapted to estimate the parameters of the three-chamber model from the data presented in this section. The proportionality relations used in this adaptation are summarised in the following matrix:

$$\begin{array}{c} \\ E_{\mathrm{h}} \\ E_{\mathrm{a}} \\ E_{\mathrm{v}} \\ R_{\mathrm{i}} \\ R_{\mathrm{o}} \\ V_{\mathrm{s,3}} \end{array} \begin{array}{c} \begin{array}{ccccccc} \Delta P_{\mathrm{a}} & \Delta P_{\mathrm{v}} & \Delta V_{\mathrm{s,h}} & \bar{P}_{\mathrm{a}} & \bar{P}_{\mathrm{v}} & \bar{V}_{\mathrm{s,h}} & \max_T \frac{\mathrm{d}P_{\mathrm{a}}(t)}{\mathrm{d}t} \end{array} \\ \begin{pmatrix} 0 & 0 & 0 & 0 & 0 & -1 & 0 \\ 1 & 0 & 0 & 0 & 0 & 0 & 0 \\ 0 & 1 & 0 & 0 & 0 & 0 & 0 \\ 0 & 0 & 0 & 0 & 1 & 0 & 0 \\ 0 & 0 & 0 & 0 & 0 & 0 & -1 \\ 0 & 0 & 1 & 0 & 0 & 0 & 0 \end{pmatrix} \end{array} = \mathbf{M}. \tag{10.11}$$

The proportionality relations for E_h and E_a are adapted from the initial version of the method [113], while the one for R_o is adapted from a later version [93]. In the initial version of the method, R_c was also linked to $\bar{P}_a$. However, in this work, R_c is exactly computed from $\bar{P}_a$ and other measurements. Consequently, the proportionality between R_c and $\bar{P}_a$ does not appear in the matrix. The relation between E_v (or R_i) and its corresponding output can be directly inferred from Equation 9.54 (or 9.28). Finally, the proportionality between $V_{s,3}$ and $\Delta V_{s,h}$ is inherent to the model equations and is not an approximation.

Implementation

Matlab (2014b, MathWorks, Natick, MA) was used to solve model equations and perform parameter identification procedures. It was run on a standard laptop computer. The model was simulated for 100 cardiac periods, to let transient effects disappear. Then, the values obtained during the 101st period were used to compute the output vector.

The seven parameter identification methods have different termination criteria, related to the size of the step taken in the parameter space, to the size of the decrease in ψ_2 value, or to the values of the components e_i. To fairly compare the methods, they were all simulated with very strict termination criteria, and each function evaluation was recorded. Then, using the recorded results, the same termination criteria were applied to all methods. The criteria were:

- A maximum of 100 function evaluations,
- A tolerance of 0.01 on the optimal function value. In other words, a method was not considered successful, and thus not stopped, until [194]:

$$\psi_2 - \psi_2(\mathbf{p}^*) \leq 0.01(1 + |\psi_2(\mathbf{p}^*)|), \tag{10.12}$$

  where $\psi_2(\mathbf{p}^*)$ is the optimal value of ψ_2. For parameter identifications performed using *in silico* reference data, $\psi_2(\mathbf{p}^*)$ was known and equal to zero. For parameter identifications performed using experimental reference data, $\psi_2(\mathbf{p}^*)$ was taken as the lowest ψ_2 value found across all methods and all function evaluations.

The TRR, interior point, active set and SQP methods require the user to provide upper and lower bounds on the possible parameter values. These bounds were set at 10 and 0.1 times the initial parameter values.

10.3.2 Test 1: *In Silico* Reference Data

Methodology

First, zero-noise, *in silico* reference data $\mathbf{y}^{\text{ref}}$ was generated using the four parameter sets displayed in Table 10.1. Parameter sets A and B produce simulations representing the haemodynamics of a patient with high (A) or low (B) cardiac contractility, E_{h}. Parameter set C produces simulations representing the effects of dobutamine, defined here as high contractility, E_{h} and low cardiac period, T. Parameter set D represents a case with low venous elastance, E_{v}. These four sets cover a representative spread of parameter values that might be encountered clinically.

Table 10.1: Reference parameter sets.

Parameter	Units	A	B	C	D
T	s	0.8	0.8	0.5	1.1
R_{c}	mmHg s/ml	1.5	1.1	2.7	3.7
$e(t)$	-	$\exp\left[-W\left((t \bmod T) - \frac{T}{2}\right)^2\right]$			
W	s^{-2}	17	80	60	19
R_{i}	mmHg s/ml	0.04	0.05	0.04	0.04
R_{o}	mmHg s/ml	0.2	0.05	0.01	0.02
E_{h}	mmHg/ml	4.7	1.4	4	2.6
E_{a}	mmHg/ml	1.2	1	3	1.4
E_{v}	mmHg/ml	0.1	0.2	0.2	0.008
$V_{\text{s},3}$	ml	400	250	140	600

Let $\mathbf{p}^{\text{ref}}$ be a set of reference parameters and $\mathbf{p}[n]$ be the parameter vector obtained at the nth iteration of the parameter identification process. The relative error vector $\mathbf{r}$ between reference and identified parameters was defined:

$$r_j[n] = \frac{p_j^{\text{ref}} - p_j[n]}{p_j^{\text{ref}}}, \text{ for } i = 1 \text{ to } 6. \tag{10.13}$$

As previously explained, the number of components in $\mathbf{r}$ is 6, for parameters E_{h}, E_{a}, E_{v}, R_{i}, R_{o} and $V_{\text{s},3}$, since R_{c} can be directly computed from the available data using Equation 9.36, and T and $e(t)$ are assumed known. The total relative error between reference and identified parameter values was defined:

$$\|\mathbf{r}\|_1 = |r_1| + |r_2| + |r_3| + |r_4| + |r_5| + |r_6|. \tag{10.14}$$

Equation 10.14 is thus a measure of method accuracy in a noise-free case, when the true parameter values are known.

Results: Ability to Retrieve the Reference Parameters

Table 10.2 summarises the outcomes of the parameter identification procedures carried out using the seven methods of Section 10.2 on the four *in silico* reference datasets of Table 10.1. All methods reached a ψ_2 value lower than 0.01 for at least one dataset. TRR and active set reached it for all 4 datasets, proportional, for 3 datasets, and SQP, for 2 datasets.

Results: Convergence Speed and Number of Function Evaluations

Figure 10.1 displays the evolution of the error, ψ_2, between reference and simulated output values during the parameter identification processes carried using the *in silico* reference parameter sets. Table 10.3 displays the number of function evaluations taken by the seven parameter identification methods to solve the four parameter identification problems on *in silico* reference data. According to these results, the TRR and active set methods were the fastest.

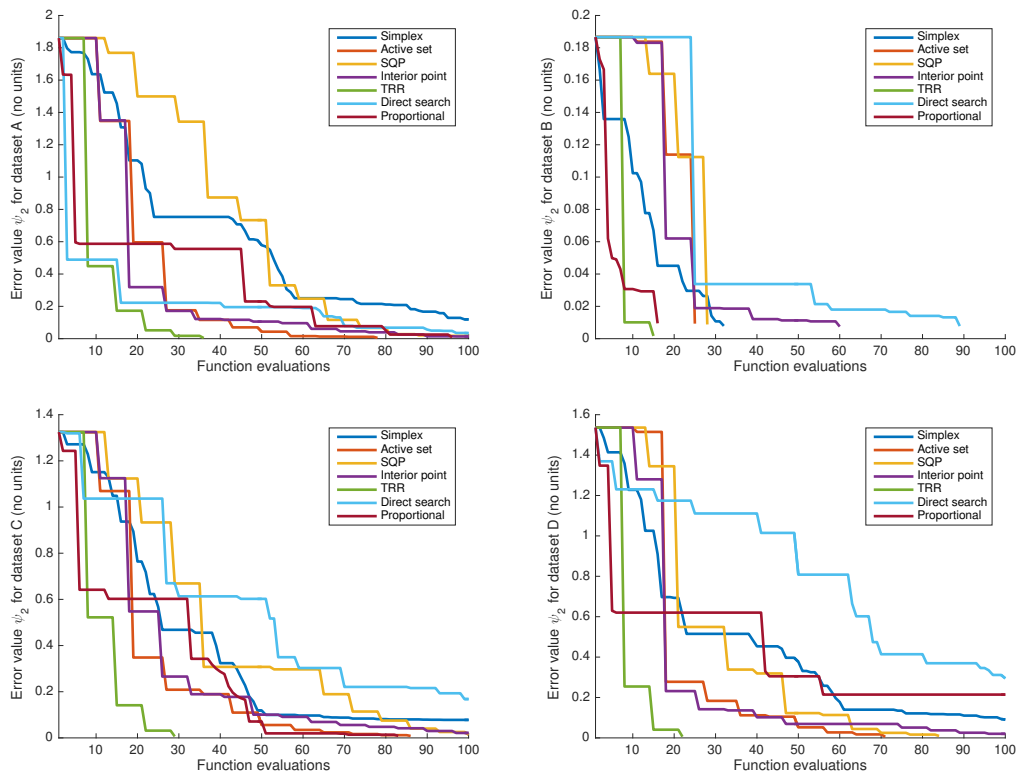

Figure 10.1: Error between reference and simulated output values for the seven parameter identification methods, tested on data from the four *in silico* reference datasets.

Table 10.2: Result of the 28 parameter identification procedures carried out on *in silico* reference data. Successful results according to Equation 10.12 are bold-faced.

Dataset	Method	r_1	r_2	r_3	r_4	r_5	r_6	Min. ψ_2
	Proportional	**-0.03**	**0.06**	**-0.03**	**0.10**	**-0.03**	**0.03**	**0.009**
	TRR	**0.07**	**-0.02**	**-0.07**	**-0.34**	**0.11**	**0.02**	**0.004**
	Interior point	0.05	-0.13	-0.11	-0.49	-0.32	0.05	0.014
A	**Active set**	**-0.03**	**-0.09**	**0.00**	**0.03**	**-0.34**	**0.03**	**0.005**
	SQP	-0.14	-0.22	-0.04	0.11	-1.26	0.05	0.018
	Simplex	-0.17	-0.10	-0.03	-0.90	-0.42	-0.20	0.120
	Direct search	-0.00	-0.27	-0.22	-0.32	-0.65	0.14	0.034
	Proportional	**0.00**	**-0.01**	**0.01**	**0.06**	**-0.43**	**-0.01**	**0.010**
	TRR	**-0.04**	**-0.04**	**0.01**	**0.00**	**-0.32**	**0.01**	**0.002**
	Interior point	**-0.11**	**-0.05**	**0.03**	**0.02**	**-0.77**	**0.01**	**0.008**
B	**Active set**	**-0.06**	**-0.02**	**-0.00**	**0.05**	**-0.62**	**-0.01**	**0.009**
	SQP	**-0.06**	**-0.03**	**-0.00**	**0.05**	**-0.62**	**-0.01**	**0.009**
	Simplex	**-0.14**	**-0.05**	**-0.00**	**0.03**	**-0.47**	**0.02**	**0.008**
	Direct search	**-0.16**	**-0.02**	**0.06**	**0.07**	**-0.46**	**0.01**	**0.008**
	Proportional	**-0.04**	**0.00**	**-0.02**	**0.14**	**-1.31**	**0.05**	**0.009**
	TRR	**0.04**	**-0.08**	**-0.03**	**-0.15**	**-1.67**	**0.01**	**0.006**
	Interior point	-0.07	-0.10	0.02	-0.09	-5.77	-0.02	0.021
C	**Active set**	**-0.05**	**-0.05**	**-0.01**	**0.05**	**-3.55**	**0.02**	**0.009**
	SQP	-0.09	-0.04	0.08	0.16	-3.37	-0.00	0.014
	Simplex	-0.00	-0.41	-0.19	-0.34	-11.98	0.14	0.078
	Direct search	-0.26	-0.43	-0.12	0.28	-3.28	0.30	0.168
	Proportional	-0.02	-0.01	-0.50	-0.53	0.29	0.15	0.214
	TRR	**0.05**	**-0.06**	**-0.09**	**-0.06**	**-0.21**	**0.09**	**0.006**
	Interior point	-0.04	-0.11	-0.01	0.04	-3.06	0.05	0.020
D	**Active set**	**-0.05**	**0.01**	**0.03**	**0.05**	**-1.13**	**-0.03**	**0.005**
	SQP	**-0.05**	**-0.04**	**0.03**	**0.08**	**-1.87**	**-0.00**	**0.010**
	Simplex	-0.02	-0.44	-0.13	-0.23	-6.88	0.08	0.091
	Direct search	0.05	-0.86	-0.08	-0.67	-15.99	0.00	0.295

10.3.3 Test 2: Experimental Reference Data

Methodology

As a second test, experimental animal data was used for parameter identification. This data came from measurements on three anaesthetized pigs. The pigs

Table 10.3: Number of function evaluations taken by the seven parameter identification methods to determine parameters for the four *in silico* reference datasets.

Evaluations	A	B	C	D
Proportional	96	16	83	100
TRR	36	42	29	22
Interior point	100	60	100	100
Active set	78	25	86	71
SQP	100	28	100	84
Simplex	100	32	100	100
Direct search	100	89	100	100

were mechanically ventilated at a positive end-expiratory pressure of 5 cmH_2O. Catheters (Transonic, NY) provided continuous recording of left ventricular pressure and volume and aortic pressure. SV, aortic PP, MAP, mean left ventricular volume (MLVV), aortic $\mathrm{d}P/\mathrm{d}t_{\max}$, T, $e(t)$, t_{BE} and t_{EE} were inferred from these measurements. A PiCCO monitor provided recording of CVP and vena cava PP. These experiments were approved by the Ethics Commission for the Use of Animals at the University of Liège, and details on the experimental procedure can also be found in Chapter 12.

The following correspondence was established between measurements and reference output values:

- Aortic PP was taken as $\Delta P_{\mathrm{a}}^{\mathrm{ref}}$,
- Vena cava PP was taken as $\Delta P_{\mathrm{v}}^{\mathrm{ref}}$,
- SV was taken as $\Delta V_{\mathrm{s,h}}^{\mathrm{ref}}$,
- MAP was taken as $\bar{P}_{\mathrm{a}}^{\mathrm{ref}}$,
- CVP was taken as $\bar{P}_{\mathrm{v}}^{\mathrm{ref}}$,
- MLVV was taken as $\bar{V}_{\mathrm{s,h}}^{\mathrm{ref}}$, thus assuming zero cardiac unstressed volume: $V_{\mathrm{u,h}} = 0$,
- Aortic $\mathrm{d}P/\mathrm{d}t_{\max}$ was taken as $\max_T \mathrm{d}P_{\mathrm{a}}^{\mathrm{ref}}/\mathrm{d}t$

Datasets E, F and G correspond to the basal state of pigs number 1, 2 and 3, while dataset H was recorded on pig number 3 after dobutamine infusion. The quality of the parameter estimation was assessed using only the error function ψ_2, since there are no reference parameter values in this case.

Results: Final Error Value

Table 10.4 displays the final ψ_2 value for the seven parameter identification methods tested on the four experimental datasets. Overall, the gradient-based meth-

ods, comprising the active set, SQP, interior point ant TRR methods, were able to find the lowest error values when applied to experimental data. The simplex method performed slightly worse than the gradient-based methods and the direct search and proportional methods were the worst in finding the lowest error values. The proportional method is strongly penalised by its bad performance on dataset G, as it performed very well on the other datasets.

Table 10.4: Minimum error value for the four parameter identification problems using experimental data. Successful results according to Equation 10.12 are bold-faced.

Minimum ψ_2	E	F	G	H
Proportional	**0.008**	0.040	3.217	**0.005**
TRR	**0.003**	0.011	**0.592**	**0.007**
Interior point	**0.005**	0.051	0.696	**0.007**
Active set	0.246	0.011	0.832	0.443
SQP	0.049	0.011	0.604	**0.004**
Simplex	0.170	0.260	1.735	0.043
Direct search	0.032	0.126	3.231	0.056

In terms of successful parameter identification procedures according to Equation 10.12, the TRR method was best, as it was successful in 3 of 4 cases. The interior point and proportional methods were successful in 2 cases and the SQP method, in 1 case. No parameter identification method was successful for dataset F. For this dataset, the direct search method reached the lowest error of 0.0006 after 1292 function evaluations. However, note that the optimal values for parameters R_i and R_o was slightly below the lower bound set on these parameters for the TRR, active set, interior point and SQP methods. This observation explains why none of these methods was able to retrieve the optimal parameter values, even if three of them, TRR, active set and SQP, stopped very close.

Results: Convergence Speed and Number of Function Evaluations

Figure 10.2 displays the evolution of the error between reference and simulated output values, ψ_2, during the parameter identification processes carried using the experimental reference parameter sets.

Table 10.5 displays the number of function evaluations taken by the seven parameter identification methods to solve the four parameter identification problems on experimental reference data. The two fastest methods are the proportional and TRR.

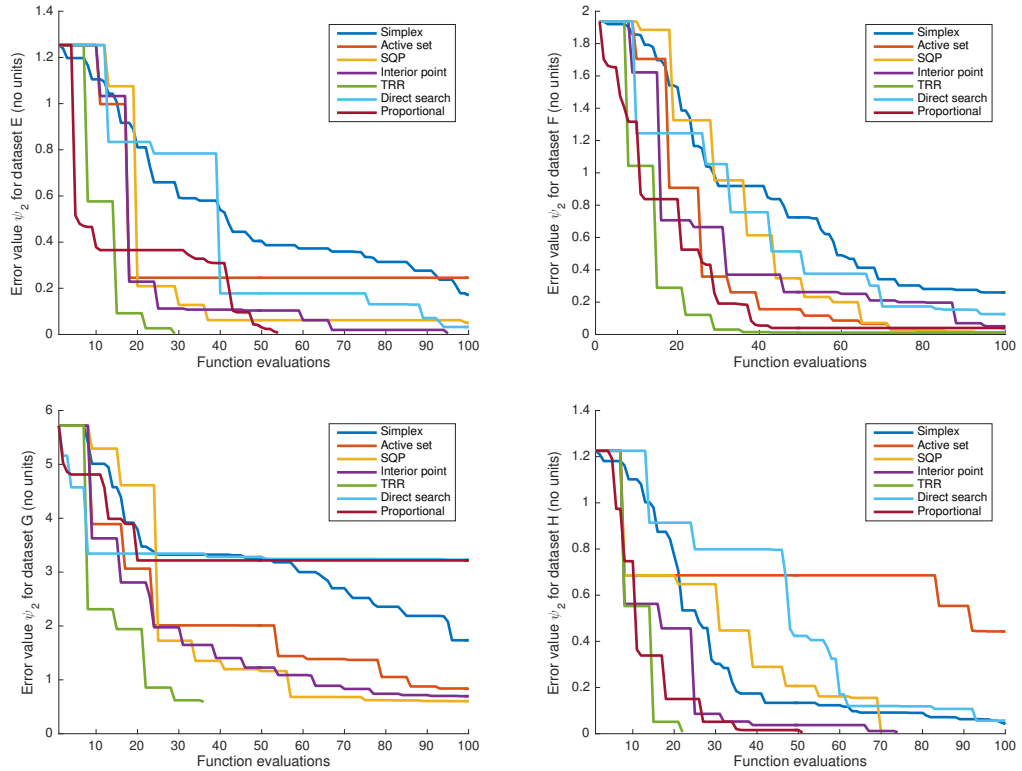

Figure 10.2: Error between reference and simulated output values for the seven parameter identification methods, tested on data from the four experimental reference datasets.

Table 10.5: Number of function evaluations taken by the seven parameter identification methods to determine parameters for the four experimental datasets.

Evaluations	A	B	C	D
Proportional	54	100	100	51
TRR	29	100	36	22
Interior point	95	100	100	74
Active set	100	100	100	100
SQP	100	100	100	70
Simplex	100	100	100	100
Direct search	100	100	100	100

10.3.4 Discussion

Seven methods were investigated in this chapter. These methods have been chosen because they are frequently applied to CVS models and/or because they are built in the widely used software Matlab, and thus, commonly used for parameter identification in general. The seven methods investigated encompass the two

main classes of identification methods, namely gradient-based and derivative-free methods. Two of these methods, TRR and proportional, work on the error vector, **e**, as a whole. The other five work on the norm of the error vector, ψ_2.

The proportional method of Hann *et al.* [113] is not always able to retrieve the parameters used to generate *in silico* reference data. It sometimes stops without having reached a low error value. However, it is one of the two fastest methods, along with the TRR method, which is related to the *a priori* information required by this algorithm.

The TRR method was, with the active set, the most effective when applied to *in silico* reference data. It also performed well on experimental data. As mentioned previously, it is one of the two fastest methods, with the proportional method. Interestingly, these two fastest methods are the two methods working on the error vector, rather than on its norm. The good performance of the TRR method indicates that the objective function ψ_2 is smooth, since the principle of the method is to approximate the objective with a quadratic function.

The interior point method reached average performance, both when retrieving reference parameter values and when minimising the error between simulations and measured reference data. This average performance is not compensated by speed, since this method also had an average speed.

The active set method retrieved the reference parameters in all cases. However, it never succeeded when tested with experimental data. On average, it was the third fastest method, after the TRR and proportional methods.

The SQP method retrieved the reference parameters in half the cases. When applied to experimental data, it achieved the second lowest errors. However, it stopped before succeeding in 3 of 4 cases. This method has an average speed.

The simplex method retrieved only one of the reference parameter sets and stopped with high error values. It is also very time-consuming. These drawbacks are probably linked to the fact that this method is derivative-free.

The other derivative-free method, the direct search method, was as unreliable with *in silico* reference data. It also had the highest errors when applied to experimental data. However, it found the lowest error for dataset F, for which no method succeeded. Its speed was the lowest in comparison to the others.

Comment on Practical Identifiability

Table 10.2 presents several cases for which the minimum ψ_2 value is lower than 0.01, but large errors are still present on the 5th parameter, R_{o}. These errors reach up to 355 %, meaning that the valve parameter R_{o} is practically difficult to identify from the selected model outputs, despite noise-free data. The 4th parameters,

R_i, also presents one occurrence of a similar issue, with an error equal to 34 %. In the successful parameter identification procedures, the final error on the other four parameters is always lower than 16 %, meaning that these parameters, E_h, E_a, E_v and $V_{\mathrm{s},3}$, are correctly retrieved.

Limitations

The results discussed in this chapter only apply to the three-chamber CVS model, with the selected output set and error function. If a different model, output set or error function is investigated, the analysis would need to be repeated. To do so, the methodology can easily be transposed, as the overall approach is general.

Precision of the Initial Values

To evaluate the quality of Equations 9.28, 9.34, 9.40, 9.49, 9.54 and 9.56 used to compute the initial parameter values, the initial total relative error $\|\mathbf{r}[1]\|_1$ between reference and identified parameters was assessed. Its value ranges from 133 to 1576 %. Interestingly, the largest errors were again related to the valve parameters. If these errors are not considered, the total initial error on the four remaining parameters (E_h, E_a, E_v and $V_{\mathrm{s},3}$) ranges from 35 to 136 %, indicating relatively good precision for the approximations of Equations 9.40, 9.49, 9.54 and 9.56.

Availability of the Experimental Data

As previously mentioned, the experimental data used in Section 10.3.3 was obtained from animal experiments in a haemodynamics laboratory. The present section discusses the availability of the same data in the ICU. First, CO, and thus, SV can clinically be obtained using the thermodilution, as explained in Section 7.3.4, or echocardiography techniques. Second, MLVV can be approximated as the mean of LVEDV and left ventricular end-systolic volume (LVESV), using:

$$\begin{aligned} \mathrm{MLVV} &\approx 0.5\,\mathrm{LVEDV} + 0.5\,\mathrm{LVESV} \\ &= \mathrm{LVEDV} - 0.5\,\mathrm{SV}. \end{aligned} \tag{10.15}$$

GEDV is measured by some cardio-vascular monitoring devices using transpulmonary thermodilution procedures, as discussed in Section 7.3.4. In turn, LVEDV can be derived from the value of GEDV [195].

Third, systemic arterial pressure can be obtained using an arterial catheter. This measurement allows the computation of arterial PP, MAP, arterial $\mathrm{d}P/\mathrm{d}t_\mathrm{max}$,

T, t_{BE} and t_{EE}, which are needed for parameter identification. Fourth, central venous pressure is provided by a central venous catheter. Its mean, CVP, and PP can then easily be obtained. Finally, practical determination of the driver function requires simultaneous measurements of left and right ventricular pressures and volumes at different afterload levels. These measurements are not generally made in a clinical setting. However, Senzaki *et al.* found that the driver function was relatively similar for any human heart [117]. This makes *a priori* generic driver functions a sensible assumption in subject-specific use.

10.4 Summary

This chapter presented seven parameter identification methods and compared their performance on the three-chamber CVS model. The seven methods were tested using *in silico* and experimental reference data and assessed on their speed and ability to decrease the error between simulations and measurements. The TRR method seems to be the best method to recommend for the three-chamber model. The proportional method also performed well, as it is specifically designed for the identification of lumped CVS models.

Overall, this chapter confirmed that identification of three-chamber CVS model parameters can be performed rapidly. Such models offer a large interest for cardiac and vascular monitoring applications. The application of these methods and models to the prediction of fluid responsiveness is the topic of the following chapters.

Part IV

Application: Prediction of Fluid Responsiveness

Introduction

In Chapter 3, SBV was introduced as a potential index of fluid responsiveness. However, the experimental procedure required to measure this parameter is very cumbersome. Mathematical models of the CVS allow to estimate model-based equivalents of this parameter, without having to perform circulatory arrests.

Part II of this work introduced two mathematical models of the CVS and their parameters, $V_{s,3}$ and $V_{s,6}$, which represent model-based equivalents of SBV. Part III explained how to identify the parameters of these two models. The last part of this work presents two applications of the previously introduced concepts to experimental data. Chapter 11 explains how to identify the total stressed volume, $V_{s,6}$, of the six-chamber model. Chapter 12 presents the identification of the three-chamber model parameters to vascular filling data and compares $V_{s,3}$ with other indices of fluid responsiveness.

Chapter 11

Parameter Identification in the Six-Chamber Model from a Preload Reduction Manoeuvre

11.1 Introduction

This chapter focuses on the computation of $V_{s,6}$, the parameter of the six-chamber model representing the total stressed blood volume in the CVS. It is an important parameter for both physicians and engineers. From the clinician's point of view, $V_{s,6}$ is interesting because it is a model-based analogue of SBV, introduced in Section 3.5. Indeed, as for its physiological counterpart SBV, if a blood volume equal to $V_{s,6}$ is removed from the six-chamber model, all pressures become zero.

As explained in Section 3.5, SBV has recently regained interest in the context of fluid therapy. In this context, Maas *et al.* have recently shown that, the lower the SBV, the higher the likelihood a patient would positively respond to fluid therapy [32]. The current method to determine SBV has several drawbacks, which have been described in Section 3.5.

To assist physicians, engineers have developed a wide range of CVS models. Such models can either be open [87,93] or closed-loop [88,92,98]. Open-loop models only represent a section of the CVS and thus, have input and output flows. Closed-loop models represent the whole CVS and thus, have neither input nor output flows. In other words, the total quantity of blood in such models is fixed and conserved, per Equation 4.16. When using a closed-loop model, it is thus paramount to know the total volume in the model. More precisely, most closed-loop CVS models rely on the concept of total stressed volume, as emphasised in Chapter 6.

However, this importance is often underestimated, because most studies focusing on CVS models aim at simulating situations in which the determinants of CO, which are contractility, preload, afterload and HR, as described in Section 2.3.5, are constant [87,93–95,98,99,101,112,141,150], while the effect of total stressed volume only appears in simulations in which these determinants change. Nevertheless, this type of simulation is the most useful, because in real life, these determinants are constantly changing due to breathing, exercise, and other factors. In addition, sudden larger changes occur in dysfunction. It is equally important clinically, where changes in state must be managed by treatment. Paradoxically, few works have sought to determine this total stressed volume and many authors do not even mention the value used in simulation.

This chapter presents a method to estimate total stressed volume, $V_{s,6}$, based on the use of the six-chamber CVS model. The model has been described in Section 6.3. Identification of the model parameters on data from preload reduction manoeuvres provides a value for $V_{s,6}$. The overall study presented is adapted from [123,196].

11.2 Methods

11.2.1 Cardio-Vascular System Model

The six-chamber model presented in Section 6.3 was used, and the following form was chosen for the driver functions [98]:

$$e_i(t) = \exp\left[-W_i\left((t \bmod T) - \frac{T}{2}\right)^2\right] \text{ with } i = \text{LV or RV}, \tag{11.1}$$

where W_i dictates the width of the Gaussian function and T is the cardiac period. This formulation of the driver functions is the simplest possible, while still being physiologically representative, and involves only two parameters. It was chosen to make the model and the parameter identification process as simple as possible, and maintain physiological relevance.

11.2.2 Rationale for Identification of $V_{s,6}$

When preload or afterload are changing, the inability to simultaneously determine venous elastances and $V_{s,6}$ highlighted in Section 9.4.1 vanishes. To show it, the six-chamber model reaction to a preload reduction manoeuvre is simulated. The preload reduction manoeuvre is modelled as a sudden twofold increase of tricuspid valve resistance R_{TV} at an instant chosen to be $t = 0$ and going on for

$t > 0$. This method of reproducing the experimental preload reduction manoeuvre is discussed in detail in Section 11.4.

The model reaction to such an increase of R_{TV} is displayed in Figure 11.1 for the two parameter sets of Table 11.1. As can be seen in this figure, the simulations before preload reduction ($t < 0$) are very similar for the two parameter sets. However, when preload is suddely reduced, pressures and volumes change differently for the two parameter sets. Note that the new steady state reached after the preload change is also different. The parameters E_{SV}, E_{PV} and $V_{\mathrm{s},6}$ are thus important when preload is varying. This idea will be used to compute $V_{\mathrm{s},6}$ from experimental data.

Table 11.1: Parameter values for the two simulations of the six-chamber CVS model presented in Figure 11.1.

Parameter	Units	Value
T	s	0.6
E_{LV}	mmHg/ml	2
E_{RV}	mmHg/ml	0.8
E_{SA}	mmHg/ml	2.5
E_{PA}	mmHg/ml	2.1
E_{SV}	mmHg/ml	0.01 (left), 0.22 (right)
E_{PV}	mmHg/ml	0.01 (left), 0.30 (right)
R_{MV}	mmHg s/ml	0.05
R_{AV}	mmHg s/ml	0.04
R_{TV}	mmHg s/ml	0.04
R_{PV}	mmHg s/ml	0.03
R_{sys}	mmHg s/ml	2.5
R_{pul}	mmHg s/ml	0.4
$V_{\mathrm{s},6}$	ml	1500 (left), 250 (right)
$e_{\mathrm{LV}}(t)$	-	$\exp\left[-80\left((t \bmod T) - \frac{T}{2}\right)^2\right]$
$e_{\mathrm{RV}}(t)$	-	$\exp\left[-80\left((t \bmod T) - \frac{T}{2}\right)^2\right]$

11.2.3 Experimental Data

To identify model parameters and prove the concept, experimental animal data were used. These data came from basal state measurements on seven pigs (num-

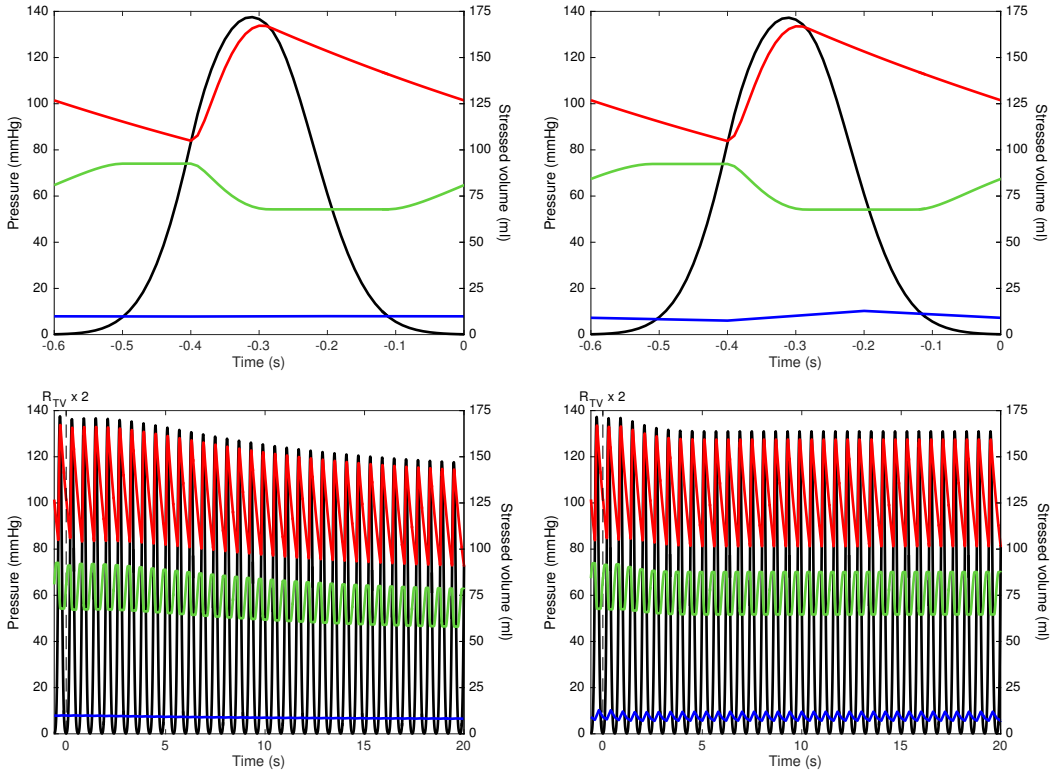

Figure 11.1: Simulations of the six-chamber CVS model using the two parameter sets of Table 11.1. Tricuspid valve resistance is doubled at $t = 0$ s. *Black*: left ventricular pressure, *blue*: pulmonary vein pressure, *red*: aortic pressure, *green*: left ventricular stressed volume.

bered 1 to 7). The ethical approval for these experiments is mentioned in Section 7.2. Detail on the experimental procedures, including detail on medication and mechanical ventilation settings are available elsewhere [197–199]. Only the elements important for the understanding of the methodology are repeated here.

As previously mentioned, the chests of the pigs were opened to enable easier access to the heart. Measurements comprised continuous recording of:

- Left and right ventricular volumes and pressures with conductance micromanometer-tipped catheters,
- Systemic arterial pressure with a micromanometer-tipped catheter inserted into the descending thoracic aorta,
- pulmonary arterial pressure with a micromanometer-tipped catheter inserted into the main pulmonary artery.

The pigs were also weighed at the beginning of the experiments.

A Fogarty balloon catheter was introduced in the inferior vena cava of each animal. After all sensors were correctly positioned, preload was transiently reduced by inflating the balloon, as illustrated in Figure 11.2. This procedure is

further referred to as a *preload reduction manoeuvre*. In two animals (numbered 1 and 3), two preload reduction manoeuvres were performed.

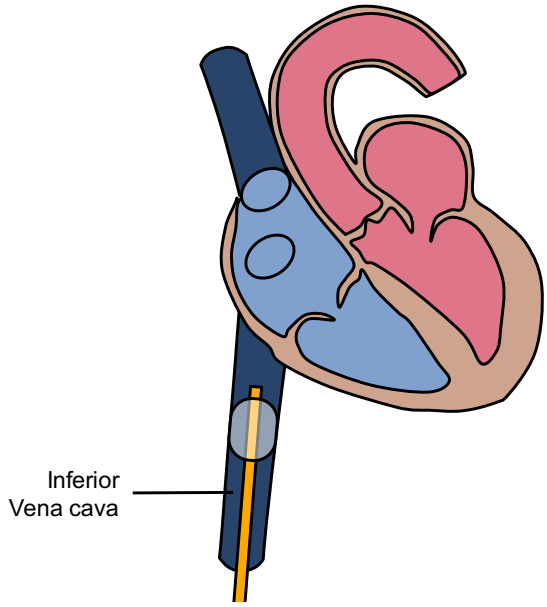

Figure 11.2: Illustration of the preload reduction manoeuvre.

In total, 9 experimental datasets were thus used, relative to seven animals. Table 11.2 summarises the following experimental data for the nine datasets:

- Mean left (MLVV) and right ventricular volumes,
- Left and right ventricular SVs,
- Mean systemic (MAP) and pulmonary arterial (MPAP) pressures,
- Systemic and pulmonary arterial PPs.

These eight indices were computed on the last heart beat before initiation of the preload reduction manoeuvre, presented in the first eight rows of Table 11.2, and on the last heart beat before stopping the preload reduction manoeuvre, which are in the last eight rows. The duration, $t_{\max}$, of each preload reduction manoeuvre is provided in Section 11.3.2.

Note that in [198] and [199], more experiments were performed to obtain data from preload reduction manoeuvres. However, the resulting measurements were not regular, due to premature ventricular contractions, and were thus not included in the present analysis. These premature contractions were probably caused by the large amount of sensors inserted in the animals' CVS and were thus not physiologically relevant to the present study.

Table 11.2: Summary of the experimental data. The asterisk (*) denotes cases for which measured pulmonary artery pressure was negative at the end of the preload reduction manoeuvre.

	Pig 1	Pig 1	Pig 2	Pig 3	Pig 3	Pig 4	Pig 5	Pig 6	Pig 7
Last heart beat before preload reduction									
MLVV (ml)	67.4	64.0	80.2	66.1	65.3	56.3	67.1	63.2	53.7
Left ventricular SV (ml)	27.0	25.1	23.4	30.8	33.9	27.5	27.6	28.1	18.3
MAP (mmHg)	123.6	112.0	74.0	117.4	110.0	117.3	74.8	80.1	58.3
Systemic arterial PP (mmHg)	30.9	24.7	19.0	30.4	26.8	33.2	34.1	37.1	21.8
Mean right ventricular volume (ml)	55.8	56.7	62.7	45.2	45.6	50.5	66.5	37.9	49.9
Right ventricular SV (ml)	17.3	16.7	18.1	10.7	10.9	14.9	20.5	17.5	12.6
MPAP (mmHg)	15.0	14.7	11.2	4.7	4.1	8.6	9.8	14.4	11.9
Pulmonary arterial PP (mmHg)	9.6	9.0	8.6	7.7	7.3	9.7	12.0	12.6	11.6
Last heart beat before stopping preload reduction									
MLVV (ml)	47.0	47.1	63.9	43.1	49.7	44.9	50.1	50.5	50.6
Left ventricular SV (ml)	8.1	7.4	18.3	9.0	20.2	13.5	11.0	20.3	15.9
MAP (mmHg)	68.9	63.8	55.4	68.5	94.5	100.1	41.4	62.8	52.3
Systemic arterial PP (mmHg)	13.8	10.6	15.7	16.5	21.2	26.4	19.4	31.9	19.4
Mean right ventricular volume (ml)	46.3	46.5	53.9	42.6	41.9	41.7	55.8	33.1	46.4
Right ventricular SV (ml)	8.7	9.2	6.6	7.9	8.1	8.6	7.2	11.7	13.2
MPAP (mmHg)	5.9	6.1	4.7	-1.8*	-0.9*	2.2*	0.8*	7.5	5.8
Pulmonary arterial PP (mmHg)	4.8	4.3	5.5	7.2*	5.6*	5.7*	4.5*	11.5	6.8

11.2.4 Parameter Identification

The parameter identification procedure involved three steps. First, initial values had to be assigned to all 16 model parameters. From simulations carried out using these values, the subset selection algorithm of Section 9.5 selected a sensitive subset of parameters to be further identified. Finally, this subset of parameters was identified using an iterative procedure.

Initial Parameter Values

To assign initial values to the model parameters, the formulae developed in Section 9.6 were used in combination with the available data.

1. The cardiac period, T, was computed by dividing the duration of the preload reduction manoeuvre by the number of cycles during the experiment. The assumption of constant cardiac period was consistent with the experimental data presented in Section 11.3.2.
2. Left ventricular end-systolic elastance, E_{LV}, and left ventricular unstressed volume $V_{\mathrm{u,LV}}$ as a byproduct, have been determined by linear regression of the left ventricular end-systolic pressure-volume points, according to the method of Kass *et al.* [179], described in Section 9.6.4. Then, the experimental driver function was computed using Equation 5.3 and the parameter W_{LV} for the driver function in Equation 11.1 was estimated by fitting Equation 11.1 to the previously computed curve.
3. Parameters E_{RV}, $V_{\mathrm{u,RV}}$ and W_{RV} were computed by an analogous procedure. In the previous computations, parameters T, W_{LV}, W_{RV}, E_{LV} and E_{RV} were computed by directly fitting the model to the data. Computation of the other parameters from the available data required some degree of approximation. When it was not possible to infer a parameter value only from the data, reference values published in the literature were used.
4. The resistance of the systemic circulation, R_{sys}, was computed using Equation 9.37.
5. The resistance of the pulmonary circulation, R_{pul}, was estimated using the pulmonary counterpart of Equation 9.37.
6. Systemic arterial elastance, E_{SA}, was estimated by fitting the measured aortic pressure during diastole to Equation 9.44.
7. The same procedure has been applied to compute E_{PA} from the measured pulmonary arterial pressure.
8. As venous pressures were not measured, Equations 9.25 or 9.28 could not be used to compute mitral and tricuspid valve resistances R_{MV} and R_{TV}. These parameters were thus initialized at values provided by Revie *et al.* [93] in

another study performed on the data used in this chapter, specifically:

$$R_{\mathrm{MV}} = 0.05 \text{ mmHg s/ml} \tag{11.2}$$

$$R_{\mathrm{TV}} = 0.04 \text{ mmHg s/ml.} \tag{11.3}$$

9. As further discussed in Section 11.3.2, measured aortic pressure is higher than measured left ventricular pressure during a large part of ejection. This discrepancy prevented the use of Equation 9.31 for computation of aortic and pulmonary valve resistances R_{AV} and R_{PV}. They were also initialised at values provided by Revie *et al.* [93]:

$$R_{\mathrm{AV}} = 0.04 \text{ mmHg s/ml} \tag{11.4}$$

$$R_{\mathrm{PV}} = 0.03 \text{ mmHg s/ml.} \tag{11.5}$$

10. Since systemic venous pressure was not measured, Equation 9.54 could not be used to compute initial systemic venous elastance E_{SV}. Therefore, a study by Zanzinger *et al.* [200] was used, where *inferior* vena cava elastance for pigs was found to be 0.44 mmHg/(ml/kg). This value was divided by 2 to account for the two venae cavae in parallel. The initial value of E_{SV} is thus 0.22 mmHg kg/ml divided by the pig's weight.
11. Since pulmonary venous pressure was also not measured, an experimental study by Barbier *et al.* was used to obtain the amplitude of pulmonary vein pressure in pigs [201]. Using this data, Equation 9.54 could be used to approximate E_{PV}.
12. To evaluate $V_{\mathrm{s},6}$, experimental pressure-volume curves on dogs published by Drees and Rothe [78] were used. These pressure-volume curves are similar to the one presented in Figure 3.8, except that the infused volume is expressed in ml/kg. From these curves, a SBV of 31.95 ml/kg was estimated, which was taken as the initial value for $V_{\mathrm{s},6}$ in the identification process.

As mentioned before, initial values of the parameters T, W_{LV}, W_{RV}, E_{LV} and E_{RV} were computed by directly fitting the model equations to the data. Consequently, it was assumed that the parameter identification process would not greatly alter these parameter values. They were thus excluded from the following selection procedure, and the remaining 1×11 parameter vector was defined:

$$\mathbf{p} = (E_{\mathrm{SA}}\ E_{\mathrm{PA}}\ R_{\mathrm{sys}}\ R_{\mathrm{pul}}\ R_{\mathrm{MV}}\ R_{\mathrm{AV}}\ R_{\mathrm{TV}}\ R_{\mathrm{PV}}\ E_{\mathrm{SV}}\ E_{\mathrm{PV}}\ V_{\mathrm{s},6}). \tag{11.6}$$

Subset Selection Algorithm

A subset of the parameter vector, $\mathbf{p}$, was selected for optimization using the dedicated algorithm presented in Section 9.5. As explained in that section, the algorithm performs a sensitivity analysis on the error vector, $\mathbf{e}$, and selects the parameters to which $\mathbf{e}$ is the most sensitive.

The output vector $\mathbf{y}^n$ for dataset number n was defined:

$$y_1^n = \frac{1}{T}\int_{-T}^{0} V_{\mathrm{LV}}(t)\,\mathrm{d}t \tag{11.7}$$

$$y_2^n = \max_{t\in[-T,0]} V_{\mathrm{LV}}(t) - \min_{t\in[0,T]} V_{\mathrm{LV}}(t) \tag{11.8}$$

$$y_3^n = \frac{1}{T}\int_{-T}^{0} P_{\mathrm{SA}}(t)\,\mathrm{d}t \tag{11.9}$$

$$y_4^n = \max_{t\in[-T,0]} P_{\mathrm{SA}}(t) - \min_{t\in[0,T]} P_{\mathrm{SA}}(t) \tag{11.10}$$

$$y_5^n = \frac{1}{T}\int_{-T}^{0} V_{\mathrm{RV}}(t)\,\mathrm{d}t \tag{11.11}$$

$$y_6^n = \max_{t\in[-T,0]} V_{\mathrm{RV}}(t) - \min_{t\in[0,T]} V_{\mathrm{RV}}(t) \tag{11.12}$$

$$y_7^n = \frac{1}{T}\int_{-T}^{0} P_{\mathrm{PA}}(t)\,\mathrm{d}t \tag{11.13}$$

$$y_8^n = \max_{t\in[-T,0]} P_{\mathrm{PA}}(t) - \min_{t\in[0,T]} P_{\mathrm{PA}}(t) \tag{11.14}$$

$$y_9^n = \frac{1}{T}\int_{t_{\max}-T}^{t_{\max}} V_{\mathrm{LV}}(t)\,\mathrm{d}t \tag{11.15}$$

$$y_{10}^n = \max_{t\in[t_{\max}-T,t_{\max}]} V_{\mathrm{LV}}(t) - \min_{t\in[t_{\max}-T,t_{\max}]} V_{\mathrm{LV}}(t) \tag{11.16}$$

$$y_{11}^n = \frac{1}{T}\int_{t_{\max}-T}^{t_{\max}} P_{\mathrm{SA}}(t)\,\mathrm{d}t \tag{11.17}$$

$$y_{12}^n = \max_{t\in[t_{\max}-T,t_{\max}]} P_{\mathrm{SA}}(t) - \min_{t\in[t_{\max}-T,t_{\max}]} P_{\mathrm{SA}}(t) \tag{11.18}$$

$$y_{13}^n = \frac{1}{T}\int_{t_{\max}-T}^{t_{\max}} V_{\mathrm{RV}}(t)\,\mathrm{d}t \tag{11.19}$$

$$y_{14}^n = \max_{t\in[t_{\max}-T,t_{\max}]} V_{\mathrm{RV}}(t) - \min_{t\in[t_{\max}-T,t_{\max}]} V_{\mathrm{RV}}(t) \tag{11.20}$$

$$y_{15}^n = \frac{1}{T}\int_{t_{\max}-T}^{t_{\max}} P_{\mathrm{PA}}(t)\,\mathrm{d}t \tag{11.21}$$

$$y_{16}^n = \max_{t\in[t_{\max}-T,t_{\max}]} P_{\mathrm{PA}}(t) - \min_{t\in[t_{\max}-T,t_{\max}]} P_{\mathrm{PA}}(t). \tag{11.22}$$

That is, the output vector contains mean values and ranges of left and right ventricular volumes, and systemic and pulmonary arterial pressures. The first eight components of $\mathbf{y}^n$ are related to the last heart beat before the preload reduction manoeuvre, whereas the 9th to 16th components of $\mathbf{y}^n$ are similar to the previous

ones, but are computed on the last heart beat before stopping the preload reduction manoeuvre. Equations 11.7 to 11.22 were used to compute the elements of Table 11.2 from experimental data. The same equations are used to compute the model output vector, $\mathbf{y}^n(\mathbf{p})$, from the simulations.

As emphasised in Table 11.2, in four experimental datasets, measured pulmonary artery pressure was negative at the end of the preload reduction manoeuvre. The corresponding components (y_{15}^n and y_{16}^n) were not included in the output vector. Hence, $\mathbf{y}^1$, $\mathbf{y}^2$, $\mathbf{y}^3$, $\mathbf{y}^8$ and $\mathbf{y}^9$ are 1×16 vectors, while $\mathbf{y}^4$, $\mathbf{y}^5$, $\mathbf{y}^6$ and $\mathbf{y}^7$ are 1×14 vectors. Cardiac pressures were not included in the output vector since they had already been used to compute parameters T, W_{LV}, W_{RV}, E_{LV} and E_{RV}.

The error vector, $\mathbf{e}^n$, for dataset n was built as the relative error between simulated and measured values, displayed in Table 11.2. More specifically, the vector $\mathbf{y}^{n,\mathrm{ref}}$ was taken as the nth column of Table 11.2. The kth component of $\mathbf{e}^n$ is thus:

$$e_k^n = \frac{y_k^{n,\mathrm{ref}} - y_k^n(\mathbf{p})}{y_k^{n,\mathrm{ref}}} \tag{11.23}$$

where $\mathbf{y}^n(\mathbf{p})$ contains the corresponding simulated values. Finally, a global 1×136 error vector, $\mathbf{e}$, was built as a concatenation of the nine error vectors $\mathbf{e}^n$ relative to each dataset:

$$\mathbf{e} = (\mathbf{e}^1\ \mathbf{e}^2\ \mathbf{e}^3\ \mathbf{e}^4\ \mathbf{e}^5\ \mathbf{e}^6\ \mathbf{e}^7\ \mathbf{e}^8\ \mathbf{e}^9) \tag{11.24}$$

and the 11×136 Jacobian matrix, defined in Equation 9.7, was computed as the derivative of this vector with respect to $\mathbf{p}$.

The reason for using a global error vector $\mathbf{e}$ was to apply the subset selection algorithm to this vector, rather than to the individual vectors $\mathbf{e}^n$. Doing so, a common parameter set is selected for all pigs during the preload reduction manoeuvre, which allows consistent comparisons between pigs. Using Equation 9.21, ρ was found to be equal to 5. In the present case, the five selected parameters were E_{SA}, E_{PA}, R_{sys}, R_{pul} and $V_{\mathrm{s},6}$. The remaining six parameters, R_{MV}, R_{AV}, R_{TV}, R_{PV}, E_{SV} and E_{PV}, were thus kept at their initial values.

Iterative Adjustment of the Selected Parameters

The five selected parameters were identified by an iterative procedure for each of the nine datasets. The objective of this procedure was to minimise ψ_2^n, the sum of squared components of $\mathbf{e}^n$. This task was performed using all seven parameter identification methods presented in Chapter 10. The initial values required

by this algorithm were the ones computed previously. All computations were performed using Matlab (2010a).

11.3 Results and Discussion

11.3.1 Sensitivity and Correlation Analyses

The sensitivities $\bar{J}_k$ computed using Equation 9.9 are displayed in Figure 11.3. The three parameters to which the error vector, **e**, is the most sensitive are $V_{s,6}$, vena cava elastance, E_{SV}, and tricuspid valve resistance, R_{TV}. The fact that E_{SV} and R_{TV} are the second and third most influent parameters is due to the way the preload reduction manoeuvre is simulated, by doubling R_{TV}, which is the resistance downstream of the systemic veins. The fourth to seventh most influent parameters are arterial elastances, E_{SA} and E_{PA}, and vascular resistances, R_{sys} and R_{pul}. The three remaining valve resistances, R_{MV}, R_{AV} and R_{PV}, and pulmonary vein elastance, E_{PV}, are the least influent parameters. This outcome emphasises the fact that valve resistances are difficult to identify from the data available, as already noted by Revie *et al.* [93].

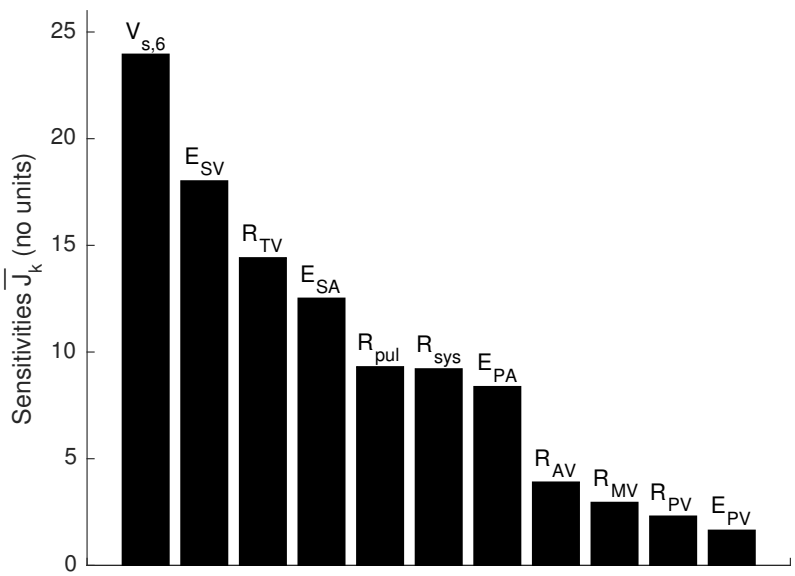

Figure 11.3: Sensitivities $\bar{J}_k$ of the error vector **e** to each parameter.

Figure 11.4 displays the symmetric correlation matrix $\mathbf{C}$[1]. The six largest correlations occurred between the following parameter pairs:

- E_{SV} and R_{TV},
- R_{AV} and R_{PV},
- $V_{\mathrm{s,6}}$ and E_{SV},
- E_{SV} and R_{PV},
- R_{pul} and E_{PV},
- R_{pul} and R_{MV}.

	E_{SA}	E_{PA}	R_{sys}	R_{pul}	R_{MV}	R_{AV}	R_{TV}	R_{PV}	E_{SV}	E_{PV}	$V_{s,6}$
E_{SA}	1.00										
E_{PA}	0.30	1.00									
R_{sys}	0.00	0.23	1.00								
R_{pul}	0.02	-0.02	0.09	1.00							
R_{MV}	-0.04	0.12	-0.03	-0.51	1.00						
R_{AV}	0.03	0.18	-0.16	-0.07	-0.02	1.00					
R_{TV}	0.04	0.09	-0.25	0.14	-0.01	0.26	1.00				
R_{PV}	0.40	0.20	-0.06	0.36	-0.41	0.70	0.39	1.00			
E_{SV}	0.14	0.18	-0.25	0.12	-0.08	0.35	0.78	0.60	1.00		
E_{PV}	0.28	0.18	0.18	-0.55	-0.07	0.02	-0.18	0.07	-0.06	1.00	
$V_{s,6}$	-0.26	-0.26	0.02	-0.01	0.11	-0.20	0.02	-0.48	-0.60	-0.22	1.00

Figure 11.4: Correlation matrix $\mathbf{C}$ between the model parameters.

The reason why the subset selection algorithm selected the parameters $V_{\mathrm{s,6}}$, E_{SA}, E_{PA}, R_{sys} and R_{pul} can be understood by comparing Figures 11.3 and 11.4. Among all six strong pairwise correlations, the parameter to which the error vector is less sensitive were never selected. Of the six remaining parameters, $V_{\mathrm{s,6}}$, E_{SA}, E_{PA}, R_{sys}, R_{pul} and R_{AV}, the five exerting the largest influence on $\mathbf{e}$ were selected.

The results presented in this section emphasise the importance of $V_{\mathrm{s,6}}$ for closed-loop CVS model simulations. The group of four parameters E_{SA}, E_{PA}, R_{sys} and R_{pul} is also shown to be relevant in a CVS model. This outcome matches and revalidates the widespread use of two-parameter *windkessel* models that include only an arterial elastance and a vascular resistance to represent the systemic or pulmonary arterial system.

[1] As can be seen in Figure 11.4, correlation between parameters is not transitive. This observation is discussed in [202].

It is worth mentioning that the sensitivity analysis and subset selection procedures were also applied to each of the nine $\mathbf{e}^n$ vectors separately. The individual sensitivities followed a pattern very similar to the one in Figure 11.3 and were also strongly correlated with the global sensitivity vector $\bar{J}_k$ (average $r^2 = 0.87$). The parameter subsets selected on the basis of the vectors $\mathbf{e}^n$ included the same five parameters, $V_{s,6}$, E_{SA}, E_{PA}, R_{sys} and R_{pul}, in 87 % of the cases and rejected the same six other ones in 92 % of the cases, thus validating the approach further.

11.3.2 Parameter Adjustment

Tables 11.3 and 11.4 shows the initial and optimised parameter values, along with the pig weights and final values of the root mean squared error (RMSE) for dataset n, equal to:

$$\mathrm{RMSE}^n = \sqrt{\frac{\psi_2^n}{N_e}} \tag{11.25}$$

In the previous equation, N_e is the number of components in $\mathbf{e}^n$, equal to 14 or 16 as explained in Section 11.2.4. The largest value of the RMSE is 29.2 %. For the corresponding dataset, $N_e = 14$ and not 16 because measured pulmonary artery pressure was negative at the end of the preload reduction manoeuvre. The overall poor quality of this dataset could justify this highest RMSE value. Figure 11.5 shows simulated and measured ventricular and arterial pressures for this worst-case dataset.

For all other datasets, the RMSE lies between 18.8 and 26.2 %. Consequently, the parameter adjustment can be qualified as good. To further emphasise this statement, Figure 11.6 shows simulated and measured left ventricular and aortic pressures for the best-case dataset (pig number 7, RMSE = 18.8 %). As can be seen on this figure, simulated and measured pressures and volumes are in very good agreement all along the preload reduction manoeuvre.

The errors between measurements and simulations have three main causes, which can be seen in Figures 11.5 and 11.6. First, in four datasets, measured pulmonary artery pressure is negative at the end of the experiment. These measurements are marked by asterisks in Table 11.2. It is uncertain whether this outcome is a measurement error or if pulmonary artery pressure was actually lower than atmospheric pressure. However, a negative pulmonary artery pressure cannot be reproduced by the CVS model, given its assumptions and formulation[2], which is

[2]In theory, the model is able to reproduce a negative pulmonary arterial pressure if stressed pulmonary arterial volume is negative. During diastole, left ventricular pressure needs to be even lower to allow ventricular filling. However, by choosing Equation 11.1 for the driver function, minimum left ventricular pressure is necessarily zero, which is a common assumption [203].

Table 11.3: Initial values of the unselected model parameters.

Parameter	Units	Pig 1	Pig 1	Pig 2	Pig 3	Pig 3	Pig 4	Pig 5	Pig 6	Pig 7
t_{max}	s	8.99	9.70	6.89	9.49	7.23	8.54	7.84	8.36	12.21
W_{LV}	s^{-2}	66.9	63.6	68.9	78.7	61.9	53.5	95.8	49.2	12.1
W_{RV}	s^{-2}	117	104	239	55.1	53.1	76.0	238	76.4	17.1
T	s	0.589	0.590	0.474	0.621	0.615	0.597	0.643	0.621	1.45
$V_{\mathrm{u,LV}}$	ml	20.6	23.1	2.99	21.8	-10.8	-13.6	32.9	-5.32	20.0
$V_{\mathrm{u,RV}}$	ml	41.7	40.6	46.0	35.5	32.8	37.6	52.3	17.5	35.1
E_{LV}	mmHg/ml	2.99	3.14	1.30	3.85	1.74	1.81	4.12	1.33	2.29
E_{RV}	mmHg/ml	2.18	1.60	1.84	3.21	2.33	1.47	2.84	1.53	1.41
E_{SV}	mmHg/ml	0.00629	0.00629	0.00710	0.00759	0.00759	0.00710	0.00677	0.00733	0.0088
E_{PV}	mmHg/ml	0.406	0.431	0.433	0.434	0.402	0.425	0.375	0.395	0.581
R_{MV}	mmHg s/ml	0.0500	0.0500	0.0500	0.0500	0.0500	0.0500	0.0500	0.0500	0.0500
R_{AV}	mmHg s/ml	0.0400	0.0400	0.0400	0.0400	0.0400	0.0400	0.0400	0.0400	0.0400
R_{TV}	mmHg s/ml	0.0400	0.0400	0.0400	0.0400	0.0400	0.0400	0.0400	0.0400	0.0400
R_{PV}	mmHg s/ml	0.0300	0.0300	0.0300	0.0300	0.0300	0.0300	0.0300	0.0300	0.0300

Table 11.4: Initial and optimised values of the selected model parameters.

Parameter	Units	Pig 1	Pig 1	Pig 2	Pig 3	Pig 3	Pig 4	Pig 5	Pig 6	Pig 7
Initial values of the selected parameters										
$V_{s,6}$	ml	1120	1120	990	927	927	990	1040	960	799
E_{SA}	mmHg/ml	2.19	2.04	1.03	2.32	1.97	2.20	1.61	2.73	2.25
E_{PA}	mmHg/ml	0.632	0.726	0.699	0.682	0.760	0.775	0.974	1.44	1.56
R_{sys}	mmHg/ml	3.29	3.17	1.69	3.52	3.02	3.31	2.00	2.18	5.45
R_{pul}	mmHg/ml	0.400	0.417	0.256	0.140	0.113	0.243	0.263	0.392	1.12
Optimised values of the selected parameters										
$V_{s,6}$	ml	535	536	436	535	498	567	342	669	256
E_{SA}	mmHg/ml	1.88	1.59	2.06	2.28	2.91	2.88	2.45	2.61	1.81
E_{PA}	mmHg/ml	0.860	0.793	2.74	2.94	7.07	9.23	0.960	2.49	1.11
R_{sys}	mmHg/ml	2.81	3.76	2.67	3.87	5.75	4.46	2.49	2.19	5.44
R_{pul}	mmHg/ml	0.122	0.134	0.0354	0.00120	0.0115	0.0427	0.212	0.0846	0.406
RMSE	-	0.212	0.213	0.262	0.247	0.292	0.231	0.211	0.202	0.188
N_e	-	16	16	16	14	14	14	14	16	16
Weight	kg	35.0	35.0	31.0	29.0	29.0	31.0	32.5	30	25
$V_{s,6}$/Weight	ml/kg	15.3	15.3	14.1	18.4	17.2	18.3	10.5	22.3	10.3

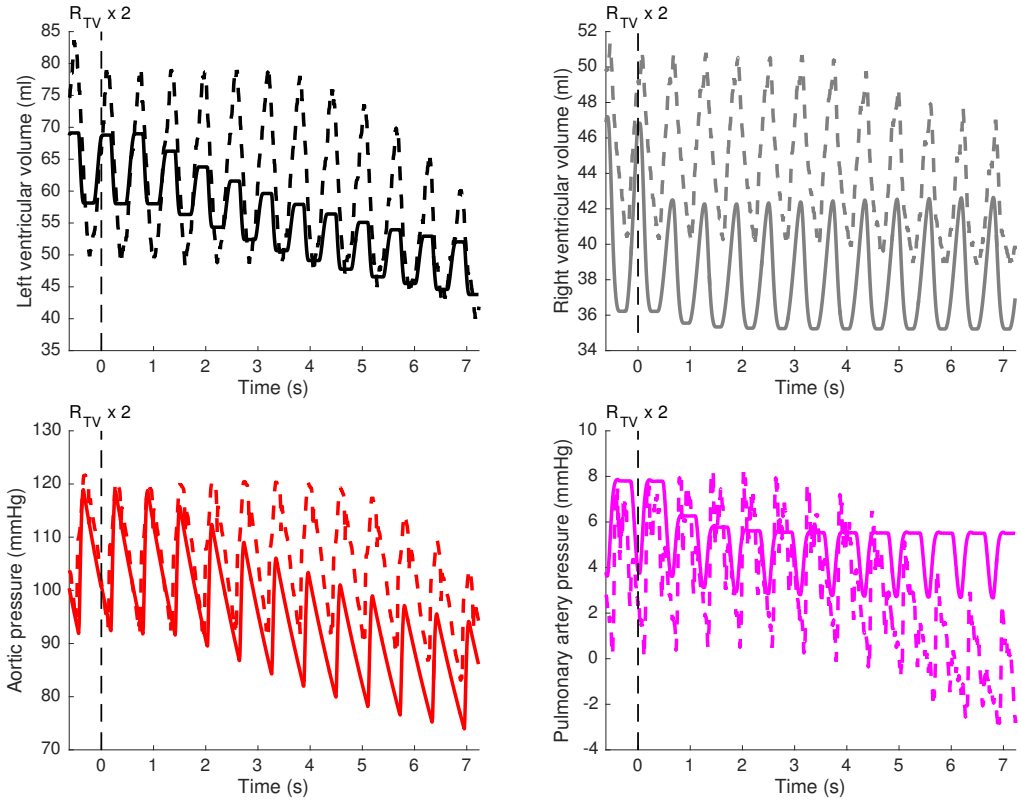

Figure 11.5: Result of parameter identification for pig number 3 (dataset 2). *Dashed lines*: measurements; *full lines*: simulations..

the reason why the objective function was modified in such cases, as explained in Section 11.2.4.

Second, for all datasets, measured aortic pressure is higher than left ventricular pressure during a large part of systole. This second outcome is probably due to an error in the calibration of the pressure catheters. Simulated arterial pressure thus has to be lower than measured, because it would otherwise prevent emptying of the ventricle.

Third, measured left and right SVs are different, as can be seen in Table 11.2. This situation cannot be reproduced by the model in steady conditions before preload reduction. Consequently, simulated SV for $t < 0$ must be a trade-off between measured left and right SVs.

Despite these discrepancies likely due to sensor errors and the difficulty of such *in vivo* measures in general, the model is able to track the pressure changes when preload is reduced. The trends appear accurately reproduced, which is, overall, clinically valuable and can thus be considered as an important success.

Therefore, the choice of the driver function is the reason why a negative pulmonary arterial pressure could not be reproduced.

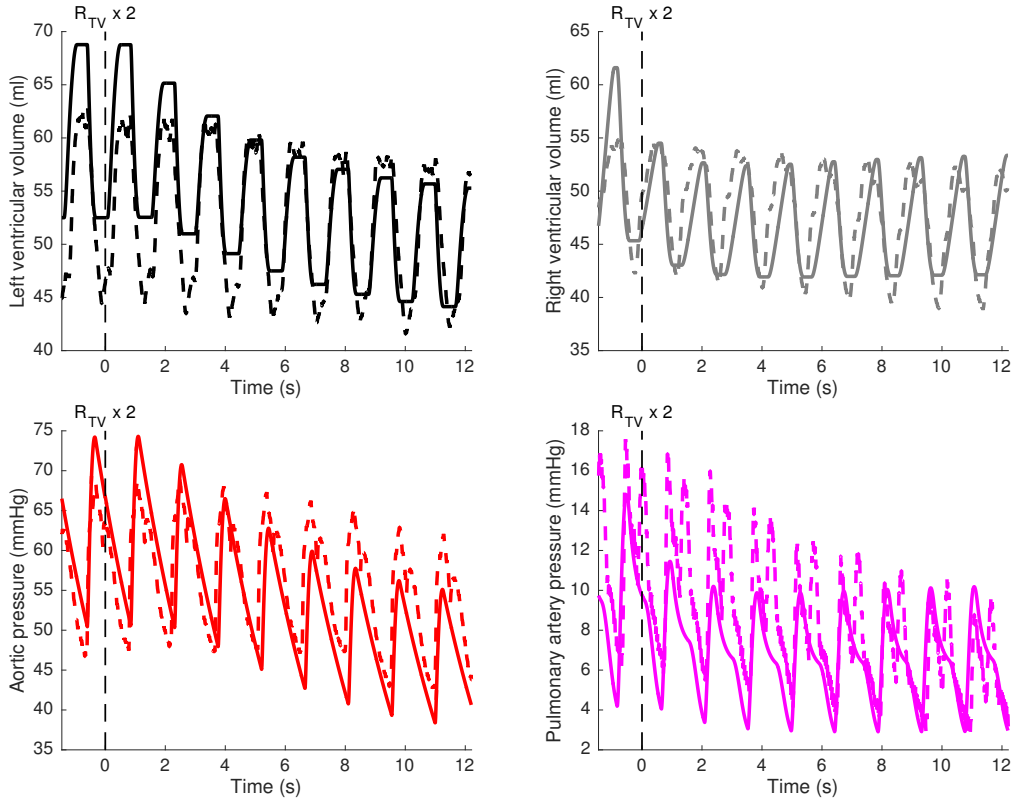

Figure 11.6: Result of parameter identification for pig number 7. *Dashed lines*: measurements; *full lines*: simulations.

Overall, these results are the first quantitative validation of the six-chamber CVS model in a situation of changing load.

Parameter Identification Methods

As previously mentioned, the seven parameter identification methods were applied to the nine available datasets. Figure 11.7 presents the total squared error reached by each parameter identification method, computed as:

$$\psi_2 = \sum_{i=1}^{136} e_i^2. \tag{11.26}$$

Interestingly, the derivative-free methods, simplex and direct search, were able to reach the lowest errors. The proportional method on its own, did not perform well, but when the results of this method were input to the simplex method, the results were the second best. The combination of these two methods offers the potential for improved speed, as the proportional method is very fast.

The good performance of derivative-free methods was not observed in Chapter 10. This observation could indicate that the error functions of this chapter are

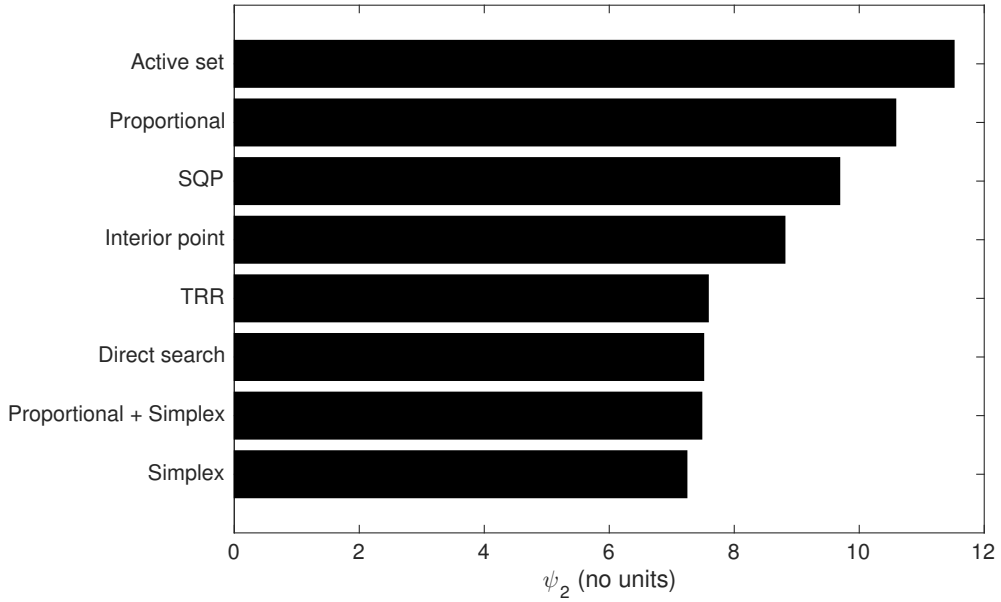

Figure 11.7: Total minimum squared error, ψ_2, reached by all parameter identification methods on the nine datasets.

not smooth, in opposition to the one used in Chapter 10. The discrepancy can also be explained by the different scale of the parameter identification problems: in this chapter, 5 parameters had to be identified from 14 to 16 measurements, while there were 6 parameters and 7 measurements in Chapter 10. Consequently, the remark that was formulated in Chapter 10 about the necessity to repeat the comparison of methods for a different parameter identification problem, can also be made here.

11.3.3 Comparison Between $V_{s,6}$ and SBV

As previously mentioned, the parameter $V_{s,6}$ is a model-based analogue of SBV. In this section, the computed values of $V_{s,6}$ are compared with SBV values provided in the literature. From the results displayed in Table 11.4, it can be observed that $V_{s,6}$ for pigs ranges from 256 to 669 ml. In humans, Maas *et al.* reported SBV values of 1265 $\pm$ 541 ml [32] (mean $\pm$ standard deviation). For comparison, the mean $V_{s,6}$ observed in the present study is 486 $\pm$ 117 ml. There is a large inter-subject variability in experimentally determined values in the present study and that of Maas *et al.* with coefficients of variation of 24 and 43 %, respectively. The experimental study of Maas *et al.* is the only one that was found providing SBV values expressed in millilitres.

The reason why no value of SBV in millilitres was found is that many investigators, when performing the experiment illustrated in Figure 3.8, infuse a quantity of fluid expressed proportionally to the animal's weight (*e.g.* 10 ml/kg). As a consequence, these experimental studies provide a *specific* value of SBV, expressed in ml/kg. For instance, in an experimental study on pigs, Ogilvie *et al.* [77] reported mean SBV values of 29, 34 and 41 ml/kg for three different ways of inducing circulatory arrest. No other experimental study on pigs was available.

Similarly, in an experiment performed on dogs, Drees and Rothe [78] found values ranging from 27.8 to 43.1 ml/kg, depending on the time elapsed between volume infusion or removal and circulatory arrest. The same authors [83] also reported values between 37.9 to 41.4 ml/kg, depending on the amount of blood that was infused or removed. Another research group [80,81] published curves of MCFP versus infused volume, such as the one in Figure 3.8, in control dogs and investigated the changes due to pharmacologic agents. In both studies, control dogs had an average SBV of 14.5 ml/kg (standard deviation was 0.2 ml/kg in the first study [80], 0.5 in the second [81]). Finally, the results of Maas *et al.* can also be divided by the mean patient weight, yielding values of 15.6 $\pm$ 6.7 ml/kg.

For comparison with these specific SBV values, specific $V_{s,6}$ values were computed and are provided in the last row of Table 11.4. The average specific $V_{s,6}$ is equal to 15.7 $\pm$ 3.6 ml/kg. The results of this study are thus of the same order of magnitude as all the previously mentioned specific SBV values, and present less variability. This observation tends to indicate that $V_{s,6}$ could be an analogue of SBV, but comparisons with other porcine studies would be better, if available.

In summary, both SBV and $V_{s,6}$, specific or not, present a large inter-subject variability. The previously reported articles have emphasised the influence of how the experiment is performed. Change of $V_{s,6}$ or SBV can also be attributed to sympathetic actions, time-dependent vascular properties, fluid exchange through the capillaries, and other factors [78]. Consequently, $V_{s,6}$ also presents an intra-subject variability. For example, compare the two $V_{s,6}$ values for pigs number 1 and 3 in Table 11.4. This outcome further highlights the need to identify this subject and condition-specific parameter directly, and in real-time, as its value may also be clinically relevant in titrating care.

11.3.4 Other Parameter Values

This section discusses values of parameters other than $V_{s,6}$. First, optimised values of the parameters are compared with their initial values. Second, the parameter values are compared with other studies performed on the same datasets.

Finally, differences in the parameters identified from datasets coming from the same animal (pigs number 1 and 3) are evaluated.

Maximal errors in the initial values of parameters E_{SA} and R_{sys} compared with optimised values were, respectively, 52 % and 36 %. This result justifies Equations 9.37 and 9.44 used to compute the initial values of these parameters and the underlying assumption of venous pressure negligible with respect to arterial pressure. Interestingly, there is a mild correlation ($r^2 = 0.51$) between initial and optimised values of R_{sys}, as shown in Figure 11.8 (left). The outlying point corresponds to the dataset associated with the highest RMSE value, as can be seen in Table 11.4. Using the information in Figure 11.8 (left), a better approximation for R_{sys} can be defined:

$$R_{\mathrm{sys}} \approx 0.83\,\frac{\bar{P}_{\mathrm{SA}}\,T}{\Delta V_{\mathrm{LV}}} + 1.2\ \mathrm{mmHg\ s/ml}. \tag{11.27}$$

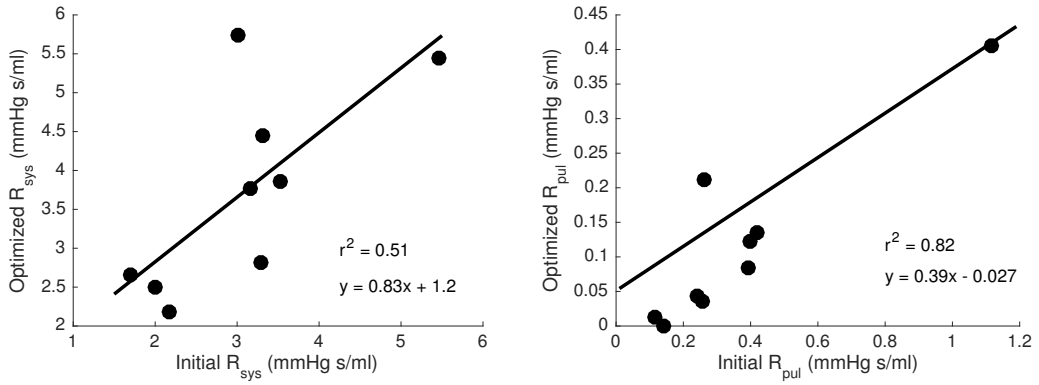

Figure 11.8: Linear correlation between initial and optimised values of R_{sys} and R_{pul}.

On the pulmonary side, the maximal errors in the initial values of parameters E_{PA} and R_{pul} were, respectively, 92 and 11,586 %. There are two main reasons for this large discrepancy between initial and optimised values of R_{pul}. First, in the datasets, pulmonary artery pressure is particularly low, sometimes even negative, as previously mentioned. Second, in the case of the pulmonary circulation, downstream pressure cannot be neglected with respect to pulmonary artery pressure [20]. The approximation $R_{\mathrm{pul}} \approx \bar{P}_{\mathrm{PA}}T/\Delta V_{\mathrm{RV}}$ is not valid. However, since downstream pressure was not available, this assumption was necessary.

As in the systemic case, there is a good correlation ($r^2 = 0.82$) between initial and optimised values of R_{pul}, shown in Figure 11.8 (right). This result suggests the following approximation:

$$R_{\mathrm{pul}} \approx 0.39\,\frac{\bar{P}_{\mathrm{PA}}\,T}{\Delta V_{\mathrm{LV}}} - 0.027\ \mathrm{mmHg\ s/ml}.$$

In other studies on the same datasets, Revie *et al.* [95, 204] identified all the parameters of the six-chamber CVS model, except $V_{s,6}$, which represents a unique feature of the present study. They published the values of the parameters R_{sys}, R_{pul}, E_{LV} and E_{RV}. When compared to the values presented in Table 11.4, only the values of R_{sys} and R_{pul} are well correlated ($r^2 = 0.79$ and 0.72, respectively). The values of E_{LV} and E_{RV} show no correlation. The reason is that Revie *et al.* assumed $V_{u,LV}$ and $V_{u,RV}$ to be zero, which is not the case, as shown in Table 11.3. As explained by these authors, their values of E_{LV} and E_{RV} do not represent left and right ventricular contractilities in a strict sense [93].

As previously explained, two preload reduction datasets were available for pigs number 1 and 3. The identified parameter values are displayed in Table 11.4. For the two parameter sets identified for pig number 1, the maximum relative differences are approximately 30 % for E_{RV} and 29 % for R_{sys}. For all other parameters, maximum relative difference is 17 %.

For pig number 3, the maximum relative differences are 591 % for $V_{u,LV}$ and 162 % for R_{pul}. These high differences are caused by the fact the two preload reduction manoeuvres did not have the same effect on the pig, as shown in Figure 11.9. In particular, the second preload reduction manoeuvre seems to have had less effect. For instance, the identified left heart contractility E_{LV} changed by 75 % between the two manoeuvres. The animals' state is continuously changing under the influence of numerous physiological reflex mechanisms. Consequently, measured pressures and volumes and thus, identified parameter values, including $V_{s,6}$, can be different for two successive measurements in a single animal. The method described in this work only aims to determine the *instantaneous* state of the animal. It cannot account for the transition between states, because the reflex mechanisms are not modelled.

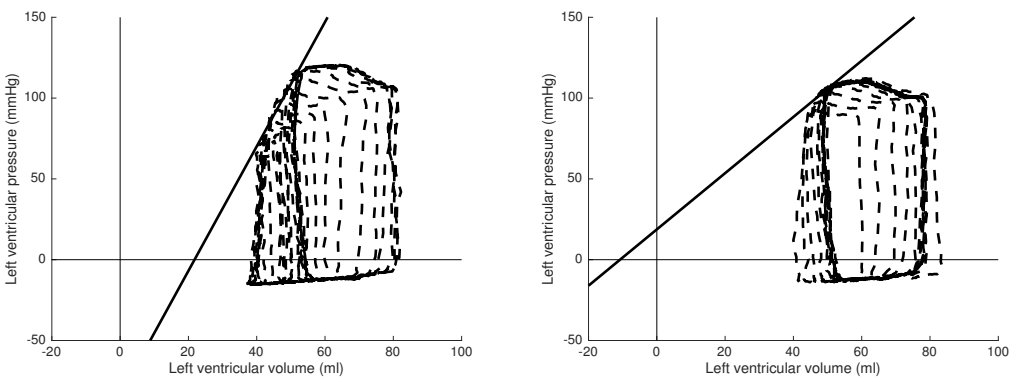

Figure 11.9: Left ventricular pressure-volume loops (*dashed line*) and end-systolic pressure-volume relationships (*full line*) for the two datasets of pig number 3.

As can be seen from Table 11.4, the unstressed volume $V_{u,LV}$ of the left ventricle is the most varying parameter (10.2 $\pm$ 16.1 ml), being sometimes even negative, as in Figure 11.9 (right). This observation has been made by many other researchers [109, 122], who questioned the physiological meaning of a negative volume. The explanation of this phenomenon is that the ESPVR is only linear on a limited volume range, but tends to become concave for low volumes, as explained in Section 5.2.1.

11.4 Limitations

This chapter presented a method to compute all the parameters of the six-chamber CVS model, including total stressed volume $V_{s,6}$, from data of preload reduction manoeuvres. In these experimental manoeuvres, one of the two input vessels to the right ventricle, the venae cavae, was occluded. In this chapter, it was assumed that this preload reduction manoeuvre could be simply modelled as a sharp doubling of the right ventricular input resistance, namely R_{TV}. This hypothesis is the main limitation and is discussed here.

First, to agree with the experimental setting, the change had to be modelled as a change in resistance, the elastance of the vessel being unaffected by the occlusion. However, the lumped nature of the model causes the venae cavae to be represented as a single elastic chamber with no resistance. The remaining choice was to alter either the resistance upstream of the elastic chamber, the resistance of the systemic circulation, R_{sys}, or the one downstream, the tricuspid valve resistance, R_{TV}. Since the resistance of the systemic circulation is mainly attributed to the capillaries, which are unaffected by the preload reduction manoeuvre, it seemed more appropriate to alter the tricuspid valve resistance, R_{TV}.

Second, it was assumed that the preload reduction manoeuvre could be modelled by doubling this resistance. Indeed, since one of the two input vessels is occluded, there is no flow in this vessel and its resistance becomes infinite. Using the rules valid for electrical circuits, the total resistance after occlusion is thus twice that before occlusion.

Finally, the preload reduction manoeuvre was reproduced by a sharp change of the resistance. It is likely that the computed $V_{s,6}$ value could change according to how fast the inferior vena cava is occluded. However, measuring the time evolution of inferior vena cava occlusion requires an echographic study, which was not available here.

The computed $V_{s,6}$ values should be compared to SBV values obtained by the experiments described in the introduction and in Figure 3.8. As mentioned previously, such experiments are invasive and risky, as they involve repetitive

circulatory arrests in all or part of the CVS and multiple fluid administrations [32, 77–83]. If the method provided here correlates well with these other approaches, it could be used as a faster replacement, also avoiding the need for circulatory arrests.

11.5 Summary

In the past, total stressed volume has been considered to be an unimportant parameter of closed-loop CVS models. Its value has been omitted from numerous studies presenting such models, despite its role in simulations with changing preload or afterload conditions. In this chapter, the importance of this parameter for CVS models was shown.

Next, a method was presented to compute this parameter along with all other parameters of the six-chamber CVS model from usual haemodynamic data. This method consists in fitting the CVS model to data from a preload reduction manoeuvre. Because data is limited and not perfect, the subset selection algorithm presented in Section 9.5 was used to select a subset of parameters to fit. The parameter $V_{s,6}$ was selected by the algorithm, which further confirms its important role. Its value could then be computed for all available datasets.

The method presented here requires many invasive data and is based on a preload reduction manoeuvre through vena cava occlusion, which is an invasive procedure, as illustrated in Figure 11.2. However, the method could be made less invasive by suppressing the need for continuous ventricular pressures and volumes measurements. As previously shown, $V_{s,6}$ is the most sensitive parameter. Therefore, it is likely to be identifiable using only arterial and/or venous pressure measurements. The second step to make the method less invasive would be to replace the vena cava occlusion by another, non-invasive, preload reduction manoeuvre, for example a passive leg raising manoeuvre or an end-expiratory occlusion test, as described in Section 3.4.5. These changes would result in a non additionally-invasive method to compute a patient's volume status. Non additionally-invasive measurements are critical to enable easy identification of a patient's volume status and whether fluid therapy should be performed, which is central to monitoring and treating CVS dysfunction.

Chapter 12

Comparison between Conventional and Model-Based Indices of Fluid Responsiveness

12.1 Introduction

The previous chapter presented a method to compute the total stressed volume parameter of the six-chamber model, $V_{s,6}$. This method has two drawbacks. First, it requires data from both the systemic and pulmonary circulations, since the six-chamber model represents these two circulations. Second, this data has to be obtained during a preload reduction manoeuvre, to eliminate the indetermination between total stressed volume and venous elastances.

In this chapter, these two limitations are overcome using the three-chamber model, and a method requiring only systemic circulation data in steady conditions, including range of venous pressure. Using this measurement eliminates the indetermination between total stressed volume and venous elastance, as discussed in Section 9.4.1.

The method is validated against experimental vascular filling data, and is also detailed in Pironet *et al.* [205]. The resulting $V_{s,3}$ value is then tested as an index of fluid responsiveness, and compared with the conventional indices introduced in Section 3.4.

12.2 Methods

12.2.1 Experimental Data

To identify the eight parameters of the three-chamber model, comprising three elastances E_h, E_a and E_v, three resistances R_i, R_o and R_c, the cardiac period T and $V_{s,3}$, experimental animal data were used. These data came from vascular filling experiments performed on eight anaesthetized pigs, weighing 20 to 41 kg. The ethical approval for these experiments is mentioned in Section 7.2. The pigs were administered a muscle relaxant (Nimbex, GlaxoSmithKline AG, Switzerland) and were mechanically ventilated at a positive end-expiratory pressure of 5 cmH_2O.

The experiments consisted in 2 to 6 successive administrations of saline solution. Pigs number 1 and 2 received slow 500 ml fluid infusions and pigs number 3 to 8 received rapid 225 ml fluid boluses. In addition, pigs number 6, 7 and 8 received dobutamine before the final 225 ml fluid bolus.

Micromanometer-tipped catheters (Transonic, NY) provided continuous recording of:

- Left ventricular pressure and volume (using the admittance technique),
- Aortic pressure,
- Inferior vena cava pressure (only for pigs number 1 and 2),
- Left atrial pressure (only for pig number 1).

A PiCCO monitor was also used for pigs number 5 to 8, providing beat-to-beat recording of:

- SV,
- CVP,
- Vena cava PP (not recorded for pig number 5).

The PiCCO was recalibrated with three thermodilutions after each fluid administration to avoid any drift in the measured SV, linked to changes in haemodynamics [162, 164], as explained in Section 7.3.5. Table 12.1 summarises the available data for each animal.

Since cardio-pulmonary interaction is not accounted for in the three-chamber model, only data during temporary interruptions of the mechanical ventilator were used. However, pausing the ventilator causes transient preload and afterload changes. Consequently, only the last heartbeat before the end of the expiratory pause was used, so that the hemodynamics were as stabilized as possible.

Table 12.1: Summary of the experimental data.

Pig number	1	2	3	4	5	6	7	8
Catheter data								
Left ventricular pressure	✓	✓	✓	✓	✓	✓	✓	✓
Left ventricular volume	✓	✓	✓	✓	(✓)	✓	✓	✓
Aortic pressure	✓	✓	✓	✓	✓	✓	✓	✓
Vena cava pressure	(✓)	✓						
Left atrial pressure	✓							
PiCCO data								
SV					✓	✓	✓	✓
CVP					✓	✓	✓	✓
Vena cava PP						✓	✓	✓
Number of fluid administrations	4	2	4	5	5	6	6	5

12.2.2 Parameter Identification

The parameter identification procedure aims to reproduce the measured signals with the model. To do so, the following correspondence was established between model outputs and experimental measurements.

- Measured left ventricular pressure and volume were taken as references for the model cardiac pressure, P_{h}, and volume, V_{h},.
- Measured aortic pressure was taken as a reference for the model arterial pressure, P_{a}.
- Measured vena cava and left atrial (only for pig number 1) pressures were considered as the reference for the model venous pressure, P_{v}.

The parameter identification procedure involved four steps, described in the following four sections. First, initial values had to be assigned to all eight model parameters. Second, an error vector was defined. From the error vector computed using the initial parameter values, the subset selection algorithm selected a sensitive subset of parameters to be further identified. Fourth, this subset of parameters was identified using an iterative procedure.

Initial Parameter Values

To assign initial values to the model parameters, the approximate formulae derived in Section 9.6 were used in combination with the available data.

1. The cardiac period, T, was computed as the time interval between two minima of the aortic pressure signal, as exemplified in Figure 2.9.
2. Input valve resistance, R_{i}, was initialized using Equation 9.26.
3. Output valve resistance, R_{o}, was initialised using Equation 9.31.
   When Equations 9.26 or 9.31 could not be used, due to missing or inconsistent data, initial valve resistances values were taken from Revie *et al.* [93]:

$$R_{\mathrm{o}} = 0.04 \text{ mmHg s/ml} \tag{12.1}$$

$$R_{\mathrm{i}} = 0.05 \text{ mmHg s/ml.} \tag{12.2}$$

4. The resistance of the circulation, R_{c}, was computed using Equation 9.37.
5. The cardiac end-systolic elastance, E_{h}, was computed using Equation 9.39. The use of this approximation is justified in the present chapter, because E_{h} need not be precisely estimated. Indeed, in the data used in this chapter, preload and afterload do not vary, in contrast to Chapter 11. Consequently, the points of end-systole do not move on the ESPVR, whose slope is thus not important.
   The driver function $e(t)$ was then obtained as:

$$e(t) = \frac{P_{\mathrm{h}}(t)}{E_{\mathrm{h}} V_{\mathrm{h}}(t)}. \tag{12.3}$$

   It was specifically found using measured left ventricular pressure for P_{h} and left ventricular volume for V_{h}. The resulting curve was then approximated by its Fourier series up to the tenth harmonic. This Fourier approximation was used to drive the three-chamber model.
6. Arterial elastance, E_{a}, was estimated by fitting Equation 9.44 to measured aortic pressure during diastole.
7. Venous elastance, E_{v}, was estimated using Equation 9.54. If ΔP_{v} was not available, it was estimated to be equal to 9 mmHg [201].
8. To determine the initial value of $V_{\mathrm{s},3}$, Equation 9.56 was used. If part of the data necessary to compute the initial value of $V_{\mathrm{s},3}$ was missing, previously published experimental results on pigs were used [196]. From these results, $V_{\mathrm{s},3}$ was estimated to be equal to 593 ml.

In the previous computations, parameters T and E_{h} were computed by directly fitting the model to the data. Consequently, it was assumed that the parameter identification process would not largely alter these parameter values. They were thus excluded from the following sensitivity analysis procedure, and the remain-

ing parameter vector was defined:

$$\mathbf{p} = (V_{s,3}\ E_a\ E_v\ R_c\ R_i\ R_o). \tag{12.4}$$

Error Vector

Table 12.2 summarizes the data included in the output vector, $\mathbf{y}$, for each pig. The error vector, $\mathbf{e}$, was then built as the relative error between simulated and measured values of these data, as dictated by Equation 9.3. The motivations for choosing the data in Table 12.2 are given in the following paragraphs.

Table 12.2: Data included in the output vector $\mathbf{y}$.

Pig number	1	2	3	4	5	6	7	8
Mean cardiac volume, $\bar{V}_h$	✓	✓	✓	✓	(✓)	✓	✓	✓
Range of cardiac volume, ΔV_h	✓	✓	✓	✓	✓	✓	✓	✓
Mean arterial pressure, $\bar{P}_a$	✓	✓	✓	✓	✓	✓	✓	✓
Range of arterial pressure, ΔP_a	✓	✓	✓	✓	✓	✓	✓	✓
Mean venous pressure, $\bar{P}_v$	✓				✓	✓	✓	✓
Range of venous pressure, ΔP_v	✓	✓				✓	✓	✓
Mean cardiac pressure, $\bar{P}_h$					✓			
Range of cardiac pressure, ΔP_h					✓			

As demonstrated in Chapter 8, using at least one volume-related piece of information, for instance ΔV_h, is necessary to ensure structural identifiability in a lumped CVS model. In this chapter, mean and range of cardiac volume were both used. For pigs number 5 to 8, two estimates of SV were available, from the ventricular pressure-volume catheter and from the PiCCO, which were averaged to obtain the reference value of ΔV_h.

Cardiac pressures were not included in the output vector since they had already been used to compute E_h and $e(t)$. However, for pig number 5, reference cardiac volume was not always reliable, as denoted by the parentheses in Tables 12.1 and 12.2. This observation, in turn, prevented the estimation of E_h and $e(t)$ as explained in the previous section. Consequently, for this animal, E_h was inserted in the parameter vector, $\mathbf{p}$, while mean cardiac pressure $\bar{P}_h$ and range of cardiac pressure ΔP_h were inserted in the output vector, $\mathbf{y}$. Additionally, measured mean vena cava pressure was negative for pig number 1, as noted by the parentheses in Table 12.1, which cannot be reproduced by the model. Since it was available, mean left atrial pressure was used as the reference for mean venous pressure instead.

Subset Selection Algorithm

A subset of the parameter vector, $\mathbf{p}$, was selected for optimization using the algorithm presented in Section 9.5. In this chapter, the subset selection algorithm was used on each individual error vector, in contrast to what was done in Chapter 11. The motivation for this change is that different data are available for each pig, as emphasised in Table 12.1.

Iterative Adjustment of the Selected Parameters

The selected parameters were computed by an iterative procedure. The objective of this procedure was to minimise the *mean absolute error (MAE)*, defined:

$$\mathrm{MAE} = \frac{\psi_1}{N_y} = \frac{1}{N_y}\sum_{i=1}^{N_y}|e_i|, \tag{12.5}$$

where N_y is the number of components in $\mathbf{y}$ and $\mathbf{e}$, equal to 4, 5, 6 or 7 in function of the available data, given in Table 12.2. This task was performed using the custom implementation of the proportional method presented in Section 10.2.1 combined with the simplex method for nonlinear optimisation presented in Section 10.2.2. The initial values needed by this algorithm were the ones computed in at the beginning of the present section. All computations were performed using Matlab (2010a).

12.3 Results and Discussion

12.3.1 Subset Selection Algorithm

Figure 12.1 shows the frequency of parameter selection by the algorithm. As can be observed in this figure, the total stressed volume, $V_{\mathrm{s},3}$, and the resistance of the circulation, R_{c}, have been selected by the algorithm for all 37 datasets, allowing the estimation of these parameters in all cases. This result emphasises the importance of $V_{\mathrm{s},3}$ for CVS model simulations, as previously pointed out in Chapter 11 for the six-chamber CVS model.

As mentioned in the previous section, cardiac elastance, E_{h}, was only submitted to the subset selection algorithm for pig number 5. For this animal, E_{h} was also selected for all datasets. Hence, this extra parameter was identified.

The valve resistances, R_{i} and R_{o}, were the least frequently selected parameters. They are indeed difficult to identify from the available data, as already noted in Chapter 10. It should also be noted that Ellwein *et al.* [88] performed a parameter sensitivity analysis in a different CVS model including 11 compartments and

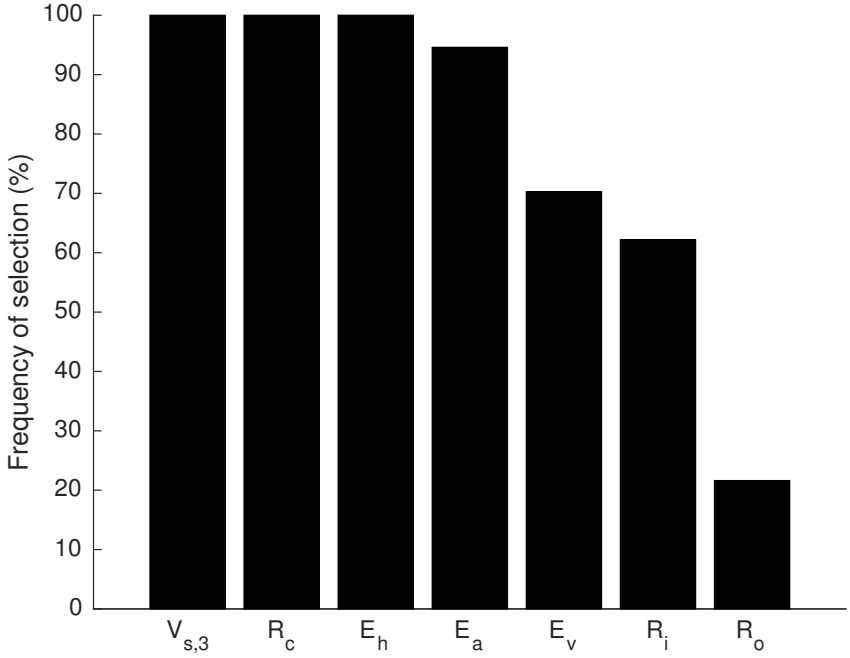

Figure 12.1: Frequency of parameter selection by the subset selection algorithm.

52 parameters. Input valve resistance was the 42nd most sensitive parameter and output valve resistance, the 46th, which matches the present results.

12.3.2 Quality of the Parameter Identification

After parameter identification on the 37 datasets, the MAE amounts to 8.58 % on average and ranges from 0.89 to 33.23 %. The quality of the parameter identification is thus very good in most cases, which also implies that the very simple three-chamber CVS model can capture the dynamics observed in the diversity of the experimental measurements obtained. For instance, pig number 6 presented a pulsus alternans, alternating strong and weak beats with a stable cardiac rhythm [14], which caused the highest MAE values. However, this condition was still correctly reproduced by the model. Additionally, pig number 8 was diagnosed in shock, which did not prevent the model from correctly representing this animal's condition, as the average MAE for this pig is 3.31 %.

The best and worst cases of parameter identification are displayed in Figures 12.2 and 12.3. The MAE for the corresponding datasets are 0.89 and 33.23 %. Simulated and measured pressures and volumes are thus in good agreement.

A frequent source of error can be evidenced using Figure 12.2. During a whole cardiac cycle, measured aortic pressure is nearly always higher than measured

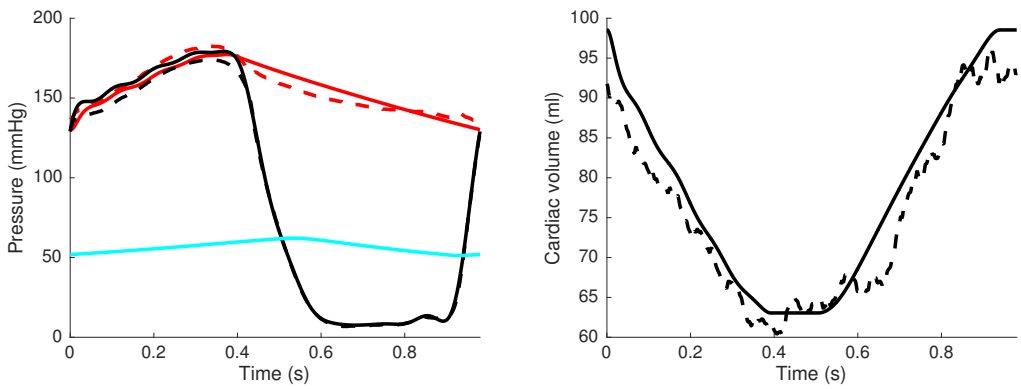

Figure 12.2: Identification result for pig number 3, after 900 ml fluid administration. *Left:* simulated (*full lines*) and reference (*dashed lines*) cardiac (*black*) and arterial (*red*) pressures, and simulated venous pressure (*light blue*). *Right:* simulated (*full line*) and reference (*dashed line*) cardiac volumes.

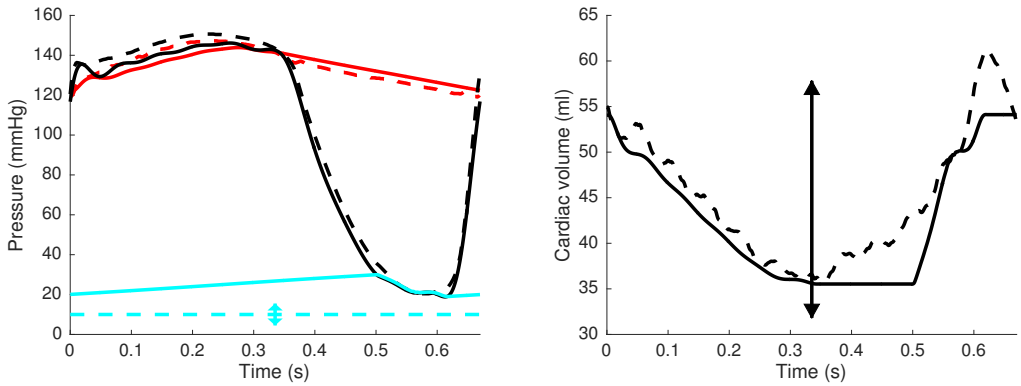

Figure 12.3: Identification result for pig number 6, after 225 ml fluid administration. *Left:* simulated (*full lines*) and reference (*dashed lines*) cardiac (*black*), arterial (*red*) and venous (*light blue*) pressures. The arrow represents vena cava PP measured by the PiCCO. *Right:* simulated (*full line*) and reference (*dashed line*) cardiac volumes. The arrow represents SV measured by the PiCCO.

left ventricular pressure. The simple valve model used in this work cannot reproduce such a situation, since the model requires arterial pressure to be lower than cardiac pressure for the output valve to open (Equation 6.6).

Another source of error is visible in Figure 12.3, where reference mean venous pressure is always lower than reference cardiac pressure. Such a situation can be physiological, as the whole right circulation is located between the two points of measurement, superior vena cava and left ventricle. However, the right circulation is not included in the model, and a venous pressure always lower than the cardiac pressure prevents cardiac filling. Consequently, for the simulated ventricle to fill, the simulated venous pressure is forced to be higher than reference cardiac pressure during filling, as in Figure 12.3.

The parameter identification method presented in this work is robust, since it was able to fit the model to various experimental data, as shown in Table 12.1, even given the following conditions:

- PiCCO data available or not,
- left atrial/vena cava pressure data available or not,
- vena cava PP data available or not,
- unreliable left ventricular volume data.

This robustness and adaptability to the available data makes the method and this simplified model serious candidates for application to ICU patient data.

12.3.3 Total Stressed Volume $V_{s,3}$ as an Index of Fluid Responsiveness

In Section 3.2, three methods were detailed to assess the performance of an index of fluid responsiveness. This section applies the three method to the computed value of $V_{s,3}$ before each fluid administration. The goal is to investigate whether $V_{s,3}$ could be used as an index of fluid responsiveness.

Linear Regression: Pooled Data

Figure 12.4 shows the relation between relative change in CO after each fluid administration and the identified $V_{s,3}$ value before the fluid administration, for pigs number 3 to 8. Pigs number 1 and 2 were excluded from this analysis, because they received different volumes of fluid, administered at a different rate, as explained in Section 12.2.1. The correlation coefficient, r, equals -0.35.

As explained in the previous section, pig number 6 presented a pulsus alternans. This condition was associated with the largest MAE and may thus have impacted the quality of the estimated $V_{s,3}$. If pig number 6 is also excluded from the linear regression analysis, the correlation coefficient becomes -0.50.

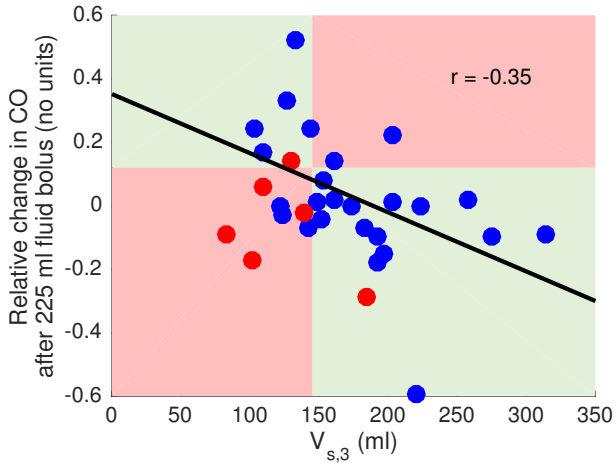

Figure 12.4: Relative change in CO after each 225 ml fluid bolus plotted versus the identified $V_{s,3}$ value before bolus, for pigs number 3 to 8. Data from pig number 6 are displayed in red. The coloured areas divide the plane along the lines $V_{s,3}$ = 145 ml and relative change in CO = 12 %.

The negative relation means that the higher the $V_{s,3}$, the lower the relative change in CO. This relation was expected, since $V_{s,3}$ represents the volume status of a subject. For instance, a high $V_{s,3}$ value means that the subject has a large intra-vascular blood volume. In this case, a fluid administration is not required and will probably not be beneficial.

The results presented in this section are similar to those of Maas *et al.* [32] for ICU patients, presented in Figure 3.1. As explained in Section 3.5, these authors observed a negative correlation between SBV and relative change in CO after fluid administrations in ICU patients. In their study, SBV was determined using 10 sequential 50 ml fluid administrations and local circulatory arrests, a time-consuming procedure, which may also be harmful if these *a priori* fluid administrations are actually not required.

In contrast, the procedure presented in this chapter does not require *a priori* fluid administration or circulatory arrests to compute the $V_{s,3}$ value. Furthermore, it is also based on data available in an ICU. Hence, it is not additionally invasive and may also be safer.

Linear Regression: Individual Data

It is also interesting to observe that the correlation presented in the previous section is even stronger for each animal taken individually. Figures 12.5 and 12.6 show the relation between relative change in CO after each fluid administration

and the identified $V_{s,3}$ value before the fluid administration, for all 8 animals separately.

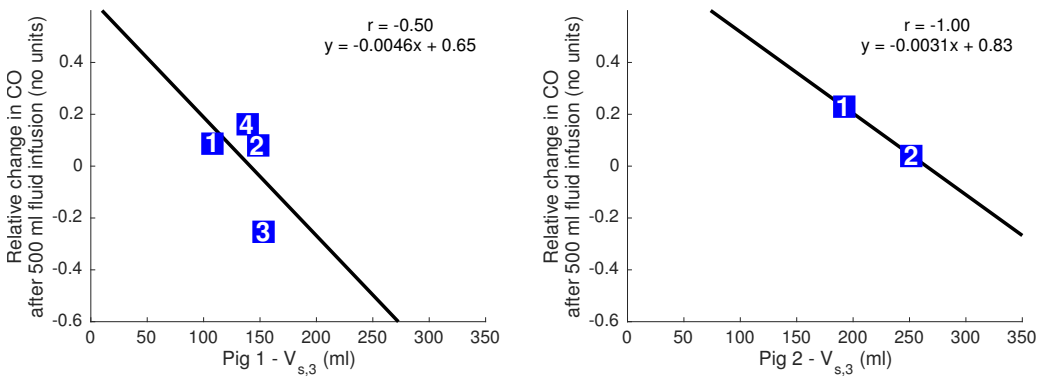

Figure 12.5: Relative change in CO after each 500 ml fluid infusion plotted versus the identified $V_{s,3}$ value before infusion, for pigs number 1 and 2. The numbers in the squares indicate the sequence of fluid administrations.

Note that the worst correlation ($r = -0.37$) is again observed for pig number 6, which presented a pulsus alternans. The lower quality of the estimated $V_{s,3}$ could explain the weaker relation between $V_{s,3}$ and relative change in CO after fluid administration.

Figures 12.5 and 12.6 also emphasise that neither $V_{s,3}$ nor CO changed monotonically during the filling experiments, which can be attributed to the numerous regulatory mechanisms acting on the CVS. Another possible reason why CO decreased after some fluid administrations can be that preload was increased so much that the heart eventually worked on the descending part of the Frank-Starling curve, as mentioned in Section 2.3.5.

Accordingly, for pigs number 7 and 8, the use of dobutamine before the final fluid bolus increased the contractility, and changed the Frank-Starling curve as shown in Figure 2.11, which explains why the last fluid administration was effective, while the previous ones were not. This effect was not observed for pig number 6. All these observations underline the complexity of predicting the effects of fluid administration and inotropes. These two treatments are often used together in the management of shock, but selecting between them is difficult [4].

t-Test

As explained in Section 3.2.2, a *t*-test and a ROC curve require setting a threshold for definition of fluid responsiveness. Maas *et al.* define a positive response as a relative change in CO larger than 12 % [32]. According to this definition,

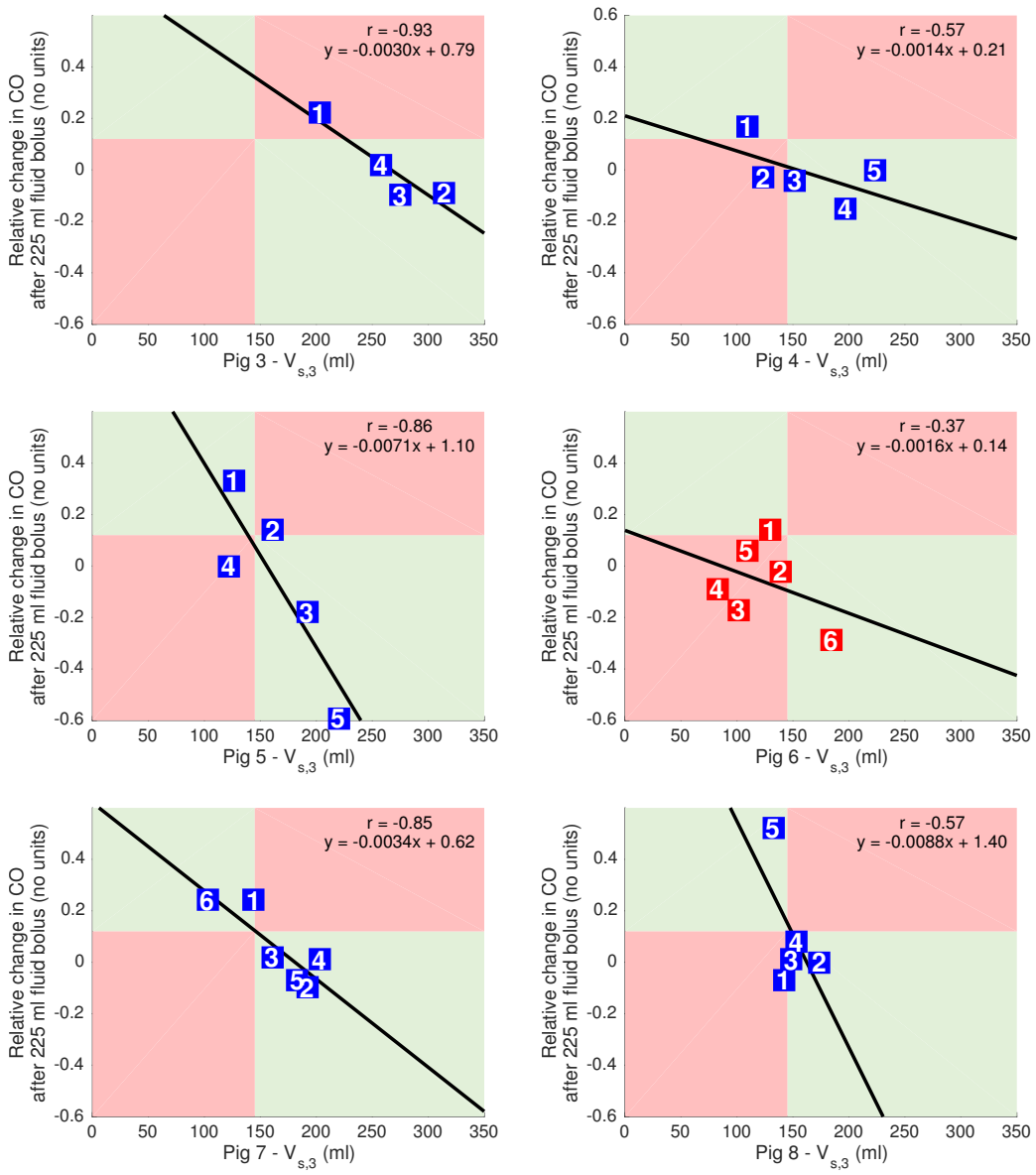

Figure 12.6: Relative change in CO after each 225 ml fluid bolus plotted versus the identified $V_{s,3}$ value before bolus, for pigs number 3 to 8. The numbers in the squares indicate the sequence of fluid administrations. The coloured areas divide the plane along the lines $V_{s,3}$ = 145 ml and relative change in CO = 12 %.

10/37 (27 %) of the fluid administrations performed in the present study were associated with a positive response. This proportion is lower than the 50 % usually reported for ICU patients [3,6,31]. However, conversely to what happens in ICUs, the pigs were healthy, except for pigs number 6 and 8, during the experiments.

The mean $V_{s,3}$ for cases associated with a positive response (138 $\pm$ 32 ml) and a negative response (176 $\pm$ 57 ml) are not significantly different ($p = 0.088$). This p-value was computed using an unpaired t-test on the combined data from pigs number 3 to 8. Leaving pig number 6 aside, the means become 140 $\pm$ 34 ml for

cases where the change in CO > 12 % and 191 ± 52 ml for cases where the change in CO ≤ 12 %, and these means are significantly different ($p = 0.026$).

Receiver-Operator Characteristic Curve

To investigate if a $V_{s,3}$ lower than a given threshold could predict a relative change in CO larger than 12 %, the ROC curve is plotted in Figure 12.7. The best threshold for $V_{s,3}$ was found to be 145 ml and is represented in Figure 12.6. This threshold was associated with a sensitivity of 0.75 and a specificity of 0.70. The area under the ROC curve was 0.70. This analysis was conducted only using the combined data from pigs number 3 to 8, since pigs number 1 and 2 received different volumes of fluid, administered in a different fashion.

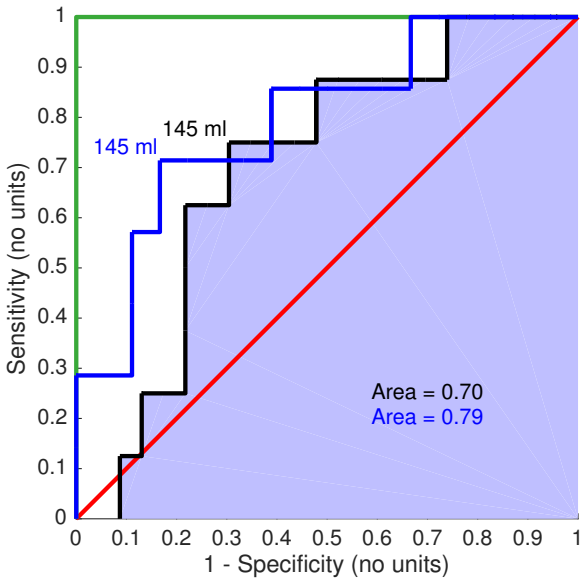

Figure 12.7: ROC curve of $V_{s,3}$ as a predictor of a relative change in CO larger than 12 % after fluid administration. The black curve was built using data from pigs number 3 to 8 and the blue one, with data from pigs number 3, 4, 5, 7 and 8.

A second ROC curve is presented in Figure 12.7, obtained by excluding pig number 6, which presented a pulsus alternans. In this case, the best threshold remains 145 ml, but is associated with a sensitivity of 0.71 and a specificity of 0.83. The area under the second ROC curve is 0.79. Both results are very good and will be compared with conventional indices of fluid responsiveness in the next section.

The imperfect values of sensitivity and specificity can be understood by noticing that the relation between $V_{s,3}$ and relative change in CO seems to be subject-specific. In particular, the slope of the relation between $V_{s,3}$ and relative change in

CO ranges from -0.0014 to -0.0088 ml^{-1}. Maas *et al.* determined only one SBV value for each subject, and thus, could not make a similar observation for SBV.

12.3.4 Conventional Indices of Fluid Responsiveness

The commonly used dynamic indices of fluid responsiveness, SVV, PPV and SPV, were introduced in Section 3.4. These indices have been computed from the measured left ventricular and aortic pressure data, before each fluid infusion. For the best comparison with $V_{s,3}$, the dynamic indices were computed on five respiratory cycles, just before the disconnection of the ventilator described in Section 12.2.1. Note that the ventilator had to be connected, since the dynamic indices are based on cardio-pulmonary interactions. The analyses presented in Section 12.3.3 for $V_{s,3}$ have been reproduced for these indices.

Linear Regression: Pooled Data

Figures 12.8 to 12.10 shows the relation between relative change in CO after each fluid administration and the values of the dynamic indices SVV, PPV and SPV before the fluid administration, for pigs number 3, 4, 5, 7 and 8. The data from pigs number 1 and 2 were excluded from the analysis because fluid was administered differently. Pig number 6 was excluded because the pulsus alternans causes changes in haemodynamic signals that are not linked to mechanical ventilation. The dynamic indices could thus not be computed for this animal.

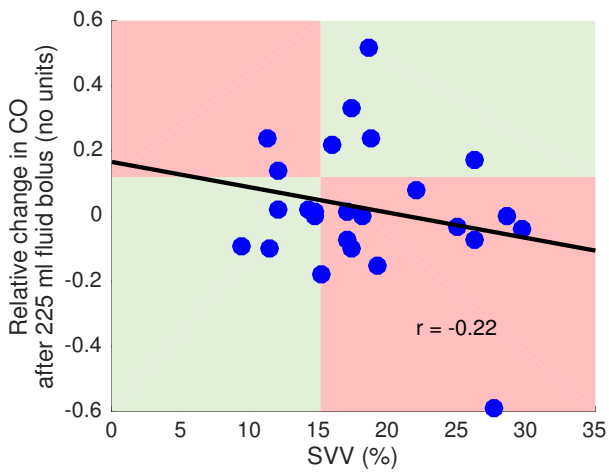

Figure 12.8: Relative change in CO after each 225 ml fluid bolus plotted versus the computed SVV value before bolus, for pigs number 3, 4, 5, 7 and 8. The coloured areas divide the plane along the lines SVV = 15.1 % and relative change in CO = 12 %.

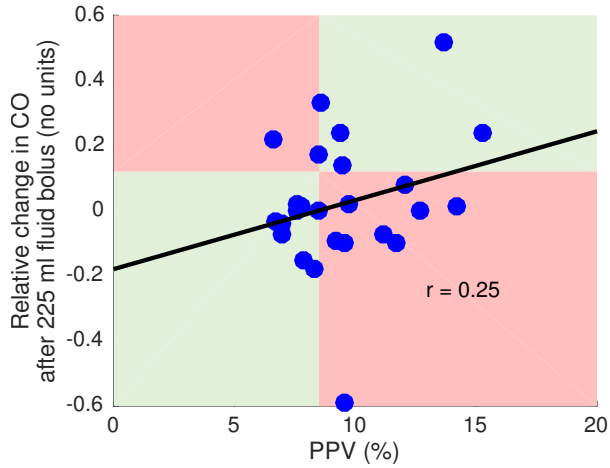

Figure 12.9: Relative change in CO after each 225 ml fluid bolus plotted versus the computed PPV value before bolus, for pigs number 3, 4, 5, 7 and 8. The coloured areas divide the plane along the lines PPV = 8.5 % and relative change in CO = 12 %.

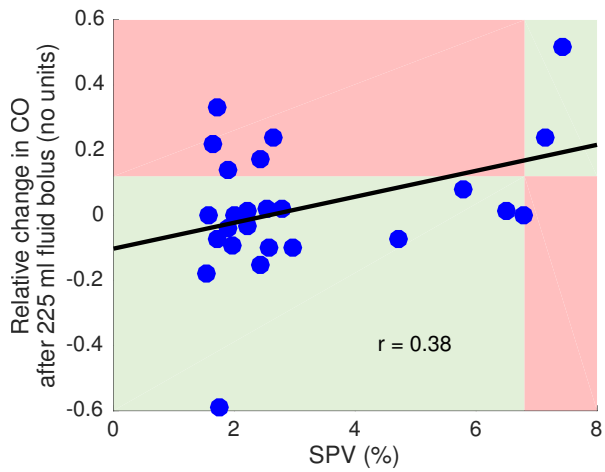

Figure 12.10: Relative change in CO after each 225 ml fluid bolus plotted versus the computed SPV value before bolus, for pigs number 3, 4, 5, 7 and 8. The coloured areas divide the plane along the lines SPV = 6.8 % and relative change in CO = 12 %.

Overall, the correlation coefficients between the dynamic indices and the relative changes in CO are smaller in absolute value than the one observed for $V_{s,3}$, which was equal to -0.5 for the same animals. In particular, the correlation coefficient for SVV is negative, as shown in Figure 12.8, while it should be positive [6].

Linear Regression: Individual Data

Table 12.3 shows the correlation coefficients, r, between relative change in CO and (1) SVV, (2) PPV and (3) SPV. Because they are only two data points for pig 2, the correlation coefficients are systematically equal to 1 or -1.

As can be seen in Table 12.3, the correlation between change in CO and SVV is negative in 4/7 cases, while it should be positive [6]. The same observation can be drawn for the correlations between

- Change in CO and PPV (negative in 3/7 cases),
- Change in CO and SPV (negative in 2/7 cases).

Both of these correlations should also be positive. On the other hand, as shown in Figures 12.5 and 12.6, change in CO was negatively correlated with $V_{s,3}$ in all cases.

Table 12.3: Correlation coefficients, r, between relative change in CO and (1) SVV, (2) PPV and (3) SPV.

Pig number	1	2	3	4	5	7	8
SVV	0.04	-1.00	0.94	0.50	-0.76	-0.29	-0.35
PPV	-0.74	1.00	-0.87	0.50	-0.37	0.66	0.48
SPV	-0.15	1.00	-0.68	0.15	0.14	0.65	0.71

t-Test

Unpaired t-tests were performed to investigate whether the mean d ynamic indices were statistically different for positive and negative responses. The results are presented in Table 12.4. As shown in this table, the mean values of SVV, PPV and SPV are very close for positive and negative responses. Consequently, there is no significant difference between these mean values and no diagnostic accuracy greater than 50 % is likely. It is also interesting to mention that the mean SVV for positive responses is lower than for negative ones, where it should be higher. In contrast, as previously mentioned, the mean $V_{s,3}$ values for positive and negative responses are significantly different ($p = 0.026$).

Receiver-Operator Characteristic Curve

The ROC curves for the dynamic indices are plotted in Figures 12.11 to 12.13 and their features are summarised in Table 12.5.

The best thresholds found for SVV, PPV and SPV are similar to those presented in the literature. For humans, the reported threshold values are:

Table 12.4: Results of the t-tests for SVV, PPV and SPV (performed using data from pigs number 3, 4, 5, 7 and 8).

Index	Mean for positive responses	Mean for negative responses	p
SVV	17.2 %	18.9 %	0.529
PPV	10.2 %	9.3 %	0.428
SPV	3.6 %	3.0 %	0.533

- 9.5 to 16 % for SVV [7,33,39,45,206],
- 4 to 17 % for PPV [7,21,25,31,36,39,53,206],
- 8.5 to 9 % for SPV [39,43].

For pigs, the values are:

- 9.5 % for SVV [207],
- 5 to 15 % for PPV [42,71,207].

As mentioned in Section 3.4.4, all these threshold values depend on many factors, including ventilator settings. They also depend on how fluid responsiveness is defined, which explains the very large variations.

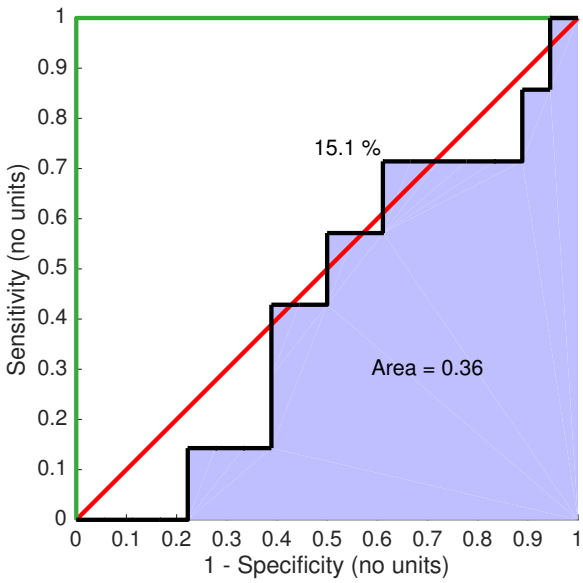

Figure 12.11: ROC curve of SVV as a predictor of a relative change in CO larger than 12 % after fluid administration. The curve was built using data from pigs number 3, 4, 5, 7 and 8.

In the present study, the dynamic indices are not able to provide both a sensitivity and a specificity larger than 0.5. Similarly, the area under the ROC curves is very close to 0.5, making them barely more (even less for SVV) efficient than flip-

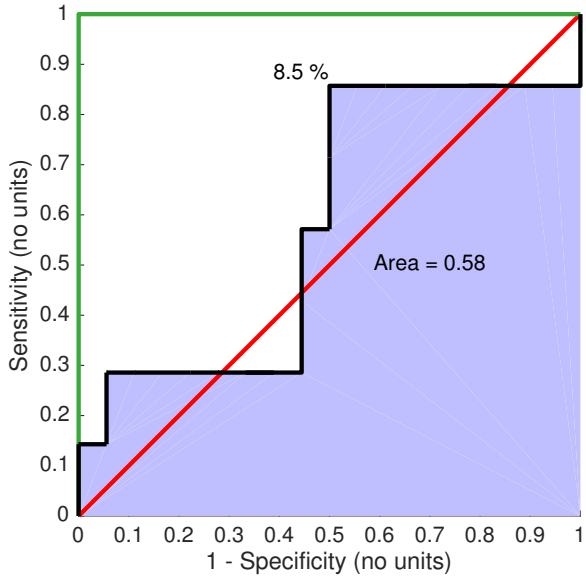

Figure 12.12: ROC curve of PPV as a predictor of a relative change in CO larger than 12 % after fluid administration. The curve was built using data from pigs number 3, 4, 5, 7 and 8.

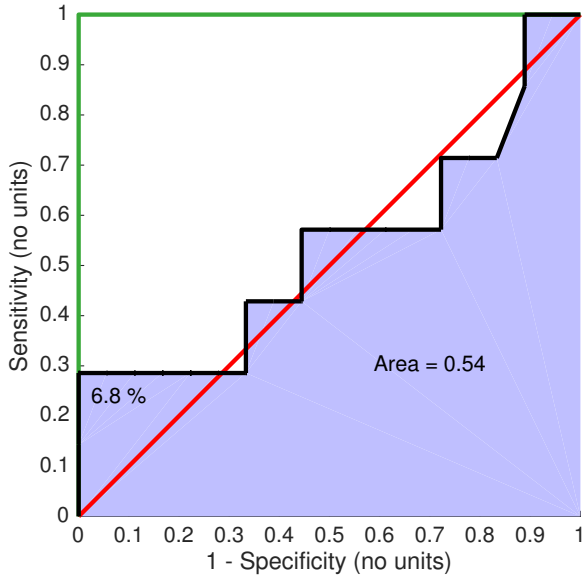

Figure 12.13: ROC curve of SPV as a predictor of a relative change in CO larger than 12 % after fluid administration. The curve was built using data from pigs number 3, 4, 5, 7 and 8.

ping a coin to make a decision about fluid administration. This last observation matches some previously published ICU results [45, 48, 60].

Table 12.5: Characteristics of the ROC curves for SVV, PPV and SPV. (The ROC curves were built using data from pigs number 3, 4, 5, 7 and 8.)

Index	Threshold	Sensitivity	Specificity	Area under ROC
SVV	15.1 %	0.71	0.39	0.36
PPV	8.5 %	0.86	0.50	0.58
SPV	6.8 %	0.29	1.00	0.54

A possible explanation for the inefficiency of dynamic indices in this diagnostic use is that the way fluid administration was performed in pigs number 3 to 8 is different from the way fluid administrations are performed in an ICU. As previously mentioned, pigs number 3 to 8 received 225 ml fluid boluses, injected in approximately two minutes. In the ICU, fluid administration is performed using continuous infusions, typically 500 ml in 30 minutes, as was done for pigs number 1 and 2. The low volume of fluid administered to pigs number 3 to 8 could explain that some animals did not respond to filling, while they would have if a larger volume had been administered. However, even when considering only the results for pigs number 1 and 2 in Table 12.3, discrepancies are still present for SVV, PPV and SPV.

12.4 Summary

This chapter presented a method to compute the $V_{s,3}$ parameter of the three-chamber model. This index was identified by adjusting the parameters of the three-chamber model to data from vascular filling experiments in pigs. The identified $V_{s,3}$ value presented a consistent association with the relative change in CO after fluid administration, as expected from the Frank-Starling mechanism and from the results of a previous study. In contrast, the clinically accepted indices, SVV, PPV and SPV, did not predict the change in CO after each fluid infusion. Importantly, the method developed in this chapter can be applied to humans, since it does not require *a priori* fluid infusions and the data required for parameter identification can be obtained in an ICU.

Chapter 13

Conclusions

Vascular filling is one of the most frequent and important interventions performed in the intensive care unit (ICU). It aims to increase cardiac output (CO) by increasing the quantity of fluid in the vasculature. However, vascular filling therapy is only effective in 50 % of cases, the rest of the fluid administrations being ineffective and potentially harmful, as an excess of fluid can cause pulmonary oedema, right ventricular dysfunction or haemodilution. Clinicians thus need robust, readily available indices to decide whether to perform vascular filling.

Currently, there exist two main types of indices to guide vascular filling. Static indices are measurements of cardiac pressures and volumes, which are assumed to represent the loading conditions of the heart. These indices have been repeatedly proven inaccurate during the last decade. Dynamic indices capture the amplitude of changes in cardiac pressures and volumes caused by mechanical ventilation and other external influences. Dynamic indices are superior to static indices, but are difficult to implement clinically.

This thesis aimed to improve the prediction of the response to vascular filling using a different approach, based on mathematical models of the cardio-vascular system (CVS). More specifically, the three goals of this thesis, as stated in the introduction, were:

- To develop simple models of the CVS usable in the ICU,
- To demonstrate that the parameters of these models can be identified from readily available ICU data, proving structural and practical identifiability,
- To verify the models using clinical data, to predict the response to vascular filling.

The present section summarises the content of this thesis and shows how these three goals were reached.

13.1 Summary

Chapter 2 first briefly presented the anatomy of the CVS. The physiology of this system was then described more extensively, including an overview of the heart's behaviour and the usual evolution of pressures and volumes during a cardiac cycle. Pressures and volumes play a major role in investigating the cardiac function and vascular state. Several indices based on pressures and volumes were defined, including CO. All these indices are constantly used in ICUs to investigate a patient's state. Finally, as CO is the most important of these indices, its four determinants, preload, afterload, contractility and heart rate, were discussed.

Vascular filling is also tightly linked to CO. As explained in Chapter 3, the goal of this therapy is to increase CO through an intravenous administration of fluid. However, because the effects of this therapy are uncertain and potentially harmful, there is a need for indices that predict the response to vascular filling, or fluid responsiveness. Prediction of fluid responsiveness can be of two types:

- Quantitative, meaning the index will predict by how much CO will change after vascular filling,
- Qualitative, meaning the index will predict if CO will change by more than a pre-defined threshold.

Static indices of fluid responsiveness are similar to the pressure and volume-based indices introduced in Chapter 2. These indices have repeatedly been proven to be poor predictors of the response to vascular filling. Dynamic indices were introduced in 2000 based on changes of the static indices caused by external influences, for instance, mechanical ventilation. They suffer many limitations, because of the numerous physiological variables influencing their values. Finally, total stressed blood volume (SBV) was introduced as another potential index. However, it cannot easily be measured in an ICU using current techniques.

Building on the physiology concepts introduced in Chapter 2, Chapters 4 presented very simple ways of modelling the passive elements of the CVS. These elements were modelled using relations between pressures and volumes, which are the most important variables to describe the functioning of the CVS. Resistance elements are tubes through which blood flows following a pressure difference. Valves are non-linear tubes through which blood is only allowed to flow in one direction. Chambers are able to store blood, causing a pressure increase. Finally, the continuity equation was introduced. For closed-loop CVS models, this equation states that blood volume equal to a constant, which represents the model-based equivalent of SBV.

Chapter 5 described different ways of modelling the most important anatomical parts of the CVS: ventricles and atria. The ventricles have been described

using two main approaches: the time-varying elastance theory and multi-scale models, based on a description of cardiac muscle units. The application of the time-varying elastance theory to the atria is very uncertain. Consequently, modelling the atria should be done using multi-scale models.

Using the building blocks developed in Chapters 4 and 5, a first simple model of the CVS was built, containing three chambers representing the heart, the arteries and the veins. A second model was also introduced, containing six chambers representing the left and right ventricles, and the systemic and pulmonary arteries and veins. The development of these models represents the achievement of the first goal of this thesis. The models were developed under several hypotheses, which were discussed and justified. These hypotheses result in the low number of parameters, which thus have the potential to be identified from the limited amounts of data available. Finally, simulations of the two models were performed to verify they produced results consistent with physiological measurements.

The next step was to identify the parameters of the two models from data available in the ICU. Chapter 7 explained what kind of data can be obtained in the ICU and the sensors and techniques to obtain such data: pressure catheters, pulmonary artery catheter, thermodilution and PiCCO. Because the models developed in this work first need to be validated, experimental data was also described, along with corresponding sensors and techniques, such as the pressure-volume catheter.

Chapter 8 presented a demonstration that parameter identification in the developed CVS models is impossible when using only pressure or volume data. More importantly, Chapter 8 also showed that that all parameters of the three-chamber CVS model could theoretically be identified from signals available in an ICU: arterial pressure, venous pressure and stroke volume (SV). The demonstration can be extended to the six-chamber CVS model, provided that measurements from pulmonary arterial and venous pressures are also available. Such a requirement can be met in an ICU by using a pulmonary artery catheter. Thanks to this demonstration, the second goal of this thesis was also reached.

Data available in the ICU are often limited to beat-to-beat indices, such as ranges and means of pressure or volume signals. Consequently, the information contained in the data is not infinite, as typically assumed in the demonstrations of identifiability, and as presented in Chapter 8. Chapter 9 introduced tools to investigate the practical consequences of the limited amount of data. For instance, a sensitivity analysis enabled investigation of the magnitude of a parameter's effect on the simulations. A correlation analysis enabled detection of whether two parameters have similar influences on the simulations. If so, these two parameters will not be practically identifiable together. The subset selection algorithm

presented combines these two approaches and excludes parameters that cannot readily be practically identified. Finally, as parameter identification is an iterative process, formulae were developed to provide precise initial values of the model parameters, which in turn reduces computational time and effort.

Several iterative methods exist to perform parameter identification. In Chapter 10, seven of these methods were introduced and compared. The proportional method was given particular focus, as it was specifically designed for parameter identification in this type of CVS models. The seven parameter identification methods were compared using the three-chamber model on two types of data:

- *In silico* data generated by the model,
- Actual experimental data.

Overall, it was shown that parameter identification in the three-chamber model can be performed rapidly from ICU data.

Chapter 11 presented a first example of parameter identification on the six-chamber model. Special attention was paid to the model-based equivalent of SBV, denoted $V_{s,6}$, as this parameter is a potential physiological, model-based index of fluid responsiveness. This parameter was shown to dictate the model's behaviour when preload and afterload are changing. Using experimental data from such a situation, this parameter could be identified based on the methodology introduced in the previous chapters. The model provided good fit to experimental data, thus providing the first validation the six-chamber model in a situation of changing determinants of CO.

In the last chapter, Chapter 12, parameters of the three-chamber model were identified from experimental data recorded during vascular filling experiments. The three-chamber model, despite its simplicity, was shown to be able to reproduce the diversity of experimental data. More importantly, the model-based version of SBV, denoted $V_{s,3}$, showed a consistent association with the change in CO after vascular filling, making it a first model-based index of fluid responsiveness. In addition, when computing the predictive power of the conventional dynamic indices of fluid responsiveness, all these dynamic indices performed poorly. In conclusion, the three-chamber model can be combined with data available in the ICU to provide an index of the response to vascular filling, thus meeting the third and final goal of this thesis.

13.2 Main Findings

While the previous section summarised the sequence of developments made in this thesis, the present section summarises the main findings and achievements. First, this thesis provided a first demonstration of the structural identifiability of a

typical, lumped CVS model. Such a demonstration is a prerequisite for parameter identification, as it proves that the process theoretically has a unique solution. Importantly, the complexity of most CVS models in the literature means they have not been shown to be structurally identifiable before performing parameter identification. Hence, this unique contribution provides a solid theoretical foundation and can be generalised to many similar physiological models.

According to the previously presented demonstration, the three-chamber CVS model developed in this thesis can be identified from data typically available in an ICU: SV, and systemic arterial and venous pressures. The six-chamber CVS model, as it represents the pulmonary circulation, requires additional information from that circulation to be identifiable. The required additional data, arterial and venous pulmonary pressures, can be obtained using an invasive sensor, the pulmonary artery catheter. Consequently, the three-chamber model is more suited for regular use in an ICU, and is thus a new, more practical minimal model for CVS monitoring and management.

As previously mentioned, this thesis also presented a first quantitative validation of the six-chamber CVS model in conditions of varying preload and afterload. Most CVS models presented in the literature are simulated in constant conditions of preload and afterload. However, as detailed in Section 3, in real life, preload and afterload are not constant, and more importantly change in typical ICU conditions. Showing that the studied CVS model can be used in varying conditions typical of the need for circulatory management, is thus a major result, since these models are to be used for prediction.

Finally, as previously emphasised, the model-based analogue of SBV, $V_{s,3}$, was computed using the three-chamber model on experimental data during vascular filling. This parameter showed a consistent association with the relative change in CO after vascular filling, for eight animals in different states, with different measurements available. Equally important, the conventional indices of fluid responsiveness, such as SVV, PPV and SPV showed a very weak efficiency in predicting the response to vascular filling. Therefore, the need for model-based indices, such as $V_{s,3}$, is strengthened.

13.3 Future Work

The work presented in this thesis yet has to be validated in humans. The method was designed with this application in mind. Since it does not require *a priori* fluid infusions and the data required for parameter identification can be obtained in an ICU, the method is readily applicable to humans. A retrospective analysis of

human data from previously performed fluid administrations is planned in the near future.

As shown in this thesis, a low value of the model parameter $V_{s,3}$ can be considered as a sign of a positive response to vascular filling. It would be useful to investigate the physiological mechanisms causing a low identified value of $V_{s,3}$ and their link to the change in CO after vascular filling. Such an investigation would allow a deeper understanding of the body's reaction to vascular filling, and would also potentially improve the quality of the model's prediction, even if it is already very good.

Finally, more reliable measurement of CO is highly needed in the ICU. Currently, CO can be measured only intermittently using echocardiography or thermodilution, as explained in Chapter 7. The continuous estimate of CO provided by the PiCCO and similar devices is only valid as long as there are no major haemodynamic changes. However, as repeatedly stated in this thesis, the efficiency of vascular filling is assessed through its effect on the measured CO. A more reliable measurement of CO would allow knowing with certainty if vascular filling was successful or not. In the particular context of the methods developed in this work, CO has been shown to be an essential measurement for parameter identification of CVS models. Since it often is the only volume-related piece of information, an unreliable CO value could have serious consequences on the identified parameter values.

Bibliography

[1] M. Cecconi, C. Hofer, J.-L. Teboul, V. Pettila, E. Wilkman, Z. Molnar, G. Della Rocca, C. Aldecoa, A. Artigas, S. Jog, M. Sander, C. Spies, J.-Y. Lefrant, and D. De Backer. Fluid challenges in intensive care: the FENICE study. *Intensive Care Medicine*, 41(9):1529–1537, 2015.

[2] T. Boulain and M. Cecconi. Can one size fit all? The fine line between fluid overload and hypovolemia. *Intensive Care Medicine*, 41(3):544–546, 2015.

[3] R. Phillips and J. Brierley. Fluid responsiveness is about stroke volume, and not pulse pressure Yogi: the power of Doppler fluid management and cardiovascular monitoring. *Journal of Clinical Monitoring and Computing*, 29(1):197–200, 2015.

[4] M. Cecconi, D. De Backer, M. Antonelli, R. Beale, J. Bakker, C. Hofer, R. Jaeschke, A. Mebazaa, M. R. Pinsky, J. L. Teboul, J. L. Vincent, and A. Rhodes. Consensus on circulatory shock and hemodynamic monitoring. task force of the european society of intensive care medicine. *Intensive Care Medicine*, 40(12):1795–1815, 2014.

[5] K. Bendjelid and J.-A. Romand. Fluid responsiveness in mechanically ventilated patients: a review of indices used in intensive care. *Intensive Care Medicine*, 29(3):352–360, 2003.

[6] F. Michard and J.-L. Teboul. Using heart-lung interactions to assess fluid responsiveness during mechanical ventilation. *Critical Care*, 4(5):282–289, 2000.

[7] F. Michard. Changes in arterial pressure during mechanical ventilation. *Anesthesiology*, 103(2):419–428, 2005.

[8] P. Coriat, M. Vrillon, A. Perel, J.-F. Baron, F. Le Bret, M. Saada, and P. Viars. A comparison of systolic blood pressure variations and echocardiographic estimates of end-diastolic left ventricular size in patients after aortic surgery. *Anesthesia & Analgesia*, 78(1):46–53, 1994.

[9] Y. Mahjoub, V. Lejeune, L. Muller, S. Perbet, L. Zieleskiewicz, F. Bart, B. Veber, C. Paugam-Burtz, S. Jaber, A. Ayham, E. Zogheib, S. Lasocki, A. Vieillard-Baron, H. Quintard, O. Joannes-Boyau, G. Plantefève, P. Montravers, S. Duperret, M. Lakhdari, N. Ammenouche, E. Lorne, M. Slama, and H. Dupont. Evaluation of pulse pressure variation validity criteria in critically ill patients: a prospective observational multicentre point-prevalence study. *British Journal of Anaesthesia*, 112(4):681–655, 2014.

[10] C. Cobelli and E. Carson. *Introduction to modeling in physiology and medicine*. Academic Press, 2008.

[11] J. G. Chase, A. J. Le Compte, J. C. Preiser, G. M. Shaw, S. Penning, and T. Desaive. Physiological modeling, tight glycemic control, and the icu clinician: what are models and how can they affect practice? *Annals of Intensive Care*, 1(1):11, 2011.

[12] P. J. Hunter, A. J. Pullan, and B. H. Smaill. Modeling total heart function. *Annual Review of Biomedical Engineering*, 5(1):147–177, 2003.

[13] S. Paeme. *Mathematical modeling of the mitral valve. From local to global hemodynamics*. PhD thesis, University of Liège, Liège, Belgium, 2014.

[14] M. Ragosta. *Textbook of Clinical Hemodynamics*. Elsevier Health Sciences, 2008.

[15] R. Klabunde and A. Dalley. *Cardiovascular physiology concepts*. Lippincott Williams & Wilkins, 2004.

[16] D. A. Reuter, T. W. Felbinger, E. Kilger, C. Schmidt, P. Lamm, and A. E. Goetz. Optimizing fluid therapy in mechanically ventilated patients after cardiac surgery by on-line monitoring of left ventricular stroke volume variations. comparison with aortic systolic pressure variations. *British Journal of Anaesthesia*, 88(1):124–126, 2002.

[17] F. Michard, D. Chemla, C. Richard, M. Wysocki, M. R. Pinsky, Y. Lecarpentier, and J.-L. Teboul. Clinical use of respiratory changes in arterial pulse pressure to monitor the hemodynamic effects of peep. *American Journal of Respiratory and Critical Care Medicine*, 159(3):935–939, 1999.

[18] P. L. Marino. *The ICU book*. Wolters Kluwer Health, 2007.

[19] J.-W. Lankhaar, N. Westerhof, T. J. Faes, C. T. Gan, K. M. Marques, A. Boonstra, F. G. van den Berg, P. E. Postmus, and A. Vonk-Noordegraaf. Pulmonary vascular resistance and compliance stay inversely related during

treatment of pulmonary hypertension. *European Heart Journal*, 29(13):1688–1695, 2008.

[20] P. Morimont, B. Lambermont, A. Ghuysen, P. Gérard, P. Kolh, P. Lancellotti, V. Tchana-Sato, T. Desaive, and V. D'Orio. Effective arterial elastance as an index of pulmonary vascular load. *American Journal of Physiology - Heart and Circulatory Physiology*, 294(6):H2736–H2742, 2008.

[21] M. Cannesson, Y. Le Manach, C. K. Hofer, J. P. Goarin, J. J. Lehot, B. Vallet, and B. Tavernier. Assessing the diagnostic accuracy of pulse pressure variations for the prediction of fluid responsiveness: a "gray zone" approach. *Anesthesiology*, 115(2):231–241, 2011.

[22] P. Morimont, B. Lambermont, T. Desaive, N. Janssen, J. G. Chase, and V. D'Orio. Arterial dP/dt_{max} accurately reflects left ventricular contractility during shock when adequate vascular filling is achieved. *BMC Cardiovascular Disorders*, 12(1):13, 2012.

[23] N. Airapetian, J. Maizel, O. Alyamani, Y. Mahjoub, E. Lorne, M. Levrard, N. Ammenouche, A. Seydi, F. Tinturier, E. Lobjoie, H. Dupont, and M. Slama. Does inferior vena cava respiratory variability predict fluid responsiveness in spontaneously breathing patients? *Critical Care*, 19(1):400, 2015.

[24] A. Lira and M. R. Pinsky. Choices in fluid type and volume during resuscitation: impact on patient outcomes. *Annals of Intensive Care*, 4(1):38, 2014.

[25] X. Yang and B. Du. Does pulse pressure variation predict fluid responsiveness in critically ill patients? A systematic review and meta-analysis. *Critical Care*, 18(6):650, 2014.

[26] W. Ganong and M. Jobin. *Physiologie médicale*. De Boeck, 2007.

[27] D. De Backer. Prédiction de la réponse au remplissage vasculaire: que faire de tous ces indices proposés ? *Réanimation*, 21(2):123–127, 2012.

[28] C. Charron, C. Fessenmeyer, C. Cosson, J. X. Mazoit, J. L. Hebert, D. Benhamou, and A. R. Edouard. The influence of tidal volume on the dynamic variables of fluid responsiveness in critically ill patients. *Anesthesia & Analgesia*, 102(5):1511–1517, 2006.

[29] M. Feissel, J. Badie, P. G. Merlani, J.-P. Faller, and K. Bendjelid. Pre-ejection period variations predict the fluid responsiveness of septic ventilated patients. *Critical Care Medicine*, 33(11):2534–2539, 2005.

[30] J. O. Auler, F. Galas, L. Hajjar, L. Santos, T. Carvalho, and F. Michard. Online monitoring of pulse pressure variation to guide fluid therapy after cardiac surgery. *Anesthesia & Analgesia*, 106(4):1201–1206, 2008.

[31] M. Biais, S. Ehrmann, A. Mari, B. Conte, Y. Mahjoub, O. Desebbe, J. Pottecher, K. Lakhal, D. Benzekri-Lefevre, N. Molinari, T. Boulain, J.-Y. Lefrant, L. Muller, and with the collaboration of AzuRea Group. Clinical relevance of pulse pressure variations for predicting fluid responsiveness in mechanically ventilated intensive care unit patients: the grey zone approach. *Critical Care*, 18(6):587, 2014.

[32] J. J. Maas, M. R. Pinsky, L. P. Aarts, and J. R. Jansen. Bedside assessment of total systemic vascular compliance, stressed volume, and cardiac function curves in intensive care unit patients. *Anesthesia & Analgesia*, 115(4):880–887, 2012.

[33] D. A. Reuter, A. Kirchner, T. W. Felbinger, F. C. Weis, E. Kilger, P. Lamm, and A. E. Goetz. Usefulness of left ventricular stroke volume variation to assess fluid responsiveness in patients with reduced cardiac function. *Critical Care Medicine*, 31(5):1399–1404, 2003.

[34] H. J. Motulsky, M. Dramaix-Wilmet, F. Nackers, and A. Robert. *Biostatistique: Une approche intuitive*. De Boeck Université. De Boeck Supérieur, 2002.

[35] C. P. Tousignant, F. Walsh, and C. D. Mazer. The use of transesophageal echocardiography for preload assessment in critically ill patients. *Anesthesia & Analgesia*, 90(2):351–355, 2000.

[36] A. Kramer, D. Zygun, H. Hawes, P. Easton, and A. Ferland. Pulse pressure variation predicts fluid responsiveness following coronary artery bypass surgery. *Chest*, 126(5):1563–1568, 2004.

[37] H. Berkenstadt, N. Margalit, M. Hadani, Z. Friedman, E. Segal, Y. Villa, and A. Perel. Stroke volume variation as a predictor of fluid responsiveness in patients undergoing brain surgery. *Anesthesia & Analgesia*, 92(4):984–989, 2001.

[38] A. Vieillard-Baron, K. Chergui, A. Rabiller, O. Peyrouset, B. Page, A. Beauchet, and F. Jardin. Superior vena caval collapsibility as a gauge of volume status in ventilated septic patients. *Intensive Care Medicine*, 30(9):1734–1739, 2004.

[39] S. Preisman, S. Kogan, H. Berkenstadt, and A. Perel. Predicting fluid responsiveness in patients undergoing cardiac surgery: functional haemodynamic parameters including the respiratory systolic variation test and static preload indicators. *British Journal of Anaesthesia*, 95(6):746–755, 2005.

[40] P. A. Wyffels, P. J. Durnez, J. Helderweirt, W. M. Stockman, and D. De Kegel. Ventilation-induced plethysmographic variations predict fluid responsiveness in ventilated postoperative cardiac surgery patients. *Anesthesia & Analgesia*, 105(2):448–452, 2007.

[41] M. I. Monge García, A. Gil Cano, and J. C. Díaz Monrové. Brachial artery peak velocity variation to predict fluid responsiveness in mechanically ventilated patients. *Critical Care*, 13(5):R142, 2009.

[42] S. T. Vistisen, J. Koefoed-Nielsen, and A. Larsson. Automated pre-ejection period variation predicts fluid responsiveness in low tidal volume ventilated pigs. *Acta Anaesthesiologica Scandinavica*, 54(2):199–205, 2010.

[43] M. Cecconi, G. Monti, M. A. Hamilton, M. Puntis, D. Dawson, M. L. Tuccillo, G. Della Rocca, R. M. Grounds, and A. Rhodes. Efficacy of functional hemodynamic parameters in predicting fluid responsiveness with pulse power analysis in surgical patients. *Minerva Anestesiologica*, 78(5):527–533, 2012.

[44] A. Yazigi, E. Khoury, S. Hlais, S. Madi-Jebara, F. Haddad, G. Hayek, and K. Jabbour. Pulse pressure variation predicts fluid responsiveness in elderly patients after coronary artery bypass graft surgery. *Journal of Cardiothoracic and Vascular Anesthesia*, 26(3):387–390, 2012.

[45] M. O. Fischer, J. Coucoravas, J. Truong, L. Zhu, J. L. Gérard, J. L. Hanouz, and J. L. Fellahi. Assessment of changes in cardiac index and fluid responsiveness: a comparison of Nexfin and transpulmonary thermodilution. *Acta Anaesthesiologica Scandinavica*, 57(6):704–712, 2013.

[46] M. O. Fischer, A. Pelissier, D. Bohadana, J. L. Gérard, J. L. Hanouz, and J. L. Fellahi. Prediction of responsiveness to an intravenous fluid challenge in patients after cardiac surgery with cardiopulmonary bypass: a comparison between arterial pulse pressure variation and digital plethysmographic variability index. *Journal of Cardiothoracic and Vascular Anesthesia*, 27(6):1087–1093, 2013.

[47] H. Ishihara, E. Hashiba, H. Okawa, J. Saito, T. Kasai, and T. Tsubo. Neither dynamic, static, nor volumetric variables can accurately predict fluid

responsiveness early after abdominothoracic esophagectomy. *Perioperative medicine*, 2(1):3, 2013.

[48] B. Lansdorp, J. Lemson, M. van Putten, A. de Keijzer, J. G. van der Hoeven, and P. Pickkers. Dynamic indices do not predict volume responsiveness in routine clinical practice. *British Journal of Anaesthesia*, 108(3):395–401, 2012.

[49] H. Charbonneau, B. Riu, M. Faron, A. Mari, M. M. Kurrek, J. Ruiz, T. Geeraerts, O. Fourcade, M. Genestal, and S. Silva. Predicting preload responsiveness using simultaneous recordings of inferior and superior vena cavae diameters. *Critical Care*, 18(5):473, 2014.

[50] C. Barbier, Y. Loubières, C. Schmit, J. Hayon, J.-L. Ricôme, F. Jardin, and A. Vieillard-Baron. Respiratory changes in inferior vena cava diameter are helpful in predicting fluid responsiveness in ventilated septic patients. *Intensive Care Medicine*, 30(9):1740–1746, 2004.

[51] C. Reuse, J. L. Vincent, and M. R. Pinsky. Measurements of right ventricular volumes during fluid challenge. *Chest*, 98(6):1450–1454, 1990.

[52] J. G. Wagner and J. W. Leatherman. Right ventricular end-diastolic volume as a predictor of the hemodynamic response to a fluid challenge. *Chest*, 113(4):1048–1054, 1998.

[53] F. Michard, S. Boussat, D. Chemla, N. Anguel, A. Mercat, Y. Lecarpentier, C. Richard, M. R. Pinsky, and J.-L. Teboul. Relation between respiratory changes in arterial pulse pressure and fluid responsiveness in septic patients with acute circulatory failure. *American Journal of Respiratory and Critical Care Medicine*, 162(1):134–138, 2000.

[54] B. Tavernier, O. Makhotine, G. Lebuffe, J. Dupont, and P. Scherpereel. Systolic pressure variation as a guide to fluid therapy in patients with sepsis-induced hypotension. *Anesthesiology*, 89(6):1313–1321, 1998.

[55] E. Bennett-Guerrero, R. A. Kahn, D. M. Moskowitz, O. Falcucci, and C. A. Bodian. Comparison of arterial systolic pressure variation with other clinical parameters to predict the response to fluid challenges during cardiac surgery. *Mount Sinai Journal of Medicine*, 69(1-2):96–100, 2002.

[56] X. Monnet, A. Bleibtreu, A. Ferré, M. Dres, R. Gharbi, C. Richard, and J.-L. Teboul. Passive leg-raising and end-expiratory occlusion tests perform better than pulse pressure variation in patients with low respiratory system compliance. *Critical Care Medicine*, 40(1):152–157, 2012.

[57] M. R. Pinsky. Heart lung interactions during mechanical ventilation. *Current Opinion in Critical Care*, 18(3):256–260, 2012.

[58] J. Mesquida, H. K. Kim, and M. R. Pinsky. *Applied Physiology in Intensive Care Medicine 1: Physiological Notes - Technical Notes - Seminal Studies in Intensive Care*, chapter Effect of tidal volume, intrathoracic pressure, and cardiac contractility on variations in pulse pressure, stroke volume, and intrathoracic blood volume, pages 255–262. Springer Berlin Heidelberg, Berlin, Heidelberg, 2012.

[59] D. A. Reuter, T. W. Felbinger, C. Schmidt, E. Kilger, O. Goedje, P. Lamm, and A. E. Goetz. Stroke volume variations for assessment of cardiac responsiveness to volume loading in mechanically ventilated patients after cardiac surgery. *Intensive Care Medicine*, 28(4):392–398, 2002.

[60] M. Biais, V. Cottenceau, L. Stecken, M. Jean, L. Ottolenghi, S. Roullet, A. Quinart, and F. Sztark. Evaluation of stroke volume variations obtained with the pressure recording analytic method. *Critical Care Medicine*, 40(4):1186–1191, 2012.

[61] J. L. Fellahi, M. O. Fischer, O. Rebet, M. Massetti, J. L. Gérard, and J. L. Hanouz. A comparison of endotracheal bioimpedance cardiography and transpulmonary thermodilution in cardiac surgery patients. *Journal of Cardiothoracic and Vascular Anesthesia*, 26(2):217–222, 2012.

[62] X. Monnet, L. Guérin, M. Jozwiak, A. Bataille, F. Julien, C. Richard, and J.-L. Teboul. Pleth variability index is a weak predictor of fluid responsiveness in patients receiving norepinephrine. *British Journal of Anaesthesia*, 110(2):207–213, 2013.

[63] K. Bendjelid, P. M. Suter, and J. A. Romand. The respiratory change in preejection period: a new method to predict fluid responsiveness. *Journal of Applied Physiology*, 96(1):337–342, 2004.

[64] F. Michard, D. Chemla, C. Richard, M. Wysocki, M. R. Pinsky, Y. Lecarpentier, and J.-L. Teboul. Clinical use of respiratory changes in arterial pulse pressure to monitor the hemodynamic effects of PEEP. *American Journal of Respiratory and Critical Care Medicine*, 159(3):935–939, 1999.

[65] M. Feissel, J. L. Teboul, P. Merlani, J. Badie, J. P. Faller, and K. Bendjelid. Plethysmographic dynamic indices predict fluid responsiveness in septic ventilated patients. *Intensive Care Medicine*, 33(6):993–999, 2007.

[66] X. Monnet, M. Dres, A. Ferré, G. Le Teuff, M. Jozwiak, A. Bleibtreu, M. C. Le Deley, D. Chemla, C. Richard, and J. L. Teboul. Prediction of fluid responsiveness by a continuous non-invasive assessment of arterial pressure in critically ill patients: comparison with four other dynamic indices. *British Journal of Anaesthesia*, 109(3):330–338, 2012.

[67] F. Michard. Volume management using dynamic parameters: the good, the bad, and the ugly. *Chest*, 128(4):1902–1903, 2005.

[68] J. Benes, J. Zatloukal, J. Kletecka, A. Simanova, L. Haidingerova, and R. Pradl. Respiratory induced dynamic variations of stroke volume and its surrogates as predictors of fluid responsiveness: applicability in the early stages of specific critical states. *Journal of Clinical Monitoring and Computing*, 28(3):225–231, 2014.

[69] F. Michard, D. Chemla, and J.-L. Teboul. Applicability of pulse pressure variation: how many shades of grey? *Critical Care*, 19(144):3, 2015.

[70] D. A. Reuter, J. Bayerlein, M. S. G. Goepfert, F. C. Weis, E. Kilger, P. Lamm, and A. E. Goetz. Influence of tidal volume on left ventricular stroke volume variation measured by pulse contour analysis in mechanically ventilated patients. *Intensive Care Medicine*, 29(3):476–480, 2003.

[71] J. Noel-Morgan, D. A. Otsuki, J. O. Auler, J. T. Fukushima, and D. T. Fantoni. Pulse pressure variation is comparable with central venous pressure to guide fluid resuscitation in experimental hemorrhagic shock with endotoxemia. *Shock*, 40(4):303–311, 2013.

[72] M. Feissel, F. Michard, J.-P. Faller, and J.-L. Teboul. The respiratory variation in inferior vena cava diameter as a guide to fluid therapy. *Intensive Care Medicine*, 30(9):1834–1837, 2004.

[73] M. I. García, M. G. Romero, A. G. Cano, H. D. Aya, A. Rhodes, R. M. Grounds, and M. Cecconi. Dynamic arterial elastance as a predictor of arterial pressure response to fluid administration: a validation study. *Critical Care*, 18(6):626, 2014.

[74] P. Lambert, E. Sloth, B. W. Smith, L. K. Hansen, J. Koefoed-Nielsen, E. Tønnesen, and A. Larsson. Does a positive end-expiratory pressure-induced reduction in stroke volume indicate preload responsiveness? An experimental study. *Acta Anaesthesiologica Scandinavica*, 51(4):415–425, 2007.

[75] L. Guérin, J.-L. Teboul, R. Persichini, M. Dres, C. Richard, and X. Monnet. Effects of passive leg raising and volume expansion on mean systemic pressure and venous return in shock in humans. *Critical Care*, 19:411, 2015.

[76] A. C. Guyton, A. W. Lindsey, and B. N. Kaufmann. Effect of mean circulatory filling pressure and other peripheral circulatory factors on cardiac output. *American Journal of Physiology - Legacy Content*, 180(3):463–468, 1955.

[77] R. I. Ogilvie, D. Zborowska-Sluis, and B. Tenaschuk. Measurement of mean circulatory filling pressure and vascular compliance in domestic pigs. *American Journal of Physiology - Heart and Circulatory Physiology*, 258(6):H1925–H1932, 1990.

[78] J. A. Drees and C. F. Rothe. Reflex venoconstriction and capacity vessel pressure-volume relationships in dogs. *Circulation Research*, 34(3):360–373, 1974.

[79] R. K. Goldberg, R. W. Lee, M. Olajos, and S. Goldman. Development of tolerance to nitroglycerin in the arterial and venous circulation of dogs. *Journal of the American College of Cardiology*, 10(6):1335–1341, 1987.

[80] R. W. Lee, R. G. Gay, L. D. Lancaster, M. Olajos, and S. Goldman. Dog model to study the effects of pharmacologic agents on the peripheral circulation: effects of milrinone. *Journal of Pharmacology and Experimental Therapeutics*, 240(3):1014–1019, 1987.

[81] R. W. Lee, T. E. Raya, R. G. Gay, M. Olajos, and S. Goldman. *Beta*-2 adrenoceptor control of the venous circulation in intact dogs. *Journal of Pharmacology and Experimental Therapeutics*, 242(3):1138–1143, 1987.

[82] R. I. Ogilvie and D. Zborowska-Sluis. Effect of chronic rapid ventricular pacing on total vascular capacitance. *Circulation*, 85(4):1524–1530, 1992.

[83] C. F. Rothe and J. A. Drees. Vascular capacitance and fluid shifts in dogs during prolonged hemorrhagic hypotension. *Circulation Research*, 38(5):347–356, 1976.

[84] R. C. P. Kerckhoffs, M. L. Neal, Q. Gu, J. B. Bassingthwaighte, J. H. Omens, and A. D. McCulloch. Coupling of a 3D finite element model of cardiac ventricular mechanics to lumped systems models of the systemic and pulmonic circulation. *Annals of Biomedical Engineering*, 35(1):1–18, 2007.

[85] H. J. Kim, I. E. Vignon-Clementel, C. A. Figueroa, J. F. LaDisa, K. E. Jansen, J. A. Feinstein, and C. A. Taylor. On coupling a lumped parameter heart model and a three-dimensional finite element aorta model. *Annals of Biomedical Engineering*, 37(11):2153–2169, 2009.

[86] D. Burkhoff and J. V. Tyberg. Why does pulmonary venous pressure rise after onset of LV dysfunction: a theoretical analysis. *American Journal of Physiology - Heart and Circulatory Physiology*, 265(5):H1819–H1828, 1993.

[87] M. Danielsen and J. T. Ottesen. Describing the pumping heart as a pressure source. *Journal of Theoretical Biology*, 212(1):71–81, 2001.

[88] L. M. Ellwein, H. T. Tran, C. Zapata, V. Novak, and M. S. Olufsen. Sensitivity analysis and model assessment: Mathematical models for arterial blood flow and blood pressure. *Cardiovascular Engineering*, 8(2):94–108, 2008.

[89] C. Hann, J. G. Chase, and G. M. Shaw. Efficient implementation of nonlinear valve law and ventricular interaction dynamics in the minimal cardiac model. *Computer Methods and Programs in Biomedicine*, 80(1):65–74, 2005.

[90] J. B. Olansen, J. W. Clark, D. Khoury, F. Ghorbel, and A. Bidani. A closed-loop model of the canine cardiovascular system that includes ventricular interaction. *Computers and Biomedical Research*, 33(4):260–295, 2000.

[91] A. Pironet, T. Desaive, S. Kosta, A. Lucas, S. Paeme, A. Collet, C. Pretty, P. Kolh, and P. C Dauby. A multi-scale cardiovascular system model can account for the load-dependence of the end-systolic pressure-volume relationship. *Biomedical Engineering OnLine*, 12(1):8, 2013.

[92] S. R. Pope, L. M. Ellwein, C. L. Zapata, V. Novak, C. T. Kelley, and M. S. Olufsen. Estimation and identification of parameters in a lumped cerebrovascular model. *Mathematical Biosciences and Engineering*, 6:93–115, 2009.

[93] J. A. Revie, D. J. Stevenson, J. G. Chase, C. Hann, B. Lambermont, A. Ghuysen, P. Kolh, G. M. Shaw, S. Heldmann, and T. Desaive. Validation of subject-specific cardiovascular system models from porcine measurements. *Computer Methods and Programs in Biomedicine*, 109(2):197–210, 2013.

[94] J. A. Revie, D. J. Stevenson, J. G. Chase, C. Hann, B. Lambermont, A. Ghuysen, P. Kolh, P. Morimont, G. M. Shaw, and T. Desaive. Clinical detection and monitoring of acute pulmonary embolism: proof of concept of a computer-based method. *Annals of Intensive Care*, 1(1):33, 2011.

[95] J. A. Revie, D. J. Stevenson, J. G. Chase, C. Pretty, B. Lambermont, A. Ghuysen, P. Kolh, G. M. Shaw, and T. Desaive. Evaluation of a model-based hemodynamic monitoring method in a porcine study of septic shock. *Computational and Mathematical Methods in Medicine*, 2013, Article ID 505417, 17 pages, 2013.

[96] W. P. Santamore and D. Burkhoff. Hemodynamic consequences of ventricular interaction as assessed by model analysis. *American Journal of Physiology - Heart and Circulatory Physiology*, 260(Suppl 1):H146–H157, 1991.

[97] E. B. Shim, H. M. Jun, C. H. Leem, S. Matusuoka, and A. Noma. A new integrated method for analyzing heart mechanics using a cell–hemodynamics–autonomic nerve control coupled model of the cardiovascular system. *Progress in Biophysics and Molecular Biology*, 96(1–3):44–59, 2008. Cardiovascular Physiome.

[98] B. W. Smith, J. G. Chase, R. I. Nokes, G. M. Shaw, and G. Wake. Minimal haemodynamic system model including ventricular interaction and valve dynamics. *Medical Engineering & Physics*, 26(2):131–139, 2004.

[99] C. Starfinger, J. G. Chase, C. Hann, G. M. Shaw, B. Lambermont, A. Ghuysen, P. Kolh, P. C. Dauby, and T. Desaive. Model-based identification and diagnosis of a porcine model of induced endotoxic shock with hemofiltration. *Mathematical Biosciences*, 216(2):132–139, 2008.

[100] C Starfinger, J. G. Chase, C. Hann, G. M. Shaw, P. Lambert, B. W. Smith, E. Sloth, A. Larsson, S. Andreassen, and S. Rees. Prediction of hemodynamic changes towards PEEP titrations at different volemic levels using a minimal cardiovascular model. *Computer Methods and Programs in Biomedicine*, 91(2):128–134, 2008.

[101] C. Starfinger, C. Hann, J. G. Chase, T. Desaive, A. Ghuysen, and G. M. Shaw. Model-based cardiac diagnosis of pulmonary embolism. *Computer Methods and Programs in Biomedicine*, 87(1):46–60, 2007.

[102] W. van Meurs. *Modeling and Simulation in Biomedical Engineering: Applications in Cardiorespiratory Physiology*. McGraw-Hill Professional, 2011.

[103] A. Pironet, T. Desaive, P. C. Dauby, J. G. Chase, and P. D. Docherty. Parameter identification methods in a model of the cardiovascular system. *IFAC-PapersOnLine*, 48(20):366–371, 2015. 9th IFAC Symposium on Biological and Medical Systems 2015, Berlin, Germany, 31 August-2 September 2015.

[104] J.-J. Wang, A. B. O'Brien, N. G. Shrive, K. H. Parker, and J. V. Tyberg. Time-domain representation of ventricular-arterial coupling as a windkessel and wave system. *American Journal of Physiology - Heart and Circulatory Physiology*, 284(4):H1358–H1368, 2003.

[105] O. Vardoulis, T. G.. Papaioannou, and N. Stergiopulos. On the estimation of total arterial compliance from aortic pulse wave velocity. *Annals of Biomedical Engineering*, 40(12):2619–2626, 2012.

[106] E. Lanzarone, P. Liani, G. Baselli, and M. L. Costantino. Model of arterial tree and peripheral control for the study of physiological and assisted circulation. *Medical Engineering & Physics*, 29(5):542–555, 2007.

[107] C. F. Babbs. Noninvasive measurement of cardiac stroke volume using pulse wave velocity and aortic dimensions: a simulation study. *Biomedical Engineering OnLine*, 13(1):137, 2014.

[108] M. Ursino. A mathematical model of the carotid baroregulation in pulsating conditions. *IEEE Transactions on Biomedical Engineering*, 46(4):382–392, April 1999.

[109] N. Westerhof, N. Stergiopulos, and M. I. Noble. *Snapshots of Hemodynamics: An Aid for Clinical Research and Graduate Education*. SpringerLink : Bücher. Springer, 2010.

[110] O. Barnea, T. W. Moore, and D. Jaron. Computer simulation of the mechanically-assisted failing canine circulation. *Annals of Biomedical Engineering*, 18(3):263–283, 1990.

[111] R. Beyar and Y. Goldstein. Model studies of the effects of the thoracic pressure on the circulation. *Annals of Biomedical Engineering*, 15(3):373–383, 1987.

[112] B. W. Smith, J. G. Chase, G. M. Shaw, and R. I. Nokes. Experimentally verified minimal cardiovascular system model for rapid diagnostic assistance. *Control Engineering Practice*, 13(9):1183–1193, 2005.

[113] C. Hann, J. G. Chase, T. Desaive, C. B. Froissart, J. A. Revie, D. J. Stevenson, B. Lambermont, A. Ghuysen, P. Kolh, and G. M. Shaw. Unique parameter identification for cardiac diagnosis in critical care using minimal data sets. *Computer Methods and Programs in Biomedicine*, 2010.

[114] J. K.-J. Li. *Dynamics of the vascular system*. World Scientific Publishing, 2004.

[115] G. Drzewiecki, S. Field, I. Moubarak, and J. K.-J. Li. Vessel growth and collapsible pressure-area relationship. *American Journal of Physiology - Heart and Circulatory Physiology*, 273(4):H2030–H2043, 1997.

[116] H. Suga, K. Sagawa, and A. A. Shoukas. Load independence of the instantaneous pressure-volume ratio of the canine left ventricle and effects of epinephrine and heart rate on the ratio. *Circulation Research*, 32(3):314–322, 1973.

[117] H. Senzaki, C.-H. Chen, and D. A. Kass. Single-beat estimation of end-systolic pressure-volume relation in humans: A new method with the potential for noninvasive application. *Circulation*, 94(10):2497–2506, 1996.

[118] D. Burkhoff. Explaining load dependence of ventricular contractile properties with a model of excitation-contraction coupling. *Journal of Molecular and Cellular Cardiology*, 26(8):959–978, 1994.

[119] S. A. Glantz and W. W. Parmley. Factors which affect the diastolic pressure-volume curve. *Circulation Research*, 42(2):171–180, 1978.

[120] M. I. Noble, E. N. Milne, R. J. Goerke, E. Carlsson, R. J. Domenech, K. B. Saunders, and J. I. Hoffman. Left ventricular filling and diastolic pressure-volume relations in the conscious dog. *Circulation Research*, 24(2):269–283, 1969.

[121] D. Burkhoff, S. Sugiura, D. T. Yue, and K. Sagawa. Contractility-dependent curvilinearity of end-systolic pressure-volume relations. *American Journal of Physiology - Heart and Circulatory Physiology*, 252(6):H1218–H1227, 1987.

[122] D. A. Kass, R. Beyar, E. Lankford, M. Heard, W. L. Maughan, and K. Sagawa. Influence of contractile state on curvilinearity of in situ end-systolic pressure-volume relations. *Circulation*, 79(1):167–178, 1989.

[123] A. Pironet, T. Desaive, J. G. Chase, P. Morimont, and P. C. Dauby. Model-based computation of total stressed blood volume from a preload reduction manoeuvre. *Mathematical Biosciences*, 265:28–39, 2015.

[124] T. E. Claessens, D. Georgakopoulos, M. Afanasyeva, S. J. Vermeersch, H. D. Millar, N. Stergiopulos, N. Westerhof, Pascal. R. Verdonck, and P. Segers. Nonlinear isochrones in murine left ventricular pressure-volume loops: how well does the time-varying elastance concept hold? *American Journal of Physiology - Heart and Circulatory Physiology*, 290(4):H1474–H1483, 2006.

[125] J.-W. Lankhaar, F. A. Rövekamp, P. Steendijk, T. J. Faes, B. E. Westerhof, T. Kind, A. Vonk-Noordegraaf, and N. Westerhof. Modeling the instantaneous pressure–volume relation of the left ventricle: a comparison of six models. *Annals of Biomedical Engineering*, 37(9):1710–1726, 2009.

[126] S. M. Davidson, D. O. Kannangara, C. G. Pretty, S. Kamoi, A. Pironet, T. Desaive, and J. G. Chase. Modelling of the nonlinear end-systolic pressure-volume relation and volume-at-zero-pressure in porcine experiments. In *Engineering in Medicine and Biology Society (EMBC), 2015. 37th Annual International Conference of the IEEE*, pages 6544–6547, Aug 2015.

[127] D. Burkhoff, P. P. de Tombe, and W. C. Hunter. Impact of ejection on magnitude and time course of ventricular pressure-generating capacity. *American Journal of Physiology*, 265(3 Pt 2):H899–H909, 1993.

[128] S. G. Shroff, J. S. Janicki, and K. T. Weber. Evidence and quantitation of left ventricular systolic resistance. *American Journal of Physiology - Heart and Circulatory Physiology*, 249(2):H358–H370, 1985.

[129] S. R. Vaartjes and H. B. Boom. Left ventricular internal resistance and unloaded ejection flow assessed from pressure-flow relations: a flow-clamp study on isolated rabbit hearts. *Circulation Research*, 60(5):727–737, 1987.

[130] D. Burkhoff, P. P de Tombe, W. C. Hunter, and D. A. Kass. Contractile strength and mechanical efficiency of left ventricle are enhanced by physiological afterload. *American Journal of Physiology - Heart and Circulatory Physiology*, 260(2):H569–H578, 1991.

[131] W. L. Maughan, A. A. Shoukas, K. Sagawa, and M. L. Weisfeldt. Instantaneous pressure-volume relationship of the canine right ventricle. *Circulation Research*, 44(3):309–315, 1979.

[132] T. Arts, T. Delhaas, P. Bovendeerd, X. Verbeek, and F. W. Prinzen. Adaptation to mechanical load determines shape and properties of heart and circulation: the CircAdapt model. *American Journal of Physiology - Heart and Circulatory Physiology*, 288(4):H1943–1954, 2005.

[133] J. A. Negroni and E. C. Lascano. Concentration and elongation of attached cross-bridges as pressure determinants in a ventricular model. *Journal of Molecular and Cellular Cardiology*, 31(8):1509–1526, 1999.

[134] A. Pironet, P. C. Dauby, S. Paeme, S. Kosta, J. G. Chase, and T. Desaive. Simulation of left atrial function using a multi-scale model of the cardiovascular system. *PLoS ONE*, 8(6):e65146, 2013.

[135] E. B. Shim, C. Hun Leem, Y. Abe, and A. Noma. A new multi-scale simulation model of the circulation: from cells to system. *Philosophical Transactions of the Royal Society of London A: Mathematical, Physical and Engineering Sciences*, 364(1843):1483–1500, 2006.

[136] J. Alexander, K. Sunagawa, N. Chang, and K. Sagawa. Instantaneous pressure-volume relation of the ejecting canine left atrium. *Circulation Research*, 61(2):209–219, 1987.

[137] B. D. Hoit, Y. Shao, M. Gabel, and R. A. Walsh. In vivo assessment of left atrial contractile performance in normal and pathological conditions using a time-varying elastance model. *Circulation*, 89(4):1829–1838, 1994.

[138] J. M. Dernellis, C. I. Stefanadis, A. A. Zacharoulis, and P. K. Toutouzas. Left atrial mechanical adaptation to long-standing hemodynamic loads based on pressure–volume relations. *The American Journal of Cardiology*, 81(9):1138–1143, 1998.

[139] M. Gare, D. A. Schwabe, D. A. Hettrick, J. R. Kersten, D. C. Warltier, and P. S. Pagel. Desflurane, sevoflurane, and isoflurane affect left atrial active and passive mechanical properties and impair left atrial-left ventricular coupling in vivo: analysis using pressure-volume relations. *Anesthesiology*, 95(3):689–698, 2001.

[140] F. Kehl, T. T. Kress, B. Mraovic, D. A. Hettrick, J. R. Kersten, D. C. Warltier, and P. S. Pagel. Propofol alters left atrial function evaluated with pressure-volume relations in vivo. *Anesthesia & Analgesia*, 94(6):1421–1426, 2002.

[141] D. C. Chung. Ventricular interaction in a closed-loop model of the canine circulation. Master's thesis, Rice University, Houston, Texas, 1996.

[142] T. Korakianitis and Y. Shi. A concentrated parameter model for the human cardiovascular system including heart valve dynamics and atrioventricular interaction. *Medical Engineering & Physics*, 28(7):613–628, 2006.

[143] V.-K. Lau and K. Sagawa. Model analysis of the contribution of atrial contraction to ventricular filling. *Annals of Biomedical Engineering*, 7(2):167–201, 1979.

[144] K. Lu, J. W. Clark, F. H. Ghorbel, D. L. Ware, and A. Bidani. A human cardiopulmonary system model applied to the analysis of the Valsalva maneuver. *American Journal of Physiology - Heart and Circulatory Physiology*, 281(6):H2661–H2679, 2001.

[145] C. Luo, D. L. Ware, J. B. Zwischenberger, and J. W. Clark. Using a human cardiopulmonary model to study and predict normal and diseased ventricular mechanics, septal interaction, and atrio-ventricular blood flow patterns. *Cardiovascular Engineering*, 7(1):17–31, 2007.

[146] K. Tse Ve Koon, V. Le Rolle, G. Carrault, and A. I. Hernandez. A cardiovascular model for the analysis of pacing configurations in cardiac resynchronization therapy. In *Computers in Cardiology, 2009*, pages 393–396. IEEE, 2009.

[147] T. A. Parlikar and G. C. Verghese. A simple cycle-averaged model for cardiovascular dynamics. In *Engineering in Medicine and Biology Society, 2005. IEEE-EMBS 2005. 27th Annual International Conference of the IEEE*, pages 5490–5494, 2005.

[148] D. Rüschen, M. Rimke, J. Gesenhues, S. Leonhard, and M. Walter. Continuous cardiac output estimation under left ventricular assistance. *IFAC-PapersOnLine*, 48(20):569–574, 2015. 9th IFAC Symposium on Biological and Medical Systems 2015, Berlin, Germany, 31 August-2 September 2015.

[149] B. W. Smith. *Minimal Haemodynamic Modelling of the Heart & Circulation for Clinical Application*. PhD thesis, University of Canterbury, Christchurch, New Zealand, 2004.

[150] M. Abdolrazaghi, M. Navidbakhsh, and K. Hassani. Mathematical modelling and electrical analog equivalent of the human cardiovascular system. *Cardiovascular Engineering*, 10(2):45–51, 2010.

[151] M. S. Olufsen, J. T. Ottesen, H. T. Tran, L. M. Ellwein, L. A. Lipsitz, and V. Novak. Blood pressure and blood flow variation during postural change from sitting to standing: model development and validation. *Journal of Applied Physiology*, 99(4):1523–1537, 2005.

[152] J. Fontecave-Jallon, E. Abdulhay, P. Calabrese, P. Baconnier, and P.-Y. Gumery. A model of mechanical interactions between heart and lungs. *Philosophical Transactions of the Royal Society A: Mathematical, Physical and Engineering Sciences*, 367(1908):4741–4757, 2009.

[153] S. de Bournonville. Cardio-pulmonary mechanics and minimum modelling in critical care. Master's thesis, Université de Liège, 2015.

[154] P. S. Pagel, F. Kehl, M. Gare, D. A. Hettrick, J. R. Kersten, and D. C. Warltier. Mechanical function of the left atrium: new insights based on analysis of

pressure-volume relations and Doppler echocardiography. *Anesthesiology*, 98(4):975–994, 2003.

[155] M. Roşca, P. Lancellotti, B. A. Popescu, and L. A. Piérard. Left atrial function: pathophysiology, echocardiographic assessment, and clinical applications. *Heart*, 97(23):1982–1989, 2011.

[156] C. Stefanadis, J. Dernellis, and P. Toutouzas. A clinical appraisal of left atrial function. *European Heart Journal*, 22(1):22–36, 2001.

[157] C. Hann, J. G. Chase, and G. M. Shaw. Integral-based identification of patient specific parameters for a minimal cardiac model. *Computer Methods and Programs in Biomedicine*, 81(2):181–192, 2006.

[158] J. Baan, E. T. van der Velde, H. de Bruin, G. J. Smeenk, J. Koops, A. D. van Dijk, D. Temmerman, J. Senden, and B. Buis. Continuous measurement of left ventricular volume in animals and humans by conductance catheter. *Circulation*, 70:812–823, 1984.

[159] Transonic Systems Inc. *Tools & Techniques for Pressure-Volume Hemodynamic Studies*, 2015.

[160] A. T. G. Kottam, J. Porterfield, K. Raghavan, D. Fernandez, M. D. Feldman, J. W. Valvano, and J. A. Pearce. Real time pressure-volume loops in mice using complex admittance: measurement and implications. In *Engineering in Medicine and Biology Society, 2006. EMBS '06. 28th Annual International Conference of the IEEE*, pages 4336–4339, 2006.

[161] W. Isakow and D. P. Schuster. Extravascular lung water measurements and hemodynamic monitoring in the critically ill: bedside alternatives to the pulmonary artery catheter. *American Journal of Physiology - Lung Cellular and Molecular Physiology*, 291(6):L1118–L1131, 2006.

[162] R. Cottis, N. Magee, and D. J. Higgins. Haemodynamic monitoring with pulse-induced contour cardiac output (PiCCO) in critical care. *Intensive and Critical Care Nursing*, 19(5):301–307, 2003.

[163] J. Jabot, X. Monnet, L. Bouchra, D. Chemla, C. Richard, and J.-L. Teboul. Cardiac function index provided by transpulmonary thermodilution behaves as an indicator of left ventricular systolic function. *Critical Care Medicine*, 37(11):2913–2918, 2009.

[164] G. Rödig, C. Prasser, C. Keyl, A. Liebold, and J. Hobbhahn. Continuous cardiac output measurement: pulse contour analysis *vs* thermodilution technique in cardiac surgical patients. *British Journal of Anaesthesia*, 82(4):525–530, 1999.

[165] É. Walter and L. Pronzato. *Identification of parametric models from experimental data*. Communications and Control Engineering. Springer, 1997.

[166] L. Ljung. *System identification: theory for the user*. PTR Prentice Hall, 1987.

[167] P. D. Docherty, J. G. Chase, T. Lotz, and T. Desaive. A graphical method for practical and informative identifiability analyses of physiological models: A case study of insulin kinetics and sensitivity. *Biomedical Engineering OnLine*, 10(1):39, 2011.

[168] H. Pohjanpalo. System identifiability based on the power series expansion of the solution. *Mathematical Biosciences*, 41(1–2):21–33, 1978.

[169] S. Kamoi, C. Pretty, P. D. Docherty, D. Squire, J. A. Revie, Y. S. Chiew, T. Desaive, G. M. Shaw, and J. G. Chase. Continuous stroke volume estimation from aortic pressure using zero dimensional cardiovascular model: Proof of concept study from porcine experiments. *PLoS ONE*, 9(7):e102476, 07 2014.

[170] A. Pironet, P. C. Dauby, J. G. Chase, J. A. Revie, P. D. Docherty, and T. Desaive. Structural identifiability analysis of a cardiovascular system model. In *Proceedings of the 19th IFAC World Congress*, pages 3869–3874, 2014.

[171] T. Abdulla, N. D. Evans, J. Yates, T. Collins, J. Mettetal, and M. Chappell. Structural identifiability and indistinguishability analyses of cardiovascular feedback models. *IFAC-PapersOnLine*, 48(20):153–158, 2015. 9th IFAC Symposium on Biological and Medical Systems 2015, Berlin, Germany, 31 August-2 September 2015.

[172] M. Burth, G. C. Verghese, and M. Velez-Reyes. Subset selection for improved parameter estimation in on-line identification of a synchronous generator. *IEEE Transactions on Power Systems*, 14(1):218–225, 1999.

[173] A. Pironet, P. C. Dauby, J. A. Revie, J. G. Chase, and T. Desaive. A new method for computing the derivatives of the mean and amplitude of physiological variables with respect to the parameters of a cardiovascular system model. *Minimally Invasive Therapy & Allied technologies : Official Journal of the Society for Minimally Invasive Therapy*, 22, 2013.

[174] M. S. Olufsen and J. T. Ottesen. A practical approach to parameter estimation applied to model predicting heart rate regulation. *Journal of Mathematical Biology*, 67(1):39–68, 2013.

[175] A. Raue, C. Kreutz, T. Maiwald, J. Bachmann, M. Schilling, U. Klingmüller, and J. Timmer. Structural and practical identifiability analysis of partially observed dynamical models by exploiting the profile likelihood. *Bioinformatics*, 25(15):1923–1929, 2009.

[176] W. Dai, L. Bansal, and J. Hahn. Parameter set selection for signal transduction pathway models including uncertainties. In *Proceedings of the 19th IFAC World Congress*, pages 815–820, 2014.

[177] J. T. Ottesen, J. Mehlsen, and M. S. Olufsen. Structural correlation method for model reduction and practical estimation of patient specific parameters illustrated on heart rate regulation. *Mathematical Biosciences*, 257:50–59, 2014. Multiscale models and methods in biomedicine.

[178] Z. Samar, T. Heldt, G. C. Verghese, and R. G. Mark. Model-based cardiovascular parameter estimation in the intensive care unit. In *Computers in Cardiology, 2005*, pages 635–638, Sept 2005.

[179] D. A. Kass, W. L. Maughan, Z. M. Guo, A. Kono, K. Sunagawa, and K. Sagawa. Comparative influence of load versus inotropic states on indexes of ventricular contractility: experimental and theoretical analysis based on pressure-volume relationships. *Circulation*, 76(6):1422–1436, 1987.

[180] S. Brimioulle, P. Wauthy, P. Ewalenko, B. Rondelet, F. Vermeulen, F. Kerbaul, and R. Naeije. Single-beat estimation of right ventricular end-systolic pressure-volume relationship. *American Journal of Physiology - Heart and Circulatory Physiology*, 284(5):H1625–H1630, 2003.

[181] C. H. Chen, B. Fetics, E. Nevo, C. E. Rochitte, K. R. Chiou, P. A. Ding, M. Kawaguchi, and D. A. Kass. Noninvasive single-beat determination of left ventricular end-systolic elastance in humans. *Journal of the American College of Cardiology*, 38(7):2028–2034, 2001.

[182] K. E. Kjørstad, C. Korvald, and T. Myrmel. Pressure-volume-based single-beat estimations cannot predict left ventricular contractility in vivo. *American Journal of Physiology - Heart and Circulatory Physiology*, 282(5):H1739–H1750, 2002.

[183] T. S. Manning, B. E. Shykoff, and J. L. Izzo. Validity and reliability of diastolic pulse contour analysis (windkessel model) in humans. *Hypertension*, 39(5):963–968, 2002.

[184] R. Mukkamala, A. T. Reisner, H.M. Hojman, R. G. Mark, and R. J. Cohen. Continuous cardiac output monitoring by peripheral blood pressure waveform analysis. *IEEE Transactions on Biomedical Engineering*, 53(3):459–467, 2006.

[185] S. R. Reuben. Compliance of the human pulmonary arterial system in disease. *Circulation Research*, 29(1):40–50, 1971.

[186] N. Westerhof, J.-W. Lankhaar, and B. E. Westerhof. The arterial windkessel. *Medical and Biological Engineering and Computing*, 47(2):131–141, 2009.

[187] D. Chemla, J.-L. Hébert, C. Coirault, K. Zamani, I. Suard, P. Colin, and Y. Lecarpentier. Total arterial compliance estimated by stroke volume-to-aortic pulse pressure ratio in humans. *American Journal of Physiology - Heart and Circulatory Physiology*, 274(2):H500–H505, 1998.

[188] S. S. Rao. *Engineering Optimization*. John Wiley & Sons, Inc., 2009.

[189] C. T. Kelley. *Iterative methods for optimization*, volume 18. SIAM, 1999.

[190] J. A. Nelder and R. Mead. A simplex method for function minimization. *The Computer Journal*, 7(4):308–313, 1965.

[191] C. Hann, J. A. Revie, D. J. Stevenson, S. Heldmann, T. Desaive, C. B. Froissart, B. Lambermont, A. Ghuysen, P. Kolh, G. M. Shaw, and J. G. Chase. Patient specific identification of the cardiac driver function in a cardiovascular system model. *Computer Methods and Programs in Biomedicine*, 101(2):201–207, 2011.

[192] A. Pironet, J. A. Revie, S. Paeme, P. C. Dauby, J. G. Chase, and T. Desaive. Development and identification of a closed-loop model of the cardiovascular system including the atria. In *Proceedings of the 8th IFAC Symposium on Biological and Medical Systems*, pages 495–500, 2012.

[193] A. R. Conn, K. Scheinberg, and L. N. Vicente. *Introduction to Derivative-free Optimization*. MPS-SIAM series on optimization. Society for Industrial and Applied Mathematics, 2009.

[194] N. Karmitsa, A. Bagirov, and M. M. Mäkelä. Comparing different nonsmooth minimization methods and software. *Optimization Methods and Software*, 27(1):131–153, 2012.

[195] A. Pironet, P. Morimont, S. Kamoi, N. Janssen, P. C. Dauby, J. G. Chase, B. Lambermont, and T. Desaive. Relation between global end-diastolic volume and left ventricular end-diastolic volume. *Critical Care*, 19(Suppl 1):P175, 2015.

[196] A. Pironet, T. Desaive, J. G. Chase, P. Morimont, and P. C. Dauby. Model-based computation of total stressed blood volume from a preload reduction experiment. In *Proceedings of the 19th IFAC World Congress*, pages 5641–5646, 2014.

[197] T. Desaive, S. Dutron, B. Lambermont, P. Kolh, C. Hann, J. G. Chase, P. C. Dauby, and A. Ghuysen. Closed-loop model of the cardiovascular system including ventricular interaction and valve dynamics: application to pulmonary embolism. In *12th International Conference on Biomedical Engineering (ICBME)*, 2005.

[198] A. Ghuysen, B. Lambermont, P. Kolh, V. Tchana-Sato, D. Magis, P. Gérard, V. Mommens, N. Janssen, T. Desaive, and V. D'Orio. Alteration of right ventricular-pulmonary vascular coupling in a porcine model of progressive pressure overloading. *Shock*, 29(2):197–204, 2008.

[199] B. Lambermont, P. Delanaye, J.-M. Dogné, A. Ghuysen, N. Janssen, B. Dubois, T. Desaive, P. Kolh, V. D'Orio, and J.-M. Krzesinski. Large-pore membrane hemofiltration increases cytokine clearance and improves right ventricular–vascular coupling during endotoxic shock in pigs. *Artificial Organs*, 30(7):560–564, 2006.

[200] J. Zanzinger, J. Czachurski, and H. Seller. Role of calcium-dependent K^+ channels in the regulation of arterial and venous tone by nitric oxide in pigs. *Pflügers Archiv*, 432(4):671–677, 1996.

[201] P. Barbier, S. Solomon, N. B. Schiller, and S. A. Glantz. Determinants of forward pulmonary vein flow: an open pericardium pig model. *Journal of the American College of Cardiology*, 35(7):1947–1959, 2000.

[202] E. Langford, N. Schwertman, and M. Owens. Is the property of being positively correlated transitive? *The American Statistician*, 55(4):322–325, 2001.

[203] P. Morimont, A. Pironet, T. Desaive, G. Chase, and B. Lambermont. Early detection of abnormal left ventricular relaxation in acute myocardial ischemia with a quadratic model. *Medical Engineering & Physics*, 36(9):1101–1105, 2014.

[204] J. A. Revie. *Model-based cardiovascular monitoring in critical care for improved diagnosis of cardiac dysfunction*. PhD thesis, University of Canterbury, 2012.

[205] A. Pironet, P. C. Dauby, J. G. Chase, S. Kamoi, N. Janssen, P. Morimont, B. Lambermont, and T. Desaive. Model-based stressed blood volume is an index of fluid responsiveness. *IFAC-PapersOnLine*, 48(20):291–296, 2015. 9th IFAC Symposium on Biological and Medical Systems 2015, Berlin, Germany, 31 August-2 September 2015.

[206] P. E. Marik and J. Lemson. Fluid responsiveness: an evolution of our understanding. *British Journal of Anaesthesia*, 112(4):617–620, 2014.

[207] J. Renner, M. Gruenewald, R. Quaden, R. Hanss, P. Meybohm, M. Steinfath, J. Scholz, and B. Bein. Influence of increased intra-abdominal pressure on fluid responsiveness predicted by pulse pressure variation and stroke volume variation in a porcine model. *Critical Care Medicine*, 37(2):650–658, 2009.

Thanks

The work that has been presented in the previous pages has been made possible by many collaborations. I here wish to thank several people for their contribution, large or small, to this thesis.

First, Thomas Desaive, my supervisor, for initially motivating me to start a Ph.D. thesis. His trusting me and giving me a first professional experience is something for which I am very grateful. Through his understanding of the world of research, I learnt the essentials of research, scientific writing, public presentation and many others. Thomas also gave me a wide number of opportunities to extend my research out of the lab, including in the wonderful country that is New Zealand.

Pierre Dauby, the head of the Thermodynamics research group, for always being interested in my research despite not being administratively obliged to do so. Pierre's scientific rigour was a source for numerous enriching, in-depth scientific discussions, to which the soundness of this work can be attributed.

Geoff Chase, my main collaborator in New Zealand, for his permanent availability. Geoff's efficiency is something with which any researcher should be inspired. I thank him for teaching me his (countless) rules of scientific writing in English. I am also grateful for his warm welcome in the country of Kiwis.

Hatim, Arnaud, Simon and Chris, my colleagues from the boy's office, for making my everyday research a multilingual, enjoyable and enriching experience.

Sarah, Sophie, Sabine and Alexandra, my colleagues from the girl's office, for making life in the office not only being about research. The girls were a very efficient party committee during these four years.

Chris, Chiew, James, Shun, Shaun, Felicity and all the other minions, my colleagues from New Zealand, for their heart-warming welcome in their country and office. I thank all of them for their availability and advices, both on scientific topics and tourism. I am also grateful to Shun and Shaun for involving me in their work, and helping me during the animal experiments of this thesis.

Paul Docherty, my main advisor on parameter identification, for his contribution to all the aspects of this thesis related to identifiability, and his comments

about the simplex method. I really appreciate his investment and interest in my work.

Philippe Morimont, an intensive care doctor from the Liège University Hospital, for the invaluable medical input he provided all through this thesis. I am grateful for his always being interested in the bizarre stuff engineers do.

Nathalie Janssen, a surgeon from the Liège University Hospital, for performing the animal experiments on which this thesis is based. She agreed to perform every strange request made from my colleagues or I during the experiments.

Philippe Kolh, Bernard Lambermont and Patrizio Lancellotti, doctors from the Liège University Hospital, for always being available to simply explaining complex medical concepts to an engineer.

Finally, my family and friends for their support and interest in my research during these four years. In particular, I wish to thank Sophie, for her support during the difficult moments of my Ph.D. and her company during the good ones.

Appendix A

Demonstration of Structural Identifiability from the Fourth Output Set

In this appendix, identifiability of the three-chamber model is demonstrated from a further reduced output set. To do so, a simplifying hypothesis is necessary, assuming values of the valve resistances are known. Thus, R_i and R_o are assumed known and are not part of the parameter vector. The reduced output set, $\mathbf{y}^4$, used here, contains:

- arterial pressure, $P_\mathrm{a}(t)$,
- integral of the ejected flow during one cardiac period, $\int_0^T Q_\mathrm{o}(t)\,\mathrm{d}t$.

In particular, this output set does not contain venous pressure. The driver function $e(t)$ is still assumed known.

A.1 During Ejection

The reasoning presented in Section 8.3.4 to obtain Equation 8.26 expressing E_h in terms of $P_\mathrm{a}(t)$, $e(t)$ and $\int_0^T Q_\mathrm{o}(t)\,\mathrm{d}t$ can be repeated here, since all these quantities are known. Cardiac elastance E_h is thus identifiable using Equation 8.26.

During ejection, cardiac pressure is higher than arterial pressure, $P_\mathrm{h}(t) > P_\mathrm{a}(t)$, and venous pressure, $P_\mathrm{h}(t) > P_\mathrm{v}(t)$. Consequently, the combination of Equations 6.5, 6.6 and 6.7 can be written:

$$\frac{\mathrm{d}V_\mathrm{s,h}(t)}{\mathrm{d}t} = -\frac{P_\mathrm{h}(t) - P_\mathrm{a}(t)}{R_\mathrm{o}} \tag{A.1}$$

Combining this equation with Equation 6.3 gives:

$$\frac{\mathrm{d}V_{\mathrm{s,h}}(t)}{\mathrm{d}t} = -\frac{E_{\mathrm{h}}e(t)V_{\mathrm{s,h}}(t) - P_{\mathrm{a}}(t)}{R_{\mathrm{o}}}. \tag{A.2}$$

Since $P_{\mathrm{a}}(t)$, E_{h}, $e(t)$ and R_{o} are known, this linear differential equation with variable coefficients can be solved for $V_{\mathrm{s,h}}(t)$ during cardiac ejection. The initial condition required for solving is obtained from Equation 8.18. Once $V_{\mathrm{s,h}}(t)$ is known, $P_{\mathrm{h}}(t)$ during ejection can be computed using Equation 6.3. It will be used further in the demonstration.

During ejection, the combination of Equations 6.4, 6.6 and 6.8 gives:

$$\frac{\mathrm{d}V_{\mathrm{s,a}}(t)}{\mathrm{d}t} = \frac{P_{\mathrm{h}}(t) - P_{\mathrm{a}}(t)}{R_{\mathrm{o}}} - \frac{P_{\mathrm{a}}(t) - P_{\mathrm{v}}(t)}{R_{\mathrm{c}}}. \tag{A.3}$$

Multiplying both sides of this equation by E_{a} and using the fact that $P_{\mathrm{a}}(t) = E_{\mathrm{a}}V_{\mathrm{s,a}}(t)$ yields:

$$\frac{\mathrm{d}P_{\mathrm{a}}(t)}{\mathrm{d}t} = \frac{E_{\mathrm{a}}}{R_{\mathrm{o}}}[P_{\mathrm{h}}(t) - P_{\mathrm{a}}(t)] - \frac{E_{\mathrm{a}}}{R_{\mathrm{c}}}[P_{\mathrm{a}}(t) - P_{\mathrm{v}}(t)]. \tag{A.4}$$

Differentiating this equation with respect to time then results in:

$$\frac{\mathrm{d}^2P_{\mathrm{a}}(t)}{\mathrm{d}t^2} = \frac{E_{\mathrm{a}}}{R_{\mathrm{o}}}\left[\frac{\mathrm{d}P_{\mathrm{h}}(t)}{\mathrm{d}t} - \frac{\mathrm{d}P_{\mathrm{a}}(t)}{\mathrm{d}t}\right] - \frac{E_{\mathrm{a}}}{R_{\mathrm{c}}}\left[\frac{\mathrm{d}P_{\mathrm{a}}(t)}{\mathrm{d}t} - \frac{\mathrm{d}P_{\mathrm{v}}(t)}{\mathrm{d}t}\right]. \tag{A.5}$$

Then, taking into account the fact that $P_{\mathrm{h}}(t) > P_{\mathrm{v}}(t)$ during ejection, Equations 6.2, 6.4, 6.5 and 6.9 can be used to substitute $\mathrm{d}P_{\mathrm{v}}(t)/\mathrm{d}t$:

$$\frac{\mathrm{d}^2P_{\mathrm{a}}(t)}{\mathrm{d}t^2} = \frac{E_{\mathrm{a}}}{R_{\mathrm{o}}}\left[\frac{\mathrm{d}P_{\mathrm{h}}(t)}{\mathrm{d}t} - \frac{\mathrm{d}P_{\mathrm{a}}(t)}{\mathrm{d}t}\right] - \frac{E_{\mathrm{a}}}{R_{\mathrm{c}}}\left\{\frac{\mathrm{d}P_{\mathrm{a}}(t)}{\mathrm{d}t} - \frac{E_{\mathrm{v}}}{R_{\mathrm{c}}}[P_{\mathrm{a}}(t) - P_{\mathrm{v}}(t)]\right\}. \tag{A.6}$$

The same two steps can be repeated twice to obtain the following two equations:

$$\begin{aligned}\frac{\mathrm{d}^3P_{\mathrm{a}}(t)}{\mathrm{d}t^3} = {} & \frac{E_{\mathrm{a}}}{R_{\mathrm{o}}}\left[\frac{\mathrm{d}^2P_{\mathrm{h}}(t)}{\mathrm{d}t^2} - \frac{\mathrm{d}^2P_{\mathrm{a}}(t)}{\mathrm{d}t^2}\right] \\ & - \frac{E_{\mathrm{a}}}{R_{\mathrm{c}}}\frac{\mathrm{d}^2P_{\mathrm{a}}(t)}{\mathrm{d}t^2} \\ & + \frac{E_{\mathrm{a}}E_{\mathrm{v}}}{R_{\mathrm{c}}^2}\left\{\frac{\mathrm{d}P_{\mathrm{a}}(t)}{\mathrm{d}t} - \frac{E_{\mathrm{v}}}{R_{\mathrm{c}}}[P_{\mathrm{a}}(t) - P_{\mathrm{v}}(t)]\right\}.\end{aligned} \tag{A.7}$$

$$\begin{aligned}\frac{\mathrm{d}^4 P_\mathrm{a}(t)}{\mathrm{d}t^4} = \frac{E_\mathrm{a}}{R_\mathrm{o}}\left[\frac{\mathrm{d}^3 P_\mathrm{h}(t)}{\mathrm{d}t^3} - \frac{\mathrm{d}^3 P_\mathrm{a}(t)}{\mathrm{d}t^3}\right] \\ - \frac{E_\mathrm{a}}{R_\mathrm{c}}\frac{\mathrm{d}^3 P_\mathrm{a}(t)}{\mathrm{d}t^3} \\ + \frac{E_\mathrm{a}E_\mathrm{v}}{R_\mathrm{c}^2}\frac{\mathrm{d}^2 P_\mathrm{a}(t)}{\mathrm{d}t^2} \\ - \frac{E_\mathrm{a}E_\mathrm{v}^2}{R_\mathrm{c}^3}\left\{\frac{\mathrm{d}P_\mathrm{a}(t)}{\mathrm{d}t} - \frac{E_\mathrm{v}}{R_\mathrm{c}}[P_\mathrm{a}(t) - P_\mathrm{v}(t)]\right\}. \end{aligned} \tag{A.8}$$

The algebraic system formed by Equations A.4, A.6, A.7 and A.8 has four equations and four unknowns, $P_\mathrm{v}(t)$, R_c, E_a and E_v, since $P_\mathrm{a}(t)$ and $P_\mathrm{h}(t)$ are known. Solving this system with a symbolic computation software (Mathematica Version 8.0, Wolfram Research Inc., Champaign, IL) shows that it has a unique solution for all t. This outcome, in turn, guarantees the identifiability of the three parameters R_c, E_a and E_v. It also provides the time course of $P_\mathrm{v}(t)$ during ejection.

A.2 During Systole

During systole, which encompasses isovolumic contraction and ejection, the input valve is closed. Hence, $Q_\mathrm{i}(t) = 0$. Combining Equations 6.2, 6.4 and 6.9 during this period gives:

$$\frac{\mathrm{d}V_\mathrm{s,v}(t)}{\mathrm{d}t} = \frac{P_\mathrm{a}(t) - E_\mathrm{v}V_\mathrm{s,v}(t)}{R_\mathrm{c}}. \tag{A.9}$$

This linear differential equation with variable coefficients can be solved for $V_\mathrm{s,v}(t)$, since $P_\mathrm{a}(t)$, E_v and R_c are now known.

To obtain the required initial condition, a series of further manipulations needs to be performed. First, at the time of input valve closing, t_EF, venous pressure equals cardiac pressure:

$$P_\mathrm{v}(t_\mathrm{EF}) = P_\mathrm{h}(t_\mathrm{EF}). \tag{A.10}$$

Using Equations 6.2 and 6.3 then yields:

$$E_\mathrm{v}V_\mathrm{s,v}(t_\mathrm{EF}) = E_\mathrm{h}e(t_\mathrm{EF})V_\mathrm{s,h}(t_\mathrm{EF}) \tag{A.11}$$

$$\Leftrightarrow V_\mathrm{s,v}(t_\mathrm{EF}) = \frac{E_\mathrm{h}}{E_\mathrm{v}}e(t_\mathrm{EF})V_\mathrm{s,h}(t_\mathrm{EF}). \tag{A.12}$$

Using the fact that cardiac volume does not change between input valve closing and output valve opening, $V_{\mathrm{s,h}}(t_{\mathrm{EF}}) = V_{\mathrm{s,h}}(t_{\mathrm{BE}})$, Equation A.12 becomes:

$$V_{\mathrm{s,v}}(t_{\mathrm{EF}}) = \frac{E_{\mathrm{h}}}{E_{\mathrm{v}}} e(t_{\mathrm{EF}}) V_{\mathrm{s,h}}(t_{\mathrm{BE}}). \tag{A.13}$$

Equations 8.18 and A.13 can be combined to obtain the needed initial condition:

$$V_{\mathrm{s,v}}(t_{\mathrm{EF}}) = \frac{P_{\mathrm{a}}(t_{\mathrm{BE}}) e(t_{\mathrm{EF}})}{E_{\mathrm{v}} e(t_{\mathrm{BE}})}. \tag{A.14}$$

Finally, since $V_{\mathrm{s,h}}(t)$, $P_{\mathrm{a}}(t)$, $V_{\mathrm{s,v}}(t)$ are available during ejection, $V_{\mathrm{s},3}$ can be computed from its definition, Equation 6.11:

$$V_{\mathrm{s},3} = V_{\mathrm{s,h}}(t) + \frac{P_{\mathrm{a}}(t)}{E_{\mathrm{a}}} + V_{\mathrm{s,v}}(t). \tag{A.15}$$

The 5 model parameters of interest can thus be computed from the restricted set of model outputs y^4. The analysis presented in this section is summarised in Table A.1 for clarity.

Table A.1: Summary of the demonstration of structural identifiability of the three-chamber CVS model from the fourth output set, y^4, with known values of the valve resistances.

Parameter	Corresponding equation(s)
R_{o}	Known
R_{i}	Known
E_{h}	8.26
R_{c}	A.4, A.6, A.7 and A.8
E_{v}	A.4, A.6, A.7 and A.8
E_{a}	A.4, A.6, A.7 and A.8
$V_{\mathrm{s},3}$	A.15

Appendix B

Investigation of the Proportionality Relation Between R_{MV} and ΔV_{LV}

The present appendix investigates the inverse proportionality relation between R_{MV} and ΔV_{LV}. This relation is one of the fundamental hypotheses of Hann *et al.*'s proportional method [113]. As previously explained, the proportional method was specifically developed for parameter identification in the six-chamber CVS model.

In the six-chamber model, during filling, the change of left ventricular stressed volume is given by Equations 6.19, 6.23 and 6.27:

$$\frac{\mathrm{d}V_{\mathrm{s,LV}}(t)}{\mathrm{d}t} = \frac{P_{\mathrm{PV}} - E_{\mathrm{LV}} e_{\mathrm{LV}}(t) V_{\mathrm{s,LV}}(t)}{R_{\mathrm{MV}}}. \tag{B.1}$$

As mentioned in Section 10.2.1, the proportional method was developed for a version of the six-chamber CVS model in which venous pressures are constant. Hence, P_{PV} is a constant in Equation B.1. Thanks to P_{PV} being constant, Equation B.1 can be solved exactly:

$$V_{\mathrm{s,LV}}(t) = \Bigg[V_{\mathrm{s,LV}}(t_{\mathrm{BF}}) + \frac{P_{\mathrm{PV}}}{R_{\mathrm{MV}}} \int_{t_{\mathrm{BF}}}^{t} \exp\left(\frac{E_{\mathrm{LV}}}{R_{\mathrm{MV}}} \mathcal{E}(u) \right) \mathrm{d}u \Bigg] \exp\left(-\frac{E_{\mathrm{LV}}}{R_{\mathrm{MV}}} \mathcal{E}(t) \right) \tag{B.2}$$

where t_{BF} denotes the beginning of filling and $\mathcal{E}$ is the indefinite integral of e_{LV}:

$$\mathcal{E}(t) = \int_{t_{\mathrm{BF}}}^{t} e_{\mathrm{LV}}(v) \, \mathrm{d}v. \tag{B.3}$$

Equation B.2 allows to compute the volume at the end of filling (at $t = t_{\mathrm{EF}}$):

$$V_{\mathrm{s,LV}}(t_{\mathrm{EF}}) = \Bigg[V_{\mathrm{s,LV}}(t_{\mathrm{BF}}) + \frac{P_{\mathrm{PV}}}{R_{\mathrm{MV}}} \int_{t_{\mathrm{BF}}}^{t_{\mathrm{EF}}} \exp\left(\frac{E_{\mathrm{LV}}}{R_{\mathrm{MV}}}\mathcal{E}(u)\right) \mathrm{d}u\Bigg] \exp\left(-\frac{E_{\mathrm{LV}}}{R_{\mathrm{MV}}}\mathcal{E}(t_{\mathrm{EF}})\right). \quad \text{(B.4)}$$

By definition, ΔV_{LV} is equal to the difference between $V_{\mathrm{s,LV}}(t_{\mathrm{EF}})$ and $V_{\mathrm{s,LV}}(t_{\mathrm{BF}})$:

$$\begin{aligned}\Delta V_{\mathrm{LV}} &= V_{\mathrm{s,LV}}(t_{\mathrm{EF}}) - V_{\mathrm{s,LV}}(t_{\mathrm{BF}}) \\ &= \left[V_{\mathrm{s,LV}}(t_{\mathrm{BF}}) + \frac{P_{\mathrm{PV}}}{R_{\mathrm{MV}}} \int_{t_{\mathrm{BF}}}^{t_{\mathrm{EF}}} \exp\left(\frac{E_{\mathrm{LV}}}{R_{\mathrm{MV}}}\mathcal{E}(u)\right) \mathrm{d}u\right] \exp\left(-\frac{E_{\mathrm{LV}}}{R_{\mathrm{MV}}}\mathcal{E}(t_{\mathrm{EF}})\right) \\ &\quad - V_{\mathrm{s,LV}}(t_{\mathrm{BF}}). \end{aligned} \quad \text{(B.5)}$$

To investigate the proportionality relation between ΔV_{LV} and R_{MV}, one needs to compute

$$\begin{aligned}\frac{\partial \Delta V_{\mathrm{LV}}}{\partial R_{\mathrm{MV}}} &= -\frac{P_{\mathrm{PV}}}{R_{\mathrm{MV}}^2} \left[\int_{t_{\mathrm{BF}}}^{t_{\mathrm{EF}}} \exp\left(\frac{E_{\mathrm{LV}}}{R_{\mathrm{MV}}}\mathcal{E}(u)\right) \mathrm{d}u\right] \exp\left(-\frac{E_{\mathrm{LV}}}{R_{\mathrm{MV}}}\mathcal{E}(t_{\mathrm{EF}})\right) \\ &\quad - \frac{E_{\mathrm{LV}} P_{\mathrm{PV}}}{R_{\mathrm{MV}}^3} \left[\int_{t_{\mathrm{BF}}}^{t_{\mathrm{EF}}} \exp\left(\frac{E_{\mathrm{LV}}}{R_{\mathrm{MV}}}\mathcal{E}(u)\right) \mathcal{E}(u)\, \mathrm{d}u\right] \exp\left(-\frac{E_{\mathrm{LV}}}{R_{\mathrm{MV}}}\mathcal{E}(t_{\mathrm{EF}})\right) \\ &\quad + \frac{E_{\mathrm{LV}}}{R_{\mathrm{MV}}^2}\mathcal{E}(t_{\mathrm{EF}}) V_{\mathrm{s,LV}}(t_{\mathrm{EF}}) \end{aligned} \quad \text{(B.6)}$$

where the last term has been simplified using Equation B.4. Using the same equation, the first term can also be simplified:

$$\begin{aligned}\frac{\partial \Delta V_{\mathrm{LV}}}{\partial R_{\mathrm{MV}}} &= -\frac{V_{\mathrm{s,LV}}(t_{\mathrm{EF}})}{R_{\mathrm{MV}}} + \frac{V_{\mathrm{s,LV}}(t_{\mathrm{BF}})}{R_{\mathrm{MV}}} \exp\left(-\frac{E_{\mathrm{LV}}}{R_{\mathrm{MV}}}\mathcal{E}(t_{\mathrm{EF}})\right) \\ &\quad - \frac{E_{\mathrm{LV}} P_{\mathrm{PV}}}{R_{\mathrm{MV}}^3} \left[\int_{t_{\mathrm{BF}}}^{t_{\mathrm{EF}}} \exp\left(\frac{E_{\mathrm{LV}}}{R_{\mathrm{MV}}}\mathcal{E}(u)\right) \mathcal{E}(u)\, \mathrm{d}u\right] \exp\left(-\frac{E_{\mathrm{LV}}}{R_{\mathrm{MV}}}\mathcal{E}(t_{\mathrm{EF}})\right) \\ &\quad + \frac{E_{\mathrm{LV}}}{R_{\mathrm{MV}}^2}\mathcal{E}(t_{\mathrm{EF}}) V_{\mathrm{s,LV}}(t_{\mathrm{EF}}). \end{aligned} \quad \text{(B.7)}$$

Grouping terms gives:

$$\frac{\partial \Delta V_{\mathrm{LV}}}{\partial R_{\mathrm{MV}}} = \frac{V_{\mathrm{s,LV}}(t_{\mathrm{EF}})}{R_{\mathrm{MV}}} \left(\frac{E_{\mathrm{LV}}}{R_{\mathrm{MV}}}\mathcal{E}(t_{\mathrm{EF}}) - 1\right) + \exp\left(-\frac{E_{\mathrm{LV}}}{R_{\mathrm{MV}}}\mathcal{E}(t_{\mathrm{EF}})\right) \Bigg[\frac{V_{\mathrm{s,LV}}(t_{\mathrm{BF}})}{R_{\mathrm{MV}}} - \frac{E_{\mathrm{LV}} P_{\mathrm{PV}}}{R_{\mathrm{MV}}^3} \int_{t_{\mathrm{BF}}}^{t_{\mathrm{EF}}} \exp\left(\frac{E_{\mathrm{LV}}}{R_{\mathrm{MV}}}\mathcal{E}(u)\right) \mathcal{E}(u)\, \mathrm{d}u\Bigg] \quad \text{(B.8)}$$

As inspection of the previous expression reveals, there is no guarantee that this derivative is positive for all values of the parameters. Figure B.1 presents a numerical evaluation of Equation B.8 with the following values, extracted from Figure 2.9 and Table 11.3:

- $V_{\mathrm{s,LV}}(t_{\mathrm{BF}}) = 50$ ml,
- $V_{\mathrm{s,LV}}(t_{\mathrm{EF}}) = 130$ ml,
- $R_{\mathrm{MV}} = 0.025$, 0.05 and 0.1 mmHg s/ml,
- E_{LV} ranging from 1.4 to 2.4 mmHg/ml,
- $E_{\mathrm{LV}} = \exp(-60((t \bmod 0.5) - 0.25)^2)$,
- $t_{\mathrm{BF}} = -0.1$ s,
- $t_{\mathrm{EF}} = 0.1$ s,
- $P_{\mathrm{PV}} = 5$ mmHg.

Figure B.1 confirms that the derivative $\partial \Delta V_{\mathrm{LV}} / \partial R_{\mathrm{MV}}$ is not always negative, depending on the values of the quantities listed above. Therefore, the hypothesis of an inverse relation between ΔV_{LV} and R_{MV} does not always hold.

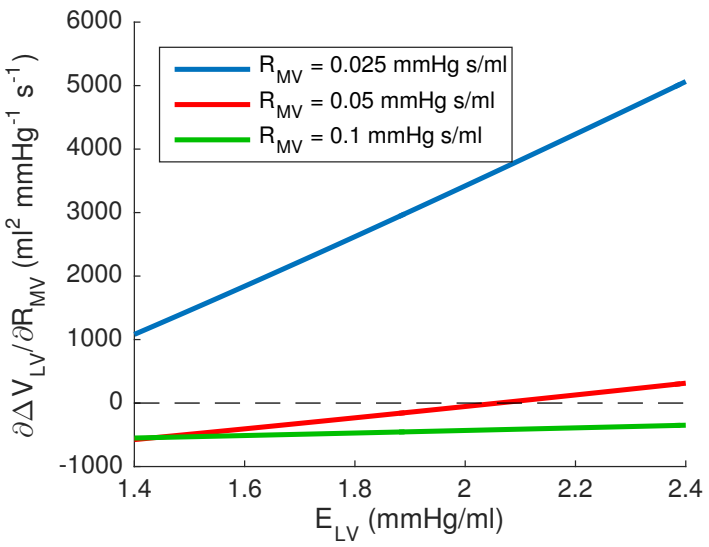

Figure B.1: Curves of $\partial \Delta V_{\mathrm{LV}} / \partial R_{\mathrm{MV}}$ for different values of the parameters E_{LV} and R_{MV}.